Boosting Max-Pressure Signal Control into Practical Implementation: Methodologies and Simulation Studies in City Networks

A DISSERTATION
SUBMITTED TO THE FACULTY OF THE GRADUATE SCHOOL
OF THE UNIVERSITY OF MINNESOTA
BY

Te Xu

IN PARTIAL FULFILLMENT OF THE REQUIREMENTS
FOR THE THE DEGREE OF
DOCTOR OF PHILOSOPHY

Adviser: Michael W. Levin

August 2023

ACKNOWLEDGEMENTS

My journey to earn a doctoral degree at the University of Minnesota, which has spanned over the last three years, has been an extraordinary experience. It began amidst the tumult of the 2020 pandemic, a challenging period during which I spent two months in Cambodia, striving to secure a student visa. I still vividly remember arriving at Minneapolis Airport on October 3, 2020, having missed the Minnesotan summer and stepping directly into winter. Yet, the people I met and worked with during this time in the biting cold were nothing short of warmhearted, supporting me through each step of my journey. It is their unwavering support that has made the completion of this dissertation possible.

At the forefront of this supportive network is my doctoral advisor, Dr. Michael Levin. I am immensely grateful for his steadfast support and guidance throughout my academic journey. Dr. Levin's deep-seated passion for academia, manifest in his enthusiasm for writing research papers and applying for grants, is infectious and inspiring. While he often pushed me out of my comfort zone with complex research questions, he was always available for discussions, encouraging me to persist in the face of adversity. Dr. Levin has an exceptional ability to gauge the amount of technical support each student needs, adapting his mentorship to cultivate independent researchers. He has often reminded me that the path to becoming an independent researcher requires me to be more autonomous each day. Even during his time off, Dr. Levin would painstakingly revise my research papers, offering feedback at any hour of the day. His dedication to his role as an educator is evident in the number of high-impact publications he has authored and the depth of knowledge his students gain in transportation science. This includes a strong grounding in mathematical modeling, rigorous proofing, and simulation techniques. This dissertation is a testament to Dr. Levin's unwavering support and mentorship. His guidance over the past years has been

invaluable, and I cannot thank him enough for his role in my academic journey.

I would like to express my sincere gratitude to Dr. Alireza Khani, Dr. Raphael Stern, and Dr. Kevin Leder for their time and effort in reading my dissertation and for their invaluable contribution as members of the dissertation committee.

I first crossed paths with Dr. Khani in 2016, though he might not recall it, when he was advising his first Ph.D. student, Dr. Yufeng Zhang, a fellow graduate from Southeast University. At that time, both Dr. Zhang and I were under the guidance of the same faculty member to complete our undergraduate dissertations. When I joined the University of Minnesota, I had the privilege of attending Dr. Khani's Transportation Networks course in Spring 2021. His teachings provided me with a deeper understanding of traffic assignment methodologies, ranging from the Method of Successive Averages (MSA) to gradient projection methods. I gained substantial insights into transportation network modeling. Dr. Khani's profound knowledge and his passion for transportation network optimization inspired me to embark on a second Master's degree in Industrial and Systems Engineering. Even more impressively, he has always treated me as his own student, willingly spending time discussing my research and providing insightful suggestions, notably in signal coordination. His steadfast support and guidance were instrumental in my successful completion of the Ph.D. program. I am extremely grateful for his contributions to my academic journey.

I vividly remember the first time I attended the CEGE Transportation Seminar hosted by Dr. Stern in Fall 2020. I was immediately impressed by Dr. Stern's excellent conversation and communication skills. He has the unique ability to maintain focus on the person he's speaking with, engaging them with intriguing topics. Dr. Stern's unwavering support and encouragement for his students is remarkable. For example, he graciously wrote a compelling recommendation letter for me, bolstering my career prospects. I recall a challenging period last summer when Dr. Stern kindly invited me out for lunch. We spent an hour discussing my future plans, and he offered a wealth of advice that proved invaluable. Moreover, Dr. Stern's profound understanding of Automated Transportation

Systems astounded me. He has an uncanny ability to identify crucial research problems and provoke insightful questions. I must express that Dr. Stern's continuous support has imbued me with the courage to keep moving forward. I am deeply grateful for his guidance and mentorship throughout my journey.

I first met Dr. Kevin Leder in September 2020 when I attended the IE 5080 course on Topics in Reinforcement Learning. My experience with the course was unique, as I was participating remotely from an Airbnb in Cambodia while waiting for my F1 Visa. I must admit, IE 5080 was among the most challenging courses during my first year of Ph.D. studies, demanding significant time and effort to complete the assignments. A distinct memory I have is when I received news during one of Dr. Leder's classes that I had to visit the U.S. Embassy to collect my passport. Upon notifying Dr. Leder of my need to delay submitting HW2, he asked me if I had taken the time to visit Angkor Wat - a moment that remains vivid in my mind. In Fall 2021, I opted for IE 5532 on Stochastic Processes, also taught by Dr. Leder. I found his teaching style, which involved systematically breaking down mathematical proofs, incredibly effective. Both reinforcement learning and stochastic processes have proven invaluable to me, not just in my academic pursuits, but also during my job hunt, where I frequently encountered related questions. These courses significantly contributed to my successful job offers. I am genuinely grateful for Dr. Leder's courses and his proficient teaching skills. Moreover, I could not have successfully completed my second Master's in Industrial and Systems Engineering without Dr. Leder's guidance and support. I deeply appreciate his contributions to my academic journey.

I am immensely appreciative of the financial support received from various institutions that made my achievements possible. My sincerest thanks go to the Department of Civil, Environmental, and Geo-Engineering for the Departmental Fellowship and the teaching assistantship, the Center for Transportation Studies for the TRB Student Travel Awards, and the University of Minnesota China Center for the Hsiao Shaw-Lundquist Fellowship. Each of these contributions played a vital role in shaping my academic journey. Moreover, I

acknowledge with gratitude the unwavering support and guidance received from the faculty and staff of the Department of Civil, Environmental, and Geo-Engineering at the University of Minnesota. Their continuous encouragement has been of great value to my progress. Special recognition must be given to Dr. Sebastian Behrens, the Director of Graduate Studies in our department, whose consistent support and inspiration were fundamental to my academic trajectory. I am equally grateful to Ms. Tiffany Ralston for her invaluable assistance in coordinating my PhD exams and orchestrating my PhD graduation milestones. Their commitment and dedication to my success have been truly remarkable.

I wish to express my heartfelt appreciation for the support I've received, both academically and personally, from Dr. Yinling Fan. As a distinguished alumna from Southeast University, now a professor in the School of Public Affairs at UMN, Dr. Fan has been a guiding light on my academic path. I have had the privilege of following her, listening attentively to her illuminating presentations in diverse locations such as Washington D.C., Nanjing, and Shenzhen. Dr. Fan's recent research focuses on vital aspects like public transportation development, emotional well-being in cities, and community-engaged transportation equity. Her work, steeped in human values, makes significant contributions to enhancing the quality of urban life. Despite her remarkable research achievements, Dr. Fan exhibits an immense dedication to her students. Particularly, she extends a hand of support to those from Southeast University aspiring for further studies, like myself. Dr. Fan is truly the cornerstone of the Southeast University community in the USA, knitting us together with a sense of unity. Her unwavering assistance, from the inception of my application process through to the completion of my Ph.D. studies, has been instrumental. I am profoundly grateful for her guidance and support throughout my academic journey.

In addition to the esteemed faculty I've already acknowledged, I'd like to extend my gratitude to my former instructors during my graduate studies at Southeast University: Dr. Zhiyuan Liu, Dr. Zhibin Li, Dr. Hao Wang, Dr. Xu Qu, and Dr. Yanjie Ji. Special recognition goes to Dr. Zhiyuan Liu. It was his course on Transportation Data Analysis

and Modeling that changed my initial reluctance towards continuing my Master's study. His efficient teaching methods and deep comprehension of Operations Research fascinated me, solidifying my belief that a remarkable teacher has the ability to simplify and demystify complex concepts. To this day, I hold Dr. Liu's course as a shining beacon of my Master's journey at Southeast University. My gratitude also extends to Dr. Yanjie Ji, who offered considerable support and encouragement during a challenging period when I broke my right arm. His aid during this trying time was invaluable. Finally, I wish to express my profound affection for Southeast University, particularly the School of Transportation Engineering. SEU was the fertile ground where my dreams were cultivated, where I was inspired and encouraged to reach new academic heights. This institution has an irreplaceable role in my journey and for this, I am eternally grateful.

I would like to express my sincere gratitude to Dr. Lijun Sun, an Associate Professor at McGill University. I am deeply thankful for the opportunity he extended to me to join his research group as a summer visiting student in 2019. My time in Montreal, Canada was one of the most enriching experiences of my life. I was fortunate to make many friends in your group and explore the beautiful city of Montreal, an experience I will forever cherish.

In addition, my heartfelt thanks go to Dr. Zheng Zhu, a Professor at Zhejiang University. During my Ph.D. application process, Dr. Zhu was serving as a Postdoctoral Researcher in Dr. Hai Yang's group in HKUST. He graciously sacrificed his personal time to refine my application email, research proposal, and my CV. More than that, Dr. Zhu's constant encouragement and faith in my abilities instilled in me the confidence I needed during this critical phase. His support has been instrumental, and for that, I am genuinely grateful.

In addition to the esteemed faculty previously acknowledged, I wish to express my heartfelt gratitude to my former instructors during my undergraduate studies at Chang'an University: Dr. Hong Chen, Dr. Haipeng Shao, and Dr. Min Zhang. Among them, my deepest thanks are reserved for Dr. Hong Chen, who played an instrumental role throughout

my undergraduate journey. I vividly recall her guidance and support during the National Transportation Science and Technology Competition, as well as her invaluable assistance during my Master's application process and the search for an advisor. Her influence on my academic path has been immeasurable.

I would like to express my heartfelt appreciation to the individuals I've had the pleasure of meeting at UMN, particularly Dr. Rongsheng Chen and Mr. Simanta Barman. Dr. Rongsheng Chen offered invaluable assistance during my arrival in the USA, a kindness that I will always remember as I wish him a prosperous career at Beijing Jiaotong University. Mr. Barman, with his remarkable mathematical acumen and proficiency in coding, has always struck me as truly gifted. The memorable and moving times we've shared over the past three years will forever remain etched in my heart. A special thanks is due to my dear friends and roommates, particularly Tianyi Li. Your support, especially when I was new to the USA, has been invaluable, and I hope that you achieve all of your dreams. I also owe a debt of gratitude to my dear friend Mingfeng Shang. I fondly remember how you helped and accompanied me when I bought my first car in the USA, and your willingness to sacrifice your time during the TRB season is deeply appreciated. My gratitude further extends to Xin Jiang (ISYE), Yifan Xu (ISYE), Xianyu Chen (CS), Shian Wang, Jingru Gao, Chen Hu, Jacob Margolis, Rui Li, Maziar Zamanpour, Di Kang, Jingran Cao (Pharmaceutical), and Behnam Davazdah Emami. Each of you has contributed significantly to my journey. If I have inadvertently missed anyone, please know that it does not diminish my appreciation for your impact on my life.

I would especially like to express my gratitude to my fellow Southeast University alumni at UMN, namely Dr. Tianhao Yan, Dr. Tao Tao, and Dr. Yufeng Zhang. Your invaluable assistance during my application process to UMN, throughout my time there, and as I completed my studies has been truly indispensable. I would also like to extend my thanks to the friends I made in the ISYE department, namely Clay Hall and Ethan Rosenthal. Being friends with both of you has been a joyous and humorous period in my life. You

invited me to birthday parties, graduation ceremonies, Halloween parties, and other events, which brought a breath of fresh air into my rigorous and demanding Ph.D. life. Clay, my friend, I wish you a fruitful career at Deloitte. Ethan, I wish you a wonderful life in Israel. Your friendships have truly enriched my time as a Ph.D. student.

I will forever cherish the support from my dear friends, the coulple Dr. Yufan He of Nvidia and Dr. Ruishen from UPenn, Dr. Yang Li of Tokyo University, the couple Han Guo & Anle Du, Dr. Yu Tu of Southeast University (SEU), Hang Gao of UC Davis, Yanzhe Dai, and Mingyang Zhang. Dr. Yufan He, my childhood friend since we were six years old, you are a hard-working, talented, and amusing individual. In my master's degree acknowledgements, I noted how you have always been a guiding light in my life, pointing me towards the correct path. Even now, you remain my exemplar, and I am grateful for your encouragement to apply for a Ph.D. and to study Artificial Intelligence. Dr. Yang Li, it was wonderful to reunite with you in Philadelphia. You are incredibly talented, not just academically but also athletically in basketball, soccer, and table tennis. I fondly recall our high school days when we played basketball every Friday afternoon. I deeply appreciate your unwavering support and the confidence you instilled in me during my challenging academic journey over the last seven years, from my master's to my Ph.D. studies. You have always been there for me, willing to lend an ear and offer advice when I needed it.

Han Guo & Anle Du, both of you are treasures in my life, my best friends since middle school. It's been three years since our last reunion, and now you two have become a lovely couple blessed with a beautiful baby, Yiyi. I eagerly await the day when I return to China and can see you again. Dr. Yu Tu, my great friend at SEU, we have shared many experiences, both in academics and on the basketball court. It was you who helped me through the challenging period when I broke my right arm, and it was you who helped me revise my knowledge during that time. I'm profoundly grateful for your support. Dr. Hang Gao, meeting you at the TRB was a joyous moment, and I thank you for being my friend. Our trip in Northern California during the fall of 2021 remains a treasured memory for me.

I would like to express my deepest appreciation to my girlfriend, Mrs. Yunfan Zeng. You are my beacon of warmth, illuminating my life amidst the cold Minnesota winters. You are confident, kind-hearted, humorous, artistic, and ceaselessly explorative. Studying, coding, traveling, and listening to symphonies together with you have been some of the best times of my life. I cannot imagine how I would have survived my final year of Ph.D. studies without you. I look forward to exploring every national park with you and embarking on annual road trips from west to east, north to south. You have brought color to my life, and I hope that for the rest of our lives, we can continue to be explorers together.

Last but certainly not least, I would like to extend my deepest gratitude for the unwavering love, support, comfort, guidance, and encouragement that I have received from my parents, Mrs. Chunhua Yuan and Mr. Shizhong Xu, and my grandparents, Mrs. Aimei Hu and Mr. Yipeng Yuan. My parents have always provided me with the utmost emotional and financial support. They've always encouraged me to pursue my dreams and not overthink. Unlike traditional Asian parents, they have given me the freedom to choose my path and never forced me into anything I did not want. When I told them I wanted to study abroad, their immediate reaction was support and encouragement. My grandparents, Mrs. Aimei Hu and Mr. Yipeng Yuan, have always been my warmest supporters. Every time I return to my grandparents' home, I am greeted with comfort, peace, and love. My grandfather, Mr. Yipeng Yuan, a well-educated engineer with extensive life and work knowledge, has been an invaluable mentor. From fishing trips to calligraphy lessons to polishing my compositions, he has been there for me. Whether discussing politics, engineering developments, macroeconomics, humanity, or history, my grandfather has an encyclopedic knowledge of it all. I am immensely grateful for the support and love you have all given me.

DEDICATION

This dissertation is dedicated to parents Chunhua Yuan and Shizhong Xu, my grand parents Aimei Hu and Yipeng Yuan.

Contents

List of Tables

List of Figures

ABSTRACT

This dissertation presents innovative modifications to the Max-Pressure (MP) control policy, an adaptive traffic signal control strategy tailored to various urban traffic conditions. The max-pressure control offers two pivotal advantages that underscore its significance for in-depth research and future implementation: Firstly, MP operates on a decentralized basis, enabling real-time solutions. Secondly, MP control guarantees maximum stability, implying it can accommodate as much given demand as any alternative signal timing strategy. Initially, the MP control policy was adapted to transit signal priority (MP-TSP). It delivered enhanced bus travel times, outperforming both fixed-time signal controls with TSP and other adaptive signal controls in efficiency. Subsequently, the pedestrian-friendly max-pressure signal controller (Ped-MP) was developed. This marked a pioneering effort in crafting an MP control to boost pedestrian access without compromising vehicle throughput. The Ped-MP, backed by analytical proof for maximum stability, illustrated an inverse relation between pedestrian delay and tolerance time during simulations on the Sioux Falls network. This suggests the potential for urban spaces that are more pedestrian-oriented, even in areas of elevated pedestrian traffic. The third innovation addressed the practical feasibility of the position-weighted back-pressure (PWBP) controller. Although the initial PWBP controller was effective in simulations, it was found to be impractical due to its need for density information from everywhere of the road link. This observation paved the way for the approximate position-weighted back-pressure (APWBP) control, which significantly reduces sensor requirements by utilizing only two loop detectors per link (one downstream and one upstream). A comparative analysis revealed that the APWBP's efficacy closely paralleled the original PWBP, validating its practicality. Finally, recognizing the MP controller's deficit in coordinated phase selection, the Smoothing-MP approach was

conceptualized. Incorporating signal coordination, this novel strategy not only maintained its maximum stability properties but also amplified traffic flow efficiency, as confirmed by mathematical proofs and numerical studies in both the Grid Network and the Downtown Austin Network.

Chapter 1

Introduction

Intersections are the major bottlenecks of city networks, which may aggravate traffic congestion due to insufficient signal timing plans, pedestrians, buses, traffic accidents, lack of maintenance, or other reasons. Traffic congestion is one of the significant problems in the urban traffic system, especially in the United States, since the vast majority of people seeking to move during peak hours use private automotive vehicles. The increase of private vehicles usage increase vehicle miles traveled, travel delay, reduce the traffic operational efficiency, especially near intersections, where vehicles need to accelerate and decelerate frequently (Saldivar-Carranza et al., 2021). As reported in the 2022 National Traffic Signal Report Card, 10 % of the travel time of an average trip was spent delayed by traffic signals. Therefore, providing a better traffic signal control system plays a significant role in the traffic network. This dissertation focusing on improving signal control, especially distributed signal control that includes multi-model traffic access, to improve traffic operation efficiency.

1.1 Intersection control

Intersection control aims to separate vehicles from different directions spatially or temporally to prevent conflicting with each other within an intersection. Initially, intersection

control started with the stop-sign-based control before traffic lights were introduced. Later on, the traffic light was introduced in 1868 in London to reduce the workload for police to control traffic. With the emergency of electricity and computerized control, traffic light technology increases intersection capacity significantly. Fixed time signal control is a simple and old form controller, with fixed green light intervals calculated in advance. However, due to the complexity and dynamics of the traffic pattern, fixed-time signal controllers are not suitable for urban traffic even they are still used in peak hours in many cities. Traffic researchers started finding more advanced way to use real-time traffic information in signal control. With the development of cameras, sensors, and loop detectors, adaptive intersection control was introduced to provide signal timing plans based on the real-time traffic pattern. There are some famous adaptive signal control frameworks, such as SCOOT (Bing and Carter, 1995), SCATS (Sims and Dobinson, 1980), RHODES (Mirchandani and Head, 2001), OPAC (Gartner, 1983), and etc.

Signal controllers are required to serve a large number of intersections to improve network-level traffic conditions. When the signal controller is applied to a city-wide network, it needs to coordinate with several intersections to let vehicles move smoothly pass through multiple intersections. However, the city-wide network size, the number of vehicles, and the number of intersections are huge which makes it is hard to obtain a ”optimal” signal-timing plan. Therefore, the coordination between intersections should be supported by an appropriate control structure. There are two main types of control structures: centralized signal control and distributed signal control. For the centralized signal control, a central controller is needed for decision making. Specifically, a central controller needs traffic data of the entire transportation network to construct an optimization model, and then it determines the global optimal controls for every intersection. Therefore, it is hard to implement the centralized traffic signal controller in large city networks. Most centralized signal controls model the traffic optimization as a mixed-integer program and simulate a signalized intersection or a signalized urban corridor, which ignores the network-level

performance.

Also, the centralized control structure is not that robust, since it requires perfect connectivity of all intersections, and a small connected error may impact the controller result a lot. Specifically, this control structure needs stable connectivity to ensure information communication, which restricts the size of the system. Malfunctions of the controller can lead to the breakdown of the entire system as the central controller makes decisions for all nodes.

Contrast to centralized signal control, a distributed control system has multiple controllers. Each controller aims to make its own decision for a small-size area or a individual intersection. Decisions of whole system are composed by each individual decision. Distributed control systems are more suitable to the city network, since it requires traffic data from upstream or downstream intersections and compute the intersection control by itself. Therefore, distributed signal controllers have more lower computation time. Although distributed signal controllers are not easy to obtain global optimality, this issue can be solved by a well-designed system structure.

1.2 Max-pressure control

Decentralized traffic signal controls, such as max-pressure (MP) control, also known as back-pressure (MP) control, have received increased attention recently. MP control was developed for wireless communication networks by Tassiulas and Ephremides (1990). In recent years, researchers began leveraging the MP policy to traffic signal control because they are decentralized signal controllers with valuable network-level properties. This thesis aims to boosting MP control in practical implementation. Wongpiromsarn et al. (2012) demonstrated their distributed traffic signal control, which is the first time that max-pressure routing has been leveraged for traffic signal problems. Later on, Varaiya (2013) developed a decentralized traffic signal control policy based on MP ideas, and proved that their policy can

guarantee maximum stability based on the store-and-forward model. Maximum stability is related to maximum throughput, which is a major goal of traffic signal timing. Specifically, throughput means the number of vehicles exiting the network, so maximum throughput refers to maximizing the number of vehicles exiting the network. "Stability" refers to queue length of a network does not grow without bounded in the long run, which also implies that the signal timing serves all demand in the transportation network. Maximum stability means the ability/capacity of a signal controller to serve as much as network-level demand as any other signal timing policy. MP control is analytically proven to achieve maximum stability which implies the controller can achieve maximum throughput when the demand can be served by some signal timing policy.

Gregoire et al. (2014a) provided a MP traffic signal controller without knowing the routing rates, only using the estimation for each possible direction. Although they proved that their proposed BP-based traffic could achieve maximum stability properties based on Lyapunov drift technologies and simulation results, they still modeled traffic flow dynamics based on the point queue model. Gregoire et al. (2014b) also developed a normalized pressure term and proposed a capacity-aware MP traffic signal controller, which can stabilize the transportation network better as congestion increases. However, their conclusion was obtained by simulation only.

Due to the complexity of the proof of maximum stability of MP-based control technologies, many past studies did not include the analytical proof of stability (Sun and Yin, 2018; Mercader et al., 2020; Dixit et al., 2020). For instance, Sun and Yin (2018) compared Varaiya (2013)'s non-cyclic MP control, a cyclic MP control, and coordinated actuated traffic signal controller in VISSIM. The results indicated that Varaiya (2013)'s non-cyclic MP control performed better than the cyclic MP control. Mercader et al. (2020) proposed a novel travel-time based MP control. The results indicated that their controller can prevent unstable traffic behavior and was implemented in a realistic intersection. Dixit et al. (2020) proposed a delay-based MP traffic signal controller that was implemented in reality based

on crowdsourced delay data.

To extend the practical application of the max-pressure signal control, many studies modified the original MP traffic signal controller proposed by Wongpiromsarn et al. (2012) and Varaiya (2013). For instance, Varaiya (2013)'s MP control actuates green lights purely based on the pressure term, which causes traffic signal phases to be actuated in arbitrary order. This arbitrary order may be confusing for drivers and may cause some vehicles to wait for a long time on low demand links. To solve this problem, both Le et al. (2015) and Levin et al. (2020) proposed a MP control with cyclic phases, and proved the stability of the proposed methods. The difference between Le et al. (2015) and Levin et al. (2020)'s studies is the cycle length in Levin et al. (2020)'s research is adaptive with a maximum value and the length can be shortened when desired, which results in better performance and an easier implementation in practice. Liu and Gayah (2022) proposed a travel-delay based MP control that tries to overcome the drawback of long waiting time of travel demand approaches. Rey and Levin (2019) noticed the emergence of autonomy trend in the transportation system and future co-existence of human-driven vehicles and autonomous vehicles on roads together. Therefore, they introduced the concept of blue phase, which was designed for autonomous vehicles usage only, in the original MP-based traffic signal controller. Their novel MP traffic control can still achieve maximum throughout. Autonomous intersection management (AIM) was introduced to coordinate intersection movement for autonomous vehicles. However, the conventional AIM algorithm cannot easily provide pedestrian access. Chen et al. (2020) proposed a MP control combined with AIM for the first time, which can maximize the network throughput of the combined vehicle and pedestrian flow. In addition, some researchers used travel time instead of queue lengths in BP control (Mercader et al., 2020). Reinforcement learning has been effectively applied in the domain of traffic control, as evidenced by works such as Ke et al. (2020), Yang et al. (2019b) and Zheng et al. (2023). Building on this, several studies have explored the integration of reinforcement learning into MP controls, including Maipradit et al. (2019), Wei et al. (2019),

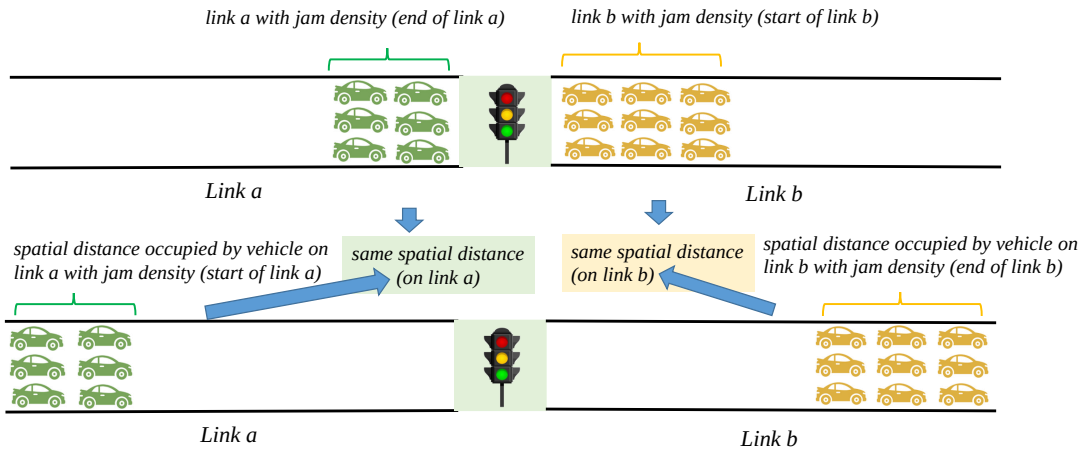

Figure 1.1: Different density distribution but have same pressure

Boukerche et al. (2021), and Wang et al. (2022). Other studies have incorporated MP control into the dispatching of shared autonomous vehicles to ensure improved passenger waiting time performance Xu et al. (2021, 2023); Robbennolt and Levin (2023).

To the best of our knowledge, most past studies about MP-based traffic signal controllers were based on the point queue or spatial queue models (Vickrey, 1969; Zhang et al., 2013), which are not able to capture the spatial distribution of vehicles along the roads (Boyles et al., 2021). However, realistic traffic does not follow a point queue model, which will obviate the mathematical guarantees of maximum throughput. For instance, different spatial distributions of vehicles may have same pressure according to Varaiya (2013). Figure 4.1 provides details about the different density spatial distribution but have same pressure scenarios. To overcome this, Li and Jabari (2019) developed a position-weighted back-pressure (PWBP) control policy which assumes that traffic follows a first-order kinematic wave model. Note that back-pressure (BP) control is the same as max-pressure (MP) control but with a different name. Li and Jabari (2019) proposed a weight function where vehicles closer to the intersection contribute more to the weight. In addition, they proved that the PWBP achieves maximum stability by Lyapunov drift technologies, and the experimental results indicated the PWBP performs better than SCOOT (Split, Cycle and Offset

Optimisation Technique), as well as in a network setting against fixed intersection control, standard BP, and capacity-aware BP (CABP). But there is a potential problem which prevents the PWBP from being implemented in practice: using loop detectors or other sensors to obtain the density at every point along a link is cost-prohibitive. Furthermore, there is no existing research introducing signal coordination into MP control.

1.3 Motivation

Although MP control has many advantages, it still faces some real-world challenges. The first challenge is that current max-pressure controller do not consider the access of public transit. Specifically, implementation of max-pressure control may cause bus service to become unreliable and increase bus users' travel time because the max-pressure controller is more likely to give phases for a large demand approach. However, bus service quality is an important factor that could promote part of the travel demand shift from driving to public transit. To achieve equity between different transportation modes, public transit priority is introduced into traffic signals to improve bus operation efficiency (Hunter-Zaworski et al., 1995; Ma et al., 2014; Ding et al., 2015; Anderson and Daganzo, 2020; Deng and Nelson, 2011; Eichler and Daganzo, 2006; Levinson et al., 2002; Bayrak and Guler, 2020; Wadjas and Furth, 2003; Yang et al., 2019a). One major approach is granting signal timing priority (also called transit signal priority, TSP) to the buses (Hunter-Zaworski et al., 1995; Currie and Shalaby, 2008; Christofa and Skabardonis, 2011; Li et al., 2011; Ma et al., 2014; Ding et al., 2015; Wadjas and Furth, 2003; Lin et al., 2019; Yang et al., 2019a; Bayrak and Guler, 2020). The other major approach is designing exclusive bus lanes, which are usually built with bus rapid transit system (Deng and Nelson, 2011; Levinson et al., 2002; Eichler and Daganzo, 2006). Both can effectively increase the operational speed of buses and increase the level of service of the public transit system.

However, previous max-pressure signal control policies assume that public transit uses

the same signal timing as private vehicles. If the operation of public transit is ignored, there may be problems at certain intersections that are neglected when implementing max-pressure controller policies. For instance, the max-pressure controller is more likely to actuate phases for high-demand approaches, which may delay buses waiting in lower-demand approaches. In order to boost the application of the max-pressure control policy, we combine the max-pressure control with TSP for the first time. Details are shown in Chapter 2.

The second challenge is that the of consideration of pedestrian access. Since walking is becoming more and more popular due to the concerns of transportation environmental impacts and increasing travel demand in urban areas, more and more researchers started focusing on providing better signal timing with pedestrian crossing (Ma et al., 2015; Zhang et al., 2018, 2019; Akyol et al., 2020). From the perspective of safety, integrating pedestrians' access in signal timing is non-negligible. The risk of pedestrian injuries or fatalities is a significant problem in our transportation systems, which is especially elevated at intersections where vehicle-pedestrian interactions occur. Therefore, it is important to consider pedestrian access at intersections, especially for the disabled, children, and elderly (Leden et al., 2006; Cafiso et al., 2011; Khosravi et al., 2018). From the point of sustainability and urban planning, promoting walking can result in health benefits (Heinrichs and Jarass, 2020; Tang et al., 2021; Park and Garcia, 2020). As the critical point to walking accessibility, crosswalks at the intersection provide the connections between sidewalks. Safety and continuous walking space encourage citizens to walk more, which further promotes sustainable development for the metropolises. Therefore, this context motivates us to find a better signal timing method to provide more friendly signal strategies for pedestrians and serve more vehicles in the urban area.

Most of the MP controls try to solve the network implementation problem but under vehicle-only scenarios. Although Chen et al. (2020) considered pedestrian access, they modeled autonomous intersection control and not traffic signals. Therefore, MP control

with pedestrian access in the human-driven vehicle environment is an open problem. To balance vehicle stability and pedestrians' waiting time, we modify Varaiya (2013)'s max-pressure policy to ensure the maximum throughput of vehicles and with bounded waiting times for pedestrians. Details are discussed in Chapter 3.

The third challenge is that most MP-based signal controls model traffic flow dynamics with the point queue or the spatial queue flow models (Vickrey, 1969; Zhang et al., 2013). The main reason that most previous research used these models is due to the complex proof of maximum stability. However, the point queue and spatial queue flow models have significant limitations in representing traffic flow dynamics, such as lacking shockwaves and queue spillback along roads. Although the spatial queue can represent queue spillback along roads, it assumes that the backward wave speed is infinity. To incorporate the impacts of realistic traffic flow dynamics and consider the realistic spatial distribution of vehicles along the road, Li and Jabari (2019) developed a position-weighted back-pressure control (PWBP) which based on the kinematic wave theory of traffic flow. Note that back-pressure (BP) control is the same as max-pressure (MP) control but with a different name. They also proved the maximum stability based on the PWBP algorithms without any non-local traffic information. However, their weight function requires integrating the density over space along the roads. While this is analytically sound, in practice, the density is unlikely to be known exactly throughout space-time. Hence, their PWBP algorithm is hard to implement in practice.

Typically, density can be measured through a limited number of loop or video detectors, which can determine the cumulative counts of vehicles at the point of detection. For instance, a link may have only 2 loop detectors – one at the upstream and downstream ends of the link. Given a flow-density relationship, the density at other points might be inferred by the kinematic wave theory (Claudel and Bayen, 2010a). Therefore, this researcher try to extend Li and Jabari (2019)'s analytical stability results to a more practical approximate position-weighted BP (APWBP) control policy. The errors in that approximation make the

maximum throughput properties unclear, requiring further methodological analysis. Therefore, in order to make MP control more practical, this research proposes an approximate position-weighted back-pressure (APWBP) traffic signal control policy, which employs kinematic wave theory to estimate traffic states based on the loop detectors installed in the upstream and downstream ends along the links. Details are discussed in Chapter 4.

The last challenge is that lack of considering signal coordination. Although max-pressure control can achieve maximum stability, but it may cause larger delay if we do not considering the coordinated movement. Signal coordination aims to smooth vehicle movements based on determining the traffic signal splits, cycle length, and offsets, which could reduce vehicle delay, vehicle travel time. Therefore, we try to introduce signal coordination into MP control for the first time in this research. Details are presented in Chapter 5.

1.4 Problem statements and contributions

Based on the objective of boosting MP control in real-world implementation, this thesis mainly includes four topics.

1.4.1 Integrating public transit signal priority into max-pressure signal control

Max-pressure signal control has been analytically proven to maximize the network throughput and stabilize queue lengths whenever possible. Since there are many transit lines operating in the metropolis, the max-pressure signal control should be extended to multi-modal transportation systems to achieve more widespread usage. The standard max-pressure controller is more likely to actuate phases during high-demand approaches, which may end up ignoring the arrival of buses, especially in bus rapid transit. In this chapter, we propose a

novel max-pressure signal control that considers transit signal priority of bus rapid transit systems to achieve both maximum stability for private vehicles and reliable transit service. This chapter revises the original max-pressure control to include constraints that provide priority for bus transit rapid system. Furthermore, this policy is decentralized which means it only relies on it relies only on the local conditions of each intersection. We set the simulation on the real-world road network with bus rapid transit systems. Numerical results show that the max-pressure signal control which considers transit signal priority can still achieve maximum stability compared with other signal control integrated with transit signal priority. Furthermore, the max-pressure control reduces private vehicle travel time and bus travel time compared to the current signal control.

1.4.2 A pedestrian-friendly max-pressure signal control policy for city networks

Previous work on max-pressure signal control with cyclic and non-cyclic phases does not include pedestrian access, which may increase pedestrians' travel time and delay or even encourage some dangerous behaviors like jaywalking. Since the movement of pedestrians is a non-negligible factor in traffic management, and many urban planning researchers have found that walking space and walking continuously have significant health, safety, and environmental impacts, a pedestrian-friendly max-pressure signal control policy is needed. In this chapter, we propose a novel pedestrian-friendly max-pressure signal control that considers pedestrian access in an urban network to achieve both maximum stability for private vehicles and a comfortable, safe walking experience. This chapter modifies the original max-pressure control to include pedestrians' access for the first time. Furthermore, this policy still inherits the decentralized property of original max-pressure control, which means it only relies on the local information of individual intersections. Simulation results indicate that although considering pedestrians' access may reduce the stable region for

vehicles, the pedestrians' travel time and delay can be reduced significantly.

1.4.3 An approximate position-weighted back-pressure traffic signal control policy for traffic networks

We use back-pressure control for this problem, since this part of research is original proposed by **?**, which named max-pressure control as back-pressure control. Actually, max-pressure control and back-pressure control are the same controller with different name. Most of the existing research on back-pressure (BP) signal control model traffic dynamics is based on the point queue model or the spatial queue model. Here back-pressure (BP) is the same control as MP control but with difference names. We use BP control in this chapter is because this research is based on the original position-weighted back-pressure signal control (PWBP) of Li and Jabari (2019). Point queue model or the spatial queue model are not able to capture the spatial pattern of traffic flow dynamics, such as the distribution of traffic density on roads. Also, most BP signal controllers are difficult to implement in reality. In order to make BP control more practical, this dissertation proposes an approximate position-weighted back-pressure (APWBP) traffic signal control policy, which employs kinematic wave theory to estimate traffic states based on the loop detectors installed in the upstream and downstream ends along the links. We prove the maximum stability of the proposed APWBP traffic signal control policy, which means APWBP can still maximize the network vehicle throughput and stabilize vehicle queueing length whenever possible. To prove the maximum stability of the proposed APWBP traffic signal control policy, we introduce a proposition that provides sufficient conditions for stability. Simulations are implemented in the well-known Sioux Falls network, and provide comparisons against the original position-weighted back-pressure signal control (PWBP) of Li and Jabari (2019). Numerical results demonstrate that the proposed APWBP can still achieve the same maximum throughput as compared with PWBP based on loop detectors installed in the upstream

and downstream of road links.

1.4.4 Introducing signal coordination into max-pressure control

Recently, traffic signal tries to coordinated-actuated traffic signal light. Signal coordination aims to smooth vehicle movements based on determining the traffic signal splits, cycle length, and offsets, which could reduce vehicle delay, vehicle travel time. There are two ways of signal coordination: active and passive. Although signal coordination has been studied for many years, it has not been introduced into max-pressure control. This chapter aims to modify original max-pressure control by defining a coordinated indicator associated with vehicle movements at each time step to determine whether this movement is allowed to move at next time step. Integrating signal coordination into max-pressure control are expected to improve average speed and decrease average delay for transportation network.

This thesis mainly focuses on answering the following questions related to mentioned four topics.

1. How can max-pressure control could be integrated with public transit signal priority and maintain network-level properties of the max-pressure control?

2. How can the max-pressure control be integrated with pedestrian access and maintain maximum stability property for vehicles?

3. How can we provide a max-pressure control that can employ kinematic wave theory to estimate traffic states based on the loop detectors installed in the upstream and downstream ends along the links and maintain network-level properties of the max-pressure control?

4. How can we introduce signal coordination into max-pressure control to reduce vehicle delay and maintain maximum stability for vehicles?

1.5 Contributions

This dissertation notably advances the MP control policy for adaptive traffic signal control, offering distinct improvements over existing methodologies. One of its paramount contributions is the innovative incorporation of transit signal priority into the MP control policy. This groundbreaking amalgamation called for intricate algorithmic modifications, ensuring a fluid integration of public transit within urban frameworks. Evaluations within the downtown Austin milieu highlighted the efficacy of integrating MP control with transit signal priority, notably reducing bus travel durations. This performance was particularly significant when compared with other fixed-time signal controls that incorporate TSP, as well as adaptive signal controls.

Furthermore, this dissertation pioneers the integration of pedestrian access within MP control, termed Ped-MP. This advancement represents a substantial leap in prioritizing pedestrian access while simultaneously maintaining vehicular efficiency. Through rigorous analytical validations and simulations conducted in the Sioux Falls domain, the Ped-MP's potential in adeptly balancing pedestrian and vehicular demands was clearly manifested.

Addressing the practical challenges of real-world applications, the study introduces the APWBP control as a solution. In light of the limitations intrinsic to the PWBP controller, the APWBP emerges as a revolutionary strategy, designed to substantially curtail sensor requirements for the tangible deployment of the MP control policy. Notably, with the integration of just two loop detectors for each road link, the APWBP's performance paralleled its antecedent, making it a remarkably viable alternative.

Lastly, to overcome the absence of coordinated phase selection in previous MP controller iterations, this research introduces a refined signal coordination MP control approach. Mathematical evaluations strongly support its inherent stability properties. Furthermore, empirical analyses conducted within the Grid and Downtown Austin networks emphasized its marked effectiveness.

1.6 Thesis organization

The remainder of the thesis includes these chapters: Chapter 2 revises the original max-pressure control to include constraints that provide priority for buses. Chapter 3 proposes a novel pedestrian-friendly max-pressure signal control named Ped-MP that considers pedestrian access in an urban network to achieve both maximum stability for private vehicles and a comfortable, safe walking experience. Chapter 4 proposes an approximate position-weighted back-pressure (APWBP) traffic signal control policy, which employs kinematic wave theory to estimate traffic states based on the loop detectors installed in the upstream and downstream ends along the links. Chapter 5 introduces signal coordination into MP control for the first time.

Chapter 2

Integrating public transit signal priority into max-pressure signal control: methodology and simulation study on a downtown network

2.1 Introduction

As a bottleneck for urban transportation networks, intersections have attracted lots of attention from researchers. To optimize signal timing and achieve maximum throughput of intersections, recent studies have proposed max-pressure-based signal control policies for adaptive adjustive signal timings (Wuthishuwong and Traechtler, 2013; Varaiya, 2013; Gregoire et al., 2014b; Xiao et al., 2014; Rey and Levin, 2019; Chen et al., 2020; Mercader et al., 2020; Levin et al., 2020; Li et al., 2021). One property of max-pressure control is it had proven to serve all demands whenever possible. max-pressure control is also decentralized, which means the network-level optimal solution can be found by a local traffic signal controller only using the traffic information from upstream and downstream links (Varaiya, 2013; Tassiulas and Ephremides, 1990).

Implementation of max-pressure control faces some real-world challenges, such as the equity between private vehicle users and public transit users. Specifically, implementation

of max-pressure control may cause bus service to become unreliable and increase bus users' travel time because the max-pressure controller is more likely to give phases for a large demand approach. However, bus service quality is an important factor that could promote part of the travel demand shift from driving to public transit. To achieve equity between different transportation modes, public transit priority is introduced to improve bus operation efficiency (Hunter-Zaworski et al., 1995; Ma et al., 2014; Ding et al., 2015; Anderson and Daganzo, 2020; Deng and Nelson, 2011; Eichler and Daganzo, 2006; Levinson et al., 2002; Bayrak and Guler, 2020; Wadjas and Furth, 2003; Yang et al., 2019a). One major approach is granting signal timing priority (also called transit signal priority, TSP) to the buses, TSP has three kinds of types: passive priority method, active priority method, and real-time priority control method (Hunter-Zaworski et al., 1995; Currie and Shalaby, 2008; Christofa and Skabardonis, 2011; Li et al., 2011; Ma et al., 2014; Ding et al., 2015; Wadjas and Furth, 2003; Lin et al., 2019; Yang et al., 2019a; Bayrak and Guler, 2020). The other major approach is designing exclusive bus lanes, which are usually built with bus rapid transit system (Deng and Nelson, 2011; Levinson et al., 2002; Eichler and Daganzo, 2006). For bus lanes, there are some other designing strategies, such as queue jumper lanes(Zhou and Gan, 2005; Truong et al., 2016) and intermittent bus lane Eichler and Daganzo (2006); Chiabaut et al. (2012); Chiabaut and Barcet (2019); Currie and Lai (2008). Both can effectively increase the operational speed of buses and increase the level of service of the public transit system.

However, previous max-pressure signal control policies assume that public transit uses the same signal timing as private vehicles. If the operation of public transit is ignored, there may be problems at certain intersections that are neglected when implementing max-pressure controller policies. For instance, the max-pressure controller is more likely to actuate phases for high-demand approaches, which may delay buses waiting in lower-demand approaches.

In order to improve the scope of the application of the max-pressure control policy, we

combine the max-pressure control with TSP for the first time. The contributions of this chapter are as follows: (1) We modify Varaiya's max-pressure control policy to give priority signals to bus rapid transit (Varaiya, 2013). Specifically, in this dissertation, we only consider situations where bus rapid transit has exclusive bus lanes. (2) We design dynamic queueing models for bus rapid transit systems and private vehicles. (3) We formulate the conflict region model, which is inspired by autonomous intersection control, for the proposed max-pressure policy to eliminate the conflicts between buses and private vehicles (Levin et al., 2019) (4) We analytically prove the max-pressure control policy considering bus rapid transit can also achieve optimal throughput at the network level. (5) We implement our simulation using the road network, bus rapid transit (BRT) system, and bus timetables from downtown Austin, Texas, USA.

2.2 Literature review

In this part, we first review related papers focusing on transit signal priority. Then we review the existing literature on max-pressure control.

2.2.1 Transit signal priority

Transit signal priority has been implemented in many cities around the world to improve bus operational performance (Hunter-Zaworski et al., 1995; Ma et al., 2014; Ding et al., 2015; Anderson and Daganzo, 2020). Many bus routes are located in a primary corridor of cites (Deng and Nelson, 2011). High-performance public transit systems can attract more travelers to transit from using private vehicles, which would reduce traffic emissions and congestion significantly. One way to enhance public transit priority is building exclusive bus lanes or intermittent bus lanes (Eichler and Daganzo, 2006; Chiabaut et al., 2012; Chiabaut and Barcet, 2019; Currie and Lai, 2008), which are part of bus rapid transit (BRT) Systems (Levinson et al., 2002; Eichler and Daganzo, 2006). Another way is designing

TSP strategies for public transit systems. Passive priority methods (pre-determined signal setting)(Lin et al., 2019), active priority methods (real-time detection of buses on the intersection arms)(Currie and Shalaby, 2008; Christofa and Skabardonis, 2011; Lin et al., 2015), and adaptive/real-time priority control method are three types of the most widely used TSP strategies(Li et al., 2011). For passive priority signal, all the phases and timing are predesigned to accommodate intersection traffic demand and buses operation. The green time extension is a typical method belonging to active transit signal priority, which required bus arrival information, such as arrival time, speed to insert phases for buses. Specifically, adaptive/real-time priority controllers are not only based on the information from detectors but also try to optimize signal timings for some performance metrics, like private vehicle delay, person delay, bus delay, etc.

Previous studies have tried to achieve more benefits from the implementation of TSP strategies. Some papers used simulation tools to test the performance of TSP (Chang et al., 2003; Wadjas and Furth, 2003; Dion et al., 2004; Stevanovic et al., 2008). Due to the complexity, these simulations only considered one intersection or arterial, rather than the whole road network. For instance, Stevanovic et al. (2008) used VISSIM and Direct COR-SIM to optimize basic signal timing parameters for transit signal priority setting. Their results showed the transit signal priority setting based on a genetic algorithm can reduce travel delay on the corridors in Albany, NY, with mixed traffic and transit operations. With the development of intelligent transportation systems, several studies aimed to leverage advanced transportation technology to make the best use of TSP. Wu et al. (2020) analyzed the transit signal priority considering buses as moving bottlenecks along an arterial with mixed traffic scenarios. They used the lax-hopf equation (Claudel and Bayen, 2010b,c) to evaluate vehicle operations at the arterial level, the results showed that implementing TSP can be better than implementing exclusive bus lanes in some scenarios. Yang et al. (2019a) used more precise and detailed information from connected vehicles for TSP implementation to minimize the delay of buses and cars. Bayrak and Guler (2020) tried to determine the

optimal transit signal priority implementation locations in an urban transportation network. They tested different scenarios aiming to minimize the total travel time of network users. Some studies used simulation-based methods to explore the TSP. Meanwhile, optimization-based methods are also popular in improving TSP strategies. Ma et al. (2014) proposed a person-capacity-based optimization method for the transit priority operation at isolated intersections. Their optimization problem was formulated as a mixed integer linear program (MILP). Christofa et al. (2013) presented a person-based traffic responsive signal control system for TSP, which was formulated as a Mixed Integer Nonlinear Program (MINLP) aiming to minimize the total person delay while providing priority to public transit vehicles. Some data-driven based methods are also used in designing TSP strategies. Ding et al. (2015) established a multi-objective TSP method that used the ARIMA–SVM hybrid model to predict bus dwell time at bus stations. The prediction model used data extracted from the BRT Line 2 from Changzhou City, China. With real-time average passenger delay, the maximum queue length, and the exhaust emissions as its optimization objectives, their proposed TSP method performed well in VISSIM simulation experiments.

Overall, existing studies of TSP have demonstrated that TSP strategies are an efficient way to improve the performance of public transit systems. These studies leveraged simulation-based and model-based methods to find the optimal locations, modified strategies to achieve better implementations with traditional vehicles. However, none of them consider the stable impacts for private vehicles. Furthermore, most of them focused only on one intersection, one bus line, or in some grid-based networks. Specifically, when TSP sacrifices the general benefits for private vehicles, the queue length of private vehicles may grow arbitrarily large around the urban network, which we call unstable scenarios.

2.2.2 Max-pressure control

Chen et al. (2020) developed the AIM-ped algorithm, which can achieve optimal through-

[H]

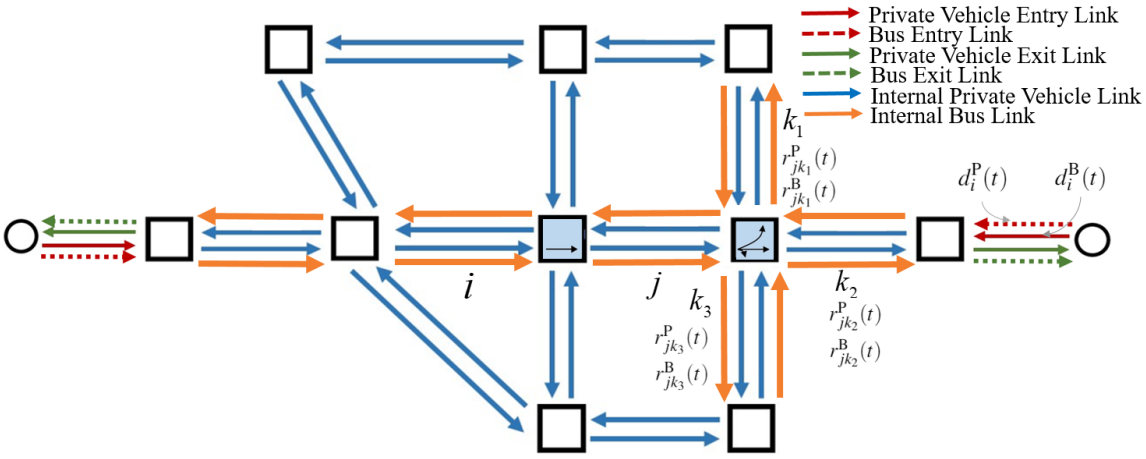

Figure 2.1: Network example

put combined with max pressure control. Their paper proved that the max-pressure controller could achieve a more realistic implementation. To reduce the negative influence brought by the original max-pressure control police, Levin et al. (2020) introduced a cyclical phase structure max-pressure controller to make the max-pressure policy more friendly for drivers' preference. The most similar previous study to this one is the paper that considered pedestrians (Chen et al., 2020). However, their simulations were only implemented on the grid-based network. Inspired by the aforementioned research, we extend the max-pressure policy to consider the transit signal priority of bus rapid transit systems in the real-world network for the first time.

2.3 Network Model

2.3.1 Road Network Model

Consider a road network $\mathcal{G} = (\mathcal{N}, \mathcal{A})$ with nodes $\mathcal{N}$ and links $\mathcal{A}$. Nodes represent intersection locations. The link set $\mathcal{A}$ is divided into three subsets, which is the entry link set $\mathcal{A}_e$,

internal link set $\mathcal{A}_i$, and the exit link set $\mathcal{A}_o$. Entry links are the source links where buses and private vehicles can enter the network. Exit links are the sink links where buses and private vehicles leave the network. Internal links connect the intersections located inside the network. Note that the bus links in this dissertation only represent exclusive bus lanes (private vehicles are not allowed to use them), which are part of bus rapid transit systems in reality. We use Γ_i^+ and Γ_j^- to represent the sets of outgoing links and incoming links of intersections respectively. One turning movement is a combination of two links. For instance, (i, j) and (j, k) are two movements respectively. We define $\mathcal{M}$ to be the set of all turning movements in the network. Let $x_{ij}^{\mathrm{P}}(t)$ be the number of private vehicles on link i waiting to move to link j, and let $x_{ij}^{\mathrm{B}}(t)$ be the number of buses waiting on link i waiting to move to link j. Let $d_i(t)$ be the demand entering the network on link $i \in \mathcal{A}_e$, which is composed by the bus demand $d_i^{\mathrm{B}}(t)$ and private vehicles' demand $d_i^{\mathrm{P}}(t)$. Turning proportion $r_{jk}^{\mathrm{B}}(t)$ is the proportion of buses entering j that will next move to k. We assume that $r_{jk}^{\mathrm{B}}(t)$ is fixed (we could get this information from the bus company or do field surveys), which represents turning movements of buses. Turning proportion $r_{jk}^{\mathrm{P}}(t)$ determines the proportion of private vehicles entering j that will next move to k, which are independent identically distributed random variables with mean $\bar{r}_{ij}^{\mathrm{P}}$. We separate the link queues by turning movements since different turning movements at intersections could not be activated at the same time in some scenarios. The capacity of bus link i is denoted by Q_i^{B}. Therefore $Q_{ij}^{\mathrm{B}} = \min(Q_i^{\mathrm{B}}, Q_j^{\mathrm{B}})$, is the maximum number of buses that can move from i to j in one time step. The capacity of private vehicle link i is denoted by Q_i^{P}. Therefore, $Q_{ij}^{\mathrm{P}} = \min(Q_i^{\mathrm{P}}, Q_j^{\mathrm{P}})$, is the maximum flow of vehicle movement (i, j). Note that, both the buses' and private vehicles' capacities represent the physical properties of the road, which means they are determined value. We assume that Q_{ij}^{B} and Q_{ij}^{P} are constants. These variables are shown in Figure 3.1.

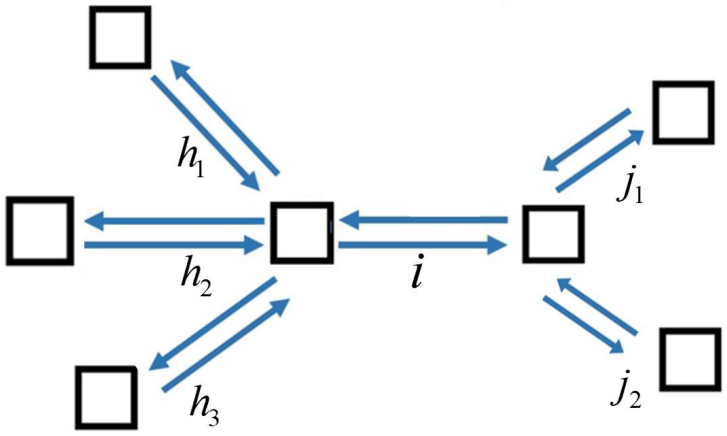

Figure 2.2: Queue evolution instruction

2.3.2 Bus queueing model

To represent the propagation of bus queueing in the network, we use the store-and-forward model of Varaiya (2013). We assume buses have entry and exit links. For the internal links, we have the following equations to represent flow conservation:

$$x_{ij}^{\mathrm{B}}(t+1) = x_{ij}^{\mathrm{B}}(t) - y_{ij}^{\mathrm{B}}(t) + \sum_{(i,j,h)\in\mathcal{A}^3} y_{hi}^{\mathrm{B}}(t) \times r_{ij}^{\mathrm{B}}(t) \tag{2.1}$$

where $y_{ij}^{\mathrm{B}}(t)$ is the number of buses from i to j at time t, which is controlled by traffic signal. $r_{ij}^{\mathrm{B}}(t)$ is the proportion of buses entering i that will next move to j. Figure 2.2 shows how the queue evolves from upstream to downstream. Flow conservation also applies to entry links, which are connected with bus terminal stations.

$$x_{ij}^{\mathrm{B}}(t+1) = x_{ij}^{\mathrm{B}}(t) - y_{ij}^{\mathrm{B}}(t) + d_{i}^{\mathrm{B}}(t) \times r_{ij}^{\mathrm{B}}(t) \tag{2.2}$$

We assume that entry link $i \in \mathcal{A}_e$, $d_i^{\mathrm{B}}(t)$ is based on the bus timetables. In reality, the

number of buses from terminal stations is varies over time throughout the day. We denote the mean value of bus entering flow as $\bar{d}_i^{\mathrm{B}}$ and further assume $d_i^{\mathrm{B}}(t)$ has maximum value $\tilde{d}_i^{\mathrm{B}}$. Intersection-controlled bus movement flow is $y_{ij}^{\mathrm{B}}(t)$. At each time step, a traffic signal phase is selected. The activation of bus turning movement (i, j) is denoted by $s_{ij}(t) \in \{0, 1\}$. $s_{ij}(t) = 1$ means movement (i, j) gets a green light, and $s_{ij}(t) = 0$ means that movement (i, j) gets a red light. The value of $y_{ij}^{\mathrm{B}}(t)$ is determined by the following equation

$$y_{ij}^{\mathrm{B}}(t) = \min\left\{Q_{ij}^{\mathrm{B}} s_{ij}(t), x_{ij}^{\mathrm{B}}(t)\right\} \tag{2.3}$$

2.3.3 Private vehicle queueing model

To represent the propagation of private vehicles queueing in the network, we use the store-and-forward model from Varaiya (2013). We assume private vehicles also have entry and exit links. For the internal links, we have the following equations:

$$x_{ij}^{\mathrm{P}}(t+1) = x_{ij}^{\mathrm{P}}(t) - y_{ij}^{\mathrm{P}}(t) + \sum_{(i,j,h)\in\mathcal{A}^3} y_{hi}^{\mathrm{P}}(t) \times r_{ij}^{\mathrm{P}}(t) \tag{2.4}$$

where $y_{ij}^{\mathrm{P}}(t)$ is the flow of private vehicles from i to j at time t, which is controlled by traffic signal. $r_{ij}^{\mathrm{P}}(t)$ is the proportion of private vehicles entering i that will next move to j. Figure 2 shows how the queue of private vehicles evolves from upstream to downstream. Flow conservation also applies to entry links, but entering flow is determined by the demand $d_i^{\mathrm{P}}(t)$.

$$x_{ij}^{\mathrm{P}}(t+1) = x_{ij}^{\mathrm{P}}(t) - y_{ij}^{\mathrm{P}}(t) + d_i^{\mathrm{P}}(t) \times r_{ij}^{\mathrm{P}}(t) \tag{2.5}$$

We assume that for entry link $i \in \mathcal{A}_e$, $d_i^{\mathrm{P}}(t)$ all t are independent identically distributed random variables with mean $\bar{d}_i^{\mathrm{P}}$. We further assume $d_i^{\mathrm{P}}(t)$ has maximum value $\tilde{d}_i^{\mathrm{P}}$.

Intersection controlled flow of private vehicles is $y_{ij}^{\mathrm{P}}(t)$. At each time step, a traffic signal phase is selected. The activation of private vehicle turning movement (i, j) is denoted by $s_{ij}(t) \in \{0, 1\}$. $s_{ij}(t) = 1$ means movement (i, j) gets a green light, and $s_{ij}(t) = 0$ means that movement (i, j) gets a red light. Noted that buses have priority in the intersections, which means if buses and private vehicles arrive at an intersection at the same time, traffic signal phases will choose 1 for buses and 0 for private vehicles. The value of $y_{ij}^{\mathrm{P}}(t)$ is determined by the following equation

$$y_{ij}^{\mathrm{P}}(t) = \min\left\{Q_{ij}^{\mathrm{P}} s_{ij}(t), x_{ij}^{\mathrm{P}}(t)\right\} \tag{2.6}$$

Furthermore, we can rewrite equations (2.4) and (2.5) as the following two equations, respectively.

$$\begin{aligned} x_{ij}^{\mathrm{P}}(t+1) = x_{ij}^{\mathrm{P}}(t) &- \min\left\{Q_{ij}^{\mathrm{P}} s_{ij}(t), x_{ij}^{\mathrm{P}}(t)\right\} \\ &+ \sum_{h \in \mathcal{A}_i^-} \min\left\{Q_{hi}^{\mathrm{P}} s_{ij}(t), x_{hi}^{\mathrm{P}}(t)\right\} \times r_{ij}^{\mathrm{P}}(t) \quad \forall i \in \mathcal{A}_{\mathrm{i}}, j \in \Gamma_i^+ \end{aligned} \tag{2.7}$$

$$x_{ij}^{\mathrm{P}}(t+1) = x_{ij}^{\mathrm{P}}(t) - \min\left\{Q_{ij}^{\mathrm{P}} s_{ij}(t), x_{ij}^{\mathrm{P}}(t)\right\} + d_i^{\mathrm{P}}(t) \times r_{ij}^{\mathrm{P}}(t) \quad \forall i \in \mathcal{A}_{\mathrm{e}}, j \in \Gamma_i^+ \tag{2.8}$$

2.3.4 Signal control and transit signal priority

The activation of turning movement for buses and private vehicles is denoted by $s_{ij}(t) \in \{0, 1\}$. Let $S_r(t)$ be an intersection matrix for intersection r, and all turning movements

activated in intersection control $S_r(t)$ matrix can not conflict with each other. Activating $S_r(t)$ at all time step, we can define the intersection control sequence $S_r = \{S_r(t), t \in T\}$ that includes signal controls for all intersections r from start to end. Let $\mathcal{S}$ be a set that includes all feasible network control matrices for all intersections, and $\mathcal{S}_r$ denotes a set including all feasible intersection matrices for intersection r. We denote the convex hull of all feasible signal control matrices as $\mathrm{Conv}(\mathcal{S})$.

We give public transit more priority than private vehicles when there are bus lanes with BRT, which means when the buses of BRT are waiting at an intersection constructed with bus lanes, the green light will be actuated to at least one phase of bus queues at the bus lanes. More specifically, the feasible signal control integrated with transit signal priority should obey the following relationships:

First, the number of signal control buses flow $y_{ij}^{\mathrm{B}}(t)$ should larger than zero if buses are waiting. That is

$$y_{ij}^{\mathrm{B}}(t) = \min\left\{Q_{ij}^{\mathrm{B}} s_{ij}(t), x_{ij}^{\mathrm{B}}(t)\right\} > 0 \qquad \text{if} \sum_{(i,j)\in\mathcal{A}^2} x_{ij}^{\mathrm{B}}(t) > 0 \tag{2.9}$$

In order to activate the phases where the buses will travel through, we have the following equation

$$\sum_{(i,j)\in\mathcal{A}^2} s_{ij}(t) \times x_{ij}^{\mathrm{B}}(t) > 0 \qquad \text{if} \sum_{(i,j)\in\mathcal{A}^2} x_{ij}^{\mathrm{B}}(t) > 0 \tag{2.10}$$

After that, we rewrite equation (2.10) as follows

$$\sum_{(i,j)\in\mathcal{A}^2} s_{ij}(t) \times x_{ij}^{\mathrm{B}}(t) - 1 \geq 0 \qquad \text{if} \sum_{(i,j)\in\mathcal{A}^2} x_{ij}^{\mathrm{B}}(t) > 0 \tag{2.11}$$

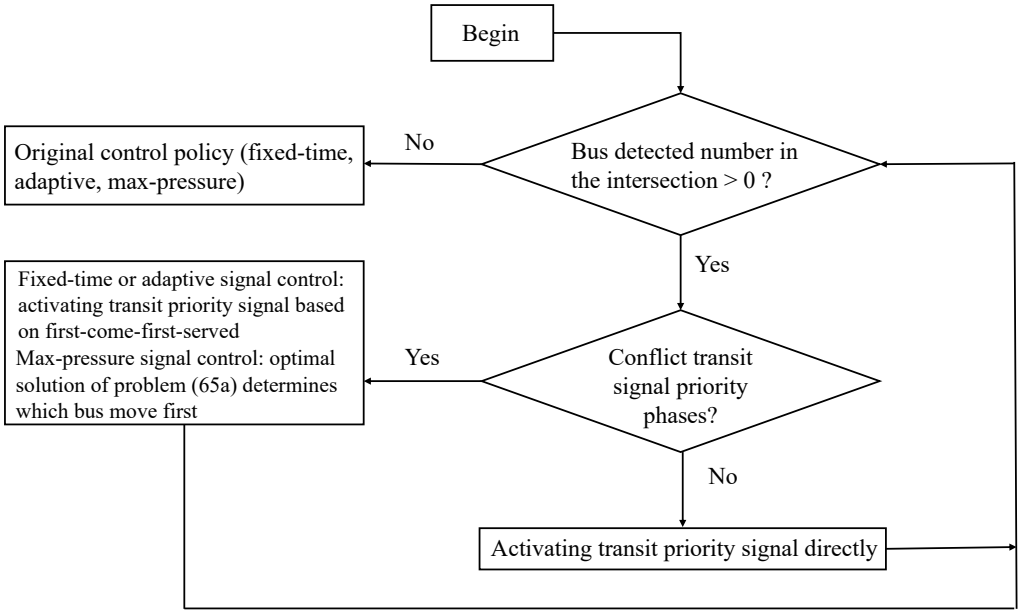

Figure 2.3: Transit signal priority

Figure 2.3 shows how the transit signal priority provide for a given fixed-time signal control, adaptive signal control, and max-pressure signal control.

Therefore, we can obtain some feasible signal controls $s_{ij}(t)$ that satisfy transit signal priority constraints, that is $s_{ij}(t) \in \mathcal{S}_p$. We define $\mathcal{S}_p$ be a set that includes all feasible network controls integrated with transit signal priority. $\mathcal{S}_p$ is a subset of $\mathcal{S}$, that is $\mathcal{S}_p \subseteq \mathcal{S}$. Furthermore, we define the convex hull of all feasible signal control integrated transit signal priority matrices as $\mathrm{Conv}(\mathcal{S}_p)$. For any given intersection control sequence, the long-term average time used for serving turning movement (i, j), which also considers transit signal priority can be calculated by equation (5.4). Let $\bar{\mathbf{s}}$ and $\mathbf{s}(t)$ be the vectors of $\bar{s}_{ij}$ and $s_{ij}(t)$ respectively.

$$\bar{s}_{ij} = \lim_{T\to\infty} \frac{1}{T} \sum_{t=1}^{T} s_{ij}(t) \tag{2.12}$$

The convex hull of $\mathcal{S}_p$, the set of feasible network controls integrated with transit signal priority, is

$$\mathrm{Conv}(\mathcal{S}_p) = \left\{ \sum_{s \in \mathcal{S}} \lambda_s S \middle| \lambda_s S \leq 0, \sum \lambda_s = 1 \right\} \tag{2.13}$$

Proposition 1. *If* $\mathbf{s}(t) \in \mathcal{S}_p$ *then there exists a* $\bar{\mathbf{s}} \in \mathrm{Conv}(\mathcal{S}_p)$ *such that*

$$\bar{\mathbf{s}} = \lim_{T \to \infty} \frac{1}{T} \sum_{t=1}^{T} \mathbf{s}(t) \tag{2.14}$$

Proof. First, we prove that $\bar{\mathbf{s}}$ is in the convex hull of $\mathcal{S}_p$. For any T, Let $T \times \lambda_{\mathbf{s}}$ be the number of times so that $\mathbf{s}(t) = \mathbf{s}$. Since $\mathbf{s}(t) \in \mathcal{S}_p$, $\sum_{\mathbf{s} \in \mathcal{S}_p} T\lambda_{\mathbf{s}} = T$, so $\lambda_{\mathbf{s}}$ is the proportions of time spent in each phase. Therefore

$$\bar{\mathbf{s}} = \lim_{T \to \infty} \frac{1}{T} \sum_{t=1}^{T} \mathbf{s}(t) \tag{2.15}$$

$$= \lim_{T \to \infty} \frac{1}{T} \sum_{t=1}^{T} \sum_{\mathbf{s} \in \mathcal{S}_p} \mathbb{I}(\mathbf{s}(t) = \mathbf{s})\mathbf{s} \tag{2.16}$$

$$= \lim_{T \to \infty} \frac{1}{T} \sum_{t=1}^{T} \sum_{\mathbf{s} \in \mathcal{S}_p} T\lambda_{\mathbf{s}}\mathbf{s} \tag{2.17}$$

$$= \sum_{\mathbf{s} \in \mathcal{S}_p} \lambda_{\mathbf{s}}\mathbf{s} \tag{2.18}$$

Since $\bar{\mathbf{s}}$ is the convex hull of of $\mathcal{S}_p$, there exists $\lambda_{\mathbf{s}}$ satisfying $\sum_{\mathbf{s} \in \mathcal{S}_p} \lambda_{\mathbf{s}} = 1$ such that

$$\bar{\mathbf{s}} = \sum_{\mathbf{s}\in\mathcal{S}_p} \lambda_{\mathbf{s}}\mathbf{s} \tag{2.19}$$

Define the indicator function as

$$\mathbb{I}(\mathbf{s}(t) = \mathbf{s}) \begin{cases} 1 & \text{if } \mathbf{s}(t) = \mathbf{s} \\ 0 & \text{if } \mathbf{s}(t) \neq \mathbf{s} \end{cases} \tag{2.20}$$

For any $\lambda_{\mathbf{s}} \in \{0, 1\}$ there exists a sequence $\lambda_{\mathbf{s}}(t)$ such that

$$\lim_{T\to\infty} \frac{1}{T} \sum_{t=1}^{T} \mathbb{I}(\mathbf{s}(t) = \mathbf{s}) = \lambda_{\mathbf{s}} \tag{2.21}$$

Since $\sum_{\mathbf{s}\in\mathcal{S}_p} \lambda_{\mathbf{s}} = 1$,

$$\lim_{T\to\infty} \frac{1}{T} \sum_{t=1}^{T} \mathbb{I}(\mathbf{s}(t) = \mathbf{s}) = 1 \tag{2.22}$$

Finally, we obtain the following equation

$$\bar{\mathbf{s}} = \lim_{T\to\infty} \frac{1}{T} \sum_{t=1}^{T} \sum_{\mathbf{s}\in\mathcal{S}_p} \mathbb{I}(\mathbf{s}(t) = \mathbf{s})\mathbf{s} = \lim_{T\to\infty} \frac{1}{T} \sum_{t=1}^{T} \mathbf{s}(t) \tag{2.23}$$

2.3.5 Stable network

Stability refers to the ability to serve all demand in the transportation network. The bus transit rapid system is always stable since the number of buses belonging to the bus transit rapid system is limited and much smaller than the number of private vehicles. We define the *stability* of the network mathematically as follows:

Definition 1. *The network is stable if the number of private vehicles remains bounded in expectation, i.e. there exists a* $\kappa < \infty$ *such that*

$$\lim_{T\to\infty} \sup \left\{ \frac{1}{T} \sum_{t=1}^{T} \sum_{(i,j)\in\mathcal{A}^2} \mathbb{E}\{x_{ij}^{\mathrm{P}}(t)\} \right\} \leq \kappa \tag{2.24}$$

It is easy to choose a demand rate vector $\bar{\mathbf{d}}^{\mathrm{P}}$ such that no traffic signal timing policy can stabilize it. For instance, we can choose a very large demand rate that exceeds the turning movement capacity. The objective of our modified max-pressure control is to stabilize any private vehicles' demand rate that could be stabilized by some signal control also considering transit signal priority of bus rapid transit. To prove the maximum-stability property, we must first define analytically the sets of demands that could be stabilized. The definition is similar to that of Varaiya (2013); Levin et al. (2020), but we should consider transit signal priority in this study.

2.3.6 Stable region

For private vehicles, since the demand of private vehicles is stochastic, the stable region is defined in terms of the average demand rates $\bar{\mathbf{d}}^{\mathrm{P}}$. Demand for entry links can be propagation to demand for entry links. Let $\mathbf{f}^{\mathrm{P}}$ be the average private vehicle traffic volume for link i. For entry links, we have

$$f_i^{\mathrm{P}} = \bar{d}_i^{\mathrm{P}} \tag{2.25}$$

For internal links of private vehicles, f_i^{P} can be determined by conservation of flow:

$$f_j^{\mathrm{P}} = \sum_{i \in \mathcal{A}} f_i^{\mathrm{P}} \bar{r}_{ij}^{\mathrm{P}} \tag{2.26}$$

By Proposition 1 of Varaiya (2013), for every demand rate $\bar{\mathbf{d}}^{\mathrm{P}}$ and turning proportions $\bar{\mathbf{r}}^{\mathrm{P}}$, there exists an unique average flow vector $\mathbf{f}^{\mathrm{P}}$. The network can be stabilized if the average private vehicle traffic flow can still be served by some traffic signals integrated with transit signal priority. That is, there must exist an average signal activation $\bar{\mathbf{s}} \in \mathrm{Conv}(\mathcal{S}_p)$. Note that, the stable region is different from Varaiya's definition Varaiya (2013), because the $\bar{\mathbf{s}} \in \mathrm{Conv}(\mathcal{S}_p)$, which includes transit signal priority.

$$f_i^{\mathrm{P}} \bar{r}_{ij}^{\mathrm{P}} \leq \bar{s}_{ij} Q_{ij}^{\mathrm{P}} \tag{2.27}$$

where $\bar{s}_{ij}$ can be obtained from equation (5.4), based on some feasible signal control consider bus priority $s_{ij}(t) \in \mathcal{S}_p$.

Let $\mathcal{D}$ be the set of demands which satisfy constraints (2.25)–(2.27). Let $\mathcal{D}^0$ be the interior of $\mathcal{D}$, where constraint (2.27) holds with strict inequality. Then there exists an $\epsilon > 0$ such that

$$f_i^{\mathrm{P}} \bar{r}_{ij}^{\mathrm{P}} - \bar{s}_{ij} Q_{ij}^{\mathrm{P}} \leq -\epsilon \tag{2.28}$$

Proposition 2. *If* $\bar{\mathbf{d}}^{\mathrm{P}} \notin \mathcal{D}$*, then there does not exist a signal control policy can stabilize the network.*

Proof. Since $\bar{\mathbf{d}}^{\mathrm{P}} \notin \mathcal{D}$, $\forall \bar{s}_{ij} \in \mathcal{S}_p$, there exists a $\theta > 0$ and at least one turning movement (i, j) satisfying $f_j^{\mathrm{P}} \bar{r}_{ij}^{\mathrm{P}} \geq \bar{s}_{ij} Q_{ij}^{\mathrm{P}} + \theta$.

Based on equation (2.4) we have

$$x_{ij}^{\mathrm{P}}(t+1) - x_{ij}^{\mathrm{P}}(t) = \sum_{(i,j,h)\in\mathcal{A}^3} y_{hi}^{\mathrm{P}}(t) r_{ij}^{\mathrm{P}}(t) - y_{ij}^{\mathrm{P}}(t) \tag{2.29}$$

Based on equation (2.29) we can obtain the following relationship:

$$\mathbb{E}\left[\sum_{t=0}^{\tau-1} \sum_{(i,j)\in\mathcal{A}^2} \left(x_{ij}^{\mathrm{P}}(t+1) - x_{ij}^{\mathrm{P}}(t)\right)\right] = \mathbb{E}\left[\sum_{(i,j)\in\mathcal{A}^2} \left(x_{ij}^{\mathrm{P}}(\tau) - x_{ij}^{\mathrm{P}}(0)\right)\right] \tag{2.30}$$

$$= \mathbb{E}\left[\sum_{t=0}^{\tau-1} \sum_{(h,i,j)\in\mathcal{A}^3} \left(y_{hi}^{\mathrm{P}}(t) r_{ij}^{\mathrm{P}}(t) - y_{ij}^{\mathrm{P}}(t)\right)\right] \tag{2.31}$$

$$= \mathbb{E}\left[\sum_{(i,j)\in\mathcal{A}^2} \left(f_j^{\mathrm{P}} \bar{r}_{ij}^{\mathrm{P}} - \bar{s}_{ij} Q_{ij}^{\mathrm{P}}\right)\right] \tag{2.32}$$

$$\geq \mathbb{E}\left[\tau\theta)\right] = \tau\theta \tag{2.33}$$

Moving $x_{ij}^{\mathrm{P}}(0)$ to the right hand side, we obtain:

$$\mathbb{E}\left[\sum_{(i,j)\in\mathcal{A}^2} x_{ij}^{\mathrm{P}}(\tau)\right] \geq \theta\tau + \mathbb{E}\left[\sum_{(i,j)\in\mathcal{A}^2} x_{ij}^{\mathrm{P}}(0)\right] \tag{2.34}$$

or equivalently

$$\mathbb{E}\left[|\mathbf{x}^{\mathrm{P}}(\tau)|\right] \geq \theta\tau + \mathbb{E}\left[|\mathbf{x}^{\mathrm{P}}(0)|\right] \tag{2.35}$$

From equation (2.35), we obtain

$$\begin{aligned}\lim_{T\to\infty} \mathbb{E}\left[\frac{1}{T}\sum_{t=1}^{T}|\mathbf{x}^{\mathrm{P}}(t)|\right] &\geq \lim_{T\to\infty} \mathbb{E}\left[\frac{1}{T}\sum_{t=1}^{T}\left[\theta t + \mathbb{E}\left[|\mathbf{x}^{\mathrm{P}}(0)|\right]\right]\right] \\ &= \lim_{T\to\infty} \mathbb{E}\left[\frac{1}{T}\sum_{t=1}^{T}(\theta t)\right] + \lim_{T\to\infty} \mathbb{E}\left[\frac{1}{T}\sum_{t=1}^{T}[|\mathbf{x}^{\mathrm{P}}(0)|]\right] = \infty\end{aligned} \tag{2.36}$$

which violates equation (2.24).

Note that if the network is unstable, the private vehicle's turning movement flow is greater than the traffic signal integrated with transit priority that can serve.

2.3.7 Stability analysis based on average signal control

We now proceed to prove that the average signal control with bus priority will stabilize any private vehicle demand $\bar{\mathbf{d}}^{\mathrm{P}} \in \mathcal{D}^0$. Since any demand $\bar{\mathbf{d}}^{\mathrm{P}} \notin \mathcal{D}$ cannot be stabilized by Proposition 2, this essentially proves that we can find an average signal control to achieve stability. The only excluded demand is on the boundary of $\mathcal{D}$, for which the Markov chain can be shown to be null recurrent but not positive recurrent. Note that we only care about the stability of private vehicles because we always give signal priority to BRT.

Lemma 1. *When $\bar{\mathbf{d}}^{\mathrm{P}} \in \mathcal{D}^0$, the average signal control resulting from equation (5.4) and satisfying constraints (2.25)–(2.27) are used, there exists a Lyapunov function $\nu(t) \geq 0$ and constants $\kappa < \infty$, $\epsilon > 0$ such that*

$$\mathbb{E}\left[\nu(t+1)-\nu(t)|\,\mathbf{x}^{\mathrm{P}}(t)\right] \leq \kappa - \epsilon|\mathbf{x}^{\mathrm{P}}(t)| \tag{2.37}$$

Proof. To calculate the queue length at time $t+1$, we apply the private vehicle queueing models shown in equation (2.7)–(2.8). Then, let $\delta_{ij}(t)$ be the difference of the queue length of private vehicles between time steps t and time steps $t+1$.

$$\begin{aligned}\delta_{ij}(t) &= x_{ij}^{\mathrm{P}}(t+1) - x_{ij}^{\mathrm{P}}(t) \\ &= -\min\left\{Q_{ij}^{\mathrm{P}} s_{ij}(t), x_{ij}^{\mathrm{P}}(t)\right\} \\ &\quad + \sum_{h\in\mathcal{A}_i^-} \min\left\{Q_{hi}^{\mathrm{P}} s_{ij}(t), x_{hi}^{\mathrm{P}}(t)\right\} \quad \times r_{ij}^{\mathrm{P}}(t) \quad \forall i \in \mathcal{A}_{\mathrm{i}}, j \in \Gamma_i^+\end{aligned} \tag{2.38}$$

$$\delta_{ij}(t) = x_{ij}^{\mathrm{P}}(t+1) - x_{ij}^{\mathrm{P}}(t) = -\min\left\{Q_{ij}^{\mathrm{P}} s_{ij}(t), x_{ij}^{\mathrm{P}}(t)\right\} + d_i^{\mathrm{P}}(t) \times r_{ij}^{\mathrm{P}}(t) \quad \forall i \in \mathcal{A}_{\mathrm{e}}, j \in \Gamma_i^+ \tag{2.39}$$

Let $\mathbf{x}^{\mathrm{P}}(t)$ be the matrix including all queue length of private vehicles. We define the Lyapunov function $\nu(t)$ as follows:

$$\nu(t) = \left|\mathbf{x}^{\mathrm{P}}(t)\right|^2 = \sum_{(i,j)\in\mathcal{A}^2} \left(x_{ij}^{\mathrm{P}}(t)\right)^2 \tag{2.40}$$

Then we expand the difference $\nu_1(t+1) - \nu_1(t)$:

$$\nu(t+1) - \nu(t) = \left|\mathbf{x}^{\mathrm{P}}(t+1)\right|^2 - \left|\mathbf{x}^{\mathrm{P}}(t)\right|^2 = \left|\mathbf{x}^{\mathrm{P}}(t) + \boldsymbol{\delta}(t)\right|^2 - \left|\mathbf{x}^{\mathrm{P}}(t)\right|^2 = 2\mathbf{x}^{\mathrm{P}}(t)^{\mathrm{T}}\boldsymbol{\delta}(t) + \left|\boldsymbol{\delta}(t)\right|^2$$

(2.41)

$$
\begin{aligned}
2\mathbf{x}^{\mathrm{P}}(t)^{\mathrm{T}}\boldsymbol{\delta}(t) = & -2x_{ij}^{\mathrm{P}}(t)\sum_{i\in\mathcal{A}}\sum_{j\in\Gamma_i^+}\min\left\{Q_{ij}^{\mathrm{P}}s_{ij}(t), x_{ij}^{\mathrm{P}}(t)\right\} \\
& + 2\sum_{h\in\Gamma_i^-}\sum_{i\in\mathcal{A}}\sum_{j\in\Gamma_i^+} x_{ij}^{\mathrm{P}}(t)\min\left\{Q_{hi}^{\mathrm{P}}s_{hi}(t), x_{hi}^{\mathrm{P}}(t)\right\} r_{ij}^{\mathrm{P}}(t) \\
& + 2\sum_{i\in\mathcal{A}_{\mathrm{e}}}\sum_{j\in\Gamma_i^+}\left(-\min\left\{Q_{ij}^{\mathrm{P}}s_{ij}(t), x_{ij}^{\mathrm{P}}(t)\right\} + d_i^{\mathrm{P}}(t)\times r_{ij}^{\mathrm{P}}(t)\right) \qquad (2.42) \\
= & 2\sum_{i\in\mathcal{A}_{\mathrm{i}}\cup\mathcal{A}_{\mathrm{e}}}\sum_{j\in\Gamma_i^+}\min\left\{Q_{ij}^{\mathrm{P}}s_{ij}(t), x_{ij}^{\mathrm{P}}(t)\right\}\left(-x_{ij}^{\mathrm{P}}(t) + \sum_{k\in\Gamma_i^+} r_{jk}^{\mathrm{P}}(t)x_{jk}^{\mathrm{P}}(t)\right) \\
& + 2\sum_{i\in\mathcal{A}_{\mathrm{e}}}\sum_{j\in\Gamma_i^+} d_i^{\mathrm{P}}(t)\times r_{ij}^{\mathrm{P}}(t)\times x_{ij}^{\mathrm{P}}(t) \qquad (2.43)
\end{aligned}
$$

Replacing the turning proportion $r_{ij}^{\mathrm{P}}(t)$ with average value $\bar{r}_{ij}^{\mathrm{P}}$, since $\lim_{T\to\infty}\frac{1}{T}\sum_{t=1}^{T}\sum_{(i,j)\in\mathcal{A}^2} r_{ij}^{\mathrm{P}}(t)$ $= \sum_{(i,j)\in\mathcal{A}}\bar{r}_{ij}^{\mathrm{P}}$ since $r_{ij}^{\mathrm{P}}(t)$ is a random variable. Therefore we have the following equation:

$$
\begin{aligned}
& \mathbb{E}\left[\mathbf{x}^{\mathrm{P}}(t)^{\mathrm{T}}\boldsymbol{\delta}(t)|\mathbf{x}^{\mathrm{P}}(t)\right] \\
& = \sum_{i\in\mathcal{A}_{\mathrm{i}}\cup\mathcal{A}_{\mathrm{e}}}\sum_{j\in\Gamma_i^+}\mathbb{E}\left[\min\left\{Q_{ij}^{\mathrm{P}}s_{ij}(t), x_{ij}^{\mathrm{P}}(t)\right\}\times(-x_{ij}^{\mathrm{P}}(t))\middle|\mathbf{x}^{\mathrm{P}}(t)\right] \\
& \quad + \sum_{i\in\mathcal{A}_{\mathrm{i}}\cup\mathcal{A}_{\mathrm{e}}}\sum_{j\in\Gamma_i^+}\mathbb{E}\left[\min\left\{Q_{ij}^{\mathrm{P}}s_{ij}(t), x_{ij}^{\mathrm{P}}(t)\right\}\middle|\mathbf{x}^{\mathrm{P}}(t)\right]\times\left(\sum_{k\in\Gamma_i^+}\bar{r}_{jk}^{\mathrm{P}}x_{jk}^{\mathrm{P}}(t)\right) \\
& \quad + \sum_{i\in\mathcal{A}_{\mathrm{e}}}\sum_{j\in\Gamma_i^+}\mathbb{E}\left[d_i^{\mathrm{P}}(t)\bar{r}_{ij}^{\mathrm{P}}x_{ij}^{\mathrm{P}}(t)\middle|\mathbf{x}^{\mathrm{P}}(t)\right] \qquad (2.44)
\end{aligned}
$$

Then we obtain

$$\begin{aligned}
&\mathbb{E}\left[\mathbf{x}^{\mathrm{P}}(t)^{\mathrm{T}}\boldsymbol{\delta}(t)|\mathbf{x}^{\mathrm{P}}(t)\right] \\
&= \sum_{i\in\mathcal{A}_{\mathrm{i}}\cup\mathcal{A}_{\mathrm{e}}} \mathbb{E}\left[\min\left\{Q_{ij}^{\mathrm{P}}s_{ij}(t), x_{ij}^{\mathrm{P}}(t)\right\}\middle|\mathbf{x}^{\mathrm{P}}(t)\right] \times \left(-x_{ij}^{\mathrm{P}}(t) + \sum_{k\in\Gamma_i^+}\bar{r}_{jk}^{\mathrm{P}}x_{jk}^{\mathrm{P}}(t)\right) \\
&\quad + \sum_{i\in\mathcal{A}_{\mathrm{e}}} \bar{d}_i^{\mathrm{P}}\bar{r}_{ij}^{\mathrm{P}}x_{ij}^{\mathrm{P}}(t) \qquad (2.45)
\end{aligned}$$

For the last term of equation (2.45), $\sum_{i\in\mathcal{A}_{\mathrm{e}}} \bar{d}_i^{\mathrm{P}}\bar{r}_{ij}^{\mathrm{P}}x_{ij}^{\mathrm{P}}(t)$, we have

$$\begin{aligned}
\sum_{i\in\mathcal{A}_{\mathrm{e}}} \bar{d}_i^{\mathrm{P}}\bar{r}_{ij}^{\mathrm{P}}x_{ij}^{\mathrm{P}}(t) &= \sum_{i\in\mathcal{A}_{\mathrm{e}}} f_i^{\mathrm{P}}\bar{r}_{ij}^{\mathrm{P}}x_{ij}^{\mathrm{P}}(t) = \sum_{i\in\mathcal{A}_{\mathrm{e}}} f_{ij}^{\mathrm{P}}x_{ij}^{\mathrm{P}}(t) && (2.46)\\
&= \sum_{i\in\mathcal{A}_{\mathrm{i}}\cup\mathcal{A}_{\mathrm{e}}} f_i^{\mathrm{P}}\bar{r}_{ij}^{\mathrm{P}}x_{ij}^{\mathrm{P}}(t) - \sum_{j\in\mathcal{A}_{\mathrm{i}}} f_j^{\mathrm{P}}\bar{r}_{jk}^{\mathrm{P}}x_{jk}^{\mathrm{P}}(t) && (2.47)\\
&= \sum_{i\in\mathcal{A}_{\mathrm{i}}\cup\mathcal{A}_{\mathrm{e}}} f_i^{\mathrm{P}}\bar{r}_{ij}^{\mathrm{P}}x_{ij}^{\mathrm{P}}(t) - \sum_{j\in\Gamma_i^+}\left[\sum_{i\in\mathcal{A}_{\mathrm{i}}\cup\mathcal{A}_{\mathrm{e}}} f_i^{\mathrm{P}}\bar{r}_{ij}^{\mathrm{P}}\right]\sum_{k\in\Gamma_i^+}\bar{r}_{jk}^{\mathrm{P}}x_{jk}^{\mathrm{P}}(t) && (2.48)\\
&= \sum_{i\in\mathcal{A}_{\mathrm{i}}\cup\mathcal{A}_{\mathrm{e}}} f_i^{\mathrm{P}}\bar{r}_{ij}^{\mathrm{P}}\left(x_{ij}^{\mathrm{P}}(t) - \sum_{k\in\Gamma_i^+}\bar{r}_{jk}^{\mathrm{P}}x_{jk}^{\mathrm{P}}(t)\right) && (2.49)
\end{aligned}$$

By Proposition 12 there exists some $\bar{s}_{ij} \in \mathrm{Conv}(\mathcal{S}_p)$ such that $\mathbb{E}[s_{ij}(t)] = \bar{s}_{ij}$. Then

$$\begin{aligned}
&\mathbb{E}\left[\mathbf{x}^{\mathrm{P}}(t)^{\mathrm{T}}\boldsymbol{\delta}(t)|\mathbf{x}^{\mathrm{P}}(t)\right] \\
&= \sum_{i\in\mathcal{A}_{\mathrm{i}}\cup\mathcal{A}_{\mathrm{e}}} \left(f_i^{\mathrm{P}}\bar{r}_{ij}^{\mathrm{P}} - \mathbb{E}\left[\min\left\{Q_{ij}^{\mathrm{P}}s_{ij}(t), \mathbf{x}^{\mathrm{P}}(t)\right\}\middle|\mathbf{x}^{\mathrm{P}}(t)\right]\right)\left(x_{ij}^{\mathrm{P}}(t) - \sum_{k\in\Gamma_j^+}\bar{r}_{jk}^{\mathrm{P}}x_{jk}^{\mathrm{P}}(t)\right) \qquad (2.50)
\end{aligned}$$

$$= \sum_{i\in\mathcal{A}_{\rm i}\cup\mathcal{A}_{\rm e}} \left(f_i^{\rm P}\bar{r}_{ij}^{\rm P} - \bar{s}_{ij}Q_{ij}^{\rm P}\right)\left(x_{ij}^{\rm P}(t) - \sum_{k\in\Gamma_j^+}\bar{r}_{jk}^{\rm P}x_{jk}^{\rm P}(t)\right)$$
$$+ \sum_{i\in\mathcal{A}_{\rm i}\cup\mathcal{A}_{\rm e}}\left(\bar{s}_{ij}Q_{ij}^{\rm P} - \mathbb{E}\left[\min\left\{Q_{ij}^{\rm P}s_{ij}(t), x_{ij}^{\rm P}(t)\right\}\middle|\mathbf{x}^{\rm P}(t)\right]\right)$$
$$\times\left(x_{ij}^{\rm P}(t) - \sum_{k\in\Gamma_j^+}\bar{r}_{jk}^{\rm P}x_{jk}^{\rm P}(t)\right) \tag{2.51}$$

For the second term of equation (2.51), if $x_{ij}^{\rm P}(t) \geq Q_{ij}^{\rm P}$, then we have $\mathbb{E}\left[\min\left\{Q_{ij}^{\rm P}s_{ij}(t), x_{ij}^{\rm P}(t)\right\}\middle|\mathbf{x}^{\rm P}(t)\right] = Q_{ij}^{\rm P}\bar{s}_{ij}$. Therefore, the second term of equation (2.51) equals zero. If $x_{ij}^{\rm P}(t) < Q_{ij}^{\rm P}$, then we have $\mathbb{E}\left[\min\left\{Q_{ij}^{\rm P}s_{ij}(t), x_{ij}^{\rm P}(t)\right\}\middle|\mathbf{x}^{\rm P}(t)\right]$ $= \mathbb{E}\left[x_{ij}^{\rm P}(t)\middle|\mathbf{x}^{\rm P}(t)\right]$, which results in

$$\sum_{i\in\mathcal{A}_{\rm i}\cup\mathcal{A}_{\rm e}}\left(\bar{s}_{ij}Q_{ij}^{\rm P} - \mathbb{E}\left[x_{ij}^{\rm P}(t)\middle|\mathbf{x}^{\rm P}(t)\right]\right)$$
$$\times\left(x_{ij}^{\rm P}(t) - \sum_{k\in\Gamma_j^+}\bar{r}_{jk}^{\rm P}x_{jk}^{\rm P}(t)\right) \leq \sum_{i\in\mathcal{A}_{\rm i}\cup\mathcal{A}_{\rm e}}\bar{s}_{ij}Q_{ij}^{\rm P}x_{ij}^{\rm P}(t)$$
$$\leq \sum_{i\in\mathcal{A}_{\rm i}\cup\mathcal{A}_{\rm e}}\left(Q_{ij}^{\rm P}\right)^2 \tag{2.52}$$

Therefore, the second term of equation (2.51) is equal to zero or bounded by $\sum_{i\in\mathcal{A}_{\rm i}\cup\mathcal{A}_{\rm e}}\left(Q_{ij}^{\rm P}\right)^2$. Moving on, we focus on the first term of equation (2.51). Based on inequality (2.28), we have

$$\sum_{i\in\mathcal{A}_{\rm i}\cup\mathcal{A}_{\rm e}}\left(f_i^{\rm P}\bar{r}_{ij}^{\rm P} - \bar{s}_{ij}Q_{ij}^{\rm P}\right)\left(x_{ij}^{\rm P}(t) - \sum_{k\in\Gamma_j^+}\bar{r}_{jk}^{\rm P}x_{jk}^{\rm P}(t)\right)$$

$$\leq \sum_{i \in \mathcal{A}_{\mathrm{i}} \cup \mathcal{A}_{\mathrm{e}}} \left(f_i^{\mathrm{P}} \bar{r}_{ij}^{\mathrm{P}} - \bar{s}_{ij} Q_{ij}^{\mathrm{P}} \right) \left(x_{ij}^{\mathrm{P}}(t) \right)$$

$$\leq -\epsilon |\mathbf{x}^{\mathrm{P}}(t)| \tag{2.53}$$

Equation (2.37) satisfies the following relationship based on equations (2.52) and (2.53):

$$|\delta_{ij}(t)| = \Big| - \min \left\{ Q_{ij}^{\mathrm{P}} s_{ij}(t), x_{ij}^{\mathrm{P}}(t) \right\} + \sum_{h \in \mathcal{A}_i^-} \min \left\{ Q_{hi}^{\mathrm{P}} s_{ij}(t), x_{hi}^{\mathrm{P}}(t) \right\} \times r_{ij}^{\mathrm{P}}(t) \Big| \quad \forall i \in \mathcal{A}_{\mathrm{i}}, j \in \Gamma_i^+ \tag{2.54}$$

$$\leq \max \left\{ Q_{ij}^{\mathrm{P}}, \sum_{h \in \mathcal{A}_i^-} Q_{ij}^{\mathrm{P}} \right\} \tag{2.55}$$

Let $\hat{d}_{ij}$ be the maximum value of the demand. Then we have

$$|\delta_{ij}(t)| = \Big| - \min \left\{ Q_{ij}^{\mathrm{P}} s_{ij}(t), x_{ij}^{\mathrm{P}}(t) \right\} + d_i^{\mathrm{P}}(t) \times r_{ij}^{\mathrm{P}} \Big| \leq \max \left\{ Q_{ij}^{\mathrm{P}}, \hat{d}_{ij} \right\} \quad \forall i \in \mathcal{A}_{\mathrm{e}}, j \in \Gamma_i^+ \tag{2.56}$$

Define λ as the maximum value among Q_{ij}^{P}, $\sum_{h \in \mathcal{A}_i^-} Q_{ij}^{\mathrm{P}}$, and $\hat{d}_{ij}$, that is

$$\lambda = \max \left\{ Q_{ij}^{\mathrm{P}}, \sum_{h \in \mathcal{A}_i^-} Q_{ij}^{\mathrm{P}}, \hat{d}_{ij} \right\} \tag{2.57}$$

Because the total movement of private vehicles is *M*, we have the following inequality

$$|\delta_{ij}(t)|^2 \leq M \times \lambda^2 \tag{2.58}$$

From equations (2.53) and (2.58),

$$\begin{aligned}
&\left|\mathbf{x}^{\mathrm{P}}(t+1)\right|^2 - \left|\mathbf{x}^{\mathrm{P}}(t)\right|^2 = 2\mathbf{x}^{\mathrm{P}}(t)^{\mathrm{T}}\boldsymbol{\delta} + \left|\boldsymbol{\delta}\right|^2 \\
&\leq 2\left(\sum_{i\in\mathcal{A}_{\mathrm{i}}\cup\mathcal{A}_{\mathrm{e}}} (Q_{ij}^{\mathrm{P}})^2 - \epsilon|\mathbf{x}^{\mathrm{P}}(t)|\right) + M\lambda^2 \qquad (2.59) \\
&= \kappa - \epsilon|\mathbf{x}^{\mathrm{P}}(t)| \qquad (2.60)
\end{aligned}$$

where $\kappa = 2\sum_{i\in\mathcal{A}_{\mathrm{i}}\cup\mathcal{A}_{\mathrm{e}}} (Q_{ij}^{\mathrm{P}})^2 + M\lambda^2$.

Based on the above procedure, we find that we do not need to know the lower-bound and upper-bound of signal to prove stability. What we need is the long-time average time $\bar{s}_{ij}$ used for serving turning movement (i, j) while considering transit signal priority.

Proposition 3. *When average signal $\bar{s}_{ij}$, which satisfies the stable region constrains and obey the transit signal priority, is used and $\bar{\mathbf{d}}^{\mathrm{P}} \in \mathcal{D}^0$, the transportation network is stable.*

Proof. Inequality (2.37) holds from Lemma 4. Taking expectations and summing over $t = 1, ..., T$ gives the following inequality:

$$\mathbb{E}\left[\nu(T+1) - \nu(1)|\,\mathbf{x}^{\mathrm{P}}(t)\right] \leq \kappa T - \epsilon\sum_{t=1}^{T}|\mathbf{x}^{\mathrm{P}}(t)| \tag{2.61}$$

Then we have

$$\epsilon \frac{1}{T} \sum_{t=1}^{T} \mathbb{E}\left[|\mathbf{x}^{\mathrm{P}}(t)|\right] \leq \kappa - \frac{1}{T}\mathbb{E}\left[\nu(T+1)\right] + \frac{1}{T}\mathbb{E}\left[\nu(1)\right] \leq \kappa + \frac{1}{T}\mathbb{E}\left[\nu(1)\right] \tag{2.62}$$

which immediately implies that the stability Definition 4 is satisfied.

Furthermore, we can prove that stability is not impacted by the initial condition. For equation (2.62), we move ϵ to the right hand side and take the limit as T goes to infinity. Then the $\frac{1}{T}\mathbb{E}\left[\nu(1)\right]$ term equals zero, which yields

$$\lim_{T\to\infty} \frac{1}{T} \sum_{t=1}^{T} \mathbb{E}\left[|\mathbf{x}^{\mathrm{P}}(t)|\right] \leq \frac{\kappa}{\epsilon} \tag{2.63}$$

2.4 Modified Max-pressure Control Policy

2.4.1 Notations

Table 2.1: Notation.

$\mathcal{M}$	Set of movements
$\mathcal{N}$	Set of nodes
$\mathcal{A}$	Set of links
Γ_j^+	Set of outgoing links
Γ_j^-	Set of incoming links
$x_{ij}^{\mathrm{P}}(t)$	Number of private vehicles of the movement from link i to link j at time step t
$x_{ij}^{\mathrm{B}}(t)$	Number of buses of the movement from link i to link j at time step t
$r_{ij}^{\mathrm{P}}(t)$	Proportion of private vehicles entering i that will next move to j.
$r_{ij}^{\mathrm{B}}(t)$	Proportion of buses entering i that will next move to j.
$w_{ij}^{\mathrm{P}}(t)$	Weight of turning movement from link i to link j at time step t
$d_i^{\mathrm{B}}(t)$	Bus demand at link i
$d_i^{\mathrm{P}}(t)$	Private vehicle demand at at link i
$s_{ij}(t)$	Actuation of turning movement from link i to link j at time step t
$y_{ij}^{\mathrm{P}}(t)$	Signal control private vehicle flow from link i to link j at time step t
$y_{ij}^{\mathrm{B}}(t)$	Signal control number of buses from link i to link j at time step t
Q_{ij}^{P}	Capacity of turning movement for private vehicles from link i to link j
Q_{ij}^{B}	Capacity of turning movement for buses from link i to link j
Q_c	Capacity of conflict region
α_{ij}^n	0–1 binary dummy variable ($\alpha_{ij}^n = 1$ when private vehicles have conflict with buses)
f_i^{P}	Average private vehicle traffic volume of link i.

2.4.2 Max-pressure control policy considering public transit signal priority

This study uses the max-pressure control policy to calculate how many vehicles at the intersection should be served at every time step integrated the transit signal priority. The weight of each turning movement is the queue length of this movement (i, j) of private vehicles. The pressure calculation is shown by equation (2.64). As shown in Figure 1, the downstream turning movements of movement $(i.j)$ are composed by movement (j, k_1), (j, k_2), and (j, k_3).

$$w_{ij}^{\mathrm{P}}(t) = x_{ij}^{\mathrm{P}}(t) - \sum_{k \in \Gamma_j^+} r_{jk}^{\mathrm{P}}(t) x_{jk}^{\mathrm{P}}(t) \tag{2.64}$$

After we calculate the weight for each movement, a mixed-integer linear program is used to calculate the intersection control. In this program, we use α_{ij}^n we indicate whether the buses' movements have conflicts with private vehicles. The capacity of conflict region is Q_c, which is determined by the capacities of turning movements, $Q_c = \max_{(i,j)|c \in C_{ij}} \{Q_{ij}\}$. The total number of private vehicles and buses driving through the one conflict region per time is bounded by the capacity of the conflict region.

The max-pressure control policy considering bus priority tries to maximize the total pressure of private vehicles. Let $s_{ij}^\star(t)$ denote the max-pressure signal control at intersection n in the transportation network given the priority of bus transit, which is $s_{ij}^\star(t) = \mathrm{argmax}_{s \in \mathcal{S}_p} \left[\sum_{(i,j) \in \mathcal{M}} s_{ij}(t) Q_{ij}^{\mathrm{P}} w_{ij}^{\mathrm{P}}(t) \right]$ based on constraints (2.65b) to (2.65h). To be specific, constraint (2.65b) is combined with equation (2.11) that indicates the max-pressure control gives priority to the bus transit. Specifically, once a bus appears in the area of the intersection, our signal control $s_{ij}(t)$ will be activated ($s_{ij}(t) = 1$) in this moving direction. However, if there is no bus, $s_{ij}(t)$ is controlled by the pressure of private vehicles, which

is determined by the objective function, equation (2.65a). If two buses with conflicting movements are waiting, then one of them will be given a green light. The optimal solution to problem (2.65a) determines which bus will move first. The operation of transit signal priority is described in Figure 2.3. Private vehicles would follow the bus transit priority signal. Constraint (2.65c) indicated the movement of private vehicles should consider the capacity of this movement and whether this movement could conflict with buses or not. Constraint (2.65d) indicates the sum movements of private vehicles and buses should less equal to the capacity of the conflict region. Constraint (2.65e) indicates the movement of private vehicles should be less than or equal to the queue length of the private vehicles. Constraint (2.65f) indicates the bus movement flow is bounded by the minimum value of capacity multiples signal control or the length of bus queueing. (2.65g) means the signal control equal to 0 or 1. The constraint (2.65h) indicates the queueing length of buses, the movement of private vehicles and buses should not be negative numbers.

$$\max \quad \sum_{(i,j)\in\mathcal{M}} s_{ij}(t) Q_{ij}^{\mathrm{P}} w_{ij}^{\mathrm{P}}(t) \tag{2.65a}$$

$$\text{s.t.} \quad \sum_{(i,j)\in\mathcal{M}} x_{ij}^{\mathrm{B}}(t) \left[\sum_{(i,j)\in\mathcal{M}} s_{ij}(t) x_{ij}^{\mathrm{B}}(t) - 1 \right] \geq 0 \quad \forall (i,j) \in \mathcal{M} \tag{2.65b}$$

$$y_{ij}^{\mathrm{P}}(t) \leq s_{ij}(t) Q_{ij}^{\mathrm{P}} (1 - \alpha_{ij}^{n}) \qquad \forall (i,j) \in \mathcal{M} \tag{2.65c}$$

$$\sum_{(i,j)\in\mathcal{M}} y_{ij}^{\mathrm{P}}(t)(1 - \alpha_{ij}^{n}) + y_{ij}^{\mathrm{B}}(t) \leq Q_{\mathrm{c}} \qquad \forall (i,j) \in \mathcal{M}, \forall c \in \mathcal{C} \tag{2.65d}$$

$$y_{ij}^{\mathrm{P}}(t) \leq x_{ij}^{\mathrm{P}}(t) \qquad \forall (i,j) \in \mathcal{M} \tag{2.65e}$$

$$y_{ij}^{\mathrm{B}}(t) = \min \left\{ Q_{ij}^{\mathrm{B}} s_{ij}(t), x_{ij}^{\mathrm{B}}(t) \right\} \qquad \forall (i,j) \in \mathcal{M} \tag{2.65f}$$

$$s_{ij}(t) \forall \in \{0, 1\} \qquad \forall (i,j) \in \mathcal{M} \tag{2.65g}$$

$$x_{ij}^{\mathrm{B}}(t), y_{ij}^{\mathrm{P}}(t), y_{ij}^{\mathrm{B}}(t) \geq 0 \qquad \forall (i,j) \in \mathcal{M} \tag{2.65h}$$

Lemma 2. *If max-pressure control policy considering bus priority is used and* $\bar{\mathbf{d}}^{\mathrm{P}} \in \mathcal{D}^0$*, then we have the following inequality for* $\bar{s}_{ij}$*, which is the average signal control considering bus priority and satisfying constraints (2.25)–(2.27).*

$$\mathbb{E}\left[\sum_{(i,j)\in\mathcal{M}^2} s^{\star}_{ij}(t) Q^{\mathrm{P}}_{ij} w^{\mathrm{P}}_{ij}(t) \middle| \mathbf{x}^{\mathrm{P}}(t)\right] \geq \mathbb{E}\left[\sum_{(i,j)\in\mathcal{M}^2} \bar{s}_{ij} Q^{\mathrm{P}}_{ij} w^{\mathrm{P}}_{ij}(t) \middle| \mathbf{x}^{\mathrm{P}}(t)\right] \tag{2.66}$$

Proof. First, we have

$$\sum_{(i,j)\in\mathcal{M}^2} s^{\star}_{ij}(t) Q^{\mathrm{P}}_{ij} w^{\mathrm{P}}_{ij}(t) \geq \sum_{(i,j)\in\mathcal{M}^2} s_{ij}(t) Q^{\mathrm{P}}_{ij} w^{\mathrm{P}}_{ij}(t) \tag{2.67}$$

since $s^{\star}_{ij}(t)$, $s_{ij}(t) \in \mathcal{S}_p$, and $s^{\star}_{ij}(t)$ maximizes objective (2.65a). Then we calculate the expected value of the above equation when given the private vehicle queue length $\mathbf{x}^{\mathrm{P}}(t)$ as

$$\mathbb{E}\left[\sum_{(i,j)\in\mathcal{M}^2} s^{\star}_{ij}(t) Q^{\mathrm{P}}_{ij} w^{\mathrm{P}}_{ij}(t) \middle| \mathbf{x}^{\mathrm{P}}(t)\right] \geq \mathbb{E}\left[\sum_{(i,j)\in\mathcal{M}^2} s_{ij}(t) Q^{\mathrm{P}}_{ij} w^{\mathrm{P}}_{ij}(t) \middle| \mathbf{x}^{\mathrm{P}}(t)\right] \tag{2.68}$$

Since $s^{\star}_{ij}(t) = \operatorname{argmax}_{s\in\mathcal{S}} \sum_{(i,j)\in\mathcal{M}^2} s_{ij}(t) Q^{\mathrm{P}}_{ij} w^{\mathrm{P}}_{ij}(t)$ and based on equation (5.4), we rewrite equation (2.68) to

$$\mathbb{E}\left[\sum_{(i,j)\in\mathcal{M}^2} s^{\star}_{ij}(t) Q^{\mathrm{P}}_{ij} w^{\mathrm{P}}_{ij}(t) \middle| \mathbf{x}^{\mathrm{P}}(t)\right] \geq \mathbb{E}\left[\sum_{(i,j)\in\mathcal{M}^2} \bar{s}_{ij} Q^{\mathrm{P}}_{ij} w^{\mathrm{P}}_{ij}(t) \middle| \mathbf{x}^{\mathrm{P}}(t)\right] \tag{2.69}$$

2.4.3 Stability analysis

Now, we proceed to prove that the max-pressure signal control with bus priority defined in Section 2.4.2 will stabilize any private vehicle demand $\bar{\mathbf{d}}^{\mathrm{P}} \in \mathcal{D}^0$. Notice that the bus demand can be stabilized at any time since the number of buses is limited and much smaller than the number of private vehicles.

Lemma 3. *If max-pressure signal control with bus priority is used and* $\bar{\mathbf{d}}^{\mathrm{P}} \in \mathcal{D}^0$*, there exists a Lyapunov function* $\nu(t) \geq 0$ *and constants* $\kappa > 0$*,* $\epsilon > 0$ *such that*

$$\mathbb{E}\left[\nu(t+1) - \nu(t) | \, \mathbf{x}^{\mathrm{P}}(t)\right] \leq \kappa - \eta |\mathbf{x}^{\mathrm{P}}(t)| \tag{2.70}$$

Proof. Based on equations (2.7)–(2.44) and the definition of the pressure term (2.64), we obtain

$$\begin{aligned}\mathbb{E}\left[\mathbf{x}^{\mathrm{P}}(t)^{\mathrm{T}} \boldsymbol{\delta}(t) | \mathbf{x}^{\mathrm{P}}(t)\right] = & \sum_{i \in \mathcal{A}_{\mathrm{i}} \cup \mathcal{A}_{\mathrm{e}}} \mathbb{E}\left[\min\left\{Q_{ij}^{\mathrm{P}} s_{ij}(t), x_{ij}^{\mathrm{P}}(t)\right\} \middle| \, \mathbf{x}^{\mathrm{P}}(t)\right] \times \left(-w_{ij}^{\mathrm{P}}(t)\right) \\ & + \sum_{i \in \mathcal{A}_{\mathrm{e}}} \bar{d}_i^{\mathrm{P}} \bar{r}_{ij}^{\mathrm{P}} x_{ij}^{\mathrm{P}}(t)\end{aligned} \tag{2.71}$$

The last term of equation (2.71) can be rewritten as follows based on equations (2.25), (4.17), and (2.64):

$$\sum_{i \in \mathcal{A}_{\mathrm{e}}} \bar{d}_i^{\mathrm{P}} \bar{r}_{ij}^{\mathrm{P}} x_{ij}^{\mathrm{P}}(t) = \sum_{i \in \mathcal{A}_{\mathrm{e}}} f_{ij}^{\mathrm{P}} x_{ij}^{\mathrm{P}}(t) \tag{2.72}$$

$$= \sum_{i \in \mathcal{A}_{\mathrm{e}} \cup \mathcal{A}_{\mathrm{e}}} f_i^{\mathrm{P}} \bar{r}_{ij}^{\mathrm{P}} x_{ij}^{\mathrm{P}}(t) - \sum_{i \in \mathcal{A}_{\mathrm{i}}} f_j^{\mathrm{P}} \bar{r}_{jk}^{\mathrm{P}} x_{jk}^{\mathrm{P}}(t) \tag{2.73}$$

$$= \sum_{i\in\mathcal{A}_{\mathrm{e}}\cup\mathcal{A}_{\mathrm{e}}} f_i^{\mathrm{P}}\bar{r}_{ij}^{\mathrm{P}}x_{ij}^{\mathrm{P}}(t) - \sum_{j\in\Gamma_i^+}\left(f_i^{\mathrm{P}}\bar{r}_{ij}^{\mathrm{P}}\right)\sum_{k\in\Gamma_i^+}\bar{r}_{jk}^{\mathrm{P}}x_{jk}^{\mathrm{P}}(t) \tag{2.74}$$

$$= \sum_{i\in\mathcal{A}_{\mathrm{i}}\cup\mathcal{A}_{\mathrm{e}}} f_i^{\mathrm{P}}\bar{r}_{ij}^{\mathrm{P}}\left(w_{ij}^{\mathrm{P}}(t)\right) \tag{2.75}$$

Combining equations (2.71) and (2.75) yields

$$\begin{aligned}\mathbb{E}\left[\mathbf{x}^{\mathrm{P}}(t)^{\mathrm{T}}\boldsymbol{\delta}(t)|\mathbf{x}^{\mathrm{P}}(t)\right] = &\sum_{i\in\mathcal{A}_{\mathrm{i}}\cup\mathcal{A}_{\mathrm{e}}}\Big(f_i^{\mathrm{P}}\bar{r}_{ij}^{\mathrm{P}} \\ &-\mathbb{E}\left[\min\left\{Q_{ij}^{\mathrm{P}}s_{ij}(t), x_{ij}^{\mathrm{P}}(t)\right\}|\mathbf{x}^{\mathrm{P}}(t)\right]\Big)w_{ij}^{\mathrm{P}}(t) \qquad (2.76)\\ = &\sum_{i\in\mathcal{A}_{\mathrm{i}}\cup\mathcal{A}_{\mathrm{e}}}\left(f_i^{\mathrm{P}}\bar{r}_{ij}^{\mathrm{P}} - Q_{ij}^{\mathrm{P}}\bar{s}_{ij}\right)w_{ij}^{\mathrm{P}}(t) \\ &+\sum_{i\in\mathcal{A}_{\mathrm{i}}\cup\mathcal{A}_{\mathrm{e}}}\Big(Q_{ij}^{\mathrm{P}}\bar{s}_{ij} \\ &-\mathbb{E}\left[\min\left\{Q_{ij}^{\mathrm{P}}s_{ij}(t), x_{ij}^{\mathrm{P}}(t)\right\}|\mathbf{x}^{\mathrm{P}}(t)\right]\Big)w_{ij}^{\mathrm{P}}(t) \qquad (2.77)\end{aligned}$$

For the second term of equation (2.77), if $x_{ij}^{\mathrm{P}}(t) \geq Q_{ij}^{\mathrm{P}}$, then we have $\mathbb{E}\left[\min\left\{Q_{ij}^{\mathrm{P}}s_{ij}(t), x_{ij}^{\mathrm{P}}(t)\right\}\middle|\mathbf{x}^{\mathrm{P}}(t)\right] = Q_{ij}^{\mathrm{P}}\bar{s}_{ij}$. Therefore, the second term of equation (2.77) equals zero. If $x_{ij}^{\mathrm{P}}(t) < Q_{ij}^{\mathrm{P}}$, then we have $\mathbb{E}\left[\min\left\{Q_{ij}^{\mathrm{P}}s_{ij}(t), x_{ij}^{\mathrm{P}}(t)\right\}\middle|\mathbf{x}^{\mathrm{P}}(t)\right]$ $= \mathbb{E}\left[x_{ij}^{\mathrm{P}}(t)\middle|\mathbf{x}^{\mathrm{P}}(t)\right]$. Therefore, we obtain the following

$$\left(Q_{ij}^{\mathrm{P}}\bar{s}_{ij} - \mathbb{E}\left[x_{ij}^{\mathrm{P}}(t)\middle|\mathbf{x}^{\mathrm{P}}(t)\right]\right)w_{ij}^{\mathrm{P}}(t) \leq Q_{ij}^{\mathrm{P}}x_{ij}^{\mathrm{P}}(t) \leq \left(Q_{ij}^{\mathrm{P}}\right)^2 \tag{2.78}$$

Hence, the second term of equation (2.77) equals zero or is bounded by $\sum_{i\in\mathcal{A}_{\mathrm{i}}\cup\mathcal{A}_{\mathrm{e}}}\left(Q_{ij}^{\mathrm{P}}\right)^2$.

The max-pressure signal control $s_{ij}^{\star}(t)$ is chosen from the feasible signal control set $\mathcal{S}_p$, which obeys bus priority constraints, and $s_{ij}^{\star}(t)$ seeks to maximize the objective (2.65a). According to Lemma 2, we have

$$\mathbb{E}\left[\sum_{i\in\mathcal{A}_{\mathrm{i}}\cup\mathcal{A}_{\mathrm{e}}}\left(f_i^{\mathrm{P}}\bar{r}_{ij}^{\mathrm{P}}-s_{ij}^{\star}(t)Q_{ij}^{\mathrm{P}}\right)w_{ij}^{\mathrm{P}}(t)\middle|\, w_{ij}^{\mathrm{P}}(t)\right]$$
$$\leq \mathbb{E}\left[\sum_{i\in\mathcal{A}_{\mathrm{i}}\cup\mathcal{A}_{\mathrm{e}}}\left(f_i^{\mathrm{P}}\bar{r}_{ij}^{\mathrm{P}}-\bar{s}_{ij}Q_{ij}^{\mathrm{P}}\right)w_{ij}^{\mathrm{P}}(t)\middle|\, w_{ij}^{\mathrm{P}}(t)\right] \tag{2.79}$$

Therefore, for some feasible signal controls $s_{ij}(t)$ satisfying the stable region and integrated transit signal priority, we obtain $\bar{s}_{ij}$ based on equation (5.4). We have

$$\sum_{i\in\mathcal{A}_{\mathrm{i}}\cup\mathcal{A}_{\mathrm{e}}}\left(f_i^{\mathrm{P}}\bar{r}_{ij}^{\mathrm{P}}-\bar{s}_{ij}Q_{ij}^{\mathrm{P}}\right)w_{ij}^{\mathrm{P}}(t)\leq-\epsilon\sum_{(i,j)\in\mathcal{M}^2}\max\left\{w_{ij}^{\mathrm{P}},0\right\}\leq-\epsilon|w_{ij}^{\mathrm{P}}| \tag{2.80}$$

We know that the pressure $\mathbf{w}(t)$ is a linear function of the queue length of the private vehicles. So we can find $\beta>0$ to satisfy $\sum_{(i,j)\in\mathcal{M}^2} w_{ij}^{\mathrm{P}}\geq\beta|\mathbf{x}^{\mathrm{P}}|$. Then we have

$$-\epsilon|w_{ij}^{\mathrm{P}}|\leq-\epsilon\beta|\mathbf{x}^{\mathrm{P}}|\leq\sum_{i\in\mathcal{A}_{\mathrm{i}}\cup\mathcal{A}_{\mathrm{e}}}\left(Q_{ij}^{\mathrm{P}}\right)^2-\epsilon\beta|\mathbf{x}^{\mathrm{P}}| \tag{2.81}$$

$\delta_{ij}(t)$ is upper-bounded by $\max\left\{Q_{ij}^{\mathrm{P}},\sum_{h\in\mathcal{A}_i^-}Q_{ij}^{\mathrm{P}}\right\}$, which is the same as equation (2.55). Based on equation (2.81) and equations (2.55)–(2.58), we obtain

$$\left|\mathbf{x}^{\mathrm{P}}(t+1)\right|^2-\left|\mathbf{x}^{\mathrm{P}}(t)\right|^2=2\mathbf{x}^{\mathrm{P}}(t)^{\mathrm{T}}\boldsymbol{\delta}+\left|\boldsymbol{\delta}\right|^2$$
$$\leq 2\left(\sum_{i\in\mathcal{A}_{\mathrm{i}}\cup\mathcal{A}_{\mathrm{e}}}\left(Q_{ij}^{\mathrm{P}}\right)^2-\epsilon\beta|\mathbf{x}^{\mathrm{P}}(t)|\right)+M\lambda^2 \tag{2.82}$$
$$=\kappa-\eta|\mathbf{x}^{\mathrm{P}}(t)| \tag{2.83}$$

where $\kappa = 2 \sum_{i \in \mathcal{A}_{\mathrm{i}} \cup \mathcal{A}_{\mathrm{e}}} (Q_{ij}^{\mathrm{P}})^2 + M\lambda^2$, $\epsilon\beta = \lambda$.

Proposition 4. *When $\bar{\mathbf{d}}^{\mathrm{P}} \in \mathcal{D}^0$, then the max-pressure policy considering transit signal priority is stabilizing.*

Proof. The proof is analogous to Proposition 7. Inequality (2.70) holds from Lemma 9. Taking expectations, summing over $t = 1, ..., T$, and transferring the position of terms gives the following inequality:

$$\eta \frac{1}{T} \sum_{t=1}^{T} \mathbb{E}\left[|\mathbf{x}^{\mathrm{P}}(t)|\right] \leq \kappa - \frac{1}{T}\mathbb{E}\left[\nu(T+1)\right] + \frac{1}{T}\mathbb{E}\left[\nu(1)\right] \leq \kappa + \frac{1}{T}\mathbb{E}\left[\nu(1)\right] \tag{2.84}$$

which satisfies Definition 4 for stability.

2.5 Simulation Model and Numerical Results

To test the effects of our proposed max-pressure control policy, we set up simulations on the downtown Austin Network based on a microscopic traffic simulation tool, SUMO, interfaced with Python (Lopez et al., 2018). The demand file was from the authors' past study, which can be found on Levin et al. (2020). Note that, there are two bus lanes built in the downtown area, the Austin Metro Rapid, which is the bus rapid transit. Details are shown in Figure 2.4. We add the Metro Rapid information into the simulation settings, such as bus operational timetable and departure interval of routes and to make the simulation much closer to the real-world condition. All the bus operational information is open access to the public on the Capital Metro website.

The numerical results presented in this part compare the performance of the max-pressure control considering transit signal priority of bus rapid transit system (referred to as MP-TSP), adaptive signal control considering transit signal priority (referred to as

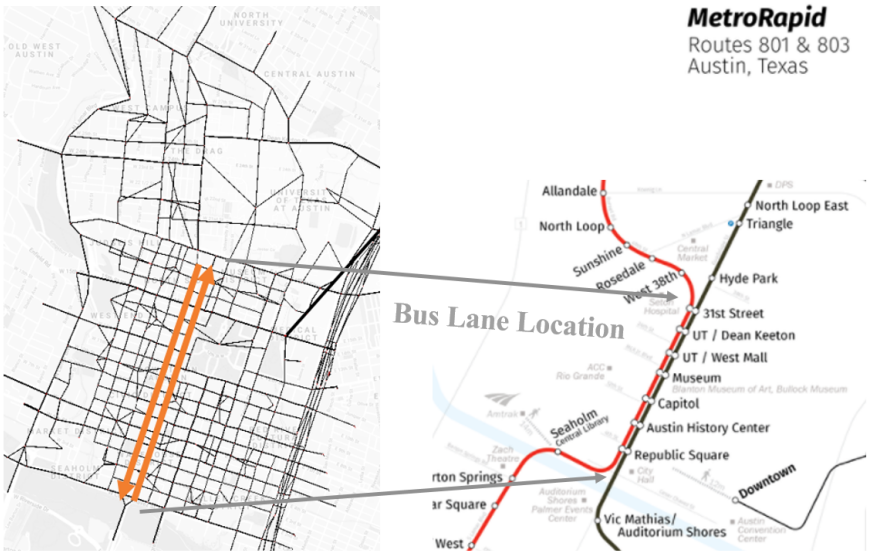

Figure 2.4: Austin Network with Bus Lanes

Adaptive-TSP), and a given fixed-time controller (referred to as FT-TSP) considering transit signal priority of bus rapid transit system. It is worth noticing that we only give transit signal priority to built-in bus lanes. While, when there is no bus lane on a BRT route, transit signal priority will fail for any signal controller in this simulation. In this simulation, there is no conflicting movement for bus lanes in the Austin network, and the transit signal priority strategy is the same for all traffic signal control policies in this disseration.

2.5.1 Stability comparison

First, we compare the stability of the network based on Definition 4. Basically, we test whether the total number of private vehicles in the network is increasing over time under different private vehicle demand level settings with 20 minutes bus departure intervals. Figure 2.5 shows an example of a stable condition and unstable condition. When the demand of private vehicles is within the stable region, the average number of private vehicles will converge to a constant. However, for unstable demand, the average number of private vehicles will increase to an arbitrarily large number.

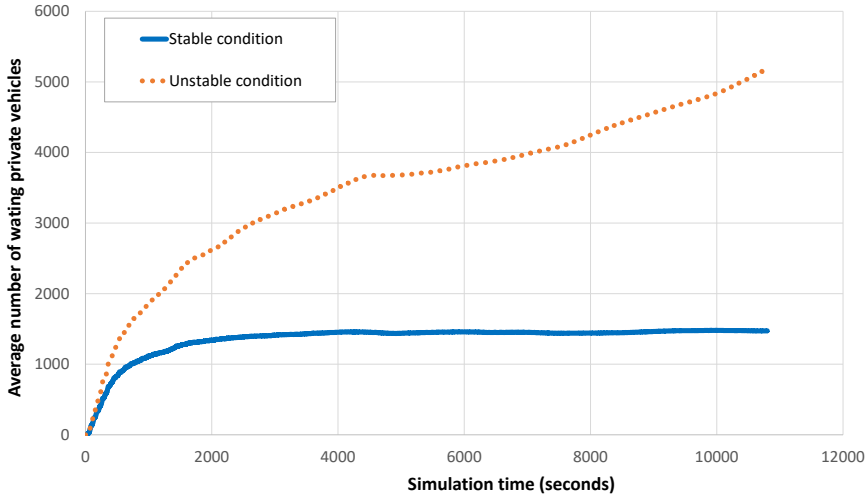

Figure 2.5: An example of stable and unstable region

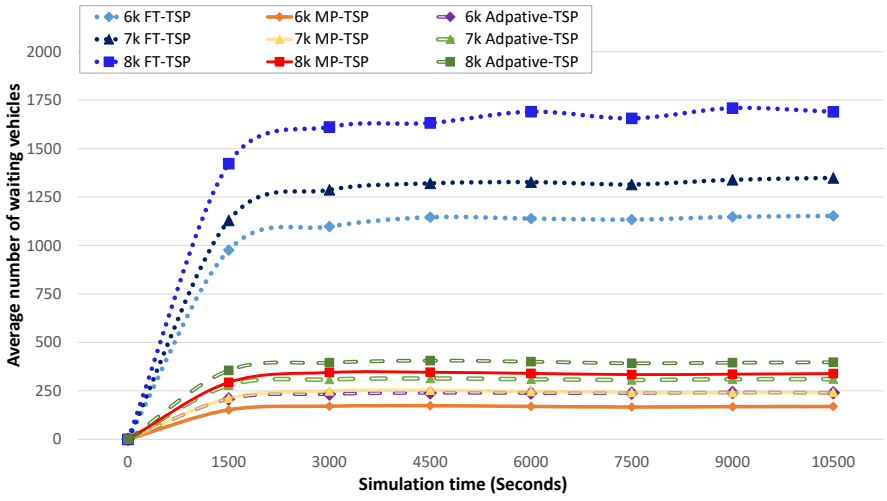

Figure 2.6: Network stability

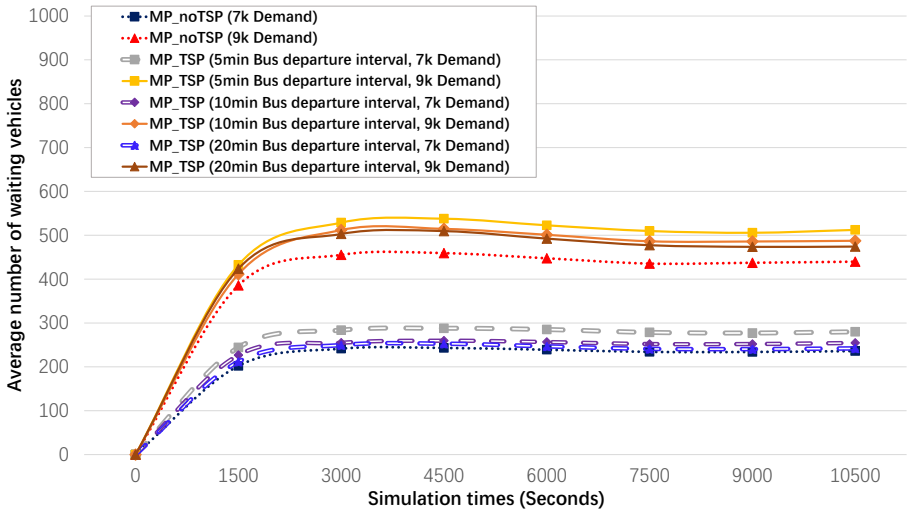

Figure 2.7: Stable region comparison between MP-noTSP and MP-TSP

Figure 2.6 compares the result of the average number of waiting private vehicles for FT-TSP, Adaptive-TSP, and MP-TSP. At the same private vehicles' demand setting, the number of waiting private vehicles by FT-TSP and Adaptive-TSP are larger than the results for MP-TSP. Furthermore, when increasing the demand level, the MP-TSP has a lower number of waiting private vehicles. These results indicate that MP-TSP has a larger stable region than FT-TSP and Adaptive-TSP, and is able to stabilize the network at a higher level of private vehicle demand, which is consistent with Section 4.2.

It is also worth exploring whether the signal priority affects the stable region. We compare the original max pressure control (referred to as MP-noTSP) from Varaiya (2013) with MP-TSP under different bus departure intervals. The results are shown in Figure 2.7. These results show that when the number of waiting private vehicles of MP-noTSP is lowest under the same demand setting. This is because, if we give more priority to transit, we will sacrifice the right of way at the intersection for private vehicles. When the bus arrival frequency is higher (bus departure interval is smaller), the number of waiting private vehicles of MP-TSP is higher. This is reasonable because the higher the bus demand, the more priority time buses are given.

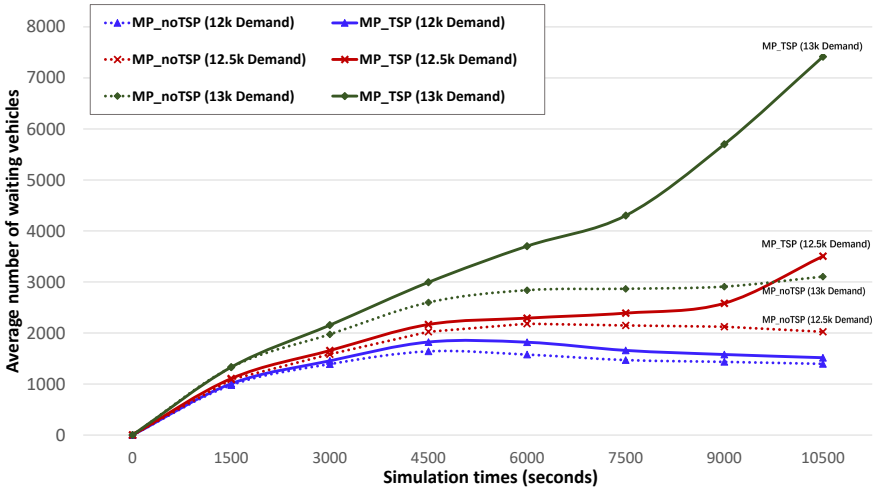

Figure 2.8: Impacts of TSP on original stable demand

From Figure 2.7, we find that TSP may "reduce" the stable region of private vehicles. Specifically, the original private vehicle demand may be within the stable region, but when TSP is considered, the private vehicle demand may fall outside of the stable region. Figure 2.8 shows the detail of throughput loss in experiments under 20 minutes bus departure intervals setting. Figure 2.8 shows that when we choose MP-noTSP, the network can serve 12500 private vehicles per hour, while when implementing MP-TSP, the network becomes unstable (the average number of waiting vehicles increases to infinity). When we add private vehicle demand to 13000 vehicles per hour, both MP-noTSP and MP-TSP cannot stabilize the network. It is worth noticing when implementing MP-TSP, the network can serve 12000 private vehicles per hour. Therefore, we may lose around 500 private vehicles network capacity when giving signal priority to public transit.

We also provide the trajectory of the proposed Lyapunov function (2.40) as figures to show the dynamic pattern of stability for FT-TSP, Adaptive-TSP, and MP-TSP. The demand setting and bus departure interval setting is the same as in Figure 5. As Figures Figure 2.9–Figure 2.11 show, the Lyapunov function value of MP-TSP is still the lowest compared with Adaptive-TSP and FT-TSP. These results indicate that MP-TSP has a larger potential

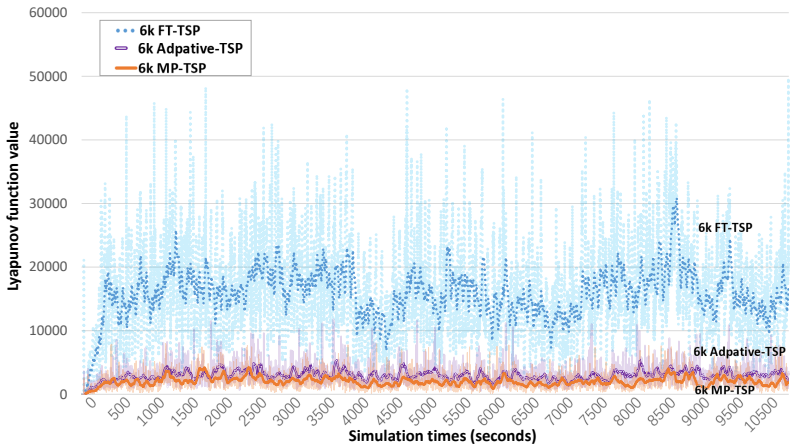

Figure 2.9: Trajectory of Lyapunov function under demand of 6000 vehicles per hour

to achieve maximum stability on a given network under different levels of demand.

2.5.2 Travel time

It is also important to explore how transit signal priority impacts vehicle travel time at the network level. The average waiting time of MP-TSP, Adaptive-TSP, and FT-TSP at different demand levels and 20 min bus departure intervals time are shown in Figure 2.12. We also provide Table 2.2 including experiment results for better comparison. As the demand increases, vehicles spend more time on the links and intersections. Therefore, the average waiting time increases. Unsurprisingly, since MP-TSP can serve more demand than Adaptive-TSP and FT-TSP, MP-TSP have lower average travel time compared with adaptive-TSP and FT-TSP. Also, it is no surprise that Adaptive-TSP make private vehicles have less travel time than FT-TSP controller since it could adjust phases duration based on loop detectors. These results also indicate that the max-pressure controller integrated with transit signal priority performs better than the adaptive signal control integrated with transit signal priority and a given fixed-time signal controller integrated with transit signal priority at different demand settings.

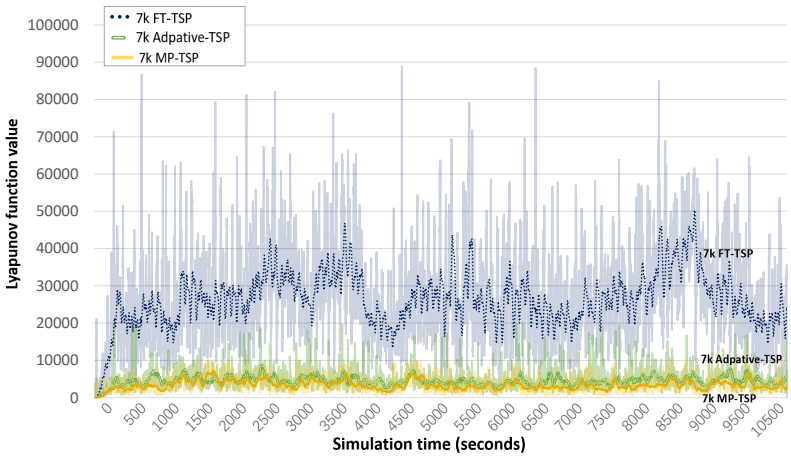

Figure 2.10: Trajectory of Lyapunov function under demand of 7000 vehicles per hour

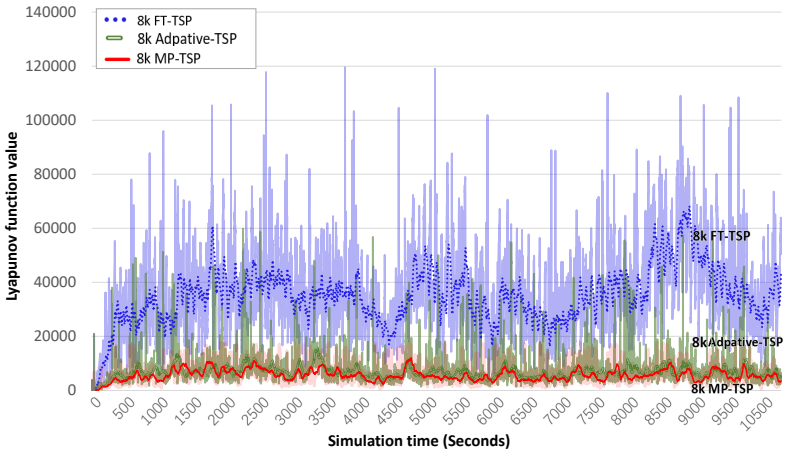

Figure 2.11: Trajectory of Lyapunov function under demand of 8000 vehicles per hour

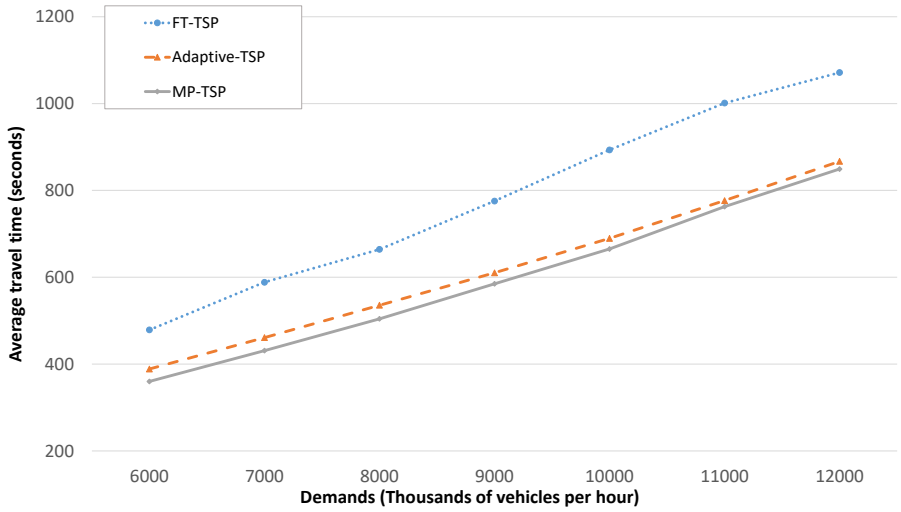

Figure 2.12: Average travel time

Table 2.2: Average travel time between MP-TSP, Adaptive-TSP, and FT-TSP

Demands	FT-TSP (seconds)	Adaptive-TSP (seconds)	MP-TSP (seconds)
6000	478.71	388.60	360.07
7000	588.50	460.96	431.15
8000	664.24	535.55	504.23
9000	775.49	610.26	584.88
10000	893.26	689.60	665.15
11000	1001.21	776.57	762.65
12000	1071.39	866.95	849.31

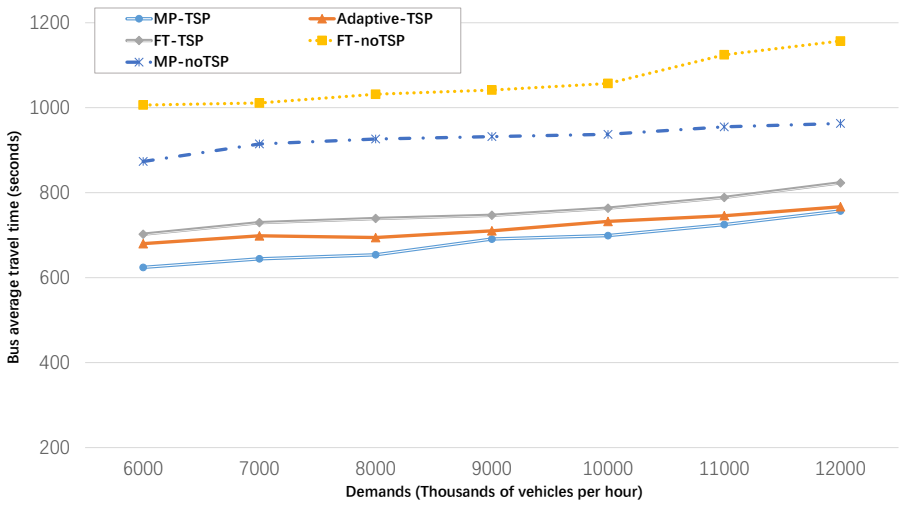

Figure 2.13: Bus average travel time

Table 2.3: Bus average travel time (seconds) in downtown area

Demands	MP-TSP	Adaptive-TSP	FT-TSP	MP-noTSP	FT-noTSP
6000	624.14	680.38	702.25	873.45	1006.31
7000	644.30	698.38	729.40	914.64	1011.02
8000	653.83	694.29	739.20	926.31	1031.59
9000	690.79	710.24	746.79	931.93	1041.52
10000	699.04	732.30	763.47	937.32	1057.03
11000	724.85	745.69	788.66	954.89	1124.51
12000	757.18	766.85	823.18	962.90	1156.84

2.5.3 Impacts on the nearby roads

How the TSP influences nearby private vehicle roads and intersections are also worth exploring. Previous studies found that TSP may increase some delay for non-transit modes in the urban network, which inspires us to figure out how MP-TSP will influence nearby private vehicle roads. We calculate how the TSP influences the private vehicle links that are

parallel to the bus links, which are denoted as the consistent direction in Figure 2.14, and the direction without bus links, which are denoted as the conflict direction in Figure 2.14. Note that for the conflict directions, we only consider the links between the nearest next intersection. We use the average queueing time of private vehicles to figure out how FT-TSP, Adaptive-TSP, and MP-TSP influence the performance in those directions. Experimental setting details are shown in Figure 2.14.

The results are shown in Figure 2.15, Figure 2.16, Table 2.4, and Table 2.5. For the consistent direction, the MP-TSP has a significantly lower queueing time compared with FT-TSP and Adaptive-TSP when the private vehicle demand increases. For instance, when the demand is 11000 private vehicles per hour, the average queueing time when implementing MP-TSP is between 50 to 60 seconds under different bus departure intervals, but the average queueing time when implementing Adaptive-TSP is between 80 to 90 seconds. Furthermore, when the demand grows larger, the queueing time of FT-TSP increases faster than the queueing time of MP-TSP. These results are consistent with the property of MP-TSP because max-pressure control can serve as much demand as possible while giving priority to bus rapid transit. When the bus rapid transit departure interval is smaller, the consistent direction has lower queueing time, since buses arrive more frequently when their departure time gap is smaller.

As for the conflicting direction, when the demand is below 10000 private vehicles per hour, MP-TSP is slightly better than FT-TSP when considering the queueing time. When the demand increases, MP-TSP is slightly worse than FT-TSP, because the max-pressure controller would give priority to bus phases and high demand approaches, which may cause some delay for conflicting movements. Furthermore, Adaptive-TSP performs best for the conflicting direction, because the adaptive signal controller can adjust its phase duration based on the dynamic private vehicle demands, but MP-TSP will give more priority for private vehicles on the consistent directions, which is the main transit corridor in the downtown Austin network. However, the travel time of private vehicles and buses at the network

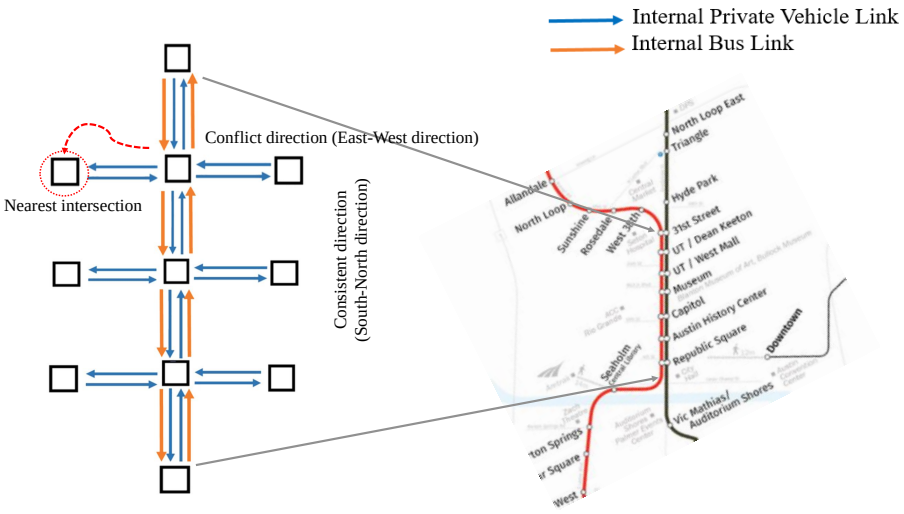

Figure 2.14: Experimental diagram

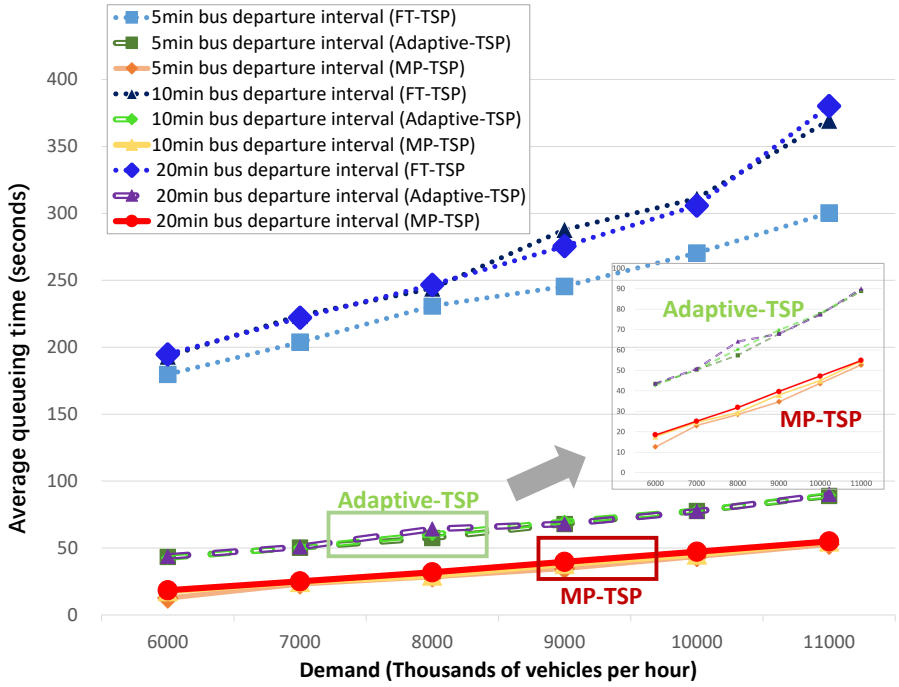

Figure 2.15: Consistent direction

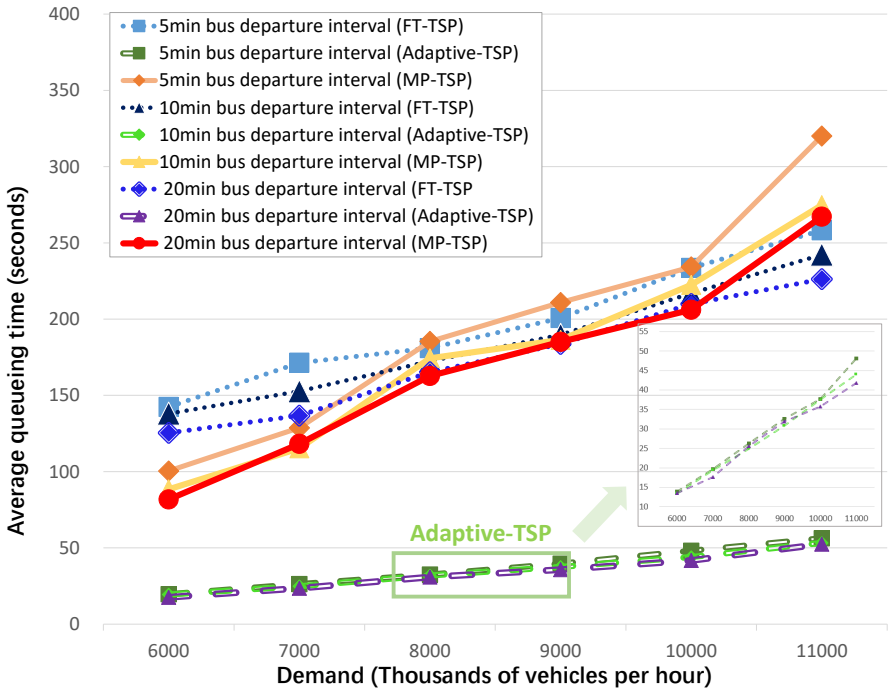

Figure 2.16: Conflict direction

level indicates that this will not influence that MP-TSP has better performance than FT-TSP and Adaptive-TSP. When the bus departure interval is smaller, the conflict direction has a larger queueing time, because the consistent direction has more priority when buses arrive more frequently in the consistent direction.

Table 2.4: Average queueing time of private vehicles among FT-TSP, Adaptive-TSP, and MP-TSP and FT-TSP in the consistent direction

5min bus headway		
FT-TSP (seconds)	Adaptive-TSP (seconds)	MP-TSP (Seconds)
179.75	42.36	12.57
203.76	50.35	23.12
230.89	57.50	27.44
245.46	67.95	34.69
270.35	76.61	43.61
299.34	88.93	52.73
10min bus headway		
FT-TSP (seconds)	Adaptive-TSP (seconds)	MP-TSP (Seconds)
193.24	42.68	17.62
223.75	50.50	24.57
244.03	60.24	29.34
287.86	69.81	37.97
311.15	77.96	45.03
369.52	89.47	54.77
20min bus headway		
FT-TSP (seconds)	Adaptive-TSP (seconds)	MP-TSP (Seconds)
194.65	44.68	18.47
222.11	51.80	25.11
246.69	63.27	31.84
275.57	69.06	39.66
305.85	78.40	47.29
380.23	90.07	54.94

Table 2.5: Average queueing time of private vehicles among FT-TSP, Adaptive-TSP, and MP-TSP and FT-TSP in the conflict direction

5min bus headway		
FT-TSP (seconds)	Adaptive-TSP (seconds)	MP-TSP (Seconds)
142.40	13.91	100.39
171.39	19.63	128.73
181.00	26.29	185.36
200.67	32.53	210.92
233.56	37.62	234.21
258.25	48.31	320.09
10min bus headway		
FT-TSP (seconds)	Adaptive-TSP (seconds)	MP-TSP (Seconds))
139.02	13.42	88.39
152.67	19.42	115.28
172.50	24.82	174.28
189.70	30.86	186.40
216.98	37.59	222.50
242.30	43.89	274.77
20min		
FT-TSP (seconds)	Adaptive-TSP (seconds)	MP-TSP (Seconds)
125.42	13.55	81.71
136.67	17.56	118.17
165.20	25.56	162.78
188.00	31.86	185.10
214.00	35.71	206.13
226.22	41.77	267.21

2.6 Conclusions

In previous studies, max-pressure control only considered the private vehicle network. However, the urban transportation network also includes other traffic modes. Chen et al. (2020) extended max-pressure signal controller to autonomous vehicles and pedestrians for the first time. To boost the scope of the application of the max-pressure control policy, we propose a modified max-pressure control policy, which considers the transit signal priority of the bus rapid transit system. We analytically proved that the MP-TSP can still achieve maximum stability.

Numerical results in the downtown Austin network suggest that, although the modified max-pressure control policy will have a lower stable region compared with the original max-pressure control policy, it will have much lower bus travel time. Also, the modified max-pressure control policy performs better than the other fixed time signal control incorporating with transit signal priority and adaptive signal control incorporating transit signal priority based on the average number of waiting private vehicles, the trajectory of the proposed Lyapunov function, the average travel time of private vehicles, and the bus average travel time. When the private vehicle links are parallel to the bus links (consistent directions), the average queueing time increase with increase of bus departure intervals, and the MP-TSP performs better than the FT-TSP and Adaptive-TSP (the second-best one). On the other hand, for the direction conflicting with bus links, the MP-TSP performs better than FT-TSP when demand is low, and the average queueing time decreases with the increase of bus departure intervals. It should be noted that Adaptive-TSP performs best in the conflict direction with bus links, this is because the adaptive signal controller can adjust its phase duration based on the dynamic private vehicle demands, but MP-TSP will give more priority for private vehicles on the consistent directions because of the arrivals of buses.We also notice that at the start points of bus lanes, where the upstream intersections are operated by origin max-pressure signal controllers, there may be a long waiting time

as demand increases, which could reduce MP-TSP travel time performance at the network level. Overall, the proposed modified max-pressure policy can serve more private vehicle demand and reduce travel time while including transit signal priority at the urban network level, which is more friendly to multi-modal traffic operations.

In the future, there are many extensions to consider. For example, streets comprise more than 80% of public space in cities, but they often fail to provide their surrounding communities with enough space where people can safely walk, bicycle, drive, take public transit, and socialize. Incorporating all of these modes into the max-pressure signal control scheme is an interesting and important challenge. In addition, the results will benefit from additional numerical analyses on the design of exclusive bus lanes, such as the layout of bus lanes, number of bus lanes, location of bus lanes with regarding the different levels of private vehicle demand.

Chapter 3

Ped-MP: A pedestrian-friendly max-pressure signal control policy for city networks

3.1 Introduction

Most past max-pressure signal controls with cyclic and non-cyclic phases do not include access for multi-modal traffic and thus are not designed for the complex multi-modal traffic dynamics in urban areas. Multi-modal traffic is very common in metropolises, such as New York City, Chicago, etc, which has inspired traffic researchers to focus on multi-modal traffic signal timing for decades (He et al., 2012, 2014). Some papers focus on providing better traffic signal timing with pedestrian crossing, since walking is becoming more and more popular due to the concerns of transportation environmental impacts and increasing travel demand in urban areas (Ma et al., 2015; Zhang et al., 2018, 2019; Akyol et al., 2020). From the perspective of safety, integrating pedestrians' access in signal timing is nonnegligible. Data from the National Highway Traffic Safety Administration (2019) shows that there were a total of 6,283 pedestrian fatalities in the United States in 2018, which represents an over 3% increase from 2017 and the most fatalities since 1990. The risk of pedestrian injuries or fatalities is a significant problem in our transportation systems, which is espe-

cially elevated at intersections where vehicle-pedestrian interactions occur. Therefore, it is important to consider pedestrian access at intersections, especially for the disabled, children, and elderly (Leden et al., 2006; Cafiso et al., 2011; Khosravi et al., 2018). From the point of sustainability and urban planning, promoting walking can result in health benefits (Heinrichs and Jarass, 2020; Tang et al., 2021; Park and Garcia, 2020). As the critical point to walking accessibility, crosswalks at the intersection provide the connections between sidewalks. Safety and continuous walking space encourage citizens to walk more, which further promotes sustainable development for the metropolises. Therefore, this context motivates us to find a better signal timing method to provide more friendly signal strategies for pedestrians and serve more vehicles in the urban area.

Many past papers considered public transit and pedestrians in traffic signal optimization problems, and their proposed methods could reduce buses and pedestrians' travel time, queue length, and delay to some extent. Most of these papers modeled the traffic optimization as mixed-integer programming and simulated on a signal intersection or a signal urban corridor, which ignored the network-level performance. Furthermore, since most of them belong to centralized signal control (Manolis et al., 2018), these traffic controllers would coordinate adjacent intersections to achieve better but are hard to implement in urban networks due to high computation time.

Most of the distributed signal controls try to solve the network implementation problem but under vehicle-only scenarios. Although Chen et al. (2020) considered pedestrian access, they modeled autonomous intersection control and not traffic signals. Therefore, MP control with pedestrian access in the human-driven vehicle environment is an open problem. To balance vehicle stability and pedestrians' waiting time, we modify Varaiya (2013)'s max-pressure policy to ensure the maximum throughput of vehicles and with bounded waiting times for pedestrians.

The contributions of this chapter are as follows: (1) We modify Varaiya (2013)'s max-pressure control policy to include pedestrian access. (2) We design dynamic queueing

models for vehicles and pedestrians. (3) We formulate a conflict region constructor, which is inspired by autonomous intersection control, for the proposed max-pressure policy to model the conflicts between vehicles and pedestrians. Our proposed conflict region logic can be implemented for some irregular network and intersections. (4) We analytically prove the max-pressure control policy considering pedestrians can also achieve maximum throughput at the network level. (5) We implement our simulation using the well-known Sioux Falls network with an added pedestrian network for the first time.

3.2 Literature review

3.2.1 Traffic signal control including pedestrians' access

It is worth mentioning that compared with vehicle traffic, pedestrian traffic is far more complex and random (Ma et al., 2015; He et al., 2012, 2014), especially at intersections. For instance, they have random routes around intersections and may expose themselves to vehicles. Researchers have been focusing on pedestrians' movements for a long time, with some of them focusing on providing convenient infrastructure for children, the elderly, and the disabled since they have lower walking speeds (Leden et al., 2006; Cafiso et al., 2011; Khosravi et al., 2018). Some researchers want to provide better walking spaces in the cities from the perspective of urban planners (Hooper et al., 2018). A walkable city (city with enough walking spaces) has many benefits, such as social, environmental, and economic benefits. Specifically, a city that has better walking space can encourage residents embrace walking rather than driving a vehicle, which makes people have more connections and reduces greenhouse gas emissions (Li et al., 2023; Liang et al., 2023). Recently, many urban planners who focus on public spaces proposed that we should balance street space for pedestrians and vehicles (Win). They proposed three ways to balance street space: (1) Improving pedestrian flow (2) Providing space for pedestrian amenities (3) Making it easier

to cross the street. The first and third points are determined by the traffic signal controller. Akyol et al. (2020) proposed an adaption of the original split, cycle, and offset optimization technique (SCOOT) to accommodate vehicle and pedestrians traffic. Using simulations in PTV-VISSIM, they found that a trade-off exists between pedestrian travel time and vehicle delay. Ma et al. (2015) established quantitative standards, which consider safety and efficiency trade-off factors for selecting pedestrian phases for signalized intersections, and results showed that their technology can select pedestrian phases properly. Zhang et al. (2018) provided a traffic light scheduling model for pedestrians-vehicles mixed-flow traffic environment. The proposed model is a mixed-integer linear program which can achieve a good balance between pedestrian demand and vehicle demand. Zhang et al. (2019) also formulated a more realistic model, the pedestrian-safety-aware traffic light strategy, in which pedestrian arrival flow and leaving flow are separately described. Based on a genetic algorithm (GA) and the harmony search, their model has better performance than traditional adaptive signal control methods.

Some researchers started to give more attention to future traffic environments with pedestrian access. Xu et al. (2022a) pointed out that although vision technologies can be applied to intersection control that integrates pedestrian access, the movement of pedestrians is hard to determine. To solve this problem, they suggested that 6G localization and tracking services offer traffic engineers new opportunities and then proposed a traffic signal control policy for pedestrians and vehicles under 6G future technology. He et al. (2012) leveraged the advantage of online data to identify the vehicle platoon and combine the request from special vehicles (public transit) to formulate a mathematical programming problem to predict future signal states. Although they did mention pedestrian access, they modeled requests for special vehicles by replacing with pedestrian crossing requests. Jin et al. (2021) proposed a deep-learning-based method for pedestrian detection in crowd management. He et al. (2014) proposed a multi-model traffic signal control policy including signal actuation and coordination, which includes pedestrian access. They built simula-

tions on a corridor and found that their method can reduce pedestrian delay and average passenger delay. However, most of these papers tried to model traffic signal optimization problems as mixed-integer programs, which are computationally difficult to implement at the network-level.

3.2.2 Max-pressure signal control

Chen et al. (2020) is the first paper that incorporated pedestrians and MP-based signal control, but their proposed method was only suitable for the environment of fully autonomous vehicles (non-signal structure) and the simulation was implemented on a grid-based network without considering realistic pedestrian phase design. Inspired by the aforementioned research and the demand for pedestrians' intersection access, we extend the max-pressure policy to consider the access of pedestrians in the realistic network.

3.3 Problem formulation

3.3.1 Math notations

Table 3.1: Notation.

$\mathcal{M}$	Set of movements (Vehicle movements $\mathcal{M}^{\mathrm{v}}$, pedestrian movement $\mathcal{M}^{\mathrm{p}}$)
$\mathcal{N}$	Set of nodes (Including vehicle nodes $\mathcal{N}^{\mathrm{v}}$ and pedestrian nodes $\mathcal{N}^{\mathrm{p}}$)
$\mathcal{A}$	Set of links (Including vehicle links $\mathcal{A}^{\mathrm{v}}$ and pedestrian links $\mathcal{A}^{\mathrm{p}}$)
Γ_j^+	Set of outgoing links
Γ_j^-	Set of incoming links
$x_{ij}^{\mathrm{v}}(t)$	Number of vehicles of the movement from link i to link j at time step t
$r_{ij}^{\mathrm{v}}(t)$	Proportion of vehicles entering i that will next move to j.
$r_{ij}^{\mathrm{p}}(t)$	Proportion of pedestrians entering i that will next move to j.
$w_{ij}^{\mathrm{v}}(t)$	Weight of vehicle turning movement from link i to link j at time step t
$d_i^{\mathrm{p}}(t)$	Pedestrian demand at entry link i
$d_i^{\mathrm{v}}(t)$	Vehicle demand at at entry link i
$s_{ij}(t)$	Actuation of turning movement from link i to link j at time step t
$y_{ij}^{\mathrm{v}}(t)$	Signal control vehicle flow from link i to link j at time step t
$s_{mb}(t)$	Actuation of crosswalk from pedestrian link m to b at time step t
$y_{ij}^{\mathrm{v}}(t)$	Signal control vehicle flow from link i to link j at time step t
$y_{ij}^{\mathrm{p}}(t)$	Signal control number of pedestrians from link i to link j at time step t
Q_{ij}^{v}	Capacity of turning movement for private vehicles from link i to link j
Q_c	Capacity of conflict region
α_{ij}^b	0–1 binary dummy variable ($\alpha_{ij}^b = 1$ when vehicles have conflict with crosswalk b)
f_i^{v}	Average vehicle traffic volume of link i.

3.3.2 Road network model with pedestrian access

Consider an urban network $\mathcal{G} = (\mathcal{N}, \mathcal{A})$ with nodes $\mathcal{N}$ and links $\mathcal{A}$. We separate the urban network into the vehicle network $\mathcal{G}^{\mathrm{v}} = (\mathcal{N}^{\mathrm{v}}, \mathcal{A}^{\mathrm{v}})$ and the pedestrian network $\mathcal{G}^{\mathrm{p}} = (\mathcal{N}^{\mathrm{p}}, \mathcal{A}^{\mathrm{p}})$, since vehicles move alone the road and pedestrians move through the sidewalks and crosswalks, and they will interact with each other at intersections. Nodes represent intersection locations. Nodes $\mathcal{N}$ are divided into vehicle nodes (intersections) $\mathcal{N}^{\mathrm{v}}$ and pedestrian nodes (intersections) $\mathcal{N}^{\mathrm{p}}$. The link set $\mathcal{A}$ is divided into three subsets, which are the entry link set $\mathcal{A}_e$, the internal link set $\mathcal{A}_i$, and the exit link set $\mathcal{A}_o$. Specifically, entry link set $\mathcal{A}_e$ can be divided into pedestrian entry links $\mathcal{A}_e^{\mathrm{p}}$ and vehicle entry links $\mathcal{A}_e^{\mathrm{v}}$, internal link set $\mathcal{A}_i$ are composed by vehicle internal links and $\mathcal{A}_i^{v}$ and pedestrian internal links $\mathcal{A}_i^{\mathrm{p}}$, and exit link set $\mathcal{A}_e$ are composed by vehicle exit links and $\mathcal{A}_e^{\mathrm{v}}$ and pedestrian exit links $\mathcal{A}_e^{\mathrm{p}}$. Note that entry links and exit links are not realistic links, which are used for loading and removing vehicles and pedestrians. Entry links are the links where pedestrians and vehicles can enter the network, which are modeled as point queues. Exit links are the sink links where pedestrians and vehicles leave the network once they reach their destination nodes

For the vehicle network $\mathcal{G}^{\mathrm{v}} = (\mathcal{N}^{\mathrm{v}}, \mathcal{A}^{\mathrm{v}})$, internal links $\mathcal{A}_i^{\mathrm{v}}$ connect the intersections located inside the vehicle network. We define $\mathcal{M}$ be the set of all turning movements in the network. We use Γ_i^+ and Γ_j^+ to represent the sets of outgoing links and incoming links of nodes (intersections) respectively. One turning movement is a combination of two links. For instance, (i, j) and (j, k) are two movements respectively. Let $x_{ij}^{\mathrm{v}}(t)$ be the number of vehicles on link i waiting to move to link j. Let $d_i^{\mathrm{v}}(t)$ be the vehicles' demand entering the network on link $i \in \mathcal{A}_e$ at time t, which are an independent identically distributed random variabled with average value $\bar{d}_i^{\mathrm{v}}$. Turning proportion $r_{jk}^{\mathrm{v}}(t)$ is the proportion of vehicles entering link j that will next move to link k at time t, which are independent identically distributed random variables with mean $\bar{r}_{ij}^{\mathrm{v}}$. Usually, the turning proportions

can be obtained from historical travel data. We separate the vehicle queues on the link by turning movements like previous work (Varaiya, 2013).

For the pedestrians network $\mathcal{G}^{\mathrm{p}} = (\mathcal{N}^{\mathrm{p}}, \mathcal{A}^{\mathrm{p}})$, the pedestrian links represent the sidewalks and crosswalks. Note that pedestrian nodes (intersections) $\mathcal{N}^{p}$ are not the physical intersections, but rather the nodes to connect sidewalks and crosswalks. Let $x_{ij}^{\mathrm{p}}(t)$ be the number of pedestrians on link i waiting to move to link j. Let $d_i^{\mathrm{p}}(t)$ be the pedestrian demand entering the network on link $i \in \mathcal{A}_e$, which are independent identically distributed random variables with average value $\bar{d}_i^{\mathrm{p}}$. Turning proportion $r_{ij}^{\mathrm{p}}(t)$ determines the proportion of pedestrians entering link i that will next move to link j, which are also independent identically distributed random variables with mean $\bar{r}_{ij}^{\mathrm{p}}$. Turning proportion $r_{ij}^{\mathrm{p}}(t)$ determines the proportion of pedestrians entering i that will next move to j, which are independent identically distributed random variables with mean $\bar{r}_{ij}^{\mathrm{p}}$. To focus on the impacts of signal control for pedestrians, we set the speed for pedestrians as constant and the capacity as infinite, which is similar to the point queue model for pedestrian propagation.

To model the vehicle and pedestrian conflicts, we use α_{ij}^{b} to indicate whether the vehicle turning movements (i, j) conflict with pedestrians' movement when pedestrians want to move across the crosswalk b. For vehicles moving through the intersections, the capacity of the conflict region is Q_c, which is determined by the capacities of turning movements, $Q_c = \max_{(i,j)|c \in C_{ij}}\{Q_{ij}\}$. The total number of vehicles driving through one conflict region per time is bounded by the capacity of the conflict region.

3.3.3 Vehicle queueing model

To calculate the vehicle queueing propagation in the network under discretized time, we use the store-and-forward model of Varaiya (2013). Vehicle queueing evolution along the internal link can be represented by the following equations:

[

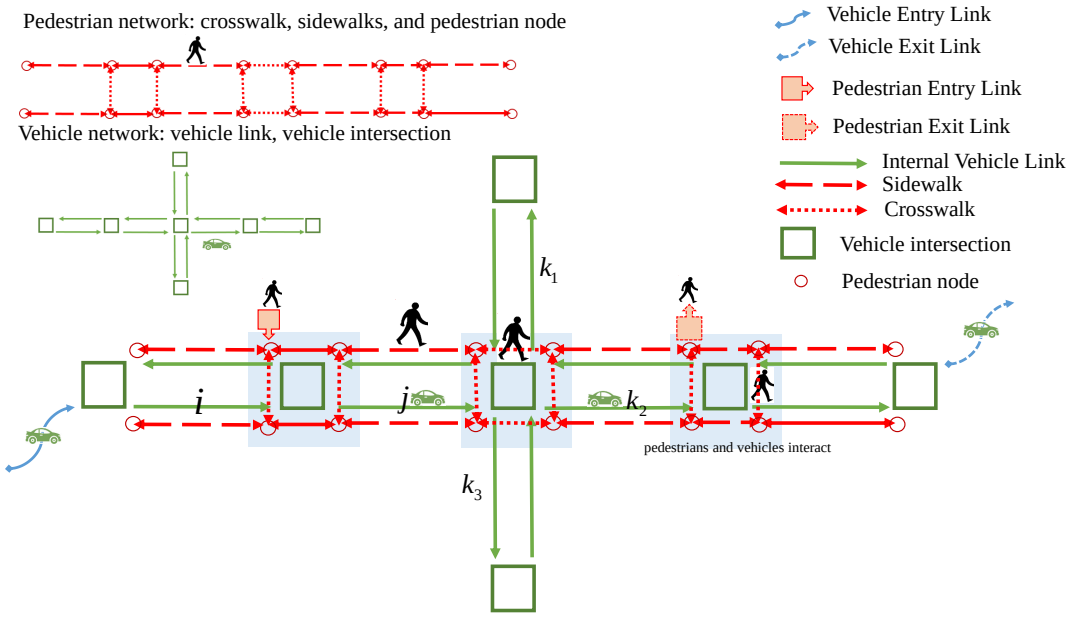

Figure 3.1: Network with pedestrian access

$$x_{ij}^{\mathrm{v}}(t+1) = x_{ij}^{\mathrm{v}}(t) - y_{ij}^{\mathrm{v}}(t) + \sum_{(i,j,h)\in(\mathcal{A}^{\mathrm{v}})^3} y_{hi}^{\mathrm{v}}(t) \times r_{ij}^{\mathrm{v}}(t) \tag{3.1}$$

where $y_{ij}^{\mathrm{v}}(t)$ is the signal controlled flow that start from link i then travels to link j. Vehicle flow conservation also applies to entry links with the following equation:

$$x_{ij}^{\mathrm{v}}(t+1) = x_{ij}^{\mathrm{v}}(t) - y_{ij}^{\mathrm{v}}(t) + d_{i}^{\mathrm{v}}(t) \times r_{ij}^{\mathrm{v}}(t) \tag{3.2}$$

The activation of vehicle turning movement (i, j) is denoted by $s_{ij}(t) \in \{0, 1\}$. The value of $y_{ij}^{\mathrm{v}}(t)$ is determined by the following equation

$$y_{ij}^{\mathrm{v}}(t) = \min\left\{Q_{ij}^{\mathrm{v}} s_{ij}(t), x_{ij}^{\mathrm{v}}(t)\right\} \tag{3.3}$$

where Q_{ij}^{v} is the capacity of turning movement from link i to link j. Specifically, $Q_{ij}^{\mathrm{v}} = \min(Q_i^{\mathrm{v}}, Q_j^{\mathrm{v}})$, is the maximum flow of vehicle movement (i, j). Note that capacity is the maximum road throughput, which we assume to be constant for each link.

3.3.4 Pedestrian queueing model

To track the propagation of pedestrians queueing in the network, we construct a store-and-forward queueing model, which is also inspired by Varaiya (2013).

$$x_{ij}^{\mathrm{p}}(t+1) = x_{ij}^{\mathrm{p}}(t) - y_{ij}^{\mathrm{p}}(t) + \sum_{(i,j,h)\in(\mathcal{A}^{\mathrm{p}})^3} y_{hi}^{\mathrm{p}}(t) \times r_{ij}^{\mathrm{p}}(t) \tag{3.4}$$

where $y_{ij}^{\mathrm{P}}(t)$ is the flow of pedestrians from i to j at time t, which is controlled by intersection signal. Flow conservation also applies to entry links of pedestrians, but entering flow is determined by the demand $d_i^{\mathrm{P}}(t)$.

$$x_{ij}^{\mathrm{p}}(t+1) = x_{ij}^{\mathrm{p}}(t) - y_{ij}^{\mathrm{p}}(t) + d_i^{\mathrm{p}}(t) \times r_{ij}^{\mathrm{p}}(t) \tag{3.5}$$

We assume that for entry link $i \in \mathcal{A}_e^{\mathrm{p}}$, $d_i^{\mathrm{p}}(t)$ are independent identically distributed random variables with mean $\bar{d}_i^{\mathrm{p}}$. We further assume $d_i^{\mathrm{p}}(t)$ has maximum value $\tilde{d}_i^{\mathrm{p}}$. Note that Varaiya (2013) did not consider the pedestrian access, but we will include the phases that consider the pedestrian and vehicle access for the intersection controls. There should be some feasible control that can accommodate pedestrian movements without conflict with

vehicles, which will be introduced in Section 3.4.

$$y_{ij}^{\mathrm{p}}(t) = \begin{cases} 0 & s_{ij}(t) = 0 \\ x_{ij}^{\mathrm{p}}(t) & s_{ij}(t) = 1 \end{cases} \tag{3.6}$$

specifically, we assume the capacity for pedestrian movements is infinity, so we can move all the number of pedestrians once they are allowed to move, and we use $s_{mb}(t)$ to denote whether crosswalks are activated or not as described in Section 3.4. Based on the conflict logic, pedestrians can move when they do not have conflicts with vehicles, or when crosswalks are forced to activate for pedestrian cross-movements.

3.3.5 Feasible signal control including pedestrian access

The activation of turning movement (i, j) for vehicles and pedestrians is denoted by $s_{ij}(t) \in \{0, 1\}$. $s_{ij}(t) = 1$ means movement (i, j) gets a green light, and $s_{ij}(t) = 0$ means that movement (i, j) gets a red light. Note that when pedestrian movements do not conflict with vehicle movements, pedestrians can still walk across the intersection. Specifically, we define pedestrian cross-movements (walking through the crosswalks) as (m, n), which are a subset of all pedestrian movements (i, j) (including cross-movements, and sidewalk-movements).

Let $S_n(t)$ be an intersection matrix for intersection n that include the movement of pedestrians and vehicles. We can define the intersection control sequence $S_n = \{S_n(t), t \in T\}$. Let $\mathcal{S}$ be a set that includes all feasible network control matrices for all intersections, and let $\mathcal{S}_n$ be the set of all feasible intersection matrices for intersection n. We denote the convex hull of all feasible signal control matrices as $Conv(\mathcal{S})$. Since we need to consider pedestrian access, Figure 3.2 shows a detailed explanation of feasible signal control including pedestrian access. Pedestrians can walk through crosswalks (crosswalks are activated)

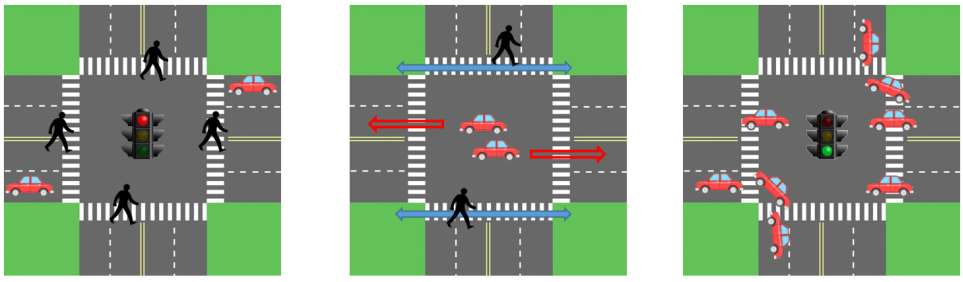

Figure 3.2: Traffic signal design with pedestrian access

when they do not have conflicts with the vehicle movements. Note that in this dissertation, vehicle movements are determined by signal phase, but Chen et al. (2020) used autonomous intersection management, which lacked signal phases.

To consider pedestrian access in the signal control, we define the activation indicator for the pedestrian cross-movement (m, b) as $s_{mb}(t)$. We keep track the pedestrian waiting time by $\phi_{mb}(t)$, that is

$$\phi_{mb}(t+1) = \begin{cases} \phi_{mb}(t) + 1 & s_{mb}(t) = 0 \\ 0 & s_{mb}(t) = 1 \end{cases} \tag{3.7}$$

We set a maximum tolerance time, $\hat{\phi}_{mb}$, which should be tested under different value settings, and we assume this number is exogenous and does not vary with time.

The pedestrian waiting time for cross-movement (m, b) at time step t is denoted as $\phi_{mb}(t)$. When the difference between pedestrian waiting time and maximum tolerance time is larger than zero, $s_{mb}(t)$ is forced to be set to 1 to activate the crosswalk for (m, b). The following equation gives a constant on the activation of pedestrian cross-movement (m, b) based on the tolerance time:

$$(1 - s_{mb}(t)) \left(\phi_{mb}(t) - \hat{\phi}_{mb} \right) \leq 0 \tag{3.8}$$

as a consequence, we are forced to activate the crosswalk at once every $\hat{\phi}_{mb}$ time steps.

When the pedestrian waiting time is less than the maximum tolerance time, $s_{mb}(t)$ could be 0 or 1, but this should depend on whether it conflicts with vehicles. The following equations represent the relationship between vehicles and pedestrians:

$$s_{mb}(t) \leq 1 - s_{ij}(t)\alpha_{ij}^{b} \tag{3.9}$$

where $\alpha_{ij}^{b} \in \{0, 1\}$ indicates whether vehicle movement (i, j) intersects with crosswalk b.

Overall, we are able to obtain feasible signal control $s_{ij}(t)$ that includes pedestrian movements and vehicle movements. For any given intersection control sequence, the long-term average time used for serving vehicle movement (i, j) including pedestrian access, can be calculated by equation (5.4). Let $\bar{\mathbf{s}}$ and $\mathbf{s}(t)$ be the vectors of $\bar{s}_{ij}$ and $s_{ij}(t)$ respectively:

$$\bar{s}_{ij} = \lim_{T \to \infty} \frac{1}{T} \sum_{t=1}^{T} s_{ij}(t) \tag{3.10}$$

The convex hull of all feasible signal control matrices $\mathcal{S}$ is given by the following equation:

$$Conv(\mathcal{S}) = \left\{ \sum_{s \in \mathcal{S}} \lambda_s S \middle| \lambda_s S \leq 0, \sum \lambda_s = 1 \right\} \tag{3.11}$$

Then we can find a set $\mathbb{S} \subset conv(\mathcal{S})$, which is the set of average control calculated by

equation (5.4) where $\mathbf{s}(t)$ satisfies pedestrian access constrains (3.7)–(3.9). After that, we can give Proposition 1, which is needed for the proof of stability.

Proposition 5. *If $\mathbf{s}(t) \in \mathcal{S}$ and $\mathbf{s}(t)$ satisfies pedestrian access constraints (3.7)–(3.9) then there exists a $\bar{\mathbf{s}} \in \mathbb{S}$ such that*

$$\bar{\mathbf{s}} = \lim_{T\to\infty} \frac{1}{T} \sum_{t=1}^{T} \mathbf{s}(t) \tag{3.12}$$

Proof. First, we prove that $\bar{\mathbf{s}}$ is in the convex hull of $\mathbb{S}$. For any T, Let $T \times \lambda_{\mathbf{s}}$ be the duration of time steps so that $\mathbf{s}(t) = \mathbf{s}$. Since $\mathbf{s}(t) \in \mathcal{S}$ and $\mathbf{s}(t)$ satisfies constraints (3.7)–(3.9), $\sum_{\mathbf{s}} T\lambda_{\mathbf{s}} = T$, so $\sum_{\mathbf{s}} \lambda_{\mathbf{s}} = 1$ is the proportions of time spent in each phase. Therefore, we define the indicator function as

$$\mathbb{I}(\mathbf{s}(t) = \mathbf{s}) \begin{cases} 1 & \text{if } \mathbf{s}(t) = \mathbf{s} \\ 0 & \text{if } \mathbf{s}(t) \neq \mathbf{s} \end{cases} \tag{3.13}$$

Then we have

$$\bar{\mathbf{s}} = \lim_{T\to\infty} \frac{1}{T} \sum_{t=1}^{T} \mathbf{s}(t) \tag{3.14}$$

$$= \lim_{T\to\infty} \frac{1}{T} \sum_{t=1}^{T} \sum_{\mathbf{s}} \mathbb{I}(\mathbf{s}(t) = \mathbf{s})\mathbf{s} \tag{3.15}$$

$$= \lim_{T\to\infty} \frac{1}{T} \sum_{t=1}^{T} \sum_{\mathbf{s}\in\mathcal{S}} T\lambda_{\mathbf{s}}\mathbf{s} \tag{3.16}$$

$$= \sum_{\mathbf{s}\in\mathcal{S}} \lambda_{\mathbf{s}}\mathbf{s} \tag{3.17}$$

Since $\bar{\mathbf{s}} \in \mathbb{S}$, there exists a $\lambda_{\mathbf{s}}$ satisfying $\sum_{\mathbf{s}\in\mathcal{S}} \lambda_{\mathbf{s}} = 1$ such that

$$\bar{\mathbf{s}} = \sum_{\mathbf{s}\in\mathcal{S}} \lambda_{\mathbf{s}}\mathbf{s} \tag{3.18}$$

3.3.6 Stable network

Stability means the ability/capacity of network-level signal controls to serve all demand in the transportation network. This dissertation only concentrates on the stability of vehicles, not of pedestrians, but we will activate pedestrian phases after a certain duration, $\hat{\phi}_{mb}$, to make sure that pedestrians can move through the network, which is introduced in Section 3.4. Hence, we define the *stability* of the network mathematically as follows when the signal control included pedestrian access:

Definition 2. *The network is strongly stable if the number of vehicles in the network is bounded in expectation, i.e. there exists a $\kappa < \infty$ such that*

$$\lim_{T\to\infty} \sup \left\{ \frac{1}{T} \sum_{t=1}^{T} \sum_{(i,j)\in\mathcal{A}^2} \mathbb{E}\{x_{ij}^{\mathrm{v}}(t)\} \right\} \leq \kappa \tag{3.19}$$

Since we can easily find a large demand rate such that no traffic control policy can serve it, it is essential to define the network stable region to prove maximum stability.

3.3.7 Stable region

MP control aims to stabilize any vehicle demand that could be stabilized by any other signal control. To prove the maximum stability property, we must define analytically the set of vehicle demands that could be stabilized. In reality, the demand for vehicles is stochastic

and the stable region is defined in terms of the average demand rates $\bar{\mathbf{d}}^{\mathrm{v}}$ to help us prove the maximum stability. Let $\mathbf{f}^{\mathrm{v}}$ be the average volume of vehicles on link i. For entry links, we have the following relationship:

$$f_i^{\mathrm{v}} = \bar{d}_i^{\mathrm{v}} \tag{3.20}$$

For internal links of vehicles, f_i^{v} can be determined by conservation of flow, which means the total flow on the downstream link are determined from all flow that on upstream link moving to the downstream link:

$$f_j^{\mathrm{v}} = \sum_{i \in \mathcal{A}_{\mathrm{v}}} f_i^{\mathrm{v}} \bar{r}_{ij}^{\mathrm{v}} \tag{3.21}$$

By Proposition 1 of Varaiya (2013), for every demand rate $\bar{\mathbf{d}}^{\mathrm{v}}$ and turning proportions $\bar{\mathbf{r}}^{\mathrm{v}}$, there exists an unique average flow vector $\mathbf{f}^{\mathrm{v}}$. In this study, the network can be stabilized if the average vehicle flow can still be served by some traffic signals considering the access of pedestrian movements. That is, there must exist an average signal activation $\bar{\mathbf{s}} \in \mathbf{S}$. It is crucial to mention that the size of the stable region in this study is smaller compared with Varaiya (2013)'s stable region, since the feasible signal phases for vehicles will be restricted by the access of pedestrian's movements by constraints equations (3.7)–(3.9). Specifically, $\bar{\mathbf{s}}$ in Varaiya (2013) are used for vehicles only, but $\bar{\mathbf{s}}$ in this research are forced to close for the activation of pedestrians movement at least every $\hat{\phi}_{mb}$ time steps.

$$f_i^{\mathrm{v}} \bar{r}_{ij}^{\mathrm{v}} \leq \bar{s}_{ij} Q_{ij}^{\mathrm{v}} \tag{3.22}$$

where $\bar{s}_{ij}$ can be obtained from equation (5.4), based on some feasible signal control that

follows pedestrian access constraints (3.7)–(3.9).

Let $\mathcal{D}$ be the set of all feasible demand vectors of vehicles $\bar{\mathrm{d}}^{\mathrm{v}}$ which satisfy constraints (5.20)–(5.22). Let $\mathcal{D}^0$ be the interior of $\mathcal{D}$, where constraints (5.22) hold with strict inequality. Then there exists an $\epsilon > 0$ such that

$$f_i^{\mathrm{v}} \bar{r}_{ij}^{\mathrm{v}} - \bar{s}_{ij} Q_{ij}^{\mathrm{v}} \leq -\epsilon \tag{3.23}$$

Proposition 6. *If $\bar{\mathrm{d}} \notin \mathcal{D}^0$, then it is impossible to find a stabilizing control.*

Proof. If the network is unstable, the vehicle's movement flow is greater than the traffic signal control policy that can serve. Since $\bar{\mathrm{d}}^{\mathrm{v}}$, $\forall \bar{s}_{ij} \in \mathcal{S}$, there exists a $\theta > 0$ and at least one turning movement (i, j) satisfying $f_j^{\mathrm{v}} \bar{r}_{ij}^{\mathrm{v}} \geq \bar{s}_{ij} Q_{ij}^{\mathrm{v}} + \theta$.

Based on equation (5.1) we have

$$x_{ij}^{\mathrm{v}}(t+1) - x_{ij}^{\mathrm{v}}(t) = \sum_{(i,j,h) \in (\mathcal{A}^{\mathrm{v}})^3} y_{hi}^{\mathrm{v}}(t) \times r_{ij}^{\mathrm{v}}(t) - y_{ij}^{\mathrm{v}}(t) \tag{3.24}$$

Based on equation (3.24) we can obtain the following relationship:

$$\begin{aligned}
&\mathbb{E}\left[\sum_{t=0}^{\tau-1} \sum_{(i,j) \in \mathcal{A}^{\mathrm{v}\,2}} \left(x_{ij}^{\mathrm{v}}(t+1) - x_{ij}^{\mathrm{v}}(t)\right)\right] \\
&= \mathbb{E}\left[\sum_{(i,j) \in \mathcal{A}^{\mathrm{v}\,2}} \left(x_{ij}^{\mathrm{v}}(\tau) - x_{ij}^{\mathrm{v}}(0)\right)\right] \qquad (3.25) \\
&= \mathbb{E}\left[\sum_{t=0}^{\tau-1} \sum_{(i,j,h) \in (\mathcal{A}^{\mathrm{v}})^3} \left(y_{hi}^{\mathrm{v}}(t) r_{ij}^{\mathrm{v}}(t) - y_{ij}^{\mathrm{v}}(t)\right)\right] \qquad (3.26)
\end{aligned}$$

$$= \mathbb{E}\left[\sum_{(i,j)\in\mathcal{A}^{\mathrm{v}\,2}} \left(f_j^{\mathrm{v}}\bar{r}_{ij}^{\mathrm{v}} - \bar{s}_{ij}Q_{ij}^{\mathrm{v}}\right)\right] \tag{3.27}$$

$$\geq \mathbb{E}\left[\tau\theta\right] = \tau\theta \tag{3.28}$$

Moving $x_{ij}^{\mathrm{v}}(0)$ to the right hand side, we obtain:

$$\mathbb{E}\left[\sum_{(i,j)\in\mathcal{A}^{\mathrm{v}\,2}} x_{ij}^{\mathrm{v}}(\tau)\right] \geq \theta\tau + \mathbb{E}\left[\sum_{(i,j)\in\mathcal{A}^{\mathrm{v}\,2}} x_{ij}^{\mathrm{v}}(0)\right] \tag{3.29}$$

or equivalently

$$\mathbb{E}\left[|\mathbf{x}^{\mathrm{v}}(\tau)|\right] \geq \theta\tau + \mathbb{E}\left[|\mathbf{x}^{\mathrm{v}}(0)|\right] \tag{3.30}$$

From equation (3.30), we obtain

$$\begin{aligned}\lim_{T\to\infty}\mathbb{E}\left[\frac{1}{T}\sum_{t=1}^{T}|\mathbf{x}^{\mathrm{v}}(t)|\right] &\geq \lim_{T\to\infty}\mathbb{E}\left[\frac{1}{T}\sum_{t=1}^{T}\left[\theta t + \mathbb{E}\left[|\mathbf{x}^{\mathrm{v}}(0)|\right]\right]\right] \\ &= \lim_{T\to\infty}\mathbb{E}\left[\frac{1}{T}\sum_{t=1}^{T}(\theta t)\right] + \lim_{T\to\infty}\mathbb{E}\left[\frac{1}{T}\sum_{t=1}^{T}[|\mathbf{x}^{\mathrm{v}}(0)|]\right] = \infty\end{aligned} \tag{3.31}$$

which violates equation (5.19).

3.3.8 Stability analysis based on the average signal control

Now we need to prove that the average signal control including pedestrian access will stabilize any demand vectors $\bar{\mathbf{d}} \in \mathcal{D}^0$. This is a prerequisite for the MP control to achieve maximum stability, since if there exits no average signal control including pedestrian access can stabilize any demand vectors $\bar{\mathbf{d}} \in \mathcal{D}^0$, MP control can not stabilize the network either. In addition, any demand $\bar{\mathbf{d}} \notin \mathcal{D}$ cannot be stabilized by Proposition 6, and this essentially proves that the average signal control can achieve stability. The only excluded demand is on the boundary of $\mathcal{D}$, for which the Markov chain can be shown to be null recurrent but not positive recurrent. Note that we only consider the stability of vehicles because pedestrians can move once the tolerance time is reached.

Lemma 4. *When $\bar{\mathbf{d}} \in \mathcal{D}^0$, there exists a Lyapunov function $\nu(t) \geq 0$ and constants $\kappa < \infty$, $\epsilon > 0$ such that*

$$\mathbb{E}\left[\nu(t+1) - \nu(t) | \, \mathbf{x}(t)\right] \leq \kappa - \epsilon |\mathbf{x}(t)| \tag{3.32}$$

Proof. To calculate the queue length at time $t+1$, we apply the vehicle queueing models shown in equation (5.1)–(5.3). Then, let $\delta_{ij}(t)$ be the difference of the queueing length of vehicles between time steps t and time steps $t+1$.

$$\begin{aligned}
\delta_{ij}(t) &= x_{ij}^{\mathrm{v}}(t+1) - x_{ij}^{\mathrm{v}}(t) \\
&= -\min\left\{Q_{ij}^{\mathrm{v}} s_{ij}(t), x_{ij}^{\mathrm{v}}(t)\right\} \\
&\quad + \sum_{h \in \mathcal{A}_i^-} \min\left\{Q_{hi}^{\mathrm{v}} s_{ij}(t), x_{hi}^{\mathrm{v}}(t)\right\} \times r_{ij}^{\mathrm{v}}(t) \quad \forall i \in \mathcal{A}_{\mathrm{i}}, j \in \Gamma_i^+
\end{aligned} \tag{3.33}$$

$$\delta_{ij}(t) = x^{\mathrm{v}}_{ij}(t+1) - x^{\mathrm{v}}_{ij}(t) = -\min\left\{Q^{\mathrm{v}}_{ij} s_{ij}(t), x^{\mathrm{v}}_{ij}(t)\right\} + d^{\mathrm{v}}_i(t) \times r^{\mathrm{v}}_{ij}(t) \quad \forall i \in \mathcal{A}_{\mathrm{e}}, j \in \Gamma^+_i \tag{3.34}$$

Let $\mathbf{x}^{\mathrm{v}}(t)$ be the matrix including all queue length of private vehicles. Hence we consider the Lyapunov function $\nu(t)$:

$$\nu(t) = \left|\mathbf{x}^{\mathrm{v}}(t)\right|^2 = \sum_{(i,j)\in\mathcal{A}^2} \left(x^{\mathrm{v}}_{ij}(t)\right)^2 \tag{3.35}$$

Then we expand the difference $\nu_1(t+1) - \nu_1(t)$:

$$\nu(t+1) - \nu(t) = \left|\mathbf{x}^{\mathrm{v}}(t+1)\right|^2 - \left|\mathbf{x}^{\mathrm{v}}(t)\right|^2 = \left|\mathbf{x}^{\mathrm{v}}(t) + \boldsymbol{\delta}(t)\right|^2 - \left|\mathbf{x}^{\mathrm{v}}(t)\right|^2 = 2\mathbf{x}^{\mathrm{v}}(t)^{\mathrm{T}}\boldsymbol{\delta}(t) + \left|\boldsymbol{\delta}(t)\right|^2 \tag{3.36}$$

The first term of equation (5.28) can be rewritten as:

$$\begin{aligned}
2\mathbf{x}^{\mathrm{v}}(t)^{\mathrm{T}}\boldsymbol{\delta}(t) =& -2x^{\mathrm{v}}_{ij}(t) \sum_{i\in\mathcal{A}} \sum_{j\in\Gamma^+_i} \min\left\{Q^{\mathrm{v}}_{ij} s_{ij}(t), x^{\mathrm{v}}_{ij}(t)\right\} \\
&+ 2 \sum_{h\in\Gamma^-_i} \sum_{i\in\mathcal{A}} \sum_{j\in\Gamma^+_i} x^{\mathrm{v}}_{ij}(t) \min\left\{Q^{\mathrm{v}}_{hi} s_{hi}(t), x^{\mathrm{v}}_{hi}(t)\right\} r^{\mathrm{v}}_{ij}(t) \\
&+ 2 \sum_{i\in\mathcal{A}_{\mathrm{e}}} \sum_{j\in\Gamma^+_i} \left(-\min\left\{Q^{\mathrm{v}}_{ij} s_{ij}(t), x^{\mathrm{v}}_{ij}(t)\right\} + d^{\mathrm{v}}_i(t) \times r^{\mathrm{v}}_{ij}(t)\right) \qquad (3.37) \\
=& 2 \sum_{i\in\mathcal{A}_{\mathrm{i}}\cup\mathcal{A}_{\mathrm{e}}} \sum_{j\in\Gamma^+_i} \min\left\{Q^{\mathrm{v}}_{ij} s_{ij}(t), x^{\mathrm{v}}_{ij}(t)\right\} \left(-x^{\mathrm{v}}_{ij}(t) + \sum_{k\in\Gamma^+_i} r^{\mathrm{v}}_{jk}(t) x^{\mathrm{v}}_{jk}(t)\right) \\
&+ 2 \sum_{i\in\mathcal{A}_{\mathrm{e}}} \sum_{j\in\Gamma^+_i} d^{\mathrm{v}}_i(t) \times r^{\mathrm{v}}_{ij}(t) \times x^{\mathrm{v}}_{ij}(t) \qquad (3.38)
\end{aligned}$$

We replace the turning proportion $r_{ij}^{\mathrm{v}}(t)$ with average value $\bar{r}_{ij}^{\mathrm{v}}$, since $\lim_{T\to\infty}\frac{1}{T}\sum_{t=1}^{T}\sum_{(i,j)\in\mathcal{A}^2} r_{ij}^{\mathrm{v}}(t) = \sum_{i,j\in\mathcal{A}} \bar{r}_{ij}^{\mathrm{v}}$, and $r_{ij}^{\mathrm{v}}(t)$ is a random variable. Therefore we have the following equation:

$$\begin{aligned}\mathbb{E}[\mathbf{x}^{\mathrm{v}}(t)^{\mathrm{T}}\boldsymbol{\delta}(t)|\mathbf{x}^{\mathrm{v}}(t)] = &\sum_{i\in\mathcal{A}_{\mathrm{i}}\cup\mathcal{A}_{\mathrm{e}}}\sum_{j\in\Gamma_i^+}\mathbb{E}\left[\min\left\{Q_{ij}^{\mathrm{v}}s_{ij}(t), x_{ij}^{\mathrm{v}}(t)\right\}\times(-x_{ij}^{\mathrm{v}}(t))\middle|\mathbf{x}^{\mathrm{v}}(t)\right]\\ &+\sum_{i\in\mathcal{A}_{\mathrm{i}}\cup\mathcal{A}_{\mathrm{e}}}\sum_{j\in\Gamma_i^+}\mathbb{E}\left[\min\left\{Q_{ij}^{\mathrm{v}}s_{ij}(t), x_{ij}^{\mathrm{v}}(t)\right\}\middle|\mathbf{x}^{\mathrm{v}}(t)\right]\\ &\times\left(\sum_{k\in\Gamma_i^+}\bar{r}_{jk}^{\mathrm{v}}x_{jk}^{\mathrm{v}}(t)\right)\\ &+\sum_{i\in\mathcal{A}_{\mathrm{e}}}\sum_{j\in\Gamma_i^+}\mathbb{E}\left[d_i^{\mathrm{v}}(t)\bar{r}_{ij}^{\mathrm{v}}x_{ij}^{\mathrm{v}}(t)\middle|\mathbf{x}^{\mathrm{v}}(t)\right]\end{aligned}\tag{3.39}$$

Then we obtain

$$\begin{aligned}&\mathbb{E}[\mathbf{x}^{\mathrm{v}}(t)^{\mathrm{T}}\boldsymbol{\delta}(t)|\mathbf{x}^{\mathrm{v}}(t)]\\ &=\sum_{i\in\mathcal{A}_{\mathrm{i}}\cup\mathcal{A}_{\mathrm{e}}}\mathbb{E}\left[\min\left\{Q_{ij}^{\mathrm{v}}s_{ij}(t), x_{ij}^{\mathrm{v}}(t)\right\}\middle|\mathbf{x}^{\mathrm{v}}(t)\right]\times\left(-x_{ij}^{\mathrm{v}}(t)+\sum_{k\in\Gamma_i^+}\bar{r}_{jk}^{\mathrm{v}}x_{jk}^{\mathrm{v}}(t)\right)\\ &+\sum_{i\in\mathcal{A}_{\mathrm{e}}}\bar{d}_i^{\mathrm{v}}\bar{r}_{ij}^{\mathrm{v}}x_{ij}^{\mathrm{v}}(t)\end{aligned}\tag{3.40}$$

For the last term of equation (5.32), $\sum_{i\in\mathcal{A}_{\mathrm{e}}}\bar{d}_i^{\mathrm{v}}\bar{r}_{ij}^{\mathrm{v}}x_{ij}^{\mathrm{v}}(t)$, we have

$$\sum_{i\in\mathcal{A}_{\mathrm{e}}}\bar{d}_i^{\mathrm{v}}\bar{r}_{ij}^{\mathrm{v}}x_{ij}^{\mathrm{v}}(t) = \sum_{i\in\mathcal{A}_{\mathrm{e}}}f_i^{\mathrm{v}}\bar{r}_{ij}^{\mathrm{v}}x_{ij}^{\mathrm{v}}(t) = \sum_{i\in\mathcal{A}_{\mathrm{e}}}f_{ij}^{\mathrm{v}}x_{ij}^{\mathrm{v}}(t)\tag{3.41}$$

$$= \sum_{i\in\mathcal{A}_{\mathrm{i}}\cup\mathcal{A}_{\mathrm{e}}}f_i^{\mathrm{v}}\bar{r}_{ij}^{\mathrm{v}}x_{ij}^{\mathrm{v}}(t) - \sum_{j\in\mathcal{A}_{\mathrm{i}}}f_j^{\mathrm{v}}\bar{r}_{jk}^{\mathrm{v}}x_{jk}^{\mathrm{v}}(t)\tag{3.42}$$

$$= \sum_{i\in\mathcal{A}_\mathrm{i}\cup\mathcal{A}_\mathrm{e}} f_i^\mathrm{v}\bar{r}_{ij}^\mathrm{v}x_{ij}^\mathrm{v}(t) - \sum_{j\in\Gamma_i^+}\left[\sum_{i\in\mathcal{A}_\mathrm{i}\cup\mathcal{A}_\mathrm{e}} f_i^\mathrm{v}\bar{r}_{ij}^\mathrm{v}\right]\sum_K \bar{r}_{jk}^\mathrm{v}x_{jk}^\mathrm{v}(t) \tag{3.43}$$

$$= \sum_{i\in\mathcal{A}_\mathrm{i}\cup\mathcal{A}_\mathrm{e}} f_i^\mathrm{v}\bar{r}_{ij}^\mathrm{v}\left(x_{ij}^\mathrm{v}(t) - \sum_k \bar{r}_{jk}^\mathrm{v}x_{jk}^\mathrm{v}(t)\right) \tag{3.44}$$

By Proposition 12 there exists some $\bar{\mathbf{s}} \in Conv(\mathcal{S})$ such that $\mathbb{E}[s_{ij}(t)] = \bar{s}_{ij}$. Then we have

$$\begin{aligned}
&\mathbb{E}[\mathbf{x}^\mathrm{v}(t)^\mathrm{T}\boldsymbol{\delta}(t)|\mathbf{x}^\mathrm{v}(t)] \\
&= \sum_{i\in\mathcal{A}_\mathrm{i}\cup\mathcal{A}_\mathrm{e}} \left(f_i^\mathrm{v}\bar{r}_{ij}^\mathrm{v} - \mathbb{E}\left[\min\left\{Q_{ij}^\mathrm{v}s_{ij}(t), \mathbf{x}^\mathrm{v}(t)\right\}\middle|\mathbf{x}^\mathrm{v}(t)\right]\right) \\
&\quad\times\left(x_{ij}^\mathrm{v}(t) - \sum_{k\in\Gamma_j^+}\bar{r}_{jk}^\mathrm{v}x_{jk}^\mathrm{v}(t)\right) \qquad (3.45) \\
&= \sum_{i\in\mathcal{A}_\mathrm{i}\cup\mathcal{A}_\mathrm{e}} \left(f_i^\mathrm{v}\bar{r}_{ij}^\mathrm{v} - \bar{s}_{ij}Q_{ij}^\mathrm{v}\right)\left(x_{ij}^\mathrm{v}(t) - \sum_{k\in\Gamma_j^+}\bar{r}_{jk}^\mathrm{v}x_{jk}^\mathrm{v}(t)\right) \\
&\quad+ \sum_{i\in\mathcal{A}_\mathrm{i}\cup\mathcal{A}_\mathrm{e}} \left(\bar{s}_{ij}Q_{ij}^\mathrm{v} - \mathbb{E}\left[\min\left\{Q_{ij}^\mathrm{v}s_{ij}(t), x_{ij}^\mathrm{v}(t)\right\}\middle|\mathbf{x}^\mathrm{v}(t)\right]\right) \\
&\quad\times\left(x_{ij}^\mathrm{v}(t) - \sum_{k\in\Gamma_j^+}\bar{r}_{jk}^\mathrm{v}x_{jk}^\mathrm{v}(t)\right) \qquad (3.46)
\end{aligned}$$

For the second term of equation (3.46), if $x_{ij}^\mathrm{v}(t) \geq Q_{ij}^\mathrm{v}$,
we have $\mathbb{E}\left[\min\left\{Q_{ij}^\mathrm{v}s_{ij}(t), x_{ij}^\mathrm{v}(t)\right\}\middle|\mathbf{x}^\mathrm{v}(t)\right] = Q_{ij}^\mathrm{v}\bar{s}_{ij}$. Therefore, the second term of equation (3.46) equals zero. If $x_{ij}^\mathrm{v}(t) < Q_{ij}^\mathrm{v}$, then we have $\mathbb{E}\left[\min\left\{Q_{ij}^\mathrm{v}s_{ij}(t), x_{ij}^\mathrm{v}(t)\right\}\middle|\mathbf{x}^\mathrm{v}(t)\right]$
$= \mathbb{E}\left[x_{ij}^\mathrm{v}(t)\middle|\mathbf{x}^\mathrm{v}(t)\right]$, which results in

$$\sum_{i\in\mathcal{A}_{\mathrm{i}}\cup\mathcal{A}_{\mathrm{e}}}\left(\bar{s}_{ij}Q_{ij}^{\mathrm{v}}-\mathbb{E}\left[x_{ij}^{\mathrm{v}}(t)\middle|\mathbf{x}^{\mathrm{v}}(t)\right]\right)$$
$$\times\left(x_{ij}^{\mathrm{v}}(t)-\sum_{k\in\Gamma_j^+}\bar{r}_{jk}^{\mathrm{v}}x_{jk}^{\mathrm{v}}(t)\right)\leq\sum_{i\in\mathcal{A}_{\mathrm{i}}\cup\mathcal{A}_{\mathrm{e}}}\bar{s}_{ij}Q_{ij}^{\mathrm{v}}x_{ij}^{\mathrm{v}}(t)$$
$$\leq\sum_{i\in\mathcal{A}_{\mathrm{i}}\cup\mathcal{A}_{\mathrm{e}}}(Q_{ij}^{\mathrm{v}})^2 \tag{3.47}$$

Therefore, the second term of equation (3.46) equals zero or is bounded by $\sum_{i\in\mathcal{A}_{\mathrm{i}}\cup\mathcal{A}_{\mathrm{e}}}(Q_{ij}^{\mathrm{v}})^2$. Moving on, we focus on the first term of equation (3.46). Based on the inequality equation (5.23), we have

$$\sum_{i\in\mathcal{A}_{\mathrm{i}}\cup\mathcal{A}_{\mathrm{e}}}\left(f_i^{\mathrm{v}}\bar{r}_{ij}^{\mathrm{v}}-\bar{s}_{ij}Q_{ij}^{\mathrm{v}}\right)$$
$$\times\left(x_{ij}^{\mathrm{v}}(t)-\sum_{k\in\Gamma_j^+}\bar{r}_{jk}^{\mathrm{v}}x_{jk}^{\mathrm{v}}(t)\right)$$
$$\leq\sum_{i\in\mathcal{A}_{\mathrm{i}}\cup\mathcal{A}_{\mathrm{e}}}\left(f_i^{\mathrm{v}}\bar{r}_{ij}^{\mathrm{v}}-\bar{s}_{ij}Q_{ij}^{\mathrm{v}}\right)\times\left(x_{ij}^{\mathrm{v}}(t)\right)$$
$$\leq-\epsilon|\mathbf{x}^{\mathrm{v}}(t)| \tag{3.48}$$

Equation (3.32) satisfies the following relationship based on equations (3.47) and (3.48). For $\delta_{ij}(t)$

$$|\delta_{ij}(t)|=\Big|-\min\left\{Q_{ij}^{\mathrm{v}}s_{ij}(t),x_{ij}^{\mathrm{v}}(t)\right\}$$
$$+\sum_{h\in\mathcal{A}_i^-}\min\left\{Q_{hi}^{\mathrm{v}}s_{ij}(t),x_{hi}^{\mathrm{v}}(t)\right\}\times r_{ij}^{\mathrm{v}}(t)\Big|\quad\forall i\in\mathcal{A}_{\mathrm{i}},j\in\Gamma_i^+ \tag{3.49}$$

$$\leq \max\left\{Q_{ij}^{\mathrm{v}}, \sum_{h\in\mathcal{A}_i^-} Q_{ij}^{\mathrm{v}}\right\} \tag{3.50}$$

Let $\hat{d}_{ij}$ be the maximum value of demand. Then we have

$$|\delta_{ij}(t)| = \left|-\min\left\{Q_{ij}^{\mathrm{v}} s_{ij}(t), x_{ij}^{\mathrm{v}}(t)\right\} + d_i^{\mathrm{v}}(t)\times r_{ij}^{\mathrm{v}}\right| \leq \max\left\{Q_{ij}^{\mathrm{v}}, \hat{d}_{ij}\right\} \quad \forall i\in\mathcal{A}_{\mathrm{e}}, j\in\Gamma_i^+ \tag{3.51}$$

Define ψ as the maximum value among, Q_{ij}^{v}, $\sum_{h\in\mathcal{A}_i^-} Q_{ij}^{\mathrm{v}}$, and $\hat{d}_{ij}$, that is

$$\psi = \max\left\{Q_{ij}^{\mathrm{v}}, \sum_{h\in\mathcal{A}_i^-} Q_{ij}^{\mathrm{v}}, \hat{d}_{ij}\right\} \tag{3.52}$$

Because the total movement of private vehicles is $\mathcal{M}$, we have the following inequality

$$|\delta_{ij}(t)|^2 \leq \boldsymbol{M}\times\psi^2 \tag{3.53}$$

From equations (3.48) and (5.49),

$$\begin{aligned}
&\left|\mathbf{x}^{\mathrm{v}}(t+1)\right|^2 - \left|\mathbf{x}^{\mathrm{v}}(t)\right|^2 = 2\mathbf{x}^{\mathrm{v}}(t)^{\mathrm{T}}\boldsymbol{\delta}(t) + \left|\boldsymbol{\delta}(t)\right|^2 \\
&\leq 2\left(\sum_{i\in\mathcal{A}_{\mathrm{i}}\cup\mathcal{A}_{\mathrm{e}}} (Q_{ij}^{\mathrm{v}})^2 - \epsilon|\mathbf{x}^{\mathrm{v}}(t)|\right) + \boldsymbol{M}\psi^2 &(3.54)\\
&= \kappa - \epsilon|\mathbf{x}^{\mathrm{v}}(t)| &(3.55)
\end{aligned}$$

where $\kappa = 2 \sum_{i \in \mathcal{A}_{\mathrm{i}} \cup \mathcal{A}_{\mathrm{e}}} (Q_{ij}^{\mathrm{v}})^2 + M\psi^2$.

Based on the above procedure, we find that we do know the lower and upper bounds of $\bar{s}_{ij}$ to prove stability. However, we need the long-time average signal activated time $\bar{s}_{ij}$ used for serving turning movement (i, j) while providing pedestrian access.

Proposition 7. *When the average signal $\bar{s}_{ij}$, which is constrained by the stable region definition, is used, and there exists $\bar{\mathbf{d}}^{\mathrm{v}} \in \mathcal{D}^0$, the transportation network is stable.*

Proof. Inequality (3.32) holds from Lemma 4. Taking expectations and summing over $t = 1, ..., T$ gives the following inequality:

$$\mathbb{E}\left[\nu(T+1) - \nu(1) | \, \mathbf{x}^{\mathrm{v}}(t)\right] \leq \kappa T - \epsilon \sum_{t=1}^{T} |\mathbf{x}^{\mathrm{P}}(t)| \tag{3.56}$$

Then we have

$$\epsilon \frac{1}{T} \sum_{t=1}^{T} \mathbb{E}\left[|\mathbf{x}^{\mathrm{v}}(t)|\right] \leq \kappa - \frac{1}{T}\mathbb{E}\left[\nu(T+1)\right] + \frac{1}{T}\mathbb{E}\left[\nu(1)\right] \leq \kappa + \frac{1}{T}\mathbb{E}\left[\nu(1)\right] \tag{3.57}$$

which implies that Definition 4 is satisfied.

Moreover, we need to mention that stability is not impacted by the initial condition. Let us move ϵ in to the right hand side and take the limit as T goes to infinity. Then the $\frac{1}{T}\mathbb{E}\left[\nu(1)\right]$ term equals zero, which yields the following inequality:

$$\lim_{T \to \infty} \frac{1}{T} \sum_{t=1}^{T} \mathbb{E}\left[|\mathbf{x}^{\mathrm{v}}(t)|\right] \leq \frac{\kappa}{\epsilon} \tag{3.58}$$

3.4 Control policy

3.4.1 Max-pressure control policy that considering pedestrian access

Now we reach the part of MP control. Since we prove that there exist average signal control $\bar{s}_{ij}$ that provide pedestrian access can stabilize the network when $\bar{\mathbf{d}}^{\mathrm{v}} \in \mathcal{D}^0$, therefore, we want to prove that MP consider pedestrian access can achieve maximum stability based on average signal control $\bar{s}_{ij}$ including pedestrian access. This study modifies the original MP control policy of Varaiya (2013) to create the pedestrian-friendly max-pressure signal control policy (Ped-MP). The weight calculation is the same as previous papers (Varaiya, 2013; Chen et al., 2020; Levin et al., 2019, 2020):

$$w_{ij}^{\mathrm{v}}(t) = x_{ij}^{\mathrm{v}}(t) - \sum_{k \in \Gamma_j^+} r_{jk}^{\mathrm{v}}(t) x_{jk}^{\mathrm{v}}(t) \tag{3.59}$$

After we calculate the weight for each movement, a mixed-integer linear program is used to calculate the intersection control. In this program, we use α_{ij}^b to indicate whether the vehicles movements have conflicts with pedestrians. The capacity of conflict region c is Q_c, which is determined by the capacities of turning movements, $Q_c = \max_{(i,j)|c \in C_{ij}} \{Q_{ij}\}$.

The modified MP control policy considering pedestrian access tries to maximize the total pressure of vehicles. $s_{ij}^\star(t)$ denotes the max-pressure signal control at intersection n in the transportation network considering the pedestrian access, which is

$$s_{ij}^\star(t) = \mathrm{argmax}_{s \in \mathcal{S}} \left[\sum_{(i,j) \in \mathcal{M}} s_{ij}(t) Q_{ij}^{\mathrm{v}} w_{ij}^{\mathrm{v}}(t) \right] \tag{3.60}$$

which should obey constraints (3.61a) to (3.61j). We include pedestrian access constraints (3.8)–(3.9) in this part as constraints (3.61b)–(3.61c) for the convenience of readers. To be

specific, constraint (3.61b) indicates the max-pressure control will consider the pedestrians waiting time. The maximum tolerance time, which is $\hat{\phi}_{mb}$ in the simulation should be tested under different value settings, and we assume this number should not change by time (input parameter for simulation). However, a short tolerance time will reduce the stable region of a vehicle significantly, so it should depend on the demand of vehicles and pedestrians in the real world. The pedestrians waiting time for cross-movement (m, b) at time step t is denoted as $\phi_{mb}(t)$ (Section 3.4). When the difference between the pedestrians' waiting time and the maximum tolerance time is large than zero, $s_{mb}(t)$ is forced to equal 1, which means, when the pedestrians have been waiting for a long time, we activate the movement for the pedestrians. When the difference between pedestrians waiting time and the maximum tolerance time less or equal to zero, $s_{mb}(t)$ could be 0 or 1, but this should depend on whether it conflicts with vehicles or not (Section 3.5). Constraint (3.61c) represent the relationship with vehicle movements and pedestrians movement, where $\alpha_{ij}^{b} \in \{0, 1\}$ indicates whether vehicle movements (i, j) intersects with crosswalk b. For instance, when vehicle movement (i, j) activated, if it intersects with crosswalk b, then $s_{mb}(t)$ is forced to be zero. However, if movement (i, j) does not conflict with crosswalk b, then $s_{mb}(t)$ is could be 0 or 1. Constraint (3.61d) limites vehicle and pedestrian movement by the capacity of the conflict region. Constraint (3.61e) includes equation (5.3) the vehicle movement flow is bounded by the minimum value of capacity multiples signal control or the length of vehicle queues. Constraint (3.61f) indicates the pedestrian flow from m to b is not permitted unless $s_{mb}(t) = 1$.

$$\max \quad \sum_{(i,j)\in\mathcal{M}^2} s_{ij}(t) Q_{ij}^{\mathrm{v}} w_{ij}^{\mathrm{v}}(t) \tag{3.61a}$$

$$\text{s.t.} \quad (1 - s_{mb}(t)) \left(\phi_{mb}(t) - \hat{\phi}_{mb}\right) \leq 0 \quad \forall b \in \mathcal{Z}, , m \in \Gamma_i^- \tag{3.61b}$$

$$s_{mb}(t) \leq 1 - s_{ij}(t)\alpha_{ij}^{b} \qquad \forall (i,j) \in \mathcal{M}, \forall b \in \mathcal{Z}, , m \in \Gamma_i^- \tag{3.61c}$$

$$\sum_{(i,j)\in\mathcal{M}} y_{ij}^{\mathrm{v}}(t)(1-\alpha_{ij}^{b}) \le Q_{\mathrm{c}} \qquad \forall (i,j)\in\mathcal{M}, \forall b\in\mathcal{Z}, \forall c\in\mathcal{C},, m\in\Gamma_i^- \tag{3.61d}$$

$$y_{ij}^{\mathrm{v}}(t) = \min\left\{Q_{ij}^{\mathrm{v}} s_{ij}(t), x_{ij}^{\mathrm{v}}(t)\right\} \qquad \forall (i,j)\in\mathcal{M} \tag{3.61e}$$

$$y_{mb}^{\mathrm{p}}(t) \in \{0, x_{mb}^{\mathrm{p}}(t)\} \qquad \forall (b)\in\mathcal{Z},, m\in\Gamma_i^- \tag{3.61f}$$

$$s_{ij}(t) \in \{0,1\} \qquad \forall (i,j)\in\mathcal{M} \tag{3.61g}$$

$$s_{mb}(t) \in \{0,1\} \qquad \forall (b)\in\mathcal{Z}, m\in\Gamma_i^- \tag{3.61h}$$

$$\alpha_{ij}^{b} \in \{0,1\} \qquad \forall (i,j)\in\mathcal{M}, \forall b\in\mathcal{Z},, m\in\Gamma_i^- \tag{3.61i}$$

$$x_{ij}^{\mathrm{v}}(t), x_{mb}^{\mathrm{p}}(t) \ge 0 \qquad \forall (i,j)\in\mathcal{M}, \forall b\in\mathcal{Z}, m\in\Gamma_i^- \tag{3.61j}$$

Lemma 5. *If the modified max-pressure signal control policy, Ped-MP, is used and* $\bar{\mathbf{d}} \in \mathcal{D}^0$*, then we have the following inequality with average signal control* $\bar{s}_{ij}$ *including pedestrian access:*

$$\mathbb{E}\left[\sum_{(i,j)\in\mathcal{M}^2} s_{ij}^{\star}(t) Q_{ij}^{\mathrm{v}} w_{ij}^{\mathrm{v}}(t) \middle| \mathbf{x}^{\mathrm{v}}(t)\right] \ge \mathbb{E}\left[\sum_{(i,j)\in\mathcal{M}^2} \bar{s}_{ij} Q_{ij}^{\mathrm{v}} w_{ij}^{\mathrm{v}}(t) \middle| \mathbf{x}^{\mathrm{v}}(t)\right] \tag{3.62}$$

Proof. First, we have the following inequality based on definition of MP control. Since $s_{ij}^{\star}(t)$, $s_{ij}(t)$ are some feasible signal control and satisfy constraints (3.61b)–(3.61c), and $s_{ij}^{\star}(t)$ maximizes objective (3.61a):

$$\sum_{(i,j)\in\mathcal{M}^2} s_{ij}^{\star}(t) Q_{ij}^{\mathrm{v}} w_{ij}^{\mathrm{v}}(t) \ge \sum_{(i,j)\in\mathcal{M}^2} s_{ij}(t) Q_{ij}^{\mathrm{v}} w_{ij}^{\mathrm{v}}(t) \tag{3.63}$$

Then calculating the expected value of the above equation when given the private vehicle queue length $\mathbf{x}^{\mathrm{v}}(t)$, we have

$$\mathbb{E}\left[\sum_{(i,j)\in\mathcal{M}^2} s^{\star}_{ij}(t)Q^{\mathrm{v}}_{ij}w^{\mathrm{v}}_{ij}(t)\middle|\mathbf{x}^{\mathrm{v}}(t)\right] \geq \mathbb{E}\left[\sum_{(i,j)\in\mathcal{M}^2} s_{ij}(t)Q^{\mathrm{v}}_{ij}w^{\mathrm{v}}_{ij}(t)\middle|\mathbf{x}^{\mathrm{v}}(t)\right] \tag{3.64}$$

Since $s^{\star}_{ij}(t) = \mathrm{argmax}_{s\in\mathcal{S}} \sum_{(i,j)\in\mathcal{M}^2} s_{ij}(t)Q^{\mathrm{v}}_{ij}w^{\mathrm{v}}_{ij}(t)$ based on equation (5.4) where $s_{ij}(t)$ satisfy constraints (3.61b)–(3.61c), we rewrite equation (5.14) as

$$\mathbb{E}\left[\sum_{(i,j)\in\mathcal{M}^2} s^{\star}_{ij}(t)Q^{\mathrm{v}}_{ij}w^{\mathrm{v}}_{ij}(t)\middle|\mathbf{x}^{\mathrm{v}}(t)\right] \geq \mathbb{E}\left[\sum_{(i,j)\in\mathcal{M}^2} \bar{s}_{ij}Q^{\mathrm{v}}_{ij}w^{\mathrm{v}}_{ij}(t)\middle|\mathbf{x}^{\mathrm{v}}(t)\right] \tag{3.65}$$

3.4.2 Stability analysis based on Ped-MP

Lemma 6. *If the modified max-pressure control policy, Ped-MP, is used and* $\bar{\mathbf{d}} \in \mathcal{D}^0$*, there exists a Lyapunov function* $\nu(t) \geq 0$ *and constants* $\kappa > 0$*,* $\epsilon > 0$ *such that*

$$\mathbb{E}\left[\nu(t+1) - \nu(t)\middle|\mathbf{x}^{\mathrm{v}}(t)\right] \leq \kappa - \eta|\mathbf{x}^{\mathrm{v}}(t)| \tag{3.66}$$

Proof. Based on equations (5.4)–(5.32) and the definition of pressure term (5.12), we obtain

$$\begin{aligned}&\mathbb{E}[\mathbf{x}^{\mathrm{v}}(t)^{\mathrm{T}}\boldsymbol{\delta}(t)|\mathbf{x}^{\mathrm{v}}(t)]\\ &\quad= \sum_{i\in\mathcal{A}_{\mathrm{i}}\cup\mathcal{A}_{\mathrm{e}}} \mathbb{E}\left[\min\left\{Q^{\mathrm{v}}_{ij}s_{ij}(t), x^{\mathrm{v}}_{ij}(t)\right\}\middle|\mathbf{x}^{\mathrm{v}}(t)\right] \times (-w^{\mathrm{v}}_{ij}(t)) + \sum_{i\in\mathcal{A}_{\mathrm{e}}} \bar{d}^{\mathrm{v}}_i \bar{r}^{\mathrm{v}}_{ij} x^{\mathrm{v}}_{ij}(t)\end{aligned} \tag{3.67}$$

The last term of equation (5.33) can be rewritten as follows based on equations (5.20), (5.21), and (5.12)

$$\sum_{i\in\mathcal{A}_\mathrm{e}} \bar{d}_i^{\mathrm{v}} \bar{r}_{ij}^{\mathrm{v}} x_{ij}^{\mathrm{v}}(t) = \sum_{i\in\mathcal{A}_\mathrm{e}} f_{ij}^{\mathrm{v}} x_{ij}^{\mathrm{v}}(t) \tag{3.68}$$

$$= \sum_{i\in\mathcal{A}_\mathrm{e}\cup\mathcal{A}_\mathrm{e}} f_i^{\mathrm{v}} \bar{r}_{ij}^{\mathrm{v}} x_{ij}^{\mathrm{v}}(t) - \sum_{i\in\mathcal{A}_\mathrm{i}} f_j^{\mathrm{v}} \bar{r}_{jk}^{\mathrm{v}} x_{jk}^{\mathrm{v}}(t) \tag{3.69}$$

$$= \sum_{i\in\mathcal{A}_\mathrm{e}\cup\mathcal{A}_\mathrm{e}} f_i^{\mathrm{v}} \bar{r}_{ij}^{\mathrm{v}} x_{ij}^{\mathrm{v}}(t) - \sum_{j\in\Gamma_i^+} \left[f_i^{\mathrm{v}} \bar{r}_{ij}^{\mathrm{v}}\right] \sum_k \bar{r}_{jk}^{\mathrm{v}} x_{jk}^{\mathrm{v}}(t) \tag{3.70}$$

$$= \sum_{i\in\mathcal{A}_\mathrm{i}\cup\mathcal{A}_\mathrm{e}} f_i^{\mathrm{v}} \bar{r}_{ij}^{\mathrm{v}} \left(w_{ij}^{\mathrm{v}}(t)\right) \tag{3.71}$$

Combining equations (5.24) and (5.37) yields

$$\mathbb{E}[\mathbf{x}^{\mathrm{v}}(t)^{\mathrm{T}} \boldsymbol{\delta}(t) | \mathbf{x}^{\mathrm{v}}(t)] \tag{3.72}$$

$$= \sum_{i\in\mathcal{A}_\mathrm{i}\cup\mathcal{A}_\mathrm{e}} \left(f_i^{\mathrm{v}} \bar{r}_{ij}^{\mathrm{v}} - \mathbb{E}\left[\min\left\{ Q_{ij}^{\mathrm{v}} s_{ij}(t), x_{ij}^{\mathrm{v}}(t) \right\} \middle| \mathbf{x}^{\mathrm{v}}(t) \right] \right) w_{ij}^{\mathrm{v}}(t)$$

$$= \sum_{i\in\mathcal{A}_\mathrm{i}\cup\mathcal{A}_\mathrm{e}} \left(f_i^{\mathrm{v}} \bar{r}_{ij}^{\mathrm{v}} - Q_{ij}^{\mathrm{v}} \bar{s}_{ij} \right) w_{ij}^{\mathrm{v}}(t)$$

$$+ \sum_{i\in\mathcal{A}_\mathrm{i}\cup\mathcal{A}_\mathrm{e}} \left(Q_{ij}^{\mathrm{v}} \bar{s}_{ij} - \mathbb{E}\left[\min\left\{ Q_{ij}^{\mathrm{v}} s_{ij}(t), x_{ij}^{\mathrm{v}}(t) \right\} \middle| \mathbf{x}^{\mathrm{v}}(t) \right] \right) w_{ij}^{\mathrm{v}}(t) \tag{3.73}$$

For the second term of equation (5.39), if $x_{ij}^{\mathrm{v}}(t) \geq Q_{ij}^{\mathrm{v}}$, then we have $\mathbb{E}\left[\min\left\{ Q_{ij}^{\mathrm{v}} s_{ij}(t), x_{ij}^{\mathrm{v}}(t) \right\} \middle| \mathbf{x}^{\mathrm{v}}(t) \right] = Q_{ij}^{\mathrm{v}} \bar{s}_{ij}$. Therefore, the second term of equation (5.39) equals zero. If $x_{ij}^{\mathrm{v}}(t) < Q_{ij}^{\mathrm{v}}$, then we have $\mathbb{E}\left[\min\left\{ Q_{ij}^{\mathrm{v}} s_{ij}(t), x_{ij}^{\mathrm{v}}(t) \right\} \middle| \mathbf{x}^{\mathrm{v}}(t) \right] = \mathbb{E}\left[x_{ij}^{\mathrm{v}}(t) \middle| \mathbf{x}^{\mathrm{v}}(t) \right]$. Therefore, we obtain the following

$$\left(Q_{ij}^{\mathrm{v}}\bar{s}_{ij}-\mathbb{E}\left[x_{ij}^{\mathrm{v}}(t)\middle|\mathbf{x}^{\mathrm{v}}(t)\right]\right)w_{ij}^{\mathrm{v}}(t)\leq Q_{ij}^{\mathrm{v}}x_{ij}^{\mathrm{v}}(t)\leq(Q_{ij}^{\mathrm{v}})^2 \tag{3.74}$$

Hence, the second term of equation (5.39) equal zero or bounded by $\sum_{i\in\mathcal{A}_{\mathrm{i}}\cup\mathcal{A}_{\mathrm{e}}}(Q_{ij}^{\mathrm{v}})^2$.

The modified max-pressure signal control $s_{ij}^{\star}(t)$ is chosen from the feasible signal control set $\mathcal{S}$ satisfying pedestrian access, and $s_{ij}^{\star}(t)$ seeks to maximize the objective (3.61a). According to Lemma 2, we have

$$\begin{aligned}&\mathbb{E}\left[\sum_{i\in\mathcal{A}_{\mathrm{i}}\cup\mathcal{A}_{\mathrm{e}}}\left[f_i^{\mathrm{v}}\bar{r}_{ij}^{\mathrm{v}}-s_{ij}^{\star}(t)Q_{ij}^{\mathrm{v}}\right]w_{ij}^{\mathrm{v}}(t)\middle|w_{ij}^{\mathrm{v}}(t)\right]\\&\quad\leq\mathbb{E}\left[\sum_{i\in\mathcal{A}_{\mathrm{i}}\cup\mathcal{A}_{\mathrm{e}}}\left[f_i^{\mathrm{v}}\bar{r}_{ij}^{\mathrm{v}}-\bar{s}_{ij}Q_{ij}^{\mathrm{v}}\right]w_{ij}^{\mathrm{v}}(t)\middle|w_{ij}^{\mathrm{v}}(t)\right]\end{aligned} \tag{3.75}$$

Therefore, for some feasible signal controls $s_{ij}(t)$ satisfying the stable region and integrated pedestrian phases, we obtain $\bar{s}_{ij}$ based on equation (5.4). We have

$$\sum_{i\in\mathcal{A}_{\mathrm{i}}\cup\mathcal{A}_{\mathrm{e}}}\left[f_i^{\mathrm{v}}\bar{r}_{ij}^{\mathrm{v}}-\bar{s}_{ij}Q_{ij}^{\mathrm{v}}\right]w_{ij}^{\mathrm{v}}(t)\leq-\epsilon\sum_{ij}\max\left\{w_{ij}^{\mathrm{v}},0\right\}\leq-\epsilon|w_{ij}^{\mathrm{v}}| \tag{3.76}$$

We know that the pressure $\mathbf{w}(t)$ is a linear function of the queue length of vehicles. So we can find $\beta>0$ to satisfy $\sum_{(i,j)\in\mathcal{M}^2}w_{ij}^{\mathrm{v}}\geq\beta|\mathbf{x}^{\mathrm{v}}|$. Then we have

$$-\epsilon|w_{ij}^{\mathrm{v}}|\leq-\epsilon\beta|\mathbf{x}^{\mathrm{v}}|\leq\sum_{i\in\mathcal{A}_{\mathrm{i}}\cup\mathcal{A}_{\mathrm{e}}}(Q_{ij}^{\mathrm{v}})^2-\epsilon\beta|\mathbf{x}^{\mathrm{v}}| \tag{3.77}$$

$\delta_{ij}(t)$ is upper-bounded by $\max\left\{Q_{ij}^{\mathrm{v}}, \sum_{h\in\mathcal{A}_i^-} Q_{ij}^{\mathrm{v}}\right\}$, which is the same as equation (5.46). Based on equation (5.44), and equations (5.46)–(5.52), we obtain

$$\begin{aligned}
&\left|\mathbf{x}^{\mathrm{v}}(t+1)\right|^2 - \left|\mathbf{x}^{\mathrm{v}}(t)\right|^2 = 2\mathbf{x}^{\mathrm{v}}(t)^{\mathrm{T}}\boldsymbol{\delta} + \left|\boldsymbol{\delta}\right|^2 \\
&\leq 2\Bigg(\sum_{i\in\mathcal{A}_{\mathrm{i}}\cup\mathcal{A}_{\mathrm{e}}} (Q_{ij}^{\mathrm{v}})^2 - \epsilon\beta|\mathbf{x}^{\mathrm{v}}(t)|\Bigg) + M\psi^2 \qquad (3.78)\\
&= \kappa - \eta|\mathbf{x}^{\mathrm{v}}(t)| \qquad (3.79)
\end{aligned}$$

where $\kappa = 2\sum_{i\in\mathcal{A}_{\mathrm{i}}\cup\mathcal{A}_{\mathrm{e}}} (Q_{ij}^{\mathrm{v}})^2 + M\psi^2$ and $\epsilon\beta = \psi$

Proposition 8. *Ped-MP is stabilizing when* $\bar{\mathbf{d}}^{\mathrm{v}} \in \mathcal{D}^0$.

Proof. The proof is analogous to Proposition 7. Inequality (5.24) holds from Lemma 9. Taking expectations, summing over $t = 1, ..., T$, and transferring the position of terms gives the following inequality:

$$\eta\frac{1}{T}\sum_{t=1}^{T}\mathbb{E}\left[|\mathbf{x}^{\mathrm{v}}(t)|\right] \leq \kappa - \frac{1}{T}\mathbb{E}\left[\nu(T+1)\right] + \frac{1}{T}\mathbb{E}\left[\nu(1)\right] \leq \kappa + \frac{1}{T}\mathbb{E}\left[\nu(1)\right] \qquad (3.80)$$

which satisfies Definition 1 for stability.

3.5 Multi-Scenario simulation and Numerical Results

To test the proposed Ped-MP performance, we set up simulations on the Sioux Falls network considering pedestrian access. Figure 3.3 provides details about the pedestrian network based on the Sioux Falls Network. There are 24 intersections and 72 links for vehicles, and 93 crosswalks for pedestrians in the Sioux Falls Network. Hourly demand for

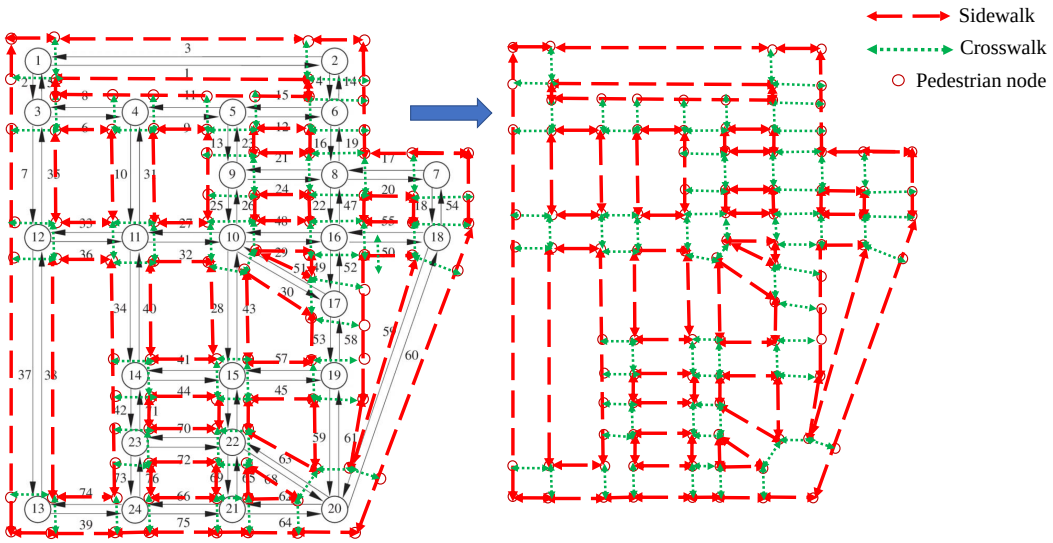

Figure 3.3: Sioux Fall network with pedestrian access

Sioux Falls network file is 15025 vehicles per hour. We randomly generate pedestrians at each each pedestrian node, and their destination is another pedestrian node. The simulation is built in Java with IBM CPLEX optimization solver. We set the simulation duration at 4 hours to ensure it is enough long to evaluate network stability. The main purpose of the simulation is to demonstrate the stability performance when including pedestrian access.

3.5.1 Stable and unstable network

In this part, we compare the stability performance based on stable network definition, Definition 1. We test different demand under under the same tolerance time. Figure 3.4 shows the results for stable network and unstable network. When demand is within the stable region, average queue length will converge to a constant, while when demand is outside of stable region, the average queue length will increase with simulation running.

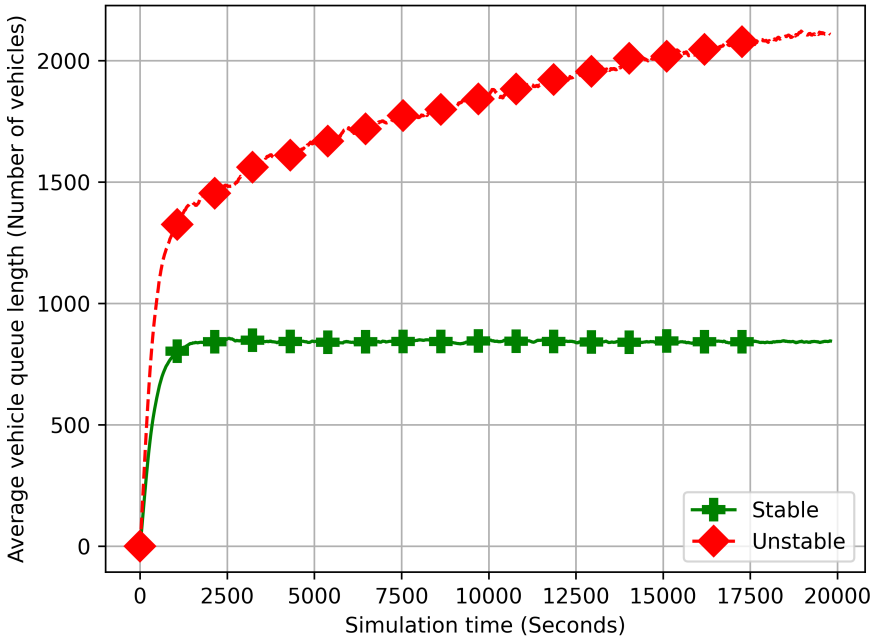

Figure 3.4: Stable and unstable network

3.5.2 Stability comparison

Firstly, we to demonstrate that the proposed Ped-MP can still achieve maximum throughput when considering pedestrian access. Figure 3.5 shows the average queue length for a current fixed-time signal control with pedestrian access compared with Ped-MP with 120 seconds tolerance time. When we load 5000 vehicles per hour into the network, the average queue length for fixed-time controller increases to infinity, but Ped-MP can still stabilize the network while including pedestrian access, which is consistent with Proposition 4.

After considering pedestrian access, we have to occupy some signal timing that could be used for vehicles. It would be interesting to check the throughput loss after considering pedestrian access with difference tolerance time. Therefore, we simulate Ped-MP with 30 seconds, 60 seconds, 90 seconds, and 120 seconds tolerance under different vehicle demand to find the maximum stable region for each Ped-MP controller and throughput loss. Figures Figure 3.6a–Figure 3.6d show that higher tolerance times for pedestrian increase the stable region for vehicles. Specifically, the maximum stable demand for Ped-MP with 30 seconds tolerance is 3000 vehicles per hour. Therefore, we can see the throughput loss lower tolerance times. We also provide Table 3.2 to show the maximum stable demand under different tolerance times.

Table 3.2: Maximum stable demand under different tolerance times

30 seconds	60 seconds	90 seconds	120 seconds
3000 vehicles/h	4750 vehicles/h	5250 vehicles/h	6000 vehicles/h

Vehicle delay is one of the most important indicators to evaluate the signal control performance, which has been used in recent MP control research (Li and Jabari, 2019; Wang et al., 2022). Here, we provide average vehicle delay dynamics under different pedestrian tolerance times (30 seconds, 60seconds, 90 seconds, 120 seconds) and different vehicle demand settings (1000 vehicles per hour, 3000 vehicles per hour, 5000 vehicles per hour) to

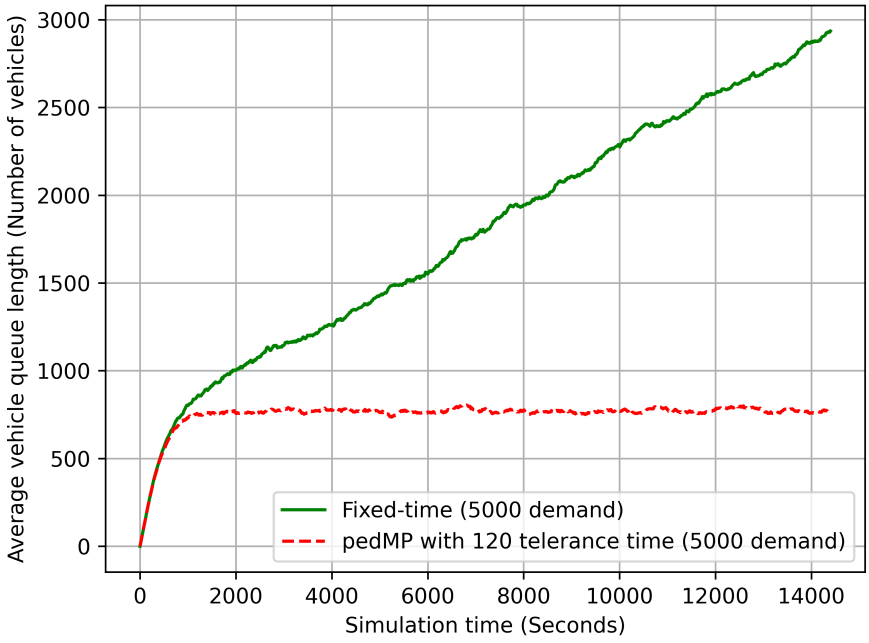

Figure 3.5: Comparison between Ped-MP and Fixed time controller

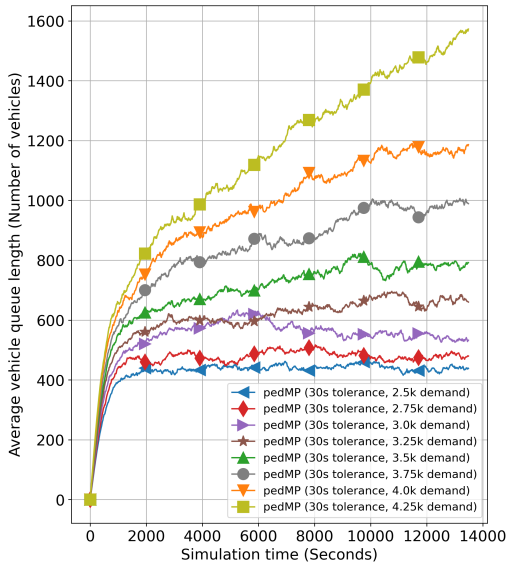

(a) Ped-MP with 30 seconds tolerance time under different demand

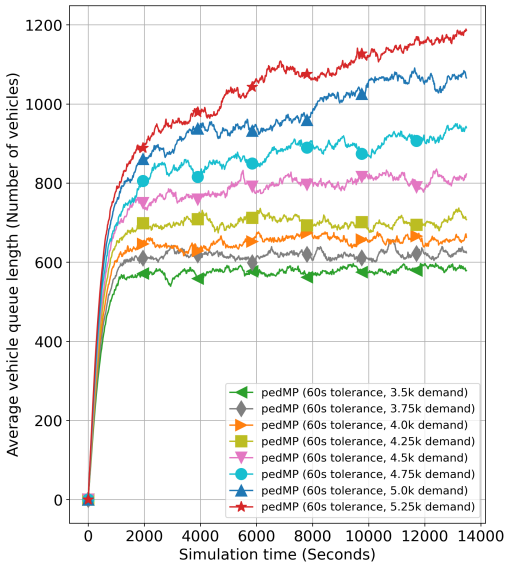

(b) Ped-MP with 60 seconds tolerance time under different demand

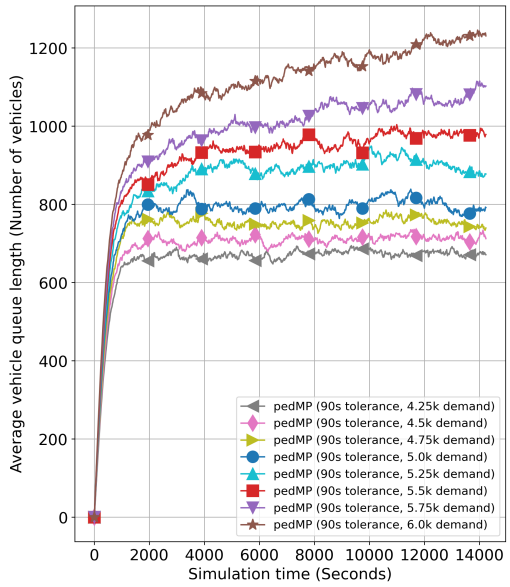

(c) Ped-MP with 90 seconds tolerance time under different demand

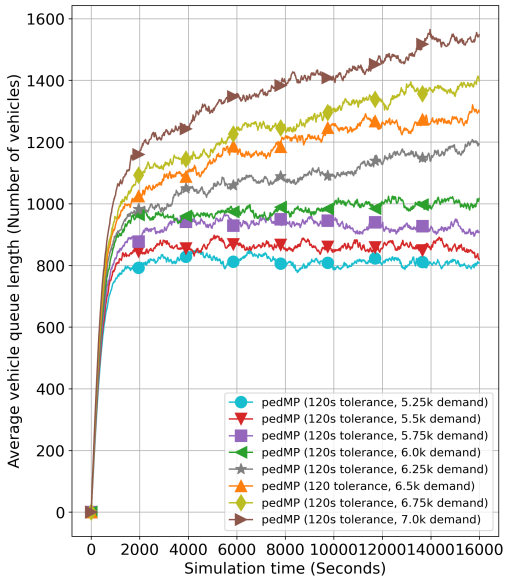

(d) Ped-MP with 120 seconds tolerance time under different demand

Figure 3.6: Throughput loss analysis

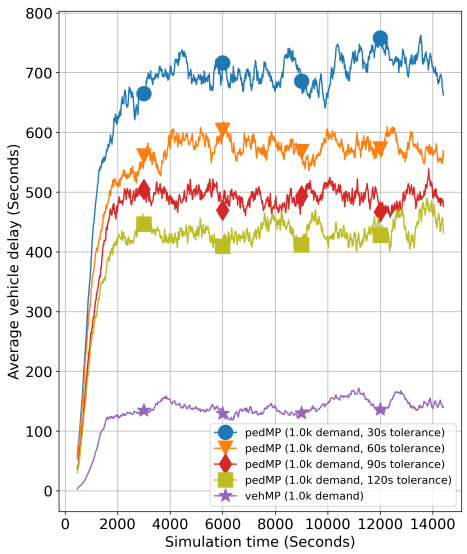

(a) 1000 vehicles hourly demand

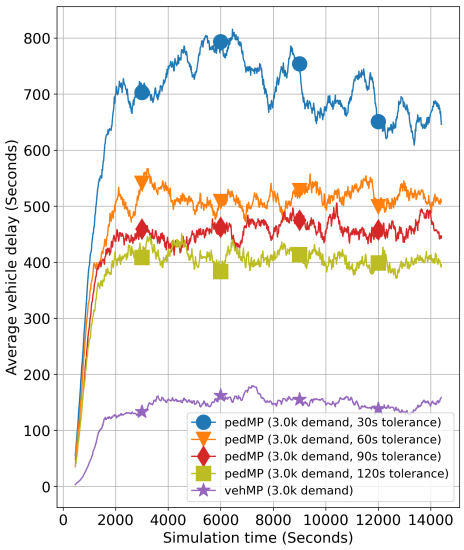

(b) 3000 vehicles hourly demand

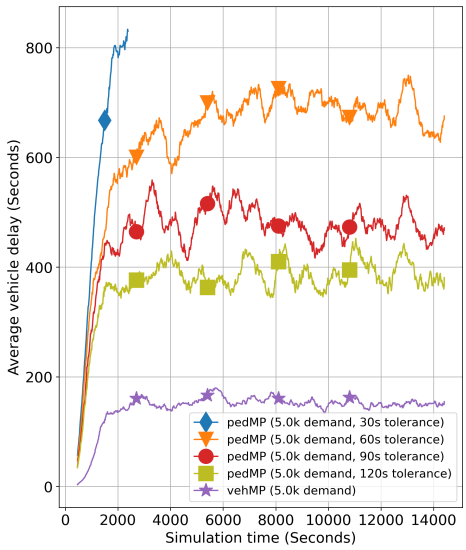

(c) 5000 vehicles hourly demand

Figure 3.7: Average vehicle delay

figure out how these factors influence vehicle delay. Figure 4.11 shows that under different demand, average vehicle delay is lowest with the original MP control proposed by Varaiya (2013), and when tolerance times increase the vehicle delay decreases since vehicles have more time to use intersections. Specifically, when demand is larger, like 5000 vehicles per hour in Figure 3.7c, vehicle delay for Ped-MP with 30 tolerance time will increase arbitrary large value, but for other tolerance time, vehicle delay fluctuates around a constant.

3.5.3 Impacts on pedestrians

One of the major goals of this dissertation is to provide a pedestrian-friendly MP control, which means we can bound pedestrian waiting times around intersections. Therefore, we want to check how Ped-MP impacts pedestrians. We provide average pedestrian delays for exploration. We simulate with 3000 vehicles per hour demand, which is in the stable region for all Ped-MP controllers under different tolerance times. Pedestrians are generated around average intersections every time step into the network, and they have a random path, which means some of them will walk through the crosswalks, and some of them will walk through sidewalks. Under these simulation scenarios, we add many pedestrians around each signal intersection to have a significantly high pedestrian demand. In this way, we provide a persuasive way to check how Ped-MP performs. Figure 3.8 provides detailed results. Unsurprisingly, the original MP control, which was proposed by Varaiya (2013), is not "friendly" to pedestrians. The delay of pedestrians increases quickly to a significantly higher value compared with all Ped-MP under different tolerance time. Also, the higher the tolerance time, the higher the pedestrian delay. For the 30 seconds tolerance time, the average delay for pedestrians fluctuates around 20 seconds. For the 60 seconds tolerance time, the average pedestrian delay fluctuates around 35 seconds, and for 90 seconds and 120 seconds tolerance time, the average delay is around 45 seconds and 55 seconds respectively. These results demonstrate that it is important to consider pedestrian access if

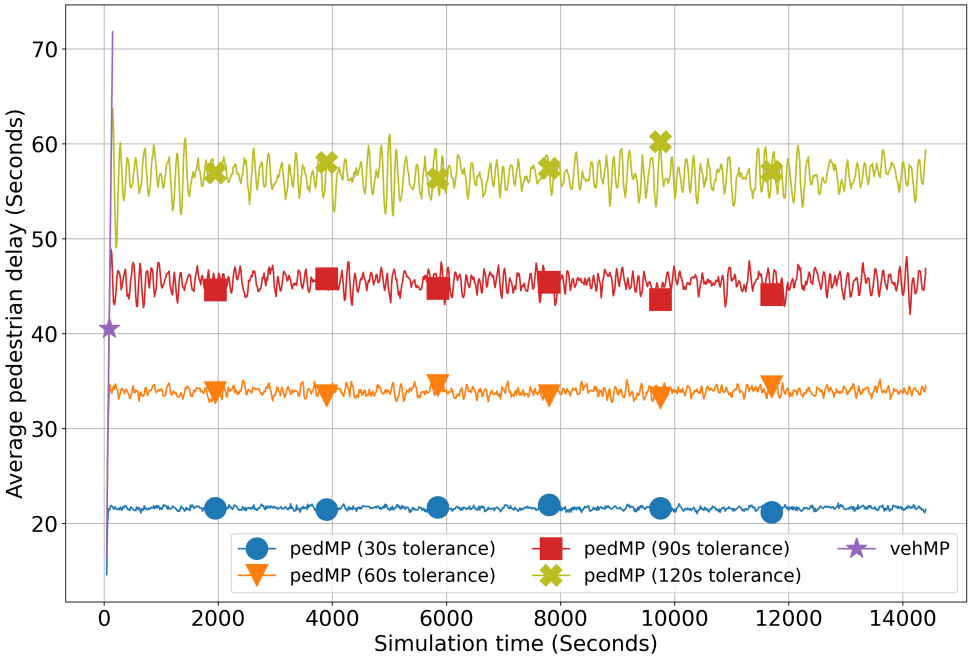

Figure 3.8: Impacts on pedestrian delay

we want to provide a more practical MP controller implement in the future, since there are large pedestrian cross demand in cities, especially in the central business district, and our proposed Ped-MP achieve good results on pedestrian delay.

3.6 Conclusions

Most previous studies about MP control policy only consider the vehicle network. There are only two previous studies that tried to include multiple modes in MP control (Chen et al., 2020; Xu et al., 2022b). To boost the scope of application of MP control, we proposed a pedestrian-friendly max-pressure signal controller, Ped-MP, for the first time. Moreover, we built a pedestrian network based on the Sioux Falls network, which makes our simulation more realistic than previous studies. We also analytically proved that our novel

Ped-MP can still achieve maximum stability.

Numerical results in the Sioux Falls network indicate that the lower tolerance time the lower pedestrian delay. It is not surprising that the performance of vehicles is best under original MP control proposed by Varaiya (2013), but these results demonstrate that we need to sacrifice vehicle performance for pedestrian access. Since the lower the tolerance time, the more thourghput loss in network. However, we find pedestrians have much less delay when we implement Ped-MP, even when we have a large number of pedestrians in the network, which means our proposed Ped-MP can provide more walkable spaces in cities and bound pedestrian wating time in the cities. Overall, the proposed Ped-MP can serve as much as vehicle demand when ever possible while including pedestrian access, which is more friendly to practical traffic operations.

In the future, there are still many extensions to consider. For example, including the information, such as number of pedestrian waiting for crossing, by advanced infrastructure sensors, will help us provide more accurate information for MP signal timing consider pedestrian access. In addition the results will benefit more from the design of pedestrian walking space, such as the design of crosswalks for pedestrian access, especially for disables.

Chapter 4

An approximate position-weighted back-pressure traffic signal control policy for traffic networks

Back-pressure (BP) control is the same control as max-pressure (MP) control with different name. We use back-pressure control in this chapter is because we modify Li and Jabari (2019)' PWBP algorithm, and they named their controller as back-pressure control.

4.1 Introduction

Researchers have focused on traffic signal optimization for a long time. Back-pressure (BP) control is one type of distributed traffic signal controls that has received increased attention recently (Varaiya, 2013; Wei et al., 2019; Levin et al., 2020; Wang et al., 2022). To avoid duplicated definitions, we use BP control to represent back-pressure based control and back-pressure control in the remaining part of this chapter. However, most BP-based signal controls model traffic flow dynamics with the point queue or the spatial queue flow models (Vickrey, 1969; Zhang et al., 2013). The main reason that most previous research used these models is due to the complex proof of maximum stability. However, the point queue and spatial queue flow models have significant limitations in representing traffic flow dynamics, such as lacking shockwaves and queue spillback along roads. Although the

spatial queue can represent queue spillback along roads, it assumes that the backward wave speed is infinity.

In BP control, although some studies used travel time to operate the traffic signal controller (Mercader et al., 2020), most past BP controllers require queue length information (number of vehicles on a road), which is used to calculate the pressure (or weight) term (Varaiya, 2013; Sun and Yin, 2018; Levin et al., 2019, 2020). Some past research assumes a fully connected traffic environment, but it wii not be achievable for several decades. To incorporate the impacts of realistic traffic flow dynamics and consider the realistic spatial distribution of vehicles along the road, Li and Jabari (2019) developed a position-weighted back-pressure control (PWBP) which based on the kinematic wave theory of traffic flow. They also proved the maximum stability based on the PWBP algorithms without any non-local traffic information. However, their weight function requires integrating the density over space along the roads. While this is analytically sound, in practice, the density is unlikely to be known exactly throughout space-time. Hence, their PWBP algorithm is hard to implement in practice.

Typically, density can be measured through a limited number of loop or video detectors, which can determine the cumulative counts of vehicles at the point of detection. For instance, a link may have only 2 loop detectors – one at the upstream and downstream ends of the link. Given a flow-density relationship, the density at other points might be inferred by the kinematic wave theory (Claudel and Bayen, 2010a). However, this is difficult to calculate quickly for a general flow-density relationship, and calibrating a general flow-density relationship to match reality is also difficult. The Newell-Daganzo method makes this calculation easy for a triangular flow-density relationship (Newell, 1993a,b,c), but the triangular flow-density relationship is only an approximation. The purpose of this dissertation is to extend Li and Jabari (2019)'s analytical stability results to a more practical approximate position-weighted BP (APWBP) control policy. The errors in that approximation make the maximum throughput properties unclear, requiring further methodological

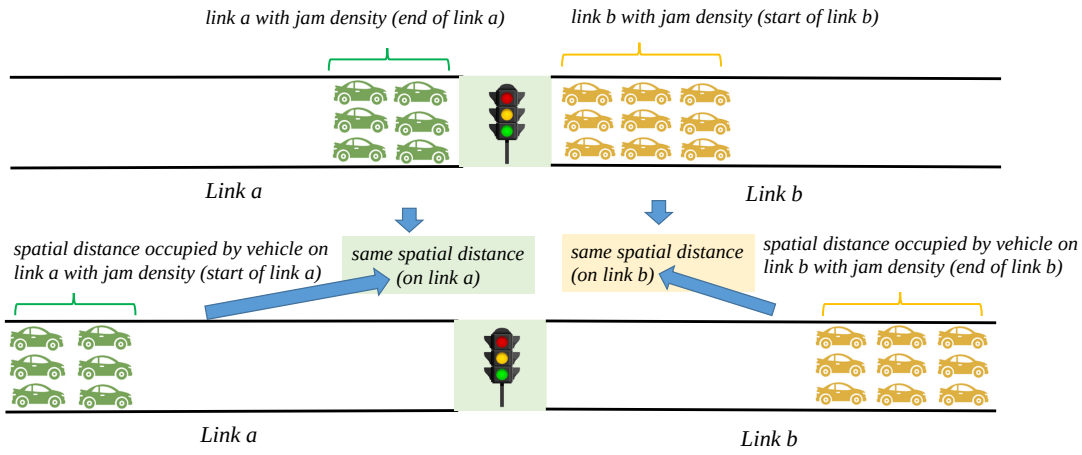

Figure 4.1: Different density distribution but have same pressure

analysis.

The contributions of this chapter are as follows: (1) We use kinematic wave theory with a triangular flow-density relationship to estimate the traffic density along the road segments to calculate BP weights. (2) Based on the estimated traffic density, we modify Li and Jabari (2019)'s PWBP traffic control algorithm and proposed approximate position-weighted BP (APWBP) control to achieve practical implementation. (3) We mathematically prove the APWBP traffic signal control policy can also achieve maximum throughput at the network level while only requiring local information, which means our proposed APWBP is still decentralized. (4) We implement APWBP and provide a comparison with PWBP proposed by Li and Jabari (2019).

4.2 Literature review

To the best of our knowledge, most past studies about BP-based traffic signal controllers were based on the point queue or spatial queue models (Vickrey, 1969; Zhang et al., 2013), which are not able to capture the spatial distribution of vehicles along the roads (Boyles et al., 2021). However, realistic traffic does not follow a point queue model, which will ob-

viate the mathematical guarantees of maximum throughput. For instance, different spatial distributions of vehicles may have same pressure according to Varaiya (2013). Figure 4.1 provides details about the different density spatial distribution but have same pressure scenarios. To overcome this, Li and Jabari (2019) developed a position-weighted BP control policy which assumes that traffic follows a first-order kinematic wave model. Li and Jabari (2019) proposed a weight function where vehicles closer to the intersection contribute more to the weight. In addition, they proved that the PWBP achieves maximum stability by Lyapunov drift technologies, and the experimental results indicated the PWBP performs better than SCOOT (Split, Cycle and Offset Optimisation Technique), as well as in a network setting against fixed intersection control, standard BP, and capacity-aware BP (CABP). But there is a potential problem which prevents the PWBP from being implemented in practice: using loop detectors or other sensors to obtain the density at every point along a link is cost-prohibitive. To address this issue, this dissertation proposes an approximate position-weighted BP (APWBP) control that model traffic flow using the kinematic wave theory, and we prove the maximum stability property of the proposed APWBP traffic signal control.

4.3 Traffic flow model

We use $x = 0$ and $x = l_a$ to represent the upstream and downstream boundaries of link a. We also use a node model to connect links to achieve traffic propagation and intersection control. Consider a traffic network $\mathcal{G} = (\mathcal{N}, \mathcal{A})$ with nodes $\mathcal{N}$ and links $\mathcal{A}$. Since these results extend directly from the results of Li and Jabari (2019), we will use the same notation. Let $\mathcal{A}_{\text{src}} \subset \mathcal{A}$ be the set of source links where vehicles enter. Let $\mathcal{M} \subset \mathcal{A}^2$ be the set of turning movements.

4.3.1 Link dynamics

We introduce the link dynamics in this section, which is defined as stochastic arc dynamics in Li and Jabari (2019). Let $\rho_a(x,t)$ and $q_a(x,t)$ be the density and flow respectively, of vehicles on on link a at time t and spatial location x. Let $\rho_a^b(x,t)$ and $q_a^b(x,t)$ be the density and flow, respectively, of vehicles on link a at time t and spatial location x that will next travel to link b. Specifically,

$$\rho_a^b(x,t) = \pi_{a,b}(t)\rho_a(x,t) \tag{4.1}$$

and

$$q_a^b(x,t) = \pi_{a,b}(t)q_a(x,t) \tag{4.2}$$

where $\pi_{a,b}(t)$ be the proportion of vehicles entering link a at time t that will next travel to link b. In addition, traffic density varies in space x and time t. Figure 4.2 provides illustration of how equation (4.1) works for better understanding.

The length of link a is denoted by l_a, so $\rho_a^b(x,t)$ and $q_a^b(x,t)$ are defined for $x \in [0, l_a]$. Flow and density follow the standard kinematic wave theory (Lighthill and Whitham, 1955), i.e. there exists a flow-density relationship $f_a^b(\rho)$ such that

$$q_a^b(x,t) = f_a^b\left(\rho_a^b(x,t)\right) \tag{4.3}$$

and

$$\frac{\partial \rho_a^b(x,t)}{\partial t} + \frac{\partial q_a^b(x,t)}{\partial x} = 0 \tag{4.4}$$

The flow density relationship $f_a^b(\rho)$ is defined for specific turning movement $(a,b) \in \mathcal{M}$ because different turning movements may have different right-of-way, e.g. restricted lanes

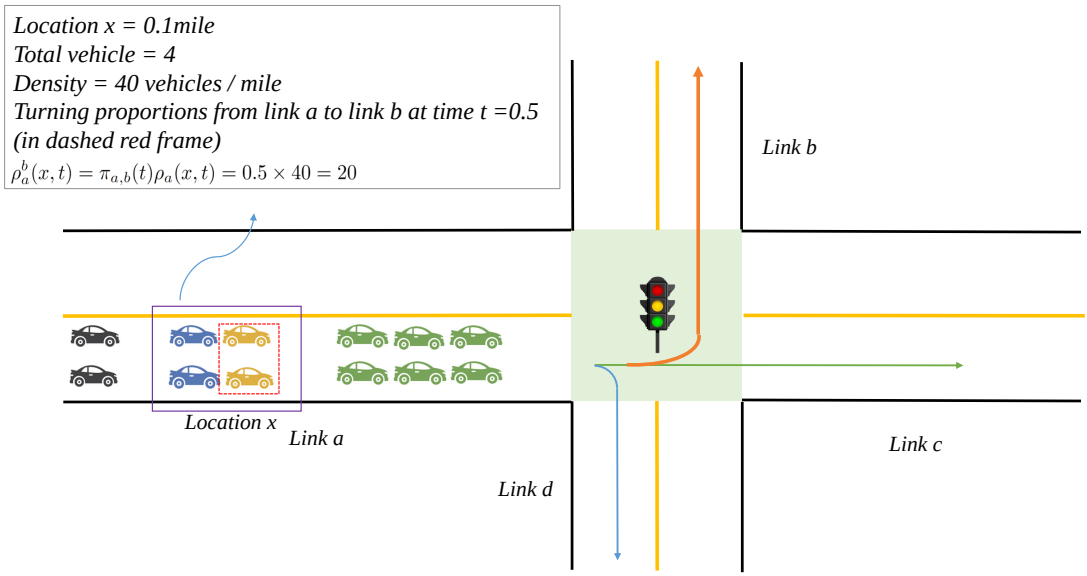

Figure 4.2: Illustration of link dynamics

of link a. We assume that the flow-density relationship is constant along the link. If applicable, a road including segments with different flow-density relationships may be separated into multiple links. Equation (4.4) represents the flow conservation law. Like Li and Jabari (2019), we make no other assumptions on $f_a^b(\rho)$, and it can be valid for both first-order and second-order models. The purpose is for $f_a^b(\rho)$ to represent as closely as possible the actual flow-density relationship of a link. Since $f_a^b(\rho)$ may be complex and is hard to calibrate for actuate traffic flow, we will use a simpler flow-density relationship to approximate the calculation of $\rho_a^b(x,t)$.

4.3.2 Boundary dynamics and intersection control

For the source links, sometimes also denoted as entry links, we use the same logic as Li and Jabari (2019) to load the inflow of network through the source links.

The flow from link a to link b is denoted by $q_{a,b}(t)$, which is the same as the boundary

flux in Li and Jabari (2019). We also define $q^b_{a,\text{in}}(t) = q^b_a(0,t)$ and $q^b_{a,\text{out}}(t) = q^b_a(l_a,t)$ to be the flow at the upstream and downstream boundaries of link a, respectively. Then conservation of flow across link boundaries is given by

$$q^b_{a,\text{in}}(t) = \pi_{a,b}(t) \sum_{(c,a)\in\mathcal{M}} q_{c,a}(t) \tag{4.5}$$

The flow across nodes is restricted by the traffic signal activation. Let $\mathbf{p}(t)$ be the signal phase activated at time t, with $p_{a,\text{out}}(t)$, or equivalently $p_{b,\text{in}}(t)$, denoting the phase at the node between links a and b of movement $(a,b) \in \mathcal{M}$. Therefore, equation (4.5) can be rewritten as

$$q^b_{a,\text{in}}(p_{a,\text{in}}(t)) = \pi_{a,b}(t) \sum_{(c,a)\in\mathcal{M}} q_{c,a}(p_{a,\text{in}}(t)) \tag{4.6}$$

Let $\delta_{a,b}\left(\rho^b_a(l_a,t)\right)$ and $\sigma_{a,b}\left(\rho_b(0,t)\right)$ be the sending and receiving flows for turning movement $(a,b) \in \mathcal{M}$, respectively. Then $q_{a,b}(t)$ is defined as

$$q_{a,b}(p_{a,\text{out}}(t)) = \mathbb{1}_{(a,b)\in p_{a,\text{out}}(t)} \min\left\{\delta_{a,b}\left(\rho^b_a(l_a,t)\right), \sigma_b\left(\rho_b(0,t)\right)\right\} \tag{4.7}$$

where $\mathbb{1}_{(a,b)\in p_{a,\text{out}}(t)}$ indicates whether movement (a,b) is permitted during phase $p_{a,\text{out}}(t)$.

At the upstream and the downstream ends for the link a $\in \mathcal{A}/\mathcal{A}_{\text{src}}$, the conservation law (4.4) can be rewritten as

$$\frac{\partial \rho^b_a(x,t)}{\partial t} = -\frac{\partial q^b_a(x,t)}{\partial x} = \begin{cases} q^b_{a,\text{in}}(p_{a,\text{in}}(t)) - q^b_{a,\text{in}}(0,t) & x = 0 \\ q^b_{a,\text{in}}(p_{a,\text{out}}(t)) - q^b_{a,\text{out}}(l_a,t) & x = l_a \end{cases} \tag{4.8}$$

As in reality, density is bounded on ordinary links by the jam density. On source links,

density may become arbitrarily large. The exogenous demand onto source link $a \in \mathcal{A}_{\text{src}}$ is given by $\frac{dA_a^b(t)}{dt}$. We assume that $\frac{dA_a^b(t)}{dt}$ is independent and identically distributed. Then the conservation law (4.4) for source links be rewritten as

$$\frac{\partial \rho_a^b(x,t)}{\partial t} = -\frac{\partial q_a^b(x,t)}{\partial x} = \frac{dA_a^b(t)}{dt} - q_{a,\text{out}}^b(p_{a,\text{out}}(t)) \tag{4.9}$$

We model source links as point queues where the occupancy can become arbitrary large. Therefore, for source links, we can drop x in equation (4.9) and rewrite it as follows:

$$\frac{\partial \rho_a^b(t)}{\partial t} = -\frac{\partial q_a^b(t)}{\partial x} = \frac{dA_a^b(t)}{dt} - q_{a,\text{out}}^b(p_{a,\text{out}}(t)) \tag{4.10}$$

4.3.3 Stable region

The stable region is the set of demands that could be stabilized. BP control aims to stabilize the maximum set of demand possible, sometimes also defined as admissible flows. We use the term stable region here, but it is synonymous with the term "network capacity region" used by Li and Jabari (2019).

Definition 3. *(Stable region). The stable region (a.k.a, capacity region) is the convex hull of the set containing all admissible flows.*

If there exists a signal control policy that can serve an arrival rate, then that arrival rate is included in the stable region. Please refer to Definition 1 in Li and Jabari (2019) for details.

4.3.4 Approximate position-weighted back-pressure (APWBP)

The weight function for the APWBP requires knowledge of the density at every point of link, which is difficult to obtain in practice. If we can estimate the density distribution

based on flow-density relationship, then the weight function (4.11) proposed by Li and Jabari (2019) can be approximated.

$$w_{a,b}(t) = \begin{cases} \left| c_{a,b}\rho_a^b(t) - \int_0^{l_b} \left|\frac{l_b - x}{l_b}\right| \sum_{(b,c)\in\mathcal{M}} c_{b,c}\pi_{b,c}(t)\rho_b^c(x,t)dx \right| & a \in \mathcal{A}_{\text{src}} \\ \left| c_{a,b}\int_0^{l_a} \left|\frac{x}{l_a}\right| \rho_a^b(x,t)dx - \int_0^{l_b} \left|\frac{l_b - x}{l_b}\right| \sum_{(b,c)\in\mathcal{M}} c_{b,c}\pi_{b,c}(t)\rho_b^c(x,t)dx \right| & a \notin \mathcal{A}_{\text{src}} \end{cases} \tag{4.11}$$

where $c_{a,b} > 0$ are constants used to provide preferential weighting to different turning movements. Then $p_{\text{PWBP}}(t)$ is defined by choosing a phase

$$p_{\text{PWBP}}(t) \in \arg\max_{\mathbf{p}\in\mathcal{P}} \sum_{(a,b)\in\mathcal{M}} w_{a,b}(t)\mathbb{E}\left[q_{a,b}(p)\right] \tag{4.12}$$

The APWBP policy $p_\diamond(t)$ of is calculated using the approximate density $\hat{\rho}_{a,b}$ to calculate the new weight function $\hat{w}_{a,b}$. The traffic volume split at time t is defined as $\pi_{a,b}(t)$, which is also known as the turning proportions. We now define the policy $p_\diamond(t)$ based on the definition of $w_{a,b}(t)$ from Li and Jabari (2019)

$$\hat{w}_{a,b}(t) = \begin{cases} \left| c_{a,b}\hat{\rho}_a^b(t) - \int_0^{l_b} \left|\frac{l_b - x}{l_b}\right| \sum_{(b,c)\in\mathcal{M}} c_{b,c}\pi_{b,c}(t)\hat{\rho}_b^c(x,t)dx \right| & a \in \mathcal{A}_{\text{src}} \\ \left| c_{a,b}\int_0^{l_a} \left|\frac{x}{l_a}\right| \hat{\rho}_a^b(x,t)dx - \int_0^{l_b} \left|\frac{l_b - x}{l_b}\right| \sum_{(b,c)\in\mathcal{M}} c_{b,c}\pi_{b,c}(t)\hat{\rho}_b^c(x,t)dx \right| & a \notin \mathcal{A}_{\text{src}} \end{cases} \tag{4.13}$$

As mentioned by Li and Jabari (2019), the core of the weight calculation is the following integral, which is the occupancy of link a that will next enter link b:

$$\int_0^{l_a} \hat{\rho}_a^b(x,t)dx \tag{4.14}$$

Therefore, the following Algorithm 1 shows how we calculate approximate weight and provide signal timing based the weight calculation. Note that we use the same method in Li and Jabari (2019) to load vehicles into the network.

Algorithm 1 Approximate position-weighted back-pressure policy (APWBP) $p_\diamond(n,t)$ for node n at time t.

function APWBP($t, \pi_{a,b}(t)_{(a,b)\in\mathcal{M}}, \{c_{a,b}\}, \delta_{a,b}, \sigma_{a,b}$, link a $(x_{i,a}, N_{i,a})$ pairs, and link b $(x_{i,b}, N_{i,b})$ pairs)
  if $a \in A_{src}$ **then**
    for $(a,b) \in \mathcal{M}_n$ **do**
      $\hat{w}_{a,b}(t) \leftarrow \left| c_{a,b}\hat{\rho}_a^b(t) - \int_0^{l_b} \left|\frac{l_b - x}{l_b}\right| \sum_{(b,c)\in\mathcal{M}} c_{b,c}\pi_{b,c}(t)\hat{\rho}_b^c(x,t)dx \right|$
    end for
  end if
  if $a \notin A_{src}$ **then**
    for $(a,b) \in \mathcal{M}_n$ **do**
      $\hat{w}_{a,b}(t) \leftarrow \left| c_{a,b} \int_0^{l_a} \left|\frac{x}{l_a}\right| \hat{\rho}_a^b(x,t)dx - \int_0^{l_b} \left|\frac{l_b - x}{l_b}\right| \sum_{(b,c)\in\mathcal{M}} c_{b,c}\pi_{b,c}(t)\hat{\rho}_b^c(x,t)dx \right|$
    end for
  end if
  for $p \in \mathcal{P}$ **do**
    $\mathbb{E}\left[q_{a,b}(p)\right] \leftarrow \mathbb{1}_{(a,b)\in p}\mathbb{E}\left[q_{a,b}(p)\right] \min\left\{\delta_{a,b}\left(\hat{\rho}_a^b(l_a,t)\right), \sigma_b\left(\hat{\rho}_b(0,t)\right)\right\}$
  end for
  $p_\diamond(n,t) \leftarrow \arg\max_{\mathbf{p}\in\mathcal{P}} \sum_{(a,b)\in\mathcal{M}} w_{a,b}(t)\mathbb{E}\left[q_{a,b}(p)\right]$
return $p_\diamond(n,t)$
end function

Now, we propose Proposition 1 to prove the proposed APWPB policy can still achieve maximum stability if on the this proposition holds. To avoid duplicating the work of Li and Jabari (2019), we state a stability condition and prove it based on their proof of the

maximum stability of $p_(t)$.

Proposition 9. *If a policy $p_\diamond(t)$ satisfies*

$$\left| \sum_{(a,b)\in\mathcal{M}} \hat{w}_{a,b}(t) q_{a,b}(p_\diamond(t)) - \max_{\mathbf{p}\in\mathcal{P}} \sum_{(a,b)\in\mathcal{M}} w_{a,b}(t)\mathbb{E}\left[q_{a,b}(p_{\text{PWBP}}(t))\right] \right| \leq \kappa \tag{4.15}$$

for some $\kappa < \infty$, then policy $p_\diamond(t)$ has maximum stability.

Proof. We build on the proof of Theorem 1 in Li and Jabari (2019) using Lyapunov function

$$\begin{aligned} V(\boldsymbol{\rho}(t)) = & \sum_{\substack{(a,b)\in\mathcal{M} \\ a\in}} c_{a,b}\rho_a^b(t)\rho_a^b(t) \\ & + \frac{1}{2}\sum_{\substack{(a,b)\in\mathcal{M} \\ a\notin}} c_{a,b} \int_0^{l_a}\int_0^{l_a} \left|\frac{l_a - x - x'}{l_a}\right| \times \rho_a^b(x,t)\rho_a^b(x',t)dx'dx \end{aligned} \tag{4.16}$$

Combining equations (51), (52), and (58) of Li and Jabari (2019), we obtain

$$\begin{aligned} \mathbb{E}\left[\dot{V}(\boldsymbol{\rho}(t))\right] \leq & \tilde{K} + \sum_{\substack{(a,b)\in\mathcal{M} \\ a\in}} c_{a,b}\mathbb{E}\left[\rho_a^b(t)\frac{dA_a^b(t)}{dt}\right] \\ & - \max_{p\in\mathcal{P}} \sum_{(a,b)\in\mathcal{M}} w_{a,b}(t)\mathbb{E}\left[q_{a,b}(p)\right] \end{aligned} \tag{4.17}$$

$$\begin{aligned} \leq & \max\left\{K^*, \tilde{K}\right\} \\ & - \epsilon^* \left(\sum_{\substack{(a,b)\in\mathcal{M} \\ a\in}} \mathbb{E}\left[\rho_a^b(t)\right] \quad + \sum_{\substack{(a,b)\in\mathcal{M} \\ a\notin}} \mathbb{E}\left[\int_0^{l_a} \rho_a^b(x,t)dx\right] \right) \end{aligned} \tag{4.18}$$

Using property (4.15) in inequality (4.17), we can obtain the inequality

$$\mathbb{E}\left[\dot{V}(\boldsymbol{\rho}(t))\right] \leq \tilde{K} + \kappa + \sum_{(a,b)\in\mathcal{M}:a\in} c_{a,b}\mathbb{E}\left[\rho_a^b(t)\frac{dA_a^b(t)}{dt}\right] - \sum_{(a,b)\in\mathcal{M}} w_{a,b}(t)q_{a,b}(p_\diamond(t)) \tag{4.19}$$

$$\leq \tilde{K} + 2\kappa \sum_{(a,b)\in\mathcal{M}:a\in} c_{a,b}\mathbb{E}\left[\rho_a^b(t)\frac{dA_a^b(t)}{dt}\right] - \max_{p\in\mathcal{P}} \sum_{(a,b)\in\mathcal{M}} w_{a,b}(t)\mathbb{E}\left[q_{a,b}(p)\right] \tag{4.20}$$

$$\leq \max\left\{K^*, \tilde{K}\right\} + 2\kappa - \epsilon^*\left(\sum_{(a,b)\in\mathcal{M}:a\in} \mathbb{E}\left[\rho_a^b(t)\right] + \sum_{(a,b)\in\mathcal{M}:a\notin} \mathbb{E}\left[\int_0^{l_a} \rho_a^b(x,t)dx\right]\right) \tag{4.21}$$

which implies network stability by Lemma 1 of Li and Jabari (2019).

After defining the APWBP and prove that APWBP can achieve maximum stability if Proposition 1 holds, we need to introduce how to approximate density along a link so that we can provide the approximated weight calculation. We also need to prove the precondition of Proposition 1, which is introduced in Section 4.4.

4.4 Density approximation

4.4.1 Shockwaves detection

In reality, it is difficult to obtain the continuous density distribution along a link, which means Li and Jabari (2019) 's PWBP is hard to implement in practice. Specifically, equation (4.14) is hard to obtain. Researchers started many years ago trying to figure out how to reconstruct traffic state information within the link with limited information (Seo et al.,

2017). Han et al. (2016) provides a link-based traffic flow model, which employs the LWR model and Newell-Daganzo method with a triangular fundamental diagram assumption (Lighthill and Whitham, 1955; Newell, 1993a,b,c, 2002; Daganzo, 2005a,b). The link-based traffic flow can be modeled traffic state information within the link. For instance, a well-known discrete version of traffic flow, the cell transmission model (Daganzo, 1995), still requires extensive information within the link to calculate the density of each cells. Therefore, it is not a good choice for the density approximation because installing loop detectors for each cell is expensive. Instead, we assume a triangular flow-density relationship and use the method of Han et al. (2016) to approximate the density from the upstream and downstream cumulative counts.

In reality, we can obtain traffic information, like the cumulative number of vehicles, from loop detectors. Note that We do not consider information obtained from connected and autonomous vehicles in this dissertation (Ma and Li, 2022; Ma et al., 2021; Ma and Wang, 2019). Based on the cumulative number of vehicles at the upstream and downstream ends of links, we are able to apply a link-based traffic flow model (Han et al., 2016) to estimate the density distribution along the link and the boundary locations of density changes.

We introduce the relevant theory from Han et al. (2016). Let $N(t, x)$ be the cumulative count, which is related to density and flow via

$$\frac{\partial N(x,t)}{\partial x} = -\rho(x,t) \tag{4.22}$$

The traffic flow-density relationship f can be rewritten as follows:

$$\frac{\partial N(x,t)}{\partial t} = f\left(\rho(x,t)\right) \tag{4.23}$$

where $f\left(\rho(x,t)\right)$ is the traffic flow obtained from the density $\rho(x,t)$.

We rewrite equation (4.4) as the following Hamilton-Jacobi equation:

$$\frac{\partial N(x,t)}{\partial x} - f\left(-\frac{\partial N(x,t)}{\partial t}\right) = 0 \tag{4.24}$$

With the simplified flow-density relationship, the triangular flow-density relationship is as follows:

$$f(\rho) = \min\left\{u_{\mathrm{f}}\rho, -\omega_{\mathrm{b}}(\rho - \rho_{\mathrm{j}})\right\} \tag{4.25}$$

where u_{f} is free-flow speed, ω_{b} is the backwards wave speed, and ρ_{j} is the maximum traffic density. This simplified flow-density relationship separates the traffic state along a link into a congested state and an uncongested state (free-flow phase).

Then, define the concave transformation of equation (4.25) as follows:

$$\varphi^*(u) = \sup_{\rho\in[0,\rho_{\mathrm{j}}]}\left\{f(\rho) - \rho u\right\} \quad \forall u \in [\omega_{\mathrm{b}}, u_{\mathrm{f}}] \tag{4.26}$$

After that, we can write Proposition 3.4 from Han et al. (2016) with some notations changed to be consistent with this dissertation.

Proposition 10. *Given $N_a(0,t)$ and $N_{a,}(l_a,t)$ for link a, the solution of the Hamilton-Jacobi equation (4.24) is the following simplified Lax-Hopf formula:*

$$N(x,t) = \min\left\{N_a\left(0, t - \frac{x}{u_{\mathrm{f}}}\right), \quad N_a\left(l_a, t - \frac{l_a - x}{\omega_{\mathrm{b}}}\right) + \rho_{\mathrm{j}}(l_a - x)\right\} \tag{4.27}$$

Note that there two expressions in equation (4.27). For an arbitrary point (x,t) within link a, if $N_a(0, t - \frac{x}{u_{\mathrm{f}}})$ is strictly less than $N_a(l_a, t - \frac{l_a - x}{\omega_{\mathrm{b}}}) + \rho_{\mathrm{j}}(l_a - x)$, then we need to track the upstream condition. If $N_a(0, t - \frac{x}{u_{\mathrm{f}}})$ strictly large than $N_a(l_a, t - \frac{l_a - x}{\omega_{\mathrm{b}}}) + \rho_{\mathrm{j}}(l_a - x)$, then the downstream condition is active at (x,t). For more details, we refer the reader to

Remark 3.5 and Figure 5 in Han et al. (2016). We also rewrite Proposition 3.6 from Han et al. (2016) as follows:

Proposition 11. *Let $N(x,t)$ be the unique solution of the Hamilton-Jacobi equation (4.24) given by the Lax-Hopf formula (4.27) from $N_a(0,t)$ and $N_a(l_a,t)$ on link a. Then the following statements hold: For any time t, if the x^* is the current shockwave position, we have*

$$N_a\left(0, t - \frac{x^*}{u_{\mathrm{f}}}\right) = N_a\left(l_a, t - \frac{l_a - x^*}{\omega_{\mathrm{b}}}\right) + \rho_{\mathrm{j}}(l_a - x^*) \tag{4.28}$$

Therefore, if the current shockwave position x^* is obtained, we know this position is the density change boundary, and density within these boundaries are the same based on the triangular flow-density relationship assumptions. Also, we can also find cumulative counts using the Newell-Daganzo method (Newell, 1993a,b,c) given a (x,t). Once we know the cumulative counts of two positions, the approximate density can be obtained from equation (4.22). Figure 4.3 illustrates the evolution of vehicle trajectories and the shockwaves. At a signalized intersection, the will be backwards forming shockwaves, backwards recovery shockwaves, and forward recovery shockwaves. Note that equation (4.28) can only provide solution of backwards forming shockwaves and forward recovery shockwaves, and we will discuss how to obtain the position of backwards forming shockwaves.

4.4.2 Some improvements to detect density boundary characteristics

It is worth mentioning that there are other causes of density variations within the link. Solving the linear equation (4.28), we can obtain the position x^* of each shockwave present at t. In a realistic traffic phenomenon, this position is the last vehicle in the vehicle's queue. However, for the shockwaves caused by the traffic light, there is another characteristic wave, called the backward recovery shockwave, which cannot be obtained by equation

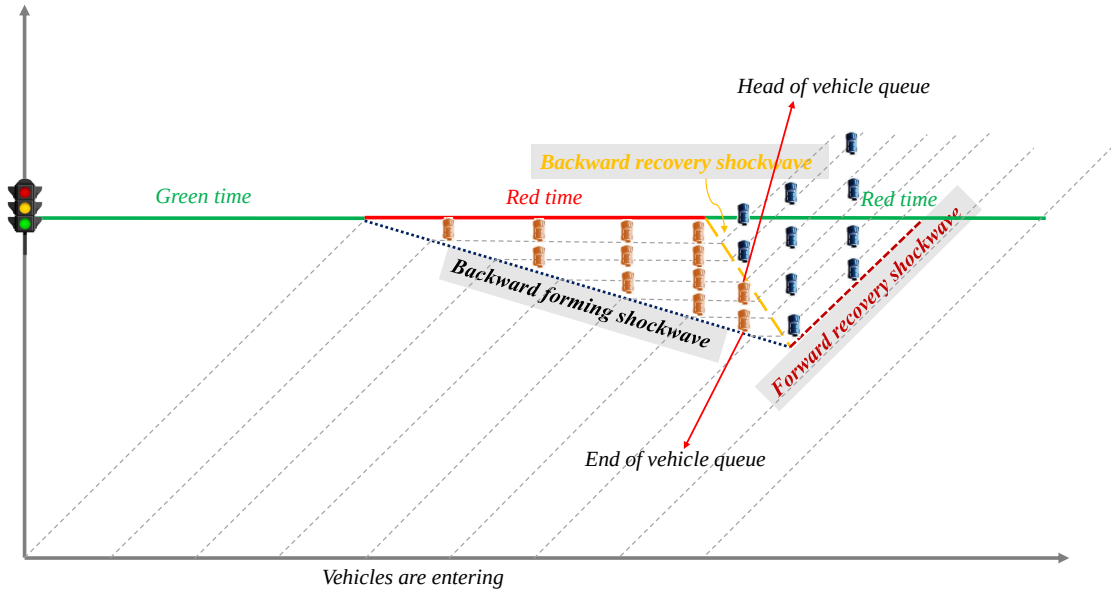

Figure 4.3: Vehicles trajectories and shockwaves in the space-time domain for a signalized intersection

(4.28). Fortunately, based on the flow-density relationship, the backward recovery shockwave is caused by a change from red light to green light, which can be detected by a change in the downstream cumulative counts. Specifically, if the traffic flow at the downstream end $q(l_a, t) = \frac{\partial N_a(l_a,t)}{\partial t}$ changes from 0 to some positive value, we know that the traffic light changed from red to green. The backward recovery shock will move upstream at backward speed ω_{b}. Note that when the backward recovery shockwave meets the backward forming shockwave, the backward recovery shock will dissipate. After that, a forward recovery shockwave forms because the last vehicle of the queue starts moving. We provide Figure 4.3 to illustrate.

Another note for the evolution of the upstream cumulative number of vehicles is that $q(0, t)$ may not be constant due to the network loading process. This will cause a flow change shockwave to move through the link at free-flow speed u_{f} .Once the upstream flow change shockwave reaches any backward forming and forward recovery shockwaves, it will

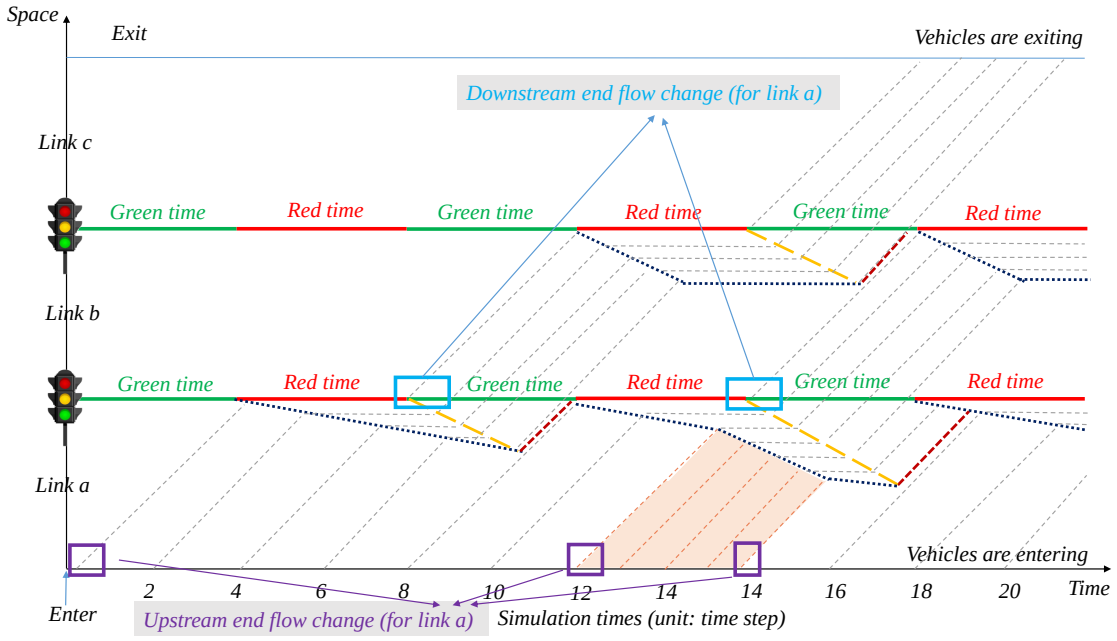

Figure 4.4: Example for upstream and downstream flow change points for link a

dissipate. Figure 4.4 provides an example of the upstream and downstream flow change (link a) and how they impact the evolution of vehicle trajectories and density distribution.

4.4.3 Density approximation algorithm and numerical example

In this part, we propose Algorithm 2 to detect the density boundary characteristic position within the link. We define X as the set of all these density boundary positions. The core idea is that Algorithm 2 makes use of both $N_a(0,t)$ and $N_a(l_a,t)$ to detect all possible density boundary positions including upstream flow change shockwaves, backward forming shockwaves, backward recovery shockwaves, and forward recovery positions. Once we obtain all these density boundary positions x^* including the flow change shockwave position, we can always find corresponding cumulative counts $N_a(x^*,t)$ based on the Newell-Daganzo method. Then the density between two boundary positions can be calculated by equation (4.22).

Algorithm 2 Density boundary positions approximated algorithm (DBPAlgos) for road section l at current time t

function DBPALGOS($t, u_f, \omega_\mathrm{b}, \rho_\mathrm{j}, N_a(0,t), N_a(l_a,t)$)
  Define an output set X
  for all roads l_a **do**
    $X \leftarrow X \cup \{0\}$
    for $i \in \left[0, \frac{l_a}{u_\mathrm{f}} - 1\right]$ and $j \in \left[0, \frac{l_a}{\omega_\mathrm{b}} - 1\right]$ **do**
      if equation (4.28) has solution x^* **then**
        if $t - \frac{x^*}{u_\mathrm{f}} \in \left[t - \left(\frac{l_a}{u_\mathrm{f}} - i\right), t - \left(\frac{l_a}{u_\mathrm{f}} - (i+1)\right)\right]$, $t - \frac{x^*}{\omega_\mathrm{b}} \in \left[t - \left(\frac{l_a}{\omega_\mathrm{b}} - i\right), t - \left(\frac{l_a}{\omega_\mathrm{b}} - (i+1)\right)\right]$, and $x^* \in [0, l_a]$ **then**
          $X \leftarrow X \cup \{x^*\}$
        end if
      end if
    end for
    for $i \in \left[0, \frac{l_a}{u_\mathrm{f}} - 2\right]$ **do**
      if $N_a\left(0, \left(t - \frac{l_a}{u_\mathrm{f}}\right) + i + 2\right) - N_a\left(0, \left(t - \frac{l_a}{u_\mathrm{f}}\right) + i + 1\right) \neq N_a\left(0, \left(t - \frac{l_a}{u_\mathrm{f}}\right) + i + 1\right) - N_a\left(0, \left(t - \frac{l_a}{u_\mathrm{f}}\right) + i\right)$ **then**
        $X \leftarrow X \cup \left\{x_\mathrm{up} = u_\mathrm{f}\left(\frac{l_a}{u_\mathrm{f}} - (i+1)\right)\right\}$
        if $x_\mathrm{up} > x^*$ **then**
          x_up is removed from X
        end if
      end if
    end for
    for $j \in \left[0, \frac{l_a}{\omega_\mathrm{b}} - 2\right]$ **do**
      if $N_a\left(l_a, \left(t - \frac{l_a}{\omega_\mathrm{b}}\right) + i + 2\right) - N_a\left(l_a, \left(t - \frac{l_a}{\omega_\mathrm{b}}\right) + i + 1\right) > 0$ and $N_a\left(l_a, \left(t - \frac{l_a}{\omega_\mathrm{b}}\right) + i + 1\right) - N_a\left(l_a, \left(t - \frac{l_a}{\omega_\mathrm{b}}\right) + i\right) = 0$ **then**
        $X \leftarrow X \cup \left\{x_\mathrm{down} = l_a - \omega_\mathrm{b}\left(\frac{l_a}{\omega_\mathrm{b}} - (i+1)\right)\right\}$
        if $x_\mathrm{down} < x^*$ **then**
          x_down is removed from X
        end if
      end if
    end for
    $X \leftarrow X \cup \{l_a\}$
  end for
return X
end function

We now provide a numerical example to help the reader understand how Algorithm 2 works. First, we need to obtain the upstream cumulative count $N_a(0,t)$ and downstream cumulative count $N_a(l_a,t)$. Consider three links, labeled a, b, and c with the same parameters, $l_a = 0.2$ mile, $u_{\mathrm{f}} = 30$ mile/hour, $\omega_{\mathrm{b}} = 15$ mile/hour, and $\rho_j = 240$ veh/mile. Defining $\Delta t = 6$ seconds, then $u_{\mathrm{f}} = 0.05$ mile/Δt, $\omega_{\mathrm{b}} = 0.025$ mile/Δt. Assume the traffic proceeds from link a to link b and then to link c, and vehicle entering flow is 2 vehicles per time step. Suppose there are two traffic signals located in between link in between link a and b, and between link b and link c. Assume that those two traffic signals have the same cycle length of $8\Delta t$ and are activated simultaneously with a green duration of $4\Delta t$ and a red duration of $4\Delta t$. We do not consider a yellow light for this small example. Our purpose in giving this example is to demonstrate the density approximation at time t based on signal timings in previous time steps. Therefore, we assume those previous signal timings are fixed. Upstream end loop detector and downstream end loop detector can collect the required data. This part leverages the dynamic network loading knowledge for calculating sending flows, receiving flows, and occupancy (Boyles et al., 2021). The corresponding space-time trajectories are shown in Figure 4.5.

We will now calculate the backward forming shockwave position at time step $t = 10$ for link a. We have $\frac{l_a}{u_{\mathrm{f}}} = 4$ and $\frac{l_a}{\omega_{\mathrm{b}}} = 8$ based on the example numbers. We find all solutions of x^* that solving the following piecewise linear equation for the for current time $t = 10$:

$$\begin{aligned} N_a(0,t') + \left(t - \frac{x^*}{u_{\mathrm{f}}} - t'\right)\left(N_a(0,t'+1) - N_a(0,t')\right) \\ = N_a(l_a,t'') + \left(t - \frac{l_a - x^*}{\omega_{\mathrm{b}}}\right)\left(N_a(l_a,t''+1) - N_a(l_a,t')\right) + \rho_{\mathrm{j}}\left(l_a - x^*\right) \end{aligned} \tag{4.29}$$

where $t' \in [6,10]$ and $t'' \in [2,10]$, since $\frac{l_a}{u_{\mathrm{f}}} = 4$ and $\frac{l_a}{\omega_{\mathrm{b}}} = 8$, we need to trace back at most $4\Delta t$ for $N_a(0,10)$ and $8\Delta t$ for $N_a(l_a,10)$. Given the traffic parameters and $N_a(0,t)$ and

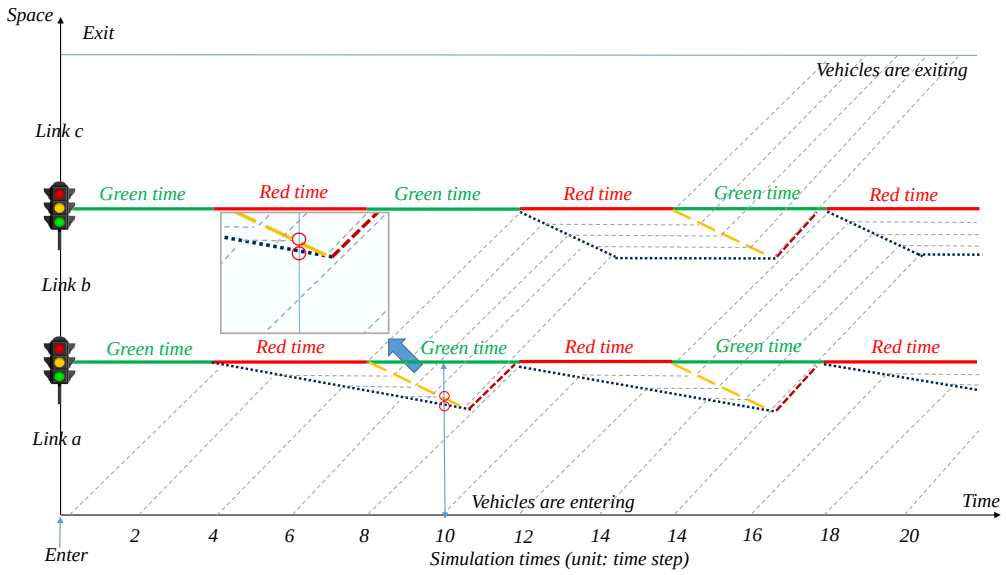

Figure 4.5: Example for density boundary detection

$N_a(l_a, t)$, the only unknown variable for equation (4.29) is x^*. Then we have:

$$\begin{aligned} N(0,t') + \left(10 - \frac{x^*}{0.05} - t'\right)\left(N_a(0,t'+1) - N_a(0,t')\right) \\ = N_a(l_a, t'') \\ + \left(t - \frac{0.2 - x^*}{0.025}\right)\left(N_a(l_a, t''+1) - N_a(l_a, t'')\right) \\ + 240(0.2 - x^*) \end{aligned} \tag{4.30}$$

equation (4.30) can be rewritten as follows:

$$20 - 40x^* = \begin{cases} 0 + 0 + 48 - 240x^* & t'' \in [2, 8] \\ 0 + (40x^* - 6) \times 4 + 48 - 48 - 240x^* & t'' \in [8, 9] \\ 4 + (40x^* - 7) \times (8 - 4) + 48 - 48 - 240x^* & t'' \in [9, 10] \end{cases} \tag{4.31}$$

The solutions are $x^* = 0.14$ and $x^* = 0.1$. Note that we obtain multiple results, and some of them may be invalid, because the corresponding t' or t'' fall outside the relevant range. The upstream feasible time range is $t - \frac{x^*}{u_\mathrm{f}} \in [6, 10]$. The downstream feasible time regions are $t - \frac{x^*}{\omega_\mathrm{b}} \in [2, 8]$, $t - \frac{x^*}{\omega_\mathrm{b}} \in [8, 9]$, and $t - \frac{x^*}{\omega_\mathrm{b}} \in [9, 10]$. Checking every x^* solution, we find the $x^* = 0.1$ is invalid, and the remaining shockwave boundary position is $x^* = 0.14$ at current time step $t = 10$.

Based on the Newell-Daganzo method, once we know $x^* = 0.14$, we can obtain the corresponding cumulative counts. Plugging $x^* = 0.14$ in to right-hand side of equation (4.28), the time step was obtained as follows:

$$\left(t - \frac{x^*}{u_\mathrm{f}}\right) = \left(10 - \frac{0.14}{0.05}\right) = 7.2\Delta t \tag{4.32}$$

Therefore, we need to trace back time step $t' = 7$ and $t' = 8$, and we assume that between two discrete time steps, the cumulative number of vehicle increase linearly. Then we have

$$N_a(0, 7.2) = N_a(0, 7) + \frac{(7.2 - 7)}{1} \times (N_a(0, 8) - N_a(0, 7)) = 14 + 0.2 \times 2 = 14.4 \tag{4.33}$$

For the backward recovery shockwave, we use the method of Section 4.2. If the traffic flow at downstream end $q(l_a, t) = \frac{\partial N_a(l_a,t)}{\partial t}$ changes from 0 to some positive values we know that the light changed from red to green. The backward recovery shockwave will move upstream at backward speed ω_b. Based on the downstream condition $N_a(l_a, t)$ at current time step $t = 10$, we obtain the following calculation for all elements in $N_a(l_a, t)$.

$$N_{a,down}(t'' = 3) - N_{a,down}(t'' = 2) = 0 - 0 = 0 \tag{4.34a}$$

$$N_{a,down}(t'' = 5) - N_{a,down}(t'' = 4) = 0 - 0 = 0 \tag{4.34b}$$

$$N_{a,down}(t'' = 6) - N_{a,down}(t'' = 5) = 0 - 0 = 0 \tag{4.34c}$$

$$N_{a,down}(t'' = 7) - N_{a,down}(t'' = 6) = 0 - 0 = 0 \tag{4.34d}$$

$$N_{a,down}(t'' = 8) - N_{a,down}(t'' = 7) = 0 - 0 = 0 \tag{4.34e}$$

$$N_{a,down}(t'' = 9) - N_{a,down}(t'' = 8) = 4 - 0 = 4 \tag{4.34f}$$

$$N_{a,down}(t'' = 10) - N_{a,down}(t'' = 9) = 8 - 4 = 4 \tag{4.34g}$$

We find that at $t'' = 8$, the traffic light changed, and the backward recovery shockwave moves for $0.025 \times (10 - 8) = 0.05$ mile, which means it is $0.2 - 0.05 = 0.15$ mile away from the upstream end. Since $0.15 > 0.14$, it is a valid solution because the backward recovery shockwave should be closer to the downstream end that the backward forming and forward recovery shockwaves, which are shown in Figure 4.5. The cumulative number of vehicles that reach this point is

$$N_a(l_a, t'' = 8) + \rho_{\text{j}}(0.2 - 0.15) = 12 \tag{4.35}$$

Now we obtain the cumulative counts, $N_a(0.14, 10) = 14.4$ of backward forming position at time step 10, and the cumulative counts of backward recovery position, that is $N_a(0.15, 10) = 12$, at time step 10. Based on equation (4.22), we have

$$\frac{\partial N(x,t)}{\partial x} = -\frac{N_a(0.14, 10) - N_a(0.15, 10)}{0.14 - 0.15} = -\frac{2}{0.14 - 0.15} = 240 \quad \text{vehicles/mile} \tag{4.36}$$

the answer is 240 vehicles/mile, which is consistent with reality, since vehicles completely jam in front of red light.

4.4.4 Sufficient conditions for network stability

We want to provide an approximated position-weight back pressure (APWBP) policy $p_\diamond(t)$ that will stabilize the network whenever possible. To do so, we compare with policy $p_{\text{PWBP}}(t)$ as defined by Li and Jabari (2019), which is proven to have the maximum-stability property. Weights $w_{a,b}(t)$ is already defined as equation (4.11)

Lemma 7. *The following calculation is bounded by some constant $\kappa < \infty$:*

$$\left| \sum_{(a,b)\in\mathcal{M}} \hat{w}_{a,b}(t) q_{a,b}(p_\diamond(t)) - \max_{\mathbf{p}\in\mathcal{P}} \sum_{(a,b)\in\mathcal{M}} w_{a,b}(t) \mathbb{E}\left[q_{a,b}(p_{\text{PWBP}}(t))\right] \right| \leq \kappa \tag{4.37}$$

Proof. Case 1: when upstream link a is a source link and downstream link b is an internal link. Equation (4.37) can be rewritten as follows:

$$\begin{aligned} \Bigg| & \underbrace{\left(c_{a,b}\hat{\rho}_a^b(t) - \int_0^{l_b} \left|\frac{l_b - x}{l_b}\right| \sum_{(b,c)\in\mathcal{M}} c_{b,c}\pi_{b,c}(t)\hat{\rho}_b^c(x,t)dx \right)}_{\text{APWBP}} q_{a,b}(p_\diamond(t)) \\ & - \underbrace{\left(c_{a,b}\rho_a^b(t) - \int_0^{l_b} \left|\frac{l_b - x}{l_b}\right| \sum_{(b,c)\in\mathcal{M}} c_{b,c}\pi_{b,c}(t)\rho_b^c(x,t)dx \right)}_{\text{PWBP}} q_{a,b}(p_{\text{PWBP}}(t)) \Bigg| \end{aligned} \tag{4.38}$$

To determine whether equation (4.38) is bounded or not, we need to maximize the difference between the first and second terms of equation (4.38). If the maximum difference is bounded, then we can determine equation (4.38) is bounded. The idea is, that we need to leverage the worst-case difference in density approximation by APWBP and PWBP. It is worth mentioning that: First, term $c_{a,b}\hat{\rho}_a^b(t)$ and $c_{a,b}\rho_a^b(t)$ are the same for APWBP and PWBP, since we use the same vehicles loading method as Li and Jabari (2019). Second, the density used by PWBP is the true density, since it assumes to be able to obtain density

at every point along a link; Third, APWBP can obtain accurate vehicle occupancy value by $N_a(0,t) - N_a(l_a,t)$ from upstream and downstream end loop detectors, which is same as PWBP. Finally, the worst traffic state that loop detectors can estimate is the jam density condition. Hence, the worst case for density difference approximated is that the density approximation by APWBP has incorrect vehicle locations, and vehicles are at jam density. If vehicle occupancy is the same and traffic condition is at the worst state, jam density, then the spatial distance occupied by vehicle Δx are the same no matter the spatial location along the link. Then we have the following equation for spatial distance occupied by the vehicle on link b.

$$\Delta x_b = \frac{\int_0^{l_b} \rho_b(x,t)dx}{\rho_{\mathrm{j}}} \tag{4.39}$$

We define the capacity of link a is q_a^{cap}, capacity of link b is q_b^{cap}. Then the movement capacity is $q_{ab}^{\mathrm{cap}} = \min\{q_a^{\mathrm{cap}}, q_b^{\mathrm{cap}}\}$. The greatest difference in the pressure weights occurs when density ρ has all of the vehicles at the end of the link (at jam density so they are as close to the end as possible) and $\hat{\rho}$ has all vehicles at the start of the link (at jam density), or vice versa. Therefore, without loss of generality, assume for APWBP, the density is approximated at the start of link, but in reality vehicles are at the end of link. Then equation (4.38) can be rewritten as follows:

$$\Bigg| \underbrace{\left(- \sum_{(b,c)\in\mathcal{M}} c_{b,c}\pi_{b,c}^2(t) \int_0^{l_b} \left(1 - \frac{x}{l_b}\right) \hat{\rho}_b(x,t)dx \right) q_{a,b}(p_\diamond(t))}_{\text{APWBP}}$$

$$- \underbrace{\left(- \sum_{(b,c)\in\mathcal{M}} c_{b,c}\pi_{b,c}^2(t) \int_0^{l_b} \left(1 - \frac{x}{l_b}\right) \rho_b(x,t)dx \right) q_{a,b}(p_{\mathrm{PWBP}}(t))}_{\mathrm{PWBP}} \Bigg| \tag{4.40}$$

$$= \Bigg| \underbrace{\left(- \sum_{(b,c)\in\mathcal{M}} c_{b,c}\pi_{b,c}^2(t) \left(\int_0^{l_b} \hat{\rho}_b(x,t)dx - \frac{1}{l_b} \int_0^{l_b} x\hat{\rho}_b(x,t)dx \right) \right) q_{a,b}(p_\diamond(t))}_{\mathrm{APWBP}}$$

$$- \underbrace{\left(- \sum_{(b,c)\in\mathcal{M}} c_{b,c}\pi_{b,c}^2(t) \left(\int_0^{l_b} \rho_b(x,t)dx - \frac{1}{l_b} \int_0^{l_b} x\rho_b(x,t)dx \right) \right) q_{a,b}(p_{\mathrm{PWBP}}(t))}_{\mathrm{PWBP}} \Bigg| \tag{4.41}$$

$$= \Bigg| \underbrace{\left(- \sum_{(b,c)\in\mathcal{M}} c_{b,c}\pi_{b,c}^2(t) \left(\int_0^{\Delta x_b} \rho_{\mathrm{j}}dx - \frac{1}{l_b} \int_0^{\Delta x_b} x\rho_{\mathrm{j}}dx \right) \right) q_{a,b}(p_\diamond(t))}_{\mathrm{APWBP}}$$

$$- \underbrace{\left(- \sum_{(b,c)\in\mathcal{M}} c_{b,c}\pi_{b,c}^2(t) \left(\int_{l_b-\Delta x_b}^{l_b} \rho_{\mathrm{j}}dx - \frac{1}{l_b} \int_{l_b-\Delta x_b}^{l_b} x\rho_{\mathrm{j}}dx \right) \right) q_{a,b}(p_{\mathrm{PWBP}}(t))}_{\mathrm{PWBP}} \Bigg| \tag{4.42}$$

$$= \Bigg| \underbrace{\left(- \sum_{(b,c)\in\mathcal{M}} c_{b,c}\pi_{b,c}^2(t) \left(\rho_{\mathrm{j}}\Delta x_b - \frac{\rho_{\mathrm{j}}(\Delta x_b)^2}{2l_b} \right) \right) q_{a,b}(p_\diamond(t))}_{\mathrm{APWBP}}$$

$$- \underbrace{\left(- \sum_{(b,c)\in\mathcal{M}} c_{b,c}\pi_{b,c}^2(t) \left(\frac{\rho_{\mathrm{j}}(\Delta x_b)^2}{2l_b} \right) \right) q_{a,b}(p_{\mathrm{PWBP}}(t))}_{\mathrm{PWBP}} \Bigg| \tag{4.43}$$

$$= \Bigg| \underbrace{\left(- \sum_{(b,c)\in\mathcal{M}} c_{b,c}\pi_{b,c}^2(t) \left(\rho_{\mathrm{j}}\Delta x_b - \frac{\rho_{\mathrm{j}}(\Delta x_b)^2}{2l_b} \right) \right) q_{a,b}(p_\diamond(t))}_{\mathrm{APWBP}}$$

$$-\underbrace{\left(-\sum_{(b,c)\in\mathcal{M}} c_{b,c}\pi_{b,c}^2(t)\left(\frac{\rho_{\mathrm{j}}(\Delta x_b)^2}{2l_b}\right)\right)q_{a,b}(p_{\mathrm{PWBP}}(t))}_{\mathrm{PWBP}}\Bigg| \tag{4.44}$$

Since $q_{a,b}(p_\diamond(t)) \leq q_{ab}^{\mathrm{cap}}$, which is the same for $q_{a,b}(p_{\mathrm{PWBP}}(t))$. We have the following relationship for equation (4.44):

$$\begin{aligned}\text{RHS of (4.44)} \leq &\Bigg|\underbrace{\left(-\sum_{(b,c)\in\mathcal{M}} c_{b,c}\pi_{b,c}^2(t)\left(\rho_{\mathrm{j}}\Delta x_b - \frac{\rho_{\mathrm{j}}(\Delta x_b)^2}{2l_b}\right)\right)q_{ab}^{\mathrm{cap}}}_{\mathrm{APWBP}} \\ &-\underbrace{\left(-\sum_{(b,c)\in\mathcal{M}} c_{b,c}\pi_{b,c}^2(t)\left(\frac{\rho_{\mathrm{j}}(\Delta x_b)^2}{l_b}\right)\right)q_{ab}^{\mathrm{cap}}}_{\mathrm{PWBP}}\Bigg| \qquad (4.45)\\ = &\left|-\sum_{(b,c)\in\mathcal{M}} c_{b,c}\pi_{b,c}^2(t)\left(\rho_{\mathrm{j}}\Delta x_b + \frac{\rho_{\mathrm{j}}(\Delta x_b)^2}{l_b}\right)\right|q_{ab}^{\mathrm{cap}} \qquad (4.46)\end{aligned}$$

Because $c_{c,b}$, $\pi_{b,c}$,l_b are given non-negative constants, $\Delta x_b \in (0, l_b)$, $\frac{\Delta x_a}{l_a} \in (0,1)$, $\frac{\Delta x_b}{l_b} \in (0,1)$, $\rho_{\mathrm{j}}\Delta x_b \in (0, Occ_{\max}^b)$, where $Occ_{\max}^b$ is maximum occupancy (positive constant) on link b. Therefore, equation (4.46) is a non-negative constant, which is the upper bound of equation (4.38). When link a is a source link, equation (4.37) is bounded by some constant $\kappa < \infty$.

Case 2: when upstream link a is internal link and downstream link b is also a internal link. Equation (4.37) can be rewritten as follows

$$\left|\left(c_{a,b}\int_0^{l_a}\left|\frac{x}{l_a}\right|\hat{\rho}_a^b(x,t)dx\right.\right.$$

$$
\begin{aligned}
&- \int_0^{l_b} \left| \frac{l_b - x}{l_b} \right| \sum_{(b,c)\in\mathcal{M}} c_{b,c}\pi_{b,c}(t)\hat{\rho}_b^c(x,t)dx \Bigg) q_{a,b}(p_\diamond(t)) \\
&- \Bigg(c_{a,b} \int_0^{l_a} \left| \frac{x}{l_a} \right| \rho_a^b(x,t)dx \\
&- \int_0^{l_b} \left| \frac{l_b - x}{l_b} \right| \sum_{(b,c)\in\mathcal{M}} c_{b,c}\pi_{b,c}(t)\rho_b^c(x,t)dx \Bigg) q_{a,b}(p_{\mathrm{PWBP}}(t)) \Bigg|
\end{aligned} \tag{4.47}
$$

The idea is similar to Case 1. We need to leverage the worst case in density distribution possible for weight calculation. The worst case is as follows: APWBP approximates vehicles on link a located at the end of link a and vehicles on link b are located at the start of link b. However, vehicles on link a located at the start of link a and vehicles on link b are located at the end of link b in reality, which can be obtained by PWBP, since it assumes to be able to obtain density at every point along a link. In addition, APWBP can obtain accurate vehicle occupancy for upstream link a by $N_a(0,t) - N_a(l_a,t)$ and downstream link b by $N_b(0,t) - N_b(l_b,t)$, which are same as PWBP. Furthermore, jam density, which is the worst traffic state that loop detectors can collect, and it is also the worst condition in reality. Spatial distances occupied by vehicles are Δx no matter which position on the link the vehicle. Therefore, we have the following equation when we include the spatial distance occupied by vehicles on link a and link b:

$$
\begin{aligned}
&\Bigg| \Bigg(c_{a,b}\pi_{a,b}(t) \int_0^{l_a} \left(\frac{x}{l_a} \right) \hat{\rho}_a(x,t)dx \\
&- \sum_{(b,c)\in\mathcal{M}} c_{b,c}\pi_{b,c}^2(t) \int_0^{l_b} \left(1 - \frac{x}{l_b} \right) \hat{\rho}_b(x,t)dx \Bigg) q_{a,b}(p_\diamond(t)) \\
&- \Bigg(c_{a,b}\pi_{a,b}(t) \int_0^{l_a} \left(\frac{x}{l_a} \right) \rho_a(x,t)dx
\end{aligned}
$$

$$
\left. - \sum_{(b,c)\in\mathcal{M}} c_{b,c}\pi_{b,c}^2(t) \int_0^{l_b} \left(1 - \frac{x}{l_b}\right) \rho_b(x,t)dx \right) q_{a,b}(p_{\mathrm{PWBP}}(t)) \Bigg| \tag{4.48}
$$

$$
\begin{aligned}
=\Bigg| & \left(\frac{c_{a,b}\pi_{a,b}(t)}{l_a} \int_0^{l_a} x\hat{\rho}_a(x,t)dx \right. \\
& \left. - \sum_{(b,c)\in\mathcal{M}} c_{b,c}\pi_{b,c}^2(t) \left(\int_0^{l_b} \hat{\rho}_b(x,t)dx - \frac{1}{l_b} \int_0^{l_b} x\hat{\rho}_b(x,t)dx \right) \right) \times q_{a,b}(p_\diamond(t)) \\
& - \left(\frac{c_{a,b}\pi_{a,b}(t)}{l_a} \int_0^{l_a} x\rho_a(x,t)dx \right. \\
& \left. - \sum_{(b,c)\in\mathcal{M}} c_{b,c}\pi_{b,c}^2(t) \left(\int_0^{l_b} \rho_b(x,t)dx - \frac{1}{l_b} \int_0^{l_b} x\rho_b(x,t)dx \right) \right) \\
& \times q_{a,b}(p_{\mathrm{PWBP}}(t)) \Bigg|
\end{aligned} \tag{4.49}
$$

$$
\begin{aligned}
=\Bigg| & \left(\frac{c_{a,b}\pi_{a,b}(t)}{l_a} \left(\int_{l_a - x_a}^{l_a} x\rho_{\mathrm{j}}dx \right) \right. \\
& \left. - \sum_{(b,c)\in\mathcal{M}} c_{b,c}\pi_{b,c}^2(t) \left(\int_0^{\Delta x_b} \rho_{\mathrm{j}}dx - \frac{1}{l_b} \int_0^{\Delta x_b} x\rho_{\mathrm{j}}dx \right) \right) \times q_{a,b}(p_\diamond(t)) \\
& - \left(\frac{c_{a,b}\pi_{a,b}(t)}{l_a} \left(\int_0^{\Delta x_a} x\rho_{\mathrm{j}}dx \right) \right. \\
& \left. - \sum_{(b,c)\in\mathcal{M}} c_{b,c}\pi_{b,c}^2(t) \left(\int_{l_b - \Delta x_b}^{l_b} \rho_{\mathrm{j}}dx - \frac{1}{l_b} \int_{l_b - \Delta x_b}^{l_b} x\rho_{\mathrm{j}}dx \right) \right) \times q_{a,b}(p_{\mathrm{PWBP}}(t)) \Bigg|
\end{aligned} \tag{4.50}
$$

$$
\begin{aligned}
=\Bigg| & \left(\frac{c_{a,b}\pi_{a,b}(t)}{l_a} \left(\rho_{\mathrm{j}} \times \frac{1}{2}(l_a^2 - (l_a - \Delta x_a)^2 \right) \right. \\
& \left. - \sum_{(b,c)\in\mathcal{M}} c_{b,c}\pi_{b,c}^2(t) \left(\rho_{\mathrm{j}}\Delta x_b - \frac{\rho_{\mathrm{j}}(\Delta x_b)^2}{2l_b} \right) \right) \\
& \times q_{a,b}(p_\diamond(t))
\end{aligned}
$$

$$
\begin{aligned}
&- \left(\frac{c_{a,b}\pi_{a,b}(t)}{l_a} \left(\frac{\rho_{\mathrm{j}}(\Delta x_a)^2}{2} \right) \right. \\
&\left. - \sum_{(b,c)\in\mathcal{M}} c_{b,c}\pi_{b,c}^2(t) \left(\frac{\rho_{\mathrm{j}}(\Delta x_b)^2}{2l_b} \right) \right) \times q_{a,b}(p_{\mathrm{PWBP}}(t)) \Bigg| \qquad (4.51) \\
= &\left| \left(\frac{c_{a,b}\pi_{a,b}(t)}{l_a} \left(\frac{\rho_{\mathrm{j}}\Delta x_a}{l_a} - \frac{\rho_{\mathrm{j}}(\Delta x_a)^2}{2l_a} \right) - \sum_{(b,c)\in\mathcal{M}} c_{b,c}\pi_{b,c}^2(t) \left(\rho_{\mathrm{j}}\Delta x_b - \frac{\rho_{\mathrm{j}}(\Delta x_b)^2}{2l_b} \right) \right) \right. \\
&\times q_{a,b}(p_\diamond(t)) \\
&\left. - \left(\frac{c_{a,b}\pi_{a,b}(t)}{l_a} \left(\frac{\rho_{\mathrm{j}}(\Delta x_a)^2}{2l_a} \right) - \sum_{(b,c)\in\mathcal{M}} c_{b,c}\pi_{b,c}^2(t) \left(\frac{\rho_{\mathrm{j}}(\Delta x_b)^2}{2l_b} \right) \right) q_{a,b}(p_{\mathrm{PWBP}}(t)) \right| \qquad (4.52)
\end{aligned}
$$

The number of vehicles that can move should be bounded by the capacity, that is $q_{a,b}(p_\diamond(t)) \leq q_{ab}^{\mathrm{cap}}$, which is same for $q_{a,b}(p_{\mathrm{PWBP}}(t))$. Then have following relationship for equation (4.52), that is

RHS of (4.52)

$$
\begin{aligned}
\leq &\left| \left(\frac{c_{a,b}\pi_{a,b}(t)}{l_a} \left(\frac{\rho_{\mathrm{j}}\Delta x_a}{l_a} - \frac{\rho_{\mathrm{j}}(\Delta x_a)^2}{2l_a} \right) - \sum_{(b,c)\in\mathcal{M}} c_{b,c}\pi_{b,c}^2(t) \left(\rho_{\mathrm{j}}\Delta x_b - \frac{\rho_{\mathrm{j}}(\Delta x_b)^2}{2l_b} \right) \right) q_{ab}^{\mathrm{cap}} \right. \\
&\left. - \left(\frac{c_{a,b}\pi_{a,b}(t)}{l_a} \left(\frac{\rho_{\mathrm{j}}(\Delta x_a)^2}{2l_a} \right) - \sum_{(b,c)\in\mathcal{M}} c_{b,c}\pi_{b,c}^2(t) \left(\frac{\rho_{\mathrm{j}}(\Delta x_b)^2}{2l_b} \right) \right) q_{ab}^{\mathrm{cap}} \right| \qquad (4.53) \\
= &\left| \left(\frac{c_{a,b}\pi_{a,b}(t)}{l_a} \left(\frac{\rho_{\mathrm{j}}\Delta x_a}{l_a} - \frac{\rho_{\mathrm{j}}(\Delta x_a)^2}{l_a} \right) - \sum_{(b,c)\in\mathcal{M}} c_{b,c}\pi_{b,c}^2(t) \left(\rho_{\mathrm{j}}\Delta x_b - \frac{\rho_{\mathrm{j}}(\Delta x_b)^2}{l_b} \right) \right| q_{ab}^{\mathrm{cap}} \qquad (4.54)
\end{aligned}
$$

Because $c_{a,b}$, $c_{c,b}$, $\pi_{a,b}$, $\pi_{b,c}$, l_a, l_b are given non-negative constants, $\Delta x_a \in (0, l_a)$, $\Delta x_b \in (0, l_b)$, $\frac{\Delta x_a}{l_a} \in (0,1)$, $\frac{\Delta x_b}{l_b} \in (0,1)$, $\rho_{\mathrm{j}}\Delta x_a \in (0, Occ_{\max}^a)$, where $Occ_{\max}$ is the maximum occupancy (positive constant) on link a, and $\rho_{\mathrm{j}}\Delta x_b \in (0, Occ_{\max}^b)$. Therefore,

equation (4.54) is a non-negative constant which is the upper bound of equations (4.37) and (4.37). Overall, when link a and link b are the internal link, equation (4.37) is bounded by some constant $\kappa < \infty$.

Corollary 1. *The proposed APWBP can still achieve maximum stability*

Proof. The difference between APBWP and PWBP is bounded by some constant κ based on Lemma 1. Combining Lemma 1 and Proposition 1, we can conclude that the APWBP can still achieve maximum stability.

4.5 Simulations and numerical results

To test the performance of our proposed APWBP, we set up simulations on the Sioux Falls network, Figure 4.6, which has been used frequently in the literature as a benchmark network. The Sioux Falls network includes 24 nodes and 72 links, which has a larger network size than the network used in Li and Jabari (2019). In addition, our phase structure is same as phases 1–4 in Li and Jabari (2019)'s four-leg isolated intersections. Hourly demand for the Sioux Falls network is 15025 vehicles per hour. The simulation experiments are written in Java using the cell transmission model with the trapezoidal flow-density relationship, which more realistic than the triangular flow-density relationship, and we used IBM CPLEX to solve the optimization. We set the simulation to 3 hours to ensure it is enough long for stability, and the time step in the simulation is 15 seconds per time step. The main purpose of the simulations is to numerically compare the stability performance between our proposed APWBP and Li and Jabari (2019)'s PWBP. However, our method is also more easily implemented in reality than Li and Jabari (2019)'s method.

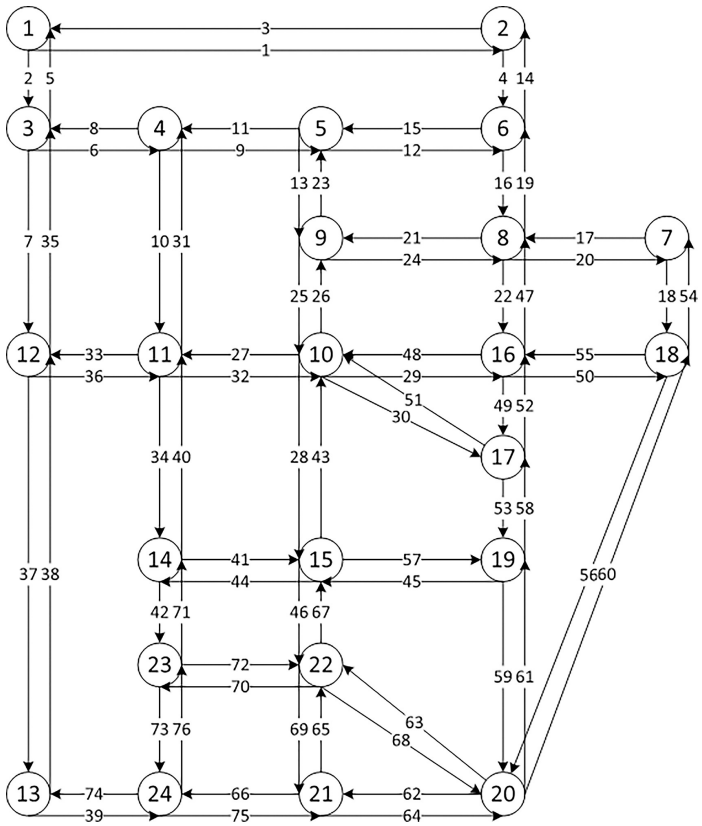

Figure 4.6: Sioux Falls Network

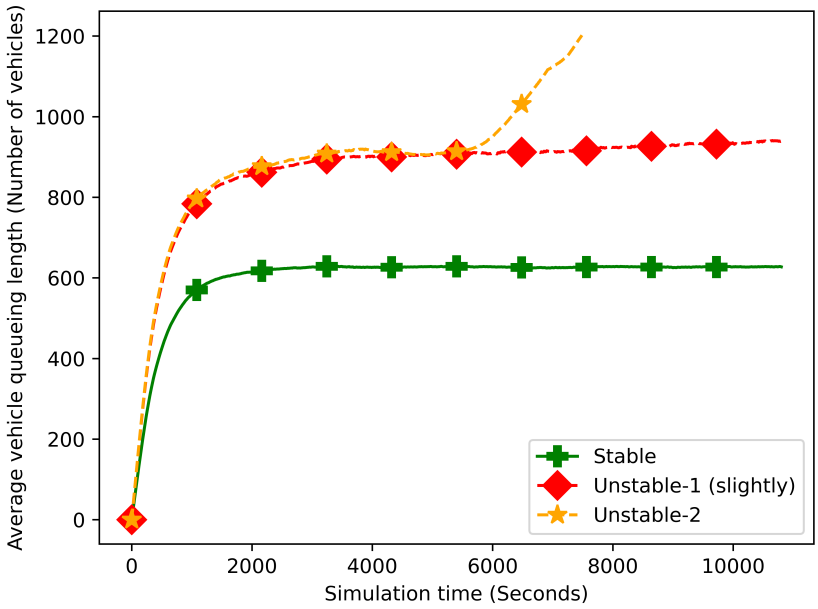

Figure 4.7: Example of stable and unstable network

4.5.1 Network stability comparisons

First, we compare the stability performance based on Definition 4. Figure 4.7 shows an example of a stable network and two examples of unstable networks. When the demand is in the stable region, the average queue length will converge to a constant as time increases. When the demand is outside of the stable region, the average queue lengths will increase to an arbitrarily large number. Depending on the magnitude of the demand, the queue lengths will increase at the different slopes. The ideal condition is a traffic signal controller that can achieve network stability.

Figure 4.8 compares the average queue lengths at different vehicle demands including stable demand and unstable demand. When the demand is in the stable region, the performances for both APWBP and PWBP are similar, that is the average queue length converges to the same constant under the same stable demand. In addition, for unstable demand, the

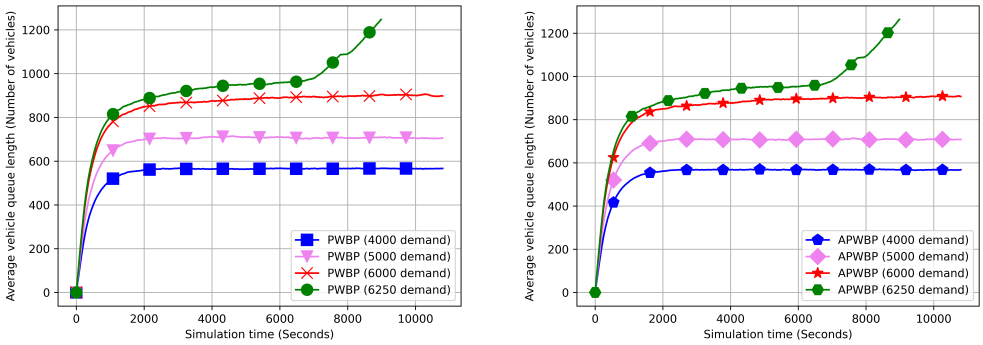

(a) Network stability for PWBP

(b) Network stability for APWBP

Figure 4.8: Average link travel time

queue length is similar for both APWBP and PWBP.

We provide more detailed information about the maximum stability in Figure 4.9. We simulate vehicle demands from 5500 to 6250 and find the maximum stable demand for APWBP and PWBP is the same, which is around 5750 vph. Therefore, Figure 4.9 also demonstrates the stability results of Section 4.4.

4.5.2 Link travel time

It is also important to compare average link travel times, since link travel time is a significant indicator of performance. Figure 4.10 shows that, as demand increases, average vehicle link travel time is longer. In addition, when demand is within the stable region, average link travel time will converge to a constant, and the travel times for APWBP and PWBP are similar.

We also provide the link travel time dynamics when the vehicle demand is 6250 vehicles per hour, which is outside of the stable region for APWBP and PWBP. Figures Figure 4.10a and Figure 4.10b show that, when vehicle demand is too large, the travel time will increase to infinity for APWBP and PWBP. Even so, the curves for signal policies still exhibit a similar pattern when demand is 6250 vehicles per hour.

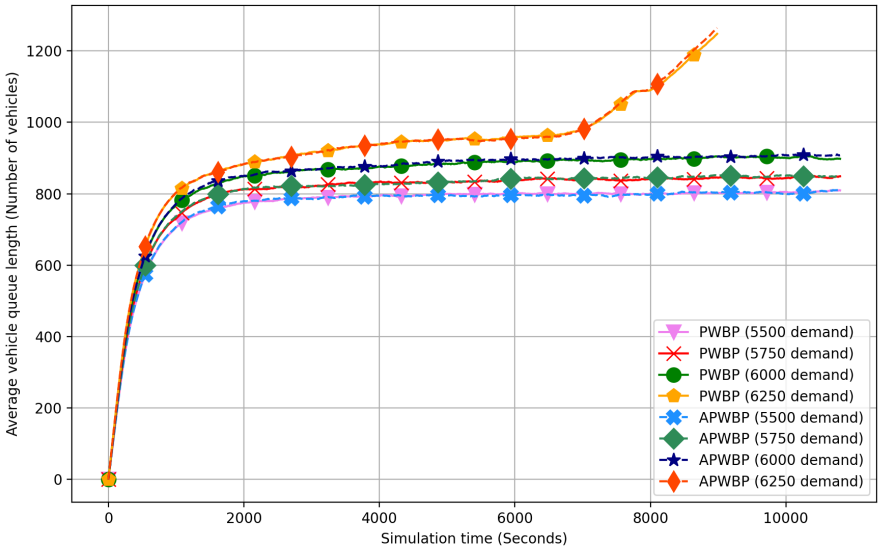

Figure 4.9: Maximum-stable demand for APWBP and PWBP

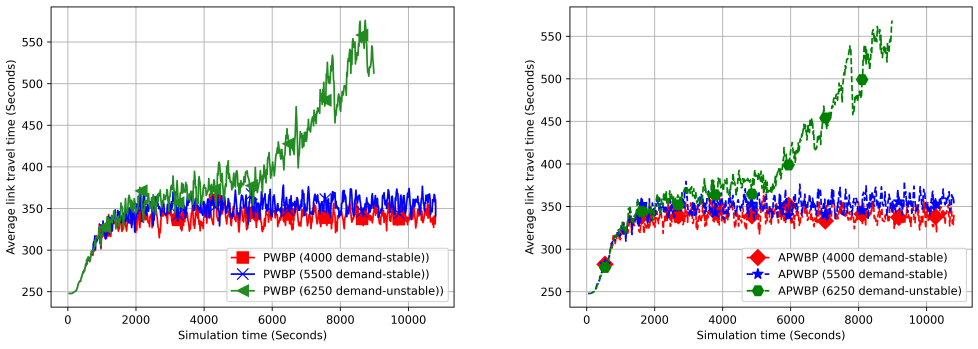

(a) Average link travel time for PWBP (b) Average link travel time for APWBP

Figure 4.10: Average link travel time

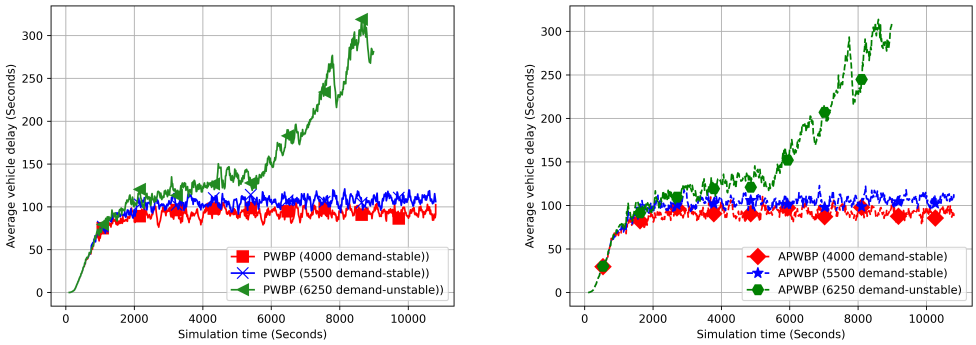

(a) Average delay for PWBP (b) Average delay for APWBP

Figure 4.11: Average delay

4.5.3 Vehicle delay

Delay is also a important indicator for traffic signal timing evaluation (Li and Jabari, 2019; Liu and Gayah, 2022; Wang et al., 2022). We also provide the average vehicle delay dynamics under stable demand and unstable demand. Unsurprisingly, under stable demand, the average vehicle delay will converge to a constant, and delay increases with the vehicle demand. In addition, the pattern of fluctuations is very similar, and the delay value will approach a constant for both APWBP and PWBP. Furthermore, when the demand is outside of the stable region, the average network delay increases to infinity for both traffic signal policies. Details are shown in Figure 4.11.

4.5.4 Fluctuated demand loading

It is also interesting to explore the ability to handle high congestion scenarios. Figure 4.12 provides the network delay dynamics and the average queue lengths dynamics when we load demand time-varying demand. Specifically, when the simulation time is between 0 to 3600 seconds, vehicle loading demand is 3000 vehicles per hour, which is within the stable region. When simulation time is between 3600 seconds to 5400 seconds, we set the vehicle

loading demand to 5250 vehicles per hour, which is still inside the stable region. Then demand is set as 6500 vehicles per hour, which is significantly larger than the stable stable region to make the network congested. After that, we drop the demand to 0 to observe the ability to release congestion for both APWBP and PWBP. Figure 4.12b demonstrates that APWBP and PWBP have the same maximum stable region and can handle network queueing length at different demands, even as demand loading fluctuates, which is consistent with Section 4.2. Figure 4.12a shows the result of network average delay. It is not surprising that the two controllers show similar delay patterns when demand loading increases from 3000 vehicles per hour to 6500 vehicles demand. But when the demand starts dropping, the delay of PWBP reduces faster than APWBP. However, they will approach a same constant when vehicle demand is within the stable region.

4.5.5 Computation times

We compare the computational efficiency of APWBP and PWBP. Table 4.1 provides results for the two controller at different vehicle demands. PWBP has lower computation time than APWBP because APWBP needs to calculate the density boundary positions every time step, then calculate the approximate position-weight for signal timing. The computation times for APWBP are roughly double that of PWBP, but they are still sufficiently low for real-time computation.

Table 4.1: Computation times for APBWP and PWBP

Demands	APWBP (seconds /3 hours simulation)	PWBP (seconds / 3 hours simulation)
3000	153.30	73.41
4000	153.47	78.39
5000	161.41	80.19
6250 (unstable)	142.73	79.13

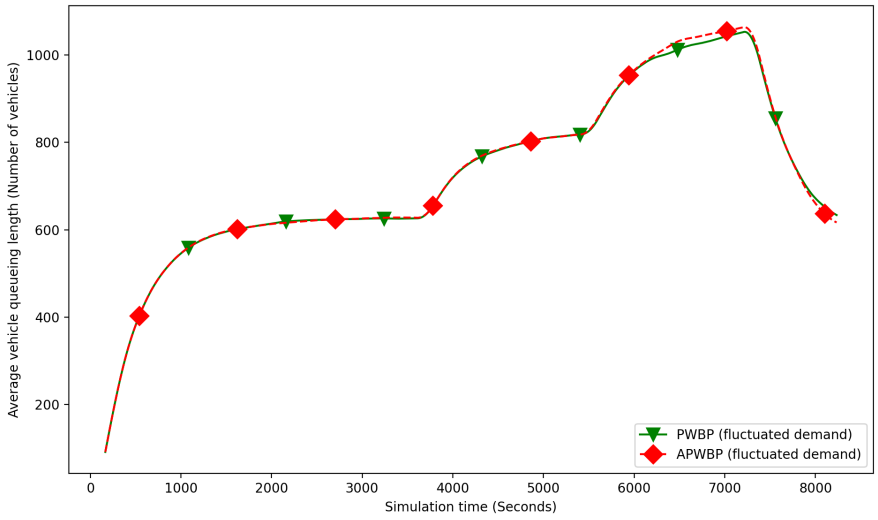

(a) Average delay dynamics

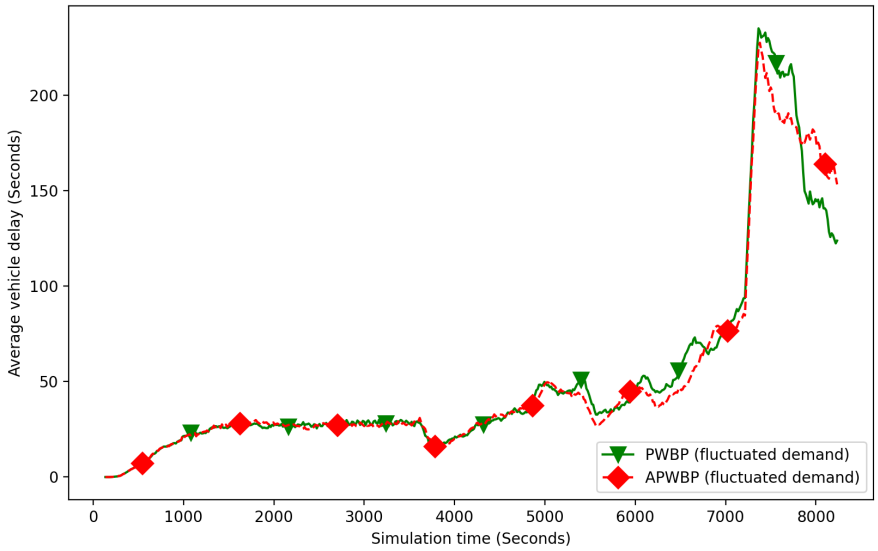

(b) Average queueing length dynamics

Figure 4.12: Ability to handle congestion

4.6 Conclusions

This study builds on the method of Li and Jabari (2019) and provides an approximate position-weighted BP (APWBP) control to reduce the sensor requirements for implementation in practice (XU et al., 2022). We use a triangular flow-density relationship to approximate the density within each link using only 2 loop detectors at the upstream and downstream ends of each link. We mathematically proved that the APWBP traffic signal controller can achieve maximum throughput at the network level.

Numerical results in the Sioux Falls network suggest that the proposed APWBP controller can capture traffic density dynamics along the link and stabilize the network at the same level as the PWBP controller. In addition, average link travel time results and average network delay results support the analytical proof, and show that proposed APWBP controller has almost the same performance as the PWBP controller. We also provide network delay dynamics and average queue length dynamics when we load demand at different rates to check the ability to handle network congestion, and the results show that PWBP can release congestion only slightly faster than APWBP based on the delay dynamics, which is shown in Figure 4.12a. Although the computation time of APWBP is higher than PWBP, we provide a way to implement it without requiring internal information along the link. We need to mention that Li and Jabari (2019) showed that PWBP performs significantly better than fixed-time controls, and APWBP should inherit much of those benefits. Overall, these results strongly support that our APWBP can achieve the same maximum throughput as Li and Jabari (2019)'s PWBP, while being easier to implement in practice.

In the future, there are many extensions to consider. For instance, integrating back-pressure control with perimeter control technologies will be interesting since perimeter control can prevent vehicles from entering congested areas, like central business districts, when the demand is approaching the maximum stable demand. Last but not least, the idea of the approximate position-weighted calculation can be leveraged to ramp meters for better

freeway control (Zhao et al., 2020; Ma and Wang, 2021).

Chapter 5

Smoothing-MP: a novel max-pressure signal control considering signal coordination to smooth traffic in urban network

5.1 Introduction

Traffic signal lights have been in use for over 100 years since the first colored traffic light was introduced in England in the 19th century Webster (1958). The goals of installing traffic signal controls include providing orderly vehicle movements, reducing conflicts, increasing traffic capacity at intersections, assigning right-of-way to increase driver confidence, reducing congestion, and more. Currently, there are two main types of traffic signal controllers widely used in cities. The first is fixed-time control, which requires historical traffic information to create signal timing plans. The other is actuated or adaptive signal controllers, which rely on sensors such as loop detectors and video detectors. However, as traffic volumes increase, traffic systems require more advanced traffic signal controllers, particularly network-level traffic signal controllers for urban traffic networks. Most existing traffic signal controllers are centralized, meaning that signals across a network are controlled together. A consequence of that approach is that the computation time increase

drastically as the network size increases. Therefore, traffic signal researchers have begun to focus on decentralized traffic signal controllers. Max-pressure (MP) control, also known as back-pressure (BP) control, is one such decentralized traffic signal control policy that has gained attention since Varaiya (2013) first proposed it for traffic signal control. It is worth noting that Tassiulas and Ephremides (1990) initially proposed the MP policy in communication and power systems before Varaiya (2013) introduced it into traffic signal control. MP control has two main advantages: provable maximum throughput for demand that can be served by any other signal control, and a well-designed decentralized structure. This means that MP control's decision-making relies only on information from upstream and downstream, allowing for excellent scalability.

Traffic patterns are not uniformly distributed throughout city networks. For example, in New York City, the most congested street is the Brooklyn-Queens Expressway, which experiences more daily congestion than other roads. Urban and traffic planners recognize that arterial corridors attract a significant portion of traffic demand in urban areas due to mixed land-use development, which includes business centers, parking lots, shopping malls, and sports and recreational areas. Therefore, arterial corridors require proper signal timing to reduce the number of stops and vehicle delays, providing smooth operation for vehicles traveling through these corridors. Traffic operational efficiency is vital for arterial corridors. Along arterial corridors, numerous continuous signalized intersections exist. If traffic lights can coordinate with one another to provide continuous green lights for vehicles traveling at appropriate speeds, the average number of stops and delays can be significantly reduced. This concept is called signal coordination (Feng, 2015).

Numerous previous research papers have demonstrated that traffic systems can benefit from proper signal coordination design strategies (Ma et al., 2018b; Yao et al., 2019; Yue, 2020). National Academies of Sciences et al. (2015) stated that the purpose of coordinating traffic signals is to facilitate smooth traffic flow along streets and highways, ultimately reducing travel times, stops, and delays. Over the past few decades, researchers

have continuously developed more advanced signal coordination systems. Some studies have focused on designing optimal bandwidth along arterial corridors, an idea originally proposed by Little et al. (1981) and called MAXBAND. However, the MAXBAND method has certain limitations, such as its underperformance in situations involving asymmetrical network demand, transit vehicles, major origin-destination flows, long arterials, and network scenarios (Zhang et al., 2016; Arsava et al., 2018; Ma et al., 2018b; Zhang et al., 2015). As a result, researchers have developed improved bandwidth-based signal coordination methods. For example, Gartner et al. (1991) proposed the MULTIBAND method to accommodate various traffic patterns for each link along an arterial corridor. Zhang et al. (2015) introduced the AM-BAND method, a type of asymmetrical MULTIBAND method that achieves superior performance along arterials. Ma et al. (2018b) developed the PM-BAND approach to integrate transit vehicles into signal coordination, while Arsava et al. (2018) created OD-NETBAND to provide optimal bandwidth for major origin-destination stream directions. Another well-known signal coordination approach is performance-based methods, which aim to minimize vehicle delays, the number of stops, and travel times. The most famous example is TRANSYT (Traffic Network Study Tools). Improved methods based on TRANSYT have been developed, such as time-dependent TRANSYT (Wong et al., 2002), GIS (Geographic Information Systems)-based TRANSYT (de Oliveira and Ribeiro, 2001), and Cohen and Liu (1986). However, most existing signal coordination research focuses on single arterial corridors. Only a few studies have mentioned that traffic engineers should consider signal coordination at the network and area-wide levels (Yan et al., 2019; Zhang et al., 2016). Moreover, most existing signal coordination policies are formulated as mixed-integer programs, which are not scalable for large city networks.

The MP control, a well-designed decentralized signal controller with provable maximum throughput, has attracted our attention. However, it has some limitations, such as activating signals in an arbitrary order (Levin et al., 2020). Some researchers have attempted to enhance the original MP control by designing a cyclic structure, as seen in

papers such as (Le et al., 2015; Levin et al., 2020). Other studies suggest that travel time or travel delay-based pressure calculations are more accurate and easier to implement in practical situations than the original queue-length based pressure calculation (Mercader et al., 2020; Liu and Gayah, 2022). MP control was modified for transit signal priority (Xu et al., 2022b) and pedestrian access (Xu et al.). However, no research has yet integrated both MP control and signal coordination. It is important to note that MP control also falls under the category of actuated or adaptive signal control, as it relies on traffic sensors installed on upstream and downstream roads. Furthermore, Das et al. (2022) indicates that coordination can be integrated with both fixed-time and actuated traffic signal control. Actuated coordination offers more advantages compared to fixed-time coordination due to its ability to respond to dynamic traffic demand on a cycle-by-cycle basis. This insight has inspired us to investigate the potential benefits of combining MP control and signal coordination to develop a novel, network-level friendly, signal-coordinated strategy.

The contributions of this dissertation are as follows: (1) We modify Varaiya (2013)'s max-pressure control policy to include signal coordination for the first time to develop Smoothing-MP. (2) We analytically prove the max-pressure control policy including signal coordination can also achieve maximum throughput at the network level without changing the stable region of the original MP control (Varaiya, 2013). (3) We implement our simulation using the Downtown Austin Network with selected coordinated corridors.

The remainder of this dissertation is organized as follows: Section 2 summarizes the related research about signal coordination methods and MP control policies. Section 3 formulates the network model with signal coordination, vehicle queueing model, stable network definition, and stable region. These contents are prerequisites for proving maximum stability for the MP control, Smoothing-MP. Section 4 proposed the Smoothing-MP and stability analysis. Section 5 presents the simulation results and we conclude in Section 6.

5.2 Literature review

In this section, we first review related papers focusing on traffic signal coordination. Then we review the existing literature on max-pressure (MP) signal control and back-pressure (BP) signal control.

5.2.1 Traffic signal coordination

Traffic engineers have observed that by implementing appropriate signal timing at a series of signalized intersections, it is possible for vehicles to travel through the entire stretch without having to stop, as long as they maintain a suitable speed. This is now the concept of signal coordination (Feng, 2015). Some past research showed that the efficiency of urban traffic systems can be improved significantly through proper signal coordination strategies (Ma et al., 2016; Yao et al., 2019; Girault et al., 2016). For instance, Girault et al. (2016) provided a comprehensive analysis of signal coordination strategies on the macroscopic fundamental diagram of urban traffic. They leveraged seven signal coordination strategies under four kinds of demand patterns to figure out the impacts of signal coordination. The results showed that good signal coordination strategies have positive impacts on the macroscopic fundamental diagram. Ma et al. (2018a) claimed that signal coordination is one of the most economical ways to reduce urban traffic congestion.

Most researchers prefer to classify signal coordination strategies into two categories: one category is to maximize the bandwidth along some corridors, and the other one is to minimize the combination of performance indexes, such as the number of stops and vehicle delay. In the category of maximizing the bandwidth, the MAXBAND method is the most representative and was proposed by Little et al. (1981). It aims to maximize the green wave bandwidth along an arterial and is solved by the branch and bound method. However, there are some limitations of the MAXBAND method such as uniform bandwidth results along an arterial and bad performance at long arterial or the network level. Later on, many

improved methods based on MAXBAND were developed. Gartner et al. (1991) proposed the MULTIBAND method, which can consider different traffic patterns along each link and provide a variable bandwidth progression in which each directional road section can obtain an individually weighted bandwidth. Note that MULTIBAND is also formulated as a mixed integer program. Zhang et al. (2016) proposed two modified MULTIBAND methods named MaxBandLA and MaxBandGN to solve traffic signal coordination problems for long arterials and grid networks respectively. To consider the major origin-destination (O-D) flows in an arterial network, Arsava et al. (2018) provided a progression optimization model named OD-NETBAND, which was formulated based on OD-BAND (a coordination strategy for arterials with major side-street traffic streams) to maximize the sum of each major OD stream's progression bandwidth. The simulation experiment is constructed under AIMSUN microscopic simulation tool. Ma et al. (2018b) proposed a partition-enable multi-mode band approach (PM-BAND), which considers transit vehicles and passenger cars together and provides signal optimization for arterials. The proposed problem was formulated as mixed-integer program which has significant performance improvements, such as much less delay and stops compared with MAXBAND and MULTIBAND.

In the category of minimizing the combination of performance index (number of stops and vehicle delays), TRANSYT is the most representative one and was developed by Dennis Roberson in the 1960s (Robertson, 1969). Some paper also classified it as performance-based method Yan et al. (2019). TRANSYT optimizes cycle length, green splits, and offsets with a predetermined phase sequence over a network of intersections (Robertson, 1969). There are also many improved traffic signal optimization methods developed based on TRANSYT. For instance, Wong (1996) proposed group-based optimization of signal timings, which formulated the traffic optimization problem as a non-linear mathematical model with an index of estimated delays and stops. However, the traffic system is a complex and dynamic system, which means the traffic demand is a time-varying variable (Vincent et al., 1980). Therefore, Wong et al. (2002) proposed a time-dependent TRAN-

SYT traffic model to be customized for dynamic traffic patterns. Then the group-based specification of signal timings is used for the proposed TRANSYT traffic model corresponding constraints on these variables. Optimization heuristics are leveraged to solve the time-dependent problem. de Oliveira and Ribeiro (2001) combined TRANSYT with the Geographic information systems (GIS) system. The advantage of combining TRANSYT with a GIS system is the convenience of data collection and data input.

Some researchers started to give more attention to future traffic environments and emergency technologies with signal coordination. Specifically, with the emergence of advanced sensors and mobile phone data, some research started focusing on developing data-driven methods to achieve signal coordination (Yao et al., 2019). For instance, Hu and Liu (2013) proposed a data-driven approach to optimize offsets for vehicle-actuated coordinated traffic signals, using the massive amount of signal status and vehicle actuation data collected from the field. The proposal was tested on a realistic scenario, a major arterial in Minnesota, USA. The result showed that the proposed method can reduce travel delays significantly. DiDi Chuxing also provided a huge set of trajectory data (Pian et al., 2020), which can provide more accurate traffic performance measures than traditional sensors. Due to the complexity of signal optimization and coordination problems, traffic signal researchers started looking at cloud computing. For instance, Zhang and Zhou (2018) proposed a coarse-grained parallel adaptive genetic algorithm (CPAGA) for the optimization of distributed coordination control, which considered the optimization of cycles, offsets, and green ratios on the cloud computing platform. The results demonstrated their proposed algorithm will not fall into a local optimum and finds a solution quickly. Learning-based methods are also becoming popular in solving transportation problems (Wei et al., 2021). Liu et al. (2021) proposed a multi-agent signal coordination framework based on reinforcement learning to achieve global optimal in the large-scale traffic network. Their proposed method is more scalable in practice. The future connected and autonomous vehicles (CAVs) environment is exciting for transportation participants (Fagnant and Kockelman, 2015). Signal con-

trol researchers also studied the opportunity brought by CAVs (Guo et al., 2019). Qi et al. (2020) invested in signalized intersection coordination design under mixed traffic flow conditions, which included human-driven vehicles and connected and autonomous vehicles. Das et al. (2022) proposed a priority-based traffic signal coordination system, which is able to consider multi-model traffic priority and vehicle actuation under the connected vehicle environment. The signal optimization model was formulated as a mixed-integer program and they tested the proposed signal control method in Anthem, Arizona, and in Portland, Oregon with satisfactory performance.

Furthermore, researchers also have a great interest in considering environmental impacts with signal coordination. Zhou et al. (2021) integrated emission reduction into signal coordination optimization problem. They formulated a bi-level multi-target optimization problem, which is able to achieve smooth traffic operation and minimize total emissions in the road network. Lv and Zhang (2012) aimed to investigate the impacts of signal coordination on traffic emissions, and the coordination quality is quantified by the platoon ratio, which is calculated by the ratio of flow rate during green to the average flow rate in the entire cycle.

However, most of these papers tried to model traffic signal coordination problems as mixed-integer programs, which are computationally difficult to solve at the network level. Although some papers try to provide a decentralized method to make signal coordination more scalable, they did not provide a rigorous mathematical proof of the maximum throughput of their signal control policy.

5.2.2 Max-pressure signal control

To the best of our understanding, no existing research has merged MP signal timing with signal coordination to streamline traffic within the urban network. Moreover, there is a lack of rigorous mathematical proofs available that incorporate signal coordination into

MP signal timing. This chapter tries to fill this gap.

5.3 Max pressure control with coordination

5.3.1 Math notations

Table 5.1: Notation.

$\mathcal{M}$	Set of movements
$\mathcal{N}$	Set of nodes
$\mathcal{A}$	Set of links
Γ_j^+	Set of outgoing links
Γ_j^-	Set of incoming links
$x_{ij}(t)$	Number of vehicles of the movement from link i to link j at time step t
$r_{ij}(t)$	Proportion of vehicles entering i that will next move to j.
$w_{ij}(t)$	Weight of vehicle turning movement from link i to link j at time step t
$d_i(t)$	Vehicle demand at at entry link i
$s_{ij}(t)$	Actuation of turning movement from link i to link j at time step t
ξ_{ij}	weight placed on coordination associated with turning movement (i, j)
$c_{ij}(t)$	signal coordination indicator associated with turning movement (i, j) at time step t
$y_{ij}(t)$	Signal control vehicle flow from link i to link j at time step t
Q_{ij}	Capacity of turning movement for private vehicles from link i to link j
f_i	Average vehicle traffic volume of link i.
M	the number of total movements of vehicles.

5.3.2 Road network model

Consider an urban network $\mathcal{G} = (\mathcal{N}, \mathcal{A})$ with nodes $\mathcal{N}$ and links $\mathcal{A}$. The link set $\mathcal{A}$ is divided into three subsets: the entry link set $\mathcal{A}_{\mathrm{e}}$, the internal link set $\mathcal{A}_{\mathrm{i}}$, and the exit link set $\mathcal{A}_{\mathrm{o}}$. The entry and exit links are not realistic links; they are used for loading and removing vehicles. Entry links represent the points where vehicles can enter the network, while exit links are the sink links where vehicles leave the network once they reach their destination nodes. The internal links $\mathcal{A}_{\mathrm{i}}$ connect the intersections located inside the vehicle network. All links are modeled are point queues. Let $\mathcal{M}$ be the set of all turning movements in the network. We use Γ_i^+ and Γ_j^+ to represent the sets of outgoing links and incoming links of nodes (intersections), respectively. One turning movement is a combination of two links, such as (i, j) and (j, k). Let $x_{ij}(t)$ be the number of vehicles on link i waiting to move to link j at time t. Let $d_i(t)$ be the demand of vehicles entering the network on link $i \in \mathcal{A}_{\mathrm{e}}$ at time t, which are independent identically distributed random variables with an average value of $\bar{d}_i$. Let $\hat{d}_i$ be the maximum value of demand. Turning proportion $r_{jk}(t)$ is the proportion of vehicles entering link j that will next move to link k at time t, which are independent identically distributed random variables with mean $\bar{r}_{jk}$. Usually, the turning proportions can be obtained from historical travel data. We separate the vehicle queues on the link by turning movements as done in previous work (Varaiya, 2013). Q_{ij} is the capacity of the turning movement from link i to link j.

5.3.3 Vehicle queueing model

We use the store-and-forward model of Varaiya (2013) to track the queue propagation in the network under discretized time. For internal links, the queue evolution can be represented by the following equations:

$$x_{ij}(t+1) = x_{ij}(t) - y_{ij}(t) + \sum_{h \in \mathcal{A}} y_{hi}(t) \times r_{ij}(t) \tag{5.1}$$

where $y_{ij}(t)$ is the signal controlled flow that start from link i then travels to link j at time step t. Vehicle flow conservation also applies to entry links with the following equation:

$$x_{ij}(t+1) = x_{ij}(t) - y_{ij}(t) + d_i(t) \times r_{ij}(t) \tag{5.2}$$

Therefore, the vehicle queue length state $\mathbf{x}(t)$ can be formulated as a stochastic Markov chain since both vehicle demand $\mathbf{d}(t)$ and turning proportion $\mathbf{r}(t)$ are independent, identically distributed random variables.

The activation of vehicle turning movement (i, j) is denoted by $s_{ij}(t) \in \{0, 1\}$, which indicates a red light or green light. The value of $y_{ij}(t)$ is determined by the following equation:

$$y_{ij}(t) = \min \{Q_{ij} s_{ij}(t), x_{ij}(t)\} \tag{5.3}$$

where Q_{ij} is the capacity of the turning movement from link i to link j. Specifically, $Q_{ij} = \min(Q_i, Q_j)$, is the maximum flow of vehicle movement (i, j). Note that capacity is the maximum road throughput, which we assume to be constant for each link.

5.3.4 Feasible signal control including signal coordination

The activation of turning movement (i, j) for vehicles is denoted by $s_{ij}(t) \in 0, 1$. $s_{ij}(t) = 1$ indicates that movement (i, j) has a green light, while $s_{ij}(t) = 0$ signifies a red light

for movement (i, j). We define $S_n(t)$ as the intersection matrix for intersection n, which encompasses the vehicle movements. The intersection control sequence S_n is defined as $S_n(t)$, for all $t \in T$. Let $\mathcal{S}$ be the set containing all feasible network control matrices for all intersections, and let $\mathcal{S}_n$ be the set of all feasible intersection matrices for intersection n. We denote the convex hull of all feasible signal control matrices as $Conv(\mathcal{S})$.

For any given intersection control sequence, the long-term average time used for serving vehicle movement (i, j) can be calculated using equation (5.4). Let $\bar{\mathbf{s}}$ and $\mathbf{s}(t)$ be the vectors of $\bar{s}_{ij}$ and $s_{ij}(t)$, respectively:

$$\bar{s}_{ij} = \lim_{T\to\infty} \frac{1}{T} \sum_{t=1}^{T} s_{ij}(t) \tag{5.4}$$

The convex hull of all feasible signal control matrices $\mathcal{S}$ is given by the following equation:

$$Conv(\mathcal{S}) = \left\{ \sum_{s\in\mathcal{S}} \lambda_s S \middle| \lambda_s S \leq 0, \sum_{s\in\mathcal{S}} \lambda_s = 1 \right\} \tag{5.5}$$

$Conv(\mathcal{S})$, is the set of average controls calculated by equation (5.4). After that, we can give Proposition 1 to relate $\mathbf{s}(t)$ to $\bar{\mathbf{s}}$.

Proposition 12. *If* $\mathbf{s}(t) \in \mathcal{S}$ *then there exists a* $\bar{\mathbf{s}} \in Conv(\mathcal{S})$ *such that*

$$\bar{\mathbf{s}} = \lim_{T\to\infty} \frac{1}{T} \sum_{t=1}^{T} \mathbf{s}(t) \tag{5.6}$$

Proof. First, we prove that $\bar{\mathbf{s}}$ is in $Conv(\mathcal{S})$. Let us define $\lambda_{\mathbf{s}}$ is the proportion of time steps

with $\mathbf{s} = \mathbf{s}(t)$. Then we can define the indicator function as

$$\mathbb{I}(\mathbf{s}(t) = \mathbf{s}) \begin{cases} 1 & \text{if } \mathbf{s}(t) = \mathbf{s} \\ 0 & \text{if } \mathbf{s}(t) \neq \mathbf{s} \end{cases} \tag{5.7}$$

Then we have

$$\bar{\mathbf{s}} = \sum_{\mathbf{s} \in \mathcal{S}} \lambda_{\mathbf{s}} \mathbf{s} \tag{5.8}$$

$$= \lim_{T \to \infty} \frac{1}{T} \sum_{t=1}^{T} \sum_{\mathbf{s} \in \mathcal{S}} T \lambda_{\mathbf{s}} \mathbf{s} \tag{5.9}$$

$$= \lim_{T \to \infty} \frac{1}{T} \sum_{t=1}^{T} \sum_{\mathbf{s}} \mathbb{I}(\mathbf{s}(t) = \mathbf{s}) \mathbf{s} \tag{5.10}$$

$$= \lim_{T \to \infty} \frac{1}{T} \sum_{t=1}^{T} \mathbf{s}(t) \tag{5.11}$$

5.3.5 Max-pressure control policy that includes signal coordination

To incorporate signal coordination into the max-pressure control, we define $c_{ij}(t)$ as the coordination indicator associated with movement (i, j) at time t. Define $\mathcal{C}$ to be the set of coordinated corridors. Each corridor $C \in \mathcal{C}$ is a subset of links (i.e., $C \subseteq \mathcal{A}$) that are intended to be coordinated. Specifically, $c_{jk}(t+1) = s_{ij}(t)$ for $(i, j, k) \in C$ for some corridor C, with $c_{ij}(t) \in \{0, 1\}$. Thus, if (i, j) has a green light at time step t, then (j, k) has a coordination indicator for a green light at time step $t + 1$. Overall, we can obtain a feasible signal control $s_{ij}(t)$ that includes signal coordination.

Now we define the MP control. This study modifies the original MP control policy of Varaiya (2013) to create the max-pressure signal control policy that considering sig-

nal coordination (Smoothing-MP). The weight calculation is the same as previous papers (Varaiya, 2013; Levin et al., 2020; Xu et al., 2022b):

$$w_{ij}(t) = x_{ij}(t) - \sum_{k \in \Gamma_j^+} r_{jk}(t) x_{jk}(t) \tag{5.12}$$

After we calculate the weight for each movement, a mixed-integer linear program is used to calculate the intersection control. The modified MP control policy considering signal coordination tries to maximize the total pressure of vehicles. $s_{ij}^{\star}(t)$ denotes the max-pressure signal control in the transportation network when considering signal coordination, which is

$$s_{ij}^{\star}(t) = \arg\max_{s \in \mathcal{S}} \left[\sum_{(i,j) \in \mathcal{M}} s_{ij}(t) Q_{ij} w_{ij}(t) + \xi_{ij} c_{ij}(t) \right] \tag{5.13}$$

Note that ξ_{ij} is the weight placed on coordination, where $\xi_{ij} \geq 0$.

To compare the modified max-pressure signal control policy, Smoothing-MP, with both Varaiya (2013)'s original max pressure control and the average signal control, we propose the following Lemma:

Lemma 8. *If the modified max-pressure signal control policy, Smoothing-MP, is used and* $\bar{\mathbf{d}} \in \mathcal{D}^0$*, then we have the following inequality with average signal control* $\bar{s}_{ij}$ *satisfying equation (5.22):*

$$\mathbb{E}\left[\sum_{(i,j) \in \mathcal{M}^2} s_{ij}^{\star}(t) Q_{ij} w_{ij}(t) + \xi_{ij} c_{ij}(t) \middle| \mathbf{x}(t) \right] \geq \mathbb{E}\left[\sum_{(i,j) \in \mathcal{M}^2} \bar{s}_{ij} Q_{ij} w_{ij}(t) \middle| \mathbf{x}(t) \right] \tag{5.14}$$

Proof. First, we have the following inequality based on definition of MP control. For all $s_{ij}(t) \in \mathcal{S}$:

$$\sum_{(i,j)\in\mathcal{M}^2} s^{\star}_{ij}(t) Q_{ij} w_{ij}(t) \geq \sum_{(i,j)\in\mathcal{M}^2} s_{ij}(t) Q_{ij} w_{ij}(t) \tag{5.15}$$

After we include signal coordination, we have the following inequality, since both ξ_{ij} and $c_{ij}(t)$ are non-negative:

$$\sum_{(i,j)\in\mathcal{M}^2} s^{\star}_{ij}(t) Q_{ij} w_{ij}(t) + \xi_{ij} c_{ij}(t) \geq \sum_{(i,j)\in\mathcal{M}^2} s^{\star}_{ij}(t) Q_{ij} w_{ij}(t) \tag{5.16}$$

Then we have

$$\sum_{(i,j)\in\mathcal{M}^2} s^{\star}_{ij}(t) Q_{ij} w_{ij}(t) + \xi_{ij} c_{ij}(t) \geq \sum_{(i,j)\in\mathcal{M}^2} s^{\star}_{ij}(t) Q_{ij} w_{ij}(t) \geq \sum_{(i,j)\in\mathcal{M}^2} s_{ij}(t) Q_{ij} w_{ij}(t) \tag{5.17}$$

Then calculating the expected value of the equation (5.15) when given the vehicle queue length $\mathbf{x}(t)$, and taking the expected value. Because there exists an $s_{ij}(t)$ with $\mathbb{E}[s_{ij}(t)] = \bar{s}_{ij}$ by Proposition 1, we have following inequality:

$$\mathbb{E}\left[\sum_{(i,j)\in\mathcal{M}^2} s^{\star}_{ij}(t) Q_{ij} w_{ij}(t) + \xi_{ij} c_{ij}(t) \middle| \mathbf{x}(t)\right] \geq \mathbb{E}\left[\sum_{(i,j)\in\mathcal{M}^2} \bar{s}_{ij} Q_{ij} w_{ij}(t) \middle| \mathbf{x}(t)\right] \tag{5.18}$$

5.4 Stability analysis

One major advantage of MP control is its mathematically proven network stability. Therefore, it is crucial to provide the stability analysis for the modified MP control, Smoothing-MP.

5.4.1 Stable network

We can mathematically define *stability* as follows:

Definition 4. *The network is strongly stable if the number of vehicles in the network is bounded in expectation, i.e. there exists a* $\kappa < \infty$ *such that*

$$\lim_{T\to\infty} \sup \left\{ \frac{1}{T} \sum_{t=1}^{T} \sum_{(i,j)\in\mathcal{A}^2} \mathbb{E}\{x_{ij}(t)\} \right\} \leq \kappa \tag{5.19}$$

Stability means the ability/capacity of network-level signal controls to serve all demand in the transportation network. If a network is stable, the total expected queue length will remain bounded in the long run. It is easy for us to find a large demand rate such that no traffic control policy can serve it, such as a very large demand that exceeds the turning movement capacity Q_{ij}. Therefore, to prove the maximum-stability property of a signal control policy, we need to define the network stable region.

5.4.2 Stable region

The primary objective of MP control is to stabilize any vehicle demand that could be stabilized by any other signal control. To prove the maximum stability property, we must analytically define the set of vehicle demands that can be stabilized. Since the demand is stochastic, the stable region is defined in terms of the average demand rates $\bar{\mathrm{d}}$.

Let $\mathbf{f}$ be the average volume of vehicles on link i. For entry links, we have the following relationship between the average volume of vehicles and demand:

$$f_i = \bar{d}_i \tag{5.20}$$

For internal links of vehicles, f_i can be determined by conservation of flow, which means the total flow on the downstream link is determined from all flow on the upstream link moving to the downstream link:

$$f_j = \sum_{i \in \mathcal{A}} f_i \bar{r}_{ij} \tag{5.21}$$

By Proposition 1 of Varaiya (2013), for every demand rate $\bar{\mathbf{d}}$ and turning proportions $\bar{\mathbf{r}}$, there exists a unique average flow vector $\mathbf{f}$. In this study, the network can be stabilized if the average vehicle flow can still be served by some traffic signals, considering the signal coordination. That is, there must exist an average signal activation $\bar{\mathbf{s}} \in \mathbf{S}$ that can serve the demand. It is crucial to mention that the stable region in this study is the same as the stable region in Varaiya (2013), since we aim to prove that our proposed signal control policy can still achieve maximum throughput.

$$f_i \bar{r}_{ij} \leq \bar{s}_{ij} Q_{ij} \tag{5.22}$$

where $\bar{s}_{ij}$ can be obtained from equation (5.4).

Let $\mathcal{D}$ be the set of all feasible demand vectors of vehicles $\bar{\mathbf{d}}$. Let $\mathcal{D}^0$ be the interior of $\mathcal{D}$, where constraints (5.22) hold with strict inequality. Then there exists an $\epsilon > 0$ such that

$$f_i \bar{r}_{ij} - \bar{s}_{ij} Q_{ij} \leq -\epsilon \tag{5.23}$$

If the network is unstable, at least one link has a flow greater than the traffic signal control policy can serve. Or we can say, If $\bar{\mathbf{d}} \notin \mathcal{D}$, then it is impossible to find a stabilizing control (Varaiya, 2013).

5.4.3 Stability analysis for Smoothing-MP

Lemma 9. *If Smoothing-MP is used and* $\bar{\mathbf{d}} \in \mathcal{D}^0$*, there exists a Lyapunov function* $\nu(t) \geq 0$ *and constants* $\kappa > 0$*,* $\epsilon > 0$ *such that*

$$\mathbb{E}\left[\nu(t+1) - \nu(t) \middle| \mathbf{x}(t)\right] \leq \kappa - \eta |\mathbf{x}(t)| \tag{5.24}$$

Proof. To calculate the queue length at time $t+1$, we apply the vehicle queueing models shown in equation (5.1)–(5.3). Then, let $\delta_{ij}(t)$ be the difference of the queueing length of vehicles between time steps t and time steps $t+1$.

$$\begin{aligned}
\delta_{ij}(t) &= x_{ij}(t+1) - x_{ij}(t) \\
&= -y_{ij}(t) + \sum_{h \in \mathcal{A}} y_{hi}(t) \cdot r_{ij}(t) \\
&= -\min\left\{Q_{ij} s_{ij}(t), x_{ij}(t)\right\} \\
&\quad + \sum_{h \in \mathcal{A}_i^-} \min\left\{Q_{hi} s_{ij}(t), x_{hi}(t)\right\} \cdot r_{ij}(t) \quad \forall i \in \mathcal{A}_{\mathrm{i}}, j \in \Gamma_i^+
\end{aligned} \tag{5.25}$$

For entry links, we have

$$\begin{aligned}\delta_{ij}(t) &= x_{ij}(t+1) - x_{ij}(t) \\ &= -y_{ij}(t) + d_i(t) \times r_{ij}(t) \\ &= -\min\left\{Q_{ij}s_{ij}(t), x_{ij}(t)\right\} + d_i(t) \times r_{ij}(t) \\ &\quad \forall i \in \mathcal{A}_{\mathrm{e}}, j \in \Gamma_i^+\end{aligned} \tag{5.26}$$

Let $\mathbf{x}(t)$ be the matrix including all queue length of private vehicles. Hence we consider the Lyapunov function $\nu(t)$:

$$\nu(t) = \left|\mathbf{x}(t)\right|^2 = \sum_{(i,j)\in\mathcal{A}^2} (x_{ij}(t))^2 \tag{5.27}$$

Then we expand the difference $\nu_1(t+1) - \nu_1(t)$:

$$\nu(t+1)-\nu(t) = \left|\mathbf{x}(t+1)\right|^2 - \left|\mathbf{x}(t)\right|^2 = \left|\mathbf{x}(t)+\boldsymbol{\delta}(t)\right|^2 - \left|\mathbf{x}(t)\right|^2 = 2\mathbf{x}(t)^{\mathrm{T}}\boldsymbol{\delta}(t) + \left|\boldsymbol{\delta}(t)\right|^2 \tag{5.28}$$

The first term of equation (5.28) can be rewritten as:

$$\begin{aligned}2\mathbf{x}(t)^{\mathrm{T}}\boldsymbol{\delta}(t) =& -2x_{ij}(t)\sum_{i\in\mathcal{A}}\sum_{j\in\Gamma_i^+}\min\left\{Q_{ij}s_{ij}(t), x_{ij}(t)\right\} \\ &+ 2\sum_{h\in\Gamma_i^-}\sum_{i\in\mathcal{A}}\sum_{j\in\Gamma_i^+} x_{ij}(t)\min\left\{Q_{hi}s_{hi}(t), x_{hi}(t)\right\} r_{ij}(t) \\ &+ 2\sum_{i\in\mathcal{A}_{\mathrm{e}}}\sum_{j\in\Gamma_i^+}\left(-\min\left\{Q_{ij}s_{ij}(t), x_{ij}(t)\right\} + d_i(t)\times r_{ij}(t)\right) \\ =& 2\sum_{i\in\mathcal{A}_{\mathrm{i}}\cup\mathcal{A}_{\mathrm{e}}}\sum_{j\in\Gamma_i^+}\min\left\{Q_{ij}s_{ij}(t), x_{ij}(t)\right\}\left(-x_{ij}(t) + \sum_{k\in\Gamma_i^+} r_{jk}(t)x_{jk}(t)\right)\end{aligned} \tag{5.29}$$

$$+ 2 \sum_{i \in \mathcal{A}_{\mathrm{e}}} \sum_{j \in \Gamma_i^+} d_i(t) \times r_{ij}(t) \times x_{ij}(t) \tag{5.30}$$

We replace the turning proportion $r_{ij}(t)$ with average value $\bar{r}_{ij}$, since $\mathbb{E}[r_{ij}(t)] = \sum_{i,j \in \mathcal{A}} \bar{r}_{ij}$. Therefore we have the following equation:

$$\begin{aligned}
\mathbb{E}[\mathbf{x}(t)^{\mathrm{T}} \boldsymbol{\delta}(t) | \mathbf{x}(t)] = & \sum_{i \in \mathcal{A}_{\mathrm{i}} \cup \mathcal{A}_{\mathrm{e}}} \sum_{j \in \Gamma_i^+} \mathbb{E}\Big[\min\{Q_{ij} s_{ij}(t), x_{ij}(t)\} \\
& \qquad \cdot (-x_{ij}(t)) \Big| \mathbf{x}(t) \Big] \\
& + \sum_{i \in \mathcal{A}_{\mathrm{i}} \cup \mathcal{A}_{\mathrm{e}}} \sum_{j \in \Gamma_i^+} \mathbb{E}\Big[\min\{Q_{ij} s_{ij}(t), x_{ij}(t)\} \\
& \qquad \Big| \mathbf{x}(t) \Big] \cdot \Big(\sum_{k \in \Gamma_i^+} \bar{r}_{jk} x_{jk}(t) \Big) \\
& + \sum_{i \in \mathcal{A}_{\mathrm{e}}} \sum_{j \in \Gamma_i^+} \mathbb{E}\Big[d_i(t) \bar{r}_{ij} x_{ij}(t) \Big| \mathbf{x}(t) \Big]
\end{aligned} \tag{5.31}$$

Then we obtain

$$\begin{aligned}
\mathbb{E}[\mathbf{x}(t)^{\mathrm{T}} \boldsymbol{\delta}(t) | \mathbf{x}(t)] = & \sum_{i \in \mathcal{A}_{\mathrm{i}} \cup \mathcal{A}_{\mathrm{e}}} \mathbb{E}\Big[\min\{Q_{ij} s_{ij}(t), x_{ij}(t)\} \Big| \mathbf{x}(t) \Big] \\
& \times \Big(- x_{ij}(t) + \sum_{k \in \Gamma_i^+} \bar{r}_{jk} x_{jk}(t) \Big) \\
& + \sum_{i \in \mathcal{A}_{\mathrm{e}}} \bar{d}_i \bar{r}_{ij} x_{ij}(t)
\end{aligned} \tag{5.32}$$

Based on equations (5.4)–(5.32) and the definition of pressure term (5.12), we obtain

$$\mathbb{E}[\mathbf{x}(t)^{\mathrm{T}}\boldsymbol{\delta}(t)|\mathbf{x}(t)] = \sum_{i\in\mathcal{A}_{\mathrm{i}}\cup\mathcal{A}_{\mathrm{e}}} \mathbb{E}\left[\min\left\{Q_{ij}s_{ij}(t), x_{ij}(t)\right\}\middle|\mathbf{x}(t)\right] \times (-w_{ij}(t)) + \sum_{i\in\mathcal{A}_{\mathrm{e}}} \bar{d}_i\bar{r}_{ij}x_{ij}(t) \tag{5.33}$$

The last term of equation (5.33) can be rewritten as follows based on equations (5.20), (5.21), and (5.12):

$$\sum_{i\in\mathcal{A}_{\mathrm{e}}} \bar{d}_i\bar{r}_{ij}x_{ij}(t) = \sum_{i\in\mathcal{A}_{\mathrm{e}}} f_{ij}x_{ij}(t) \tag{5.34}$$

$$= \sum_{i\in\mathcal{A}_{\mathrm{e}}\cup\mathcal{A}_{\mathrm{e}}} f_i\bar{r}_{ij}x_{ij}(t) - \sum_{i\in\mathcal{A}_{\mathrm{i}}} f_j\bar{r}_{jk}x_{jk}(t) \tag{5.35}$$

$$= \sum_{i\in\mathcal{A}_{\mathrm{e}}\cup\mathcal{A}_{\mathrm{e}}} f_i\bar{r}_{ij}x_{ij}(t) - \sum_{j\in\Gamma_i^+} [f_i\bar{r}_{ij}] \sum_{k\in\Gamma_i^+} \bar{r}_{jk}x_{jk}(t) \tag{5.36}$$

$$= \sum_{i\in\mathcal{A}_{\mathrm{i}}\cup\mathcal{A}_{\mathrm{e}}} f_i\bar{r}_{ij}\left(w_{ij}(t)\right) \tag{5.37}$$

Combining equations (5.33) and (5.37) yields

$$\mathbb{E}[\mathbf{x}(t)^{\mathrm{T}}\boldsymbol{\delta}(t)|\mathbf{x}(t)] = \sum_{i\in\mathcal{A}_{\mathrm{i}}\cup\mathcal{A}_{\mathrm{e}}} \left(f_i\bar{r}_{ij} - \mathbb{E}\left[\min\left\{Q_{ij}s_{ij}(t), x_{ij}(t)\right\}\middle|\mathbf{x}(t)\right]\right) w_{ij}(t) \tag{5.38}$$

$$= \sum_{i\in\mathcal{A}_{\mathrm{i}}\cup\mathcal{A}_{\mathrm{e}}} \left(f_i\bar{r}_{ij} - Q_{ij}s_{ij}^{\star}(t)\right) w_{ij}(t) + \sum_{i\in\mathcal{A}_{\mathrm{i}}\cup\mathcal{A}_{\mathrm{e}}} \left(Q_{ij}s_{ij}^{\star}(t) - \mathbb{E}\left[\min\left\{Q_{ij}s_{ij}(t), x_{ij}(t)\right\}\middle|\mathbf{x}(t)\right]\right) w_{ij}(t) \tag{5.39}$$

For the second term of equation (5.39), if $x_{ij}(t) \geq Q_{ij}$, then we have $\mathbb{E}\left[\min\left\{Q_{ij}s_{ij}(t), x_{ij}(t)\right\}\middle|\mathbf{x}(t)\right] = Q_{ij}s^{\star}_{ij}(t)$. Therefore, the second term of equation (5.39) equals zero. If $x_{ij}(t) < Q_{ij}$ and $s_{ij}(t) \neq 0$, then we have $\mathbb{E}\left[\min\left\{Q_{ij}s_{ij}(t), x_{ij}(t)\right\}\middle|\mathbf{x}(t)\right] = \mathbb{E}\left[x_{ij}(t)\middle|\mathbf{x}(t)\right]$. Therefore, we obtain the following inequality

$$\left(Q_{ij}s^{\star}_{ij}(t) - \mathbb{E}\left[x_{ij}(t)\middle|\mathbf{x}(t)\right]\right) w_{ij}(t) \leq Q_{ij}x_{ij}(t) \leq (Q_{ij})^2 \tag{5.40}$$

Hence, the second term of equation (5.39) equals zero or is bounded by $\sum_{i\in\mathcal{A}_{\mathrm{i}}\cup\mathcal{A}_{\mathrm{e}}}(Q_{ij})^2$.

The modified MP control $s^{\star}_{ij}(t)$ is chosen from the feasible signal control set $\mathcal{S}$, and $s^{\star}_{ij}(t)$ seeks to maximize the objective (5.13). According to Lemma 1, we following inequality:

$$\begin{aligned}\mathbb{E}\Bigg[\sum_{i\in\mathcal{A}_{\mathrm{i}}\cup\mathcal{A}_{\mathrm{e}}}\Big[f_i\bar{r}_{ij} - s^{\star}_{ij}(t)Q_{ij}\Big]w_{ij}(t) \\ - \xi_{ij}c_{ij}(t)\Bigg|w_{ij}(t)\Bigg] \leq \mathbb{E}\Bigg[\sum_{i\in\mathcal{A}_{\mathrm{i}}\cup\mathcal{A}_{\mathrm{e}}}\Big[f_i\bar{r}_{ij} - s^{\star}_{ij}(t)Q_{ij}\Big]w_{ij}(t) \quad \Bigg|w_{ij}(t)\Bigg]\end{aligned} \tag{5.41}$$

and

$$\begin{aligned}\mathbb{E}\Bigg[\sum_{i\in\mathcal{A}_{\mathrm{i}}\cup\mathcal{A}_{\mathrm{e}}}\Big[f_i\bar{r}_{ij} - s^{\star}_{ij}(t)Q_{ij}\Big]w_{ij}(t) \\ \Bigg|w_{ij}(t)\Bigg] \leq \mathbb{E}\Bigg[\sum_{i\in\mathcal{A}_{\mathrm{i}}\cup\mathcal{A}_{\mathrm{e}}}\Big[f_i\bar{r}_{ij} - \bar{s}_{ij}Q_{ij}\Big]w_{ij}(t) \quad \Bigg|w_{ij}(t)\Bigg]\end{aligned} \tag{5.42}$$

Therefore, for some feasible signal controls $s_{ij}(t)$ satisfying the stable region, we obtain

$\bar{s}_{ij}$ based on equation (5.4). We have the following relationship for the first term of equation (5.39) based on equation (23) when $\bar{\mathbf{d}} \in \mathcal{D}^0$:

$$\sum_{i \in \mathcal{A}_{\mathrm{i}} \cup \mathcal{A}_{\mathrm{e}}} \left[f_i \bar{r}_{ij} - \bar{s}_{ij} Q_{ij} \right] w_{ij}(t) \leq -\epsilon \sum_{ij} \max\left\{ w_{ij}, 0 \right\} \leq -\epsilon |w_{ij}| \tag{5.43}$$

We know that the pressure $\mathbf{w}(t)$ is a linear function of the queue length of vehicles. So we can find $\beta > 0$ to satisfy $\sum_{(i,j) \in \mathcal{M}^2} w_{ij} \geq \beta |\mathbf{x}|$. Then we have

$$-\epsilon |w_{ij}| \leq -\epsilon \beta |\mathbf{x}| \leq \sum_{i \in \mathcal{A}_{\mathrm{i}} \cup \mathcal{A}_{\mathrm{e}}} (Q_{ij})^2 - \epsilon \beta |\mathbf{x}| \tag{5.44}$$

Equation (5.24) satisfies the following relationship based on equations (5.42) and (5.43). For $\delta_{ij}(t)$

$$\begin{aligned} |\delta_{ij}(t)| = |&- \min\left\{ Q_{ij} s_{ij}(t), x_{ij}(t) \right\} \\ &+ \sum_{h \in \mathcal{A}_i^-} \min\left\{ Q_{hi} s_{ij}(t), x_{hi}(t) \right\} \times r_{ij}(t) \Big| \quad \forall i \in \mathcal{A}_{\mathrm{i}}, j \in \Gamma_i^+ \end{aligned} \tag{5.45}$$

$$\leq \max\left\{ Q_{ij}, \sum_{h \in \mathcal{A}_i^-} Q_{ij} \right\} \tag{5.46}$$

Then we have

$$|\delta_{ij}(t)| = |- \min\left\{ Q_{ij} s_{ij}(t), x_{ij}(t) \right\} + d_i(t) \times r_{ij}| \leq \max\left\{ Q_{ij}, \hat{d}_{ij} \right\} \quad \forall i \in \mathcal{A}_{\mathrm{e}}, j \in \Gamma_i^+ \tag{5.47}$$

Define ψ follows:

$$\psi = \max\left\{ Q_{ij}, \sum_{h \in \mathcal{A}_i^-} Q_{ij}, \hat{d}_{ij} \right\} \tag{5.48}$$

Because the number of total movements of vehicles is *M*, we have the following inequality:

$$|\delta_{ij}(t)|^2 \leq \boldsymbol{M} \times \psi^2 \tag{5.49}$$

Since $\delta_{ij}(t)$ is upper-bounded by $\max\left\{ Q_{ij}, \sum_{h \in \mathcal{A}_i^-} Q_{ij} \right\}$, we can use equation (5.44), along with equations (5.46)–(5.49), to derive the following:

$$\begin{aligned} &\left|\mathbf{x}(t+1)\right|^2 - \left|\mathbf{x}(t)\right|^2 = 2\mathbf{x}(t)^{\mathrm{T}}\boldsymbol{\delta} + \left|\boldsymbol{\delta}\right|^2 \\ &\leq 2\Bigg(\sum_{i \in \mathcal{A}_{\mathrm{i}} \cup \mathcal{A}_{\mathrm{e}}} (Q_{ij})^2 - \epsilon\beta|\mathbf{x}(t)| \Bigg) + \boldsymbol{M}\psi^2 \qquad (5.50) \\ &= \kappa - \eta|\mathbf{x}(t)| \qquad (5.51) \end{aligned}$$

where $\kappa = 2 \sum_{i \in \mathcal{A}_{\mathrm{i}} \cup \mathcal{A}_{\mathrm{e}}} (Q_{ij})^2 + \boldsymbol{M}\psi^2$ and $\epsilon\beta = \eta$.

Proposition 13. *Smoothing-MP is stabilizing when* $\bar{\mathbf{d}} \in \mathcal{D}^0$.

Proof. Inequality (5.24) holds from Lemma 9. Taking expectations, summing over $t = 1, ..., T$, and transferring the position of terms gives the following inequality:

$$\mathbb{E}\left[\nu(T+1) - \nu(1) \middle| \mathbf{x}(t)\right] \leq \kappa T - \epsilon \sum_{t=1}^{T} |\mathbf{x}(t)| \tag{5.52}$$

Then we have

$$\epsilon\frac{1}{T}\sum_{t=1}^{T}\mathbb{E}\left[|\mathbf{x}(t)|\right] \leq \kappa - \frac{1}{T}\mathbb{E}\left[\nu(T+1)\right] + \frac{1}{T}\mathbb{E}\left[\nu(1)\right] \leq \kappa + \frac{1}{T}\mathbb{E}\left[\nu(1)\right] \tag{5.53}$$

which implies that Definition 4 is satisfied.

Moreover, we need to mention that stability is not impacted by the initial condition. Let us move ϵ in to the right hand side and take the limit as T goes to infinity. Then the $\frac{1}{T}\mathbb{E}\left[\nu(1)\right]$ term approaches zero, which yields the following inequality which implies Definition 4 is satisfied:

$$\lim_{T\to\infty}\frac{1}{T}\sum_{t=1}^{T}\mathbb{E}\left[|\mathbf{x}(t)|\right] \leq \frac{\kappa}{\epsilon} \tag{5.54}$$

Since $\bar{\mathbf{d}} \in \mathcal{D}^0$ and Definition 4 is satisfied, the network achieves maximum stability under the use of Smoothing-MP.

5.5 Multi-scenario simulation and numerical results

To evaluate the performance of the proposed Smoothing-MP control, we conducted simulations on two distinct networks: the Downtown Austin Network and a Grid Network. These test networks were chosen to ensure a robust and comprehensive assessment of the new method. The simulations were implemented using the microscopic traffic simulation tool, SUMO, interfaced with Python (Lopez et al., 2018). The locations of signal coordination corridors within the Downtown Austin Network and a Grid Network (GridNet) are illustrated in Figure 5.2 and Figure 5.1, respectively. The Downtown Austin Network consists of 546 nodes and 1247 links, and the network profile could be found through the authors'

previous studies (Levin et al., 2020). This Grid Network consists of 12 nodes and 72 links. The empirical results, presented subsequently, offer a comparative evaluation between the proposed Smoothing-MP and the established MP control (Varaiya, 2013). It is worth noting that, apart from the controllers on the coordination corridors in both networks, all other signal controls adhere to the original MP control strategy.

5.5.1 Stability comparison

This section focuses on verifying the stability of the network as per Definition 4. To this end, we conduct simulations to observe the total number of vehicles within the network and monitor whether it increases over time under various vehicle demand level settings.

Figure 5.3 presents the average number of waiting vehicles within the Grid Network (GridNet). It reveals a striking consistency in the average number of waiting vehicles across different vehicle demand and coordination weight (ξ value) settings. The maximum stable region, identified across coordination weight settings (2000, 10000, 20000), lies within the range of 2400 to 2560 vehicles per hour, a value identical to that of the Original MP control. Similar observations can be made from the Austin Network results displayed in Figure 5.4. Here, too, the average number of waiting vehicles remains approximately the same under varying vehicle demand and coordination weight (ξ value) settings. The maximum stable region for the different coordination weight settings (2000, 10000, 20000) is around 13530 vehicles per hour, aligning with the Original MP control. These findings lead us to conclude that the Smoothing-MP exhibits a stable region analogous to that of the Original MP control, corroborating the definition of the stable region discussed in Section 4.2.

5.5.2 Average Speed

The goal of signal coordination is to improve the average speed along corridors. In the context of the Grid Network we use Figure 5.5a demonstrates that the average speed along the

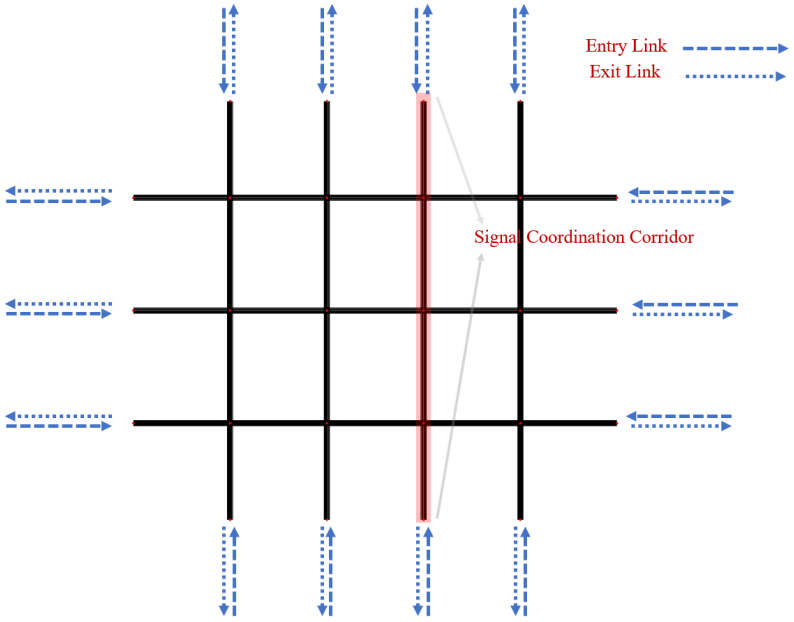

Figure 5.1: Grid Network with Signal Coordination Corridor

Figure 5.2: Austin Network with Signal Coordination corridor

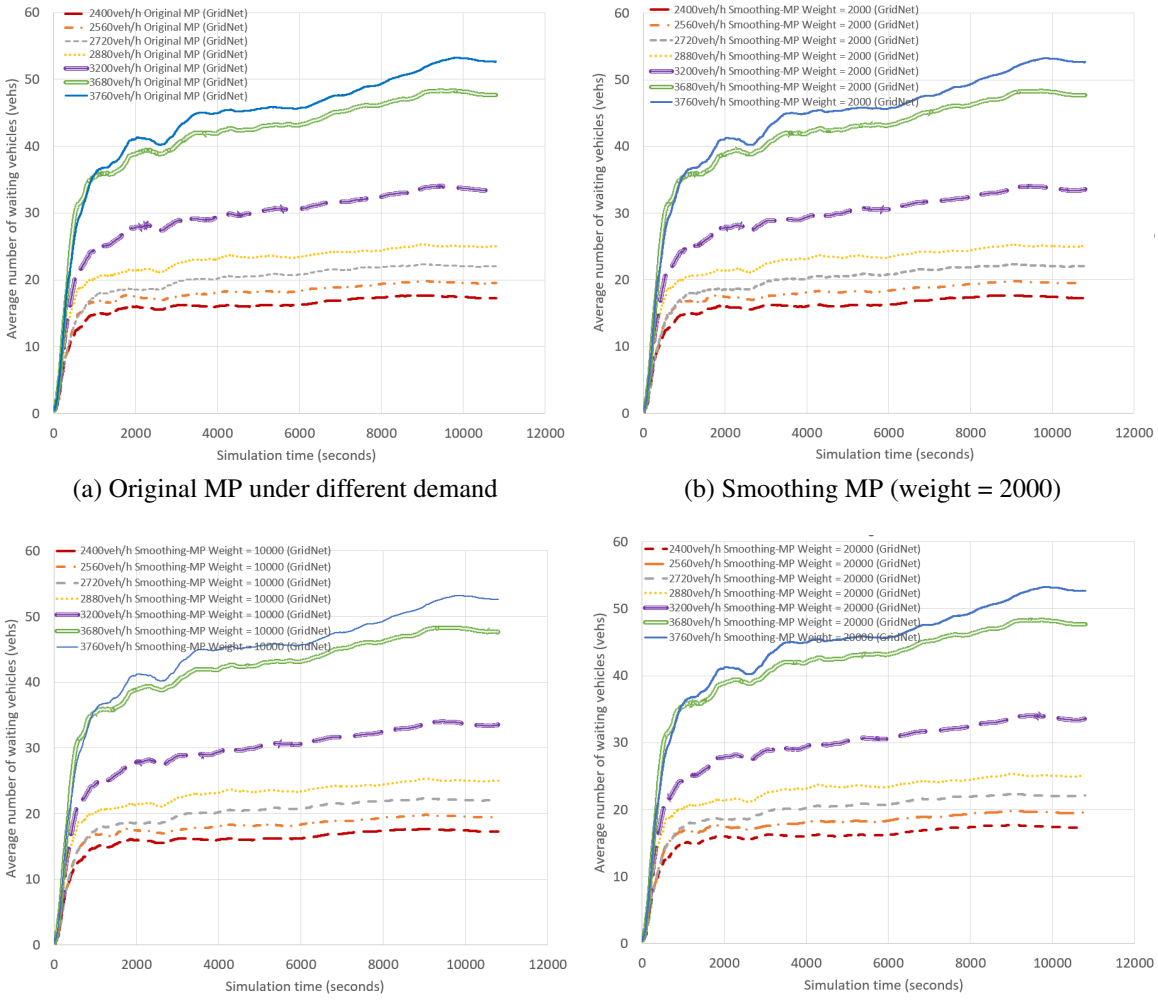

(a) Original MP under different demand

(b) Smoothing MP (weight = 2000)

(c) Smoothing MP (weight = 10000)

(d) Smoothing MP (weight = 20000)

Figure 5.3: Stability analysis (Grid Network)

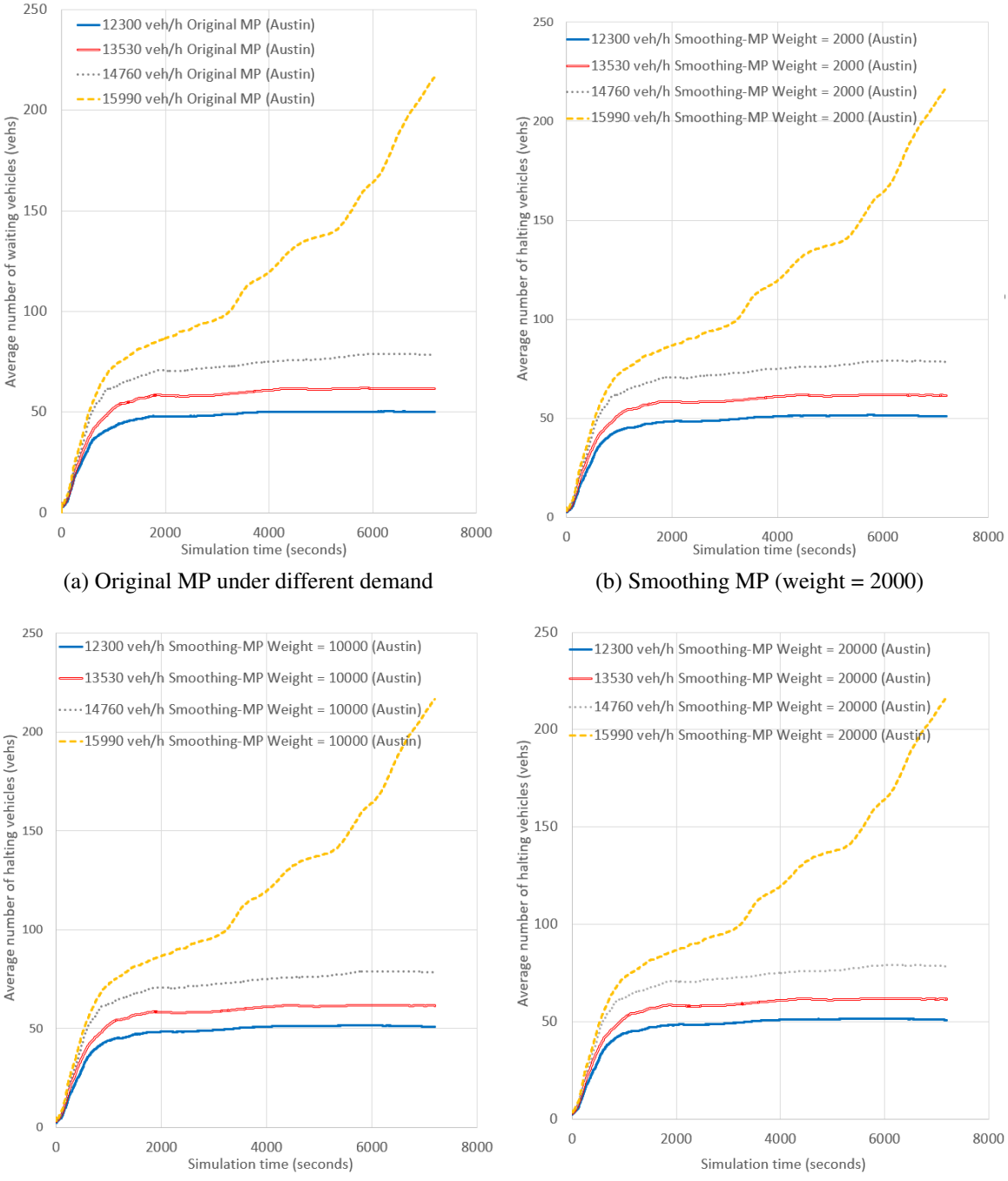

(a) Original MP under different demand

(b) Smoothing MP (weight = 2000)

(c) Smoothing MP (weight = 10000)

(d) Smoothing MP (weight = 20000)

Figure 5.4: Stability analysis (Austin Network)

corridor under the Original MP control surpasses that under the Smoothing-MP control for vehicle demand levels ranging from 800 to 3840 vehicles per hour. Conversely, Figure 5.5b illustrates that the average speed along the corridor's conflict direction is lower under the Original MP control than under the Smoothing-MP control within the same vehicle demand range.

For the Austin Network, similar patterns can be discerned, as depicted in Figure 5.6a and Figure 5.6b. The former reveals that the average speed along the corridor under the Original MP control exceeds that under the Smoothing-MP control for vehicle demand ranging from 11070 to 15990 vehicles per hour. Meanwhile, the latter indicates that the average speed along the corridor conflict direction is reduced under the Original MP control compared to the Smoothing-MP control within the same vehicle demand range.

Both Figure 5.5 and Figure 5.6 consolidate the observation that vehicle travel speed along corridors can be increased under the Smoothing-MP controller. However, this augmentation comes at the expense of reduced average speed along corresponding conflict directions.

The influence of signal coordination weight value on the average speed dynamics along corridors and their conflict directions is another significant aspect to examine. Figure 5.7a within the context of the Grid Network indicates that, given various vehicle demands, the average speed tends to increase in correlation with the signal coordination weight value along the corridor directions. In contrast, Figure 5.7b shows that the average speed decreases as the signal coordination weight value increases along the corridor conflict directions.

Analogous patterns are observed for the Austin Network, as depicted in Figure 5.8a and Figure 5.8b. As such, we can infer that higher signal coordination weight values are associated with increased average speeds along corridor directions, while a contrary pattern is evident along the corridor conflict directions.

In addition, we present a time-series plot of the average vehicle speed along the cor-

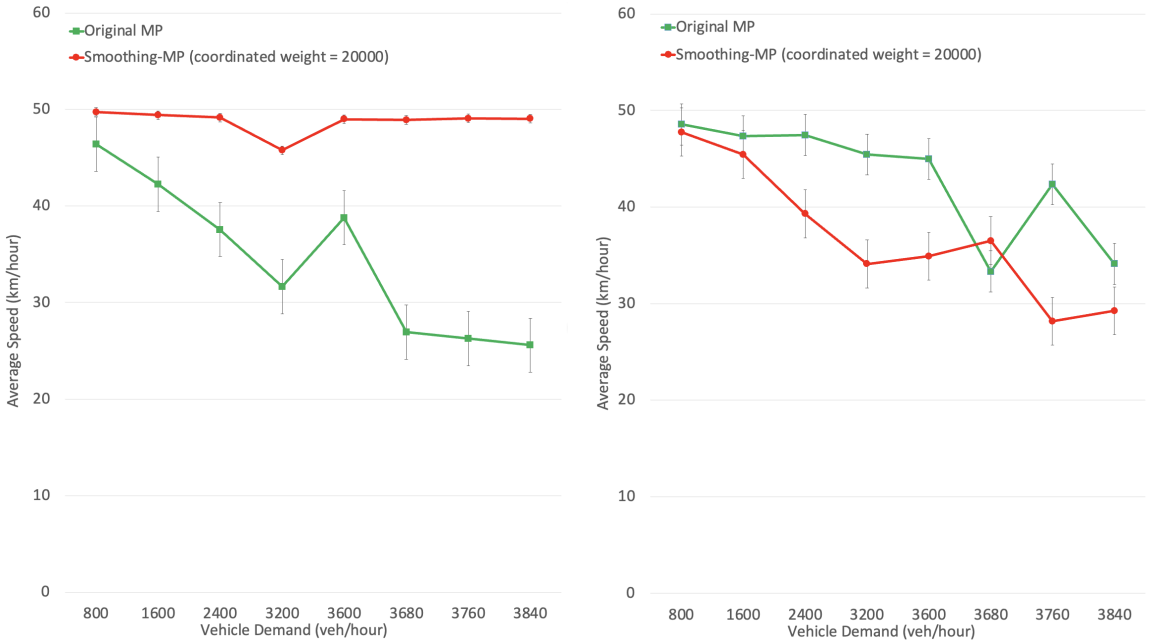

(a) Average Speed Along Corridor

(b) Average Speed Along Corridor Conflict Direction

Figure 5.5: Average Speed Comparison (Grid Network)

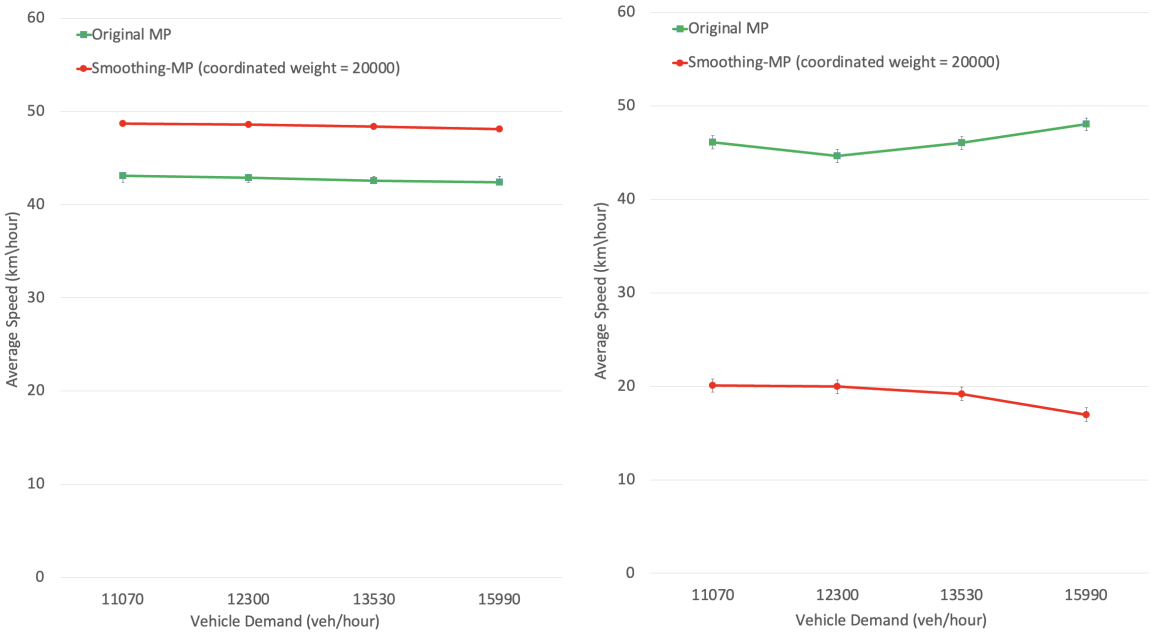

(a) Average Speed Along Corridor (b) Average Speed Along Corridor Conflict Direction

Figure 5.6: Average Speed Comparison (Austin Network)

ridor for each simulation time in Figure 5.9. Analysis of these findings suggests that the implementation of the Smoothing-MP algorithm along signal coordination corridors results in more stable and higher average vehicle speed dynamics, which approximate free flow speed. In contrast, the Original MP control produces significantly more fluctuation in the average vehicle speed along the corridor, indicating less stability than when the Smoothing-MP control is employed.

5.5.3 Average Delay

Average delay is a widely accepted metric in traffic signal studies (Liu and Gayah, 2022; Wang et al., 2022; Xu et al.). Consequently, we present the average delay values along the corridors and their corresponding conflict directions. For the Grid Network's corridor direction, the average delay tends to increase with vehicle demand. Moreover, the average

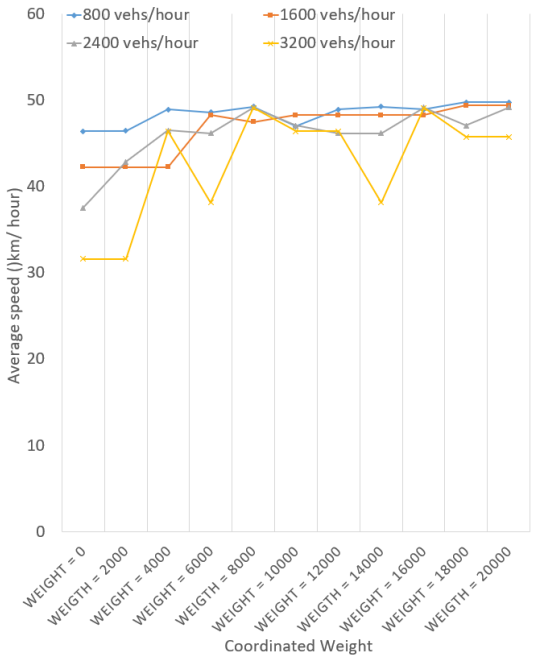

(a) Average Speed Dynamic Along Corridor

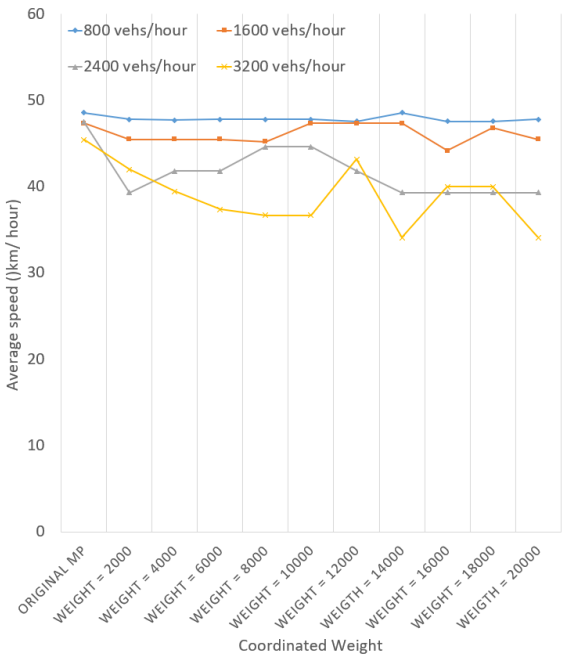

(b) Average Speed Dynamic Along Corridor Conflict Directions

Figure 5.7: Average Speed Dynamic Comparison (Grid Network)

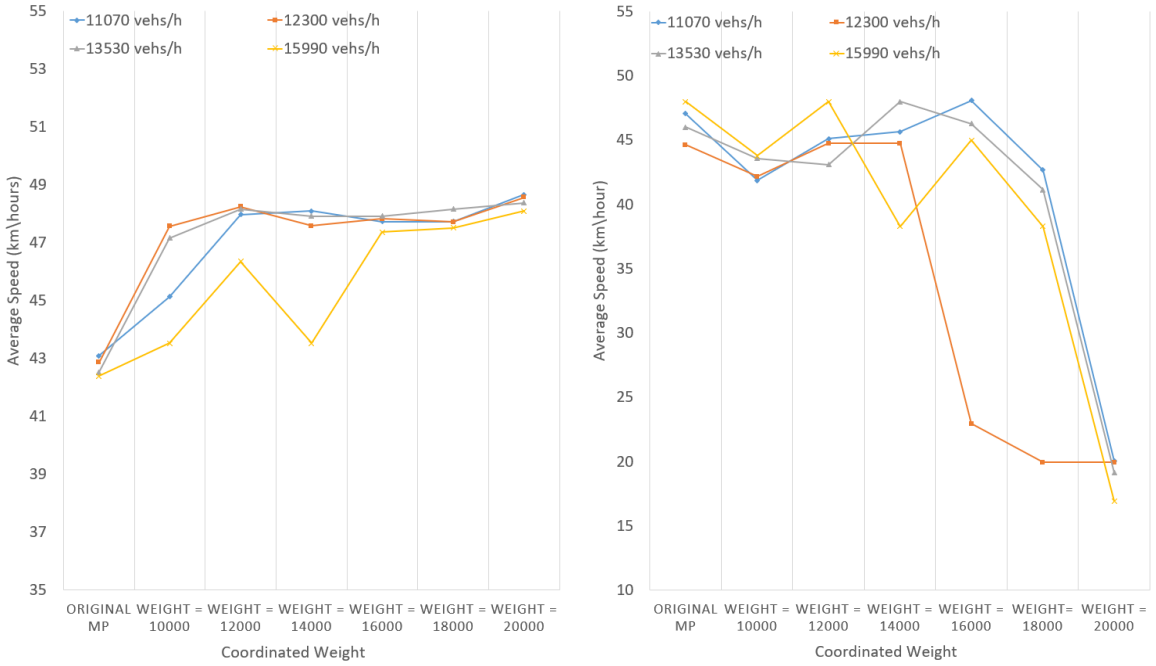

(a) Average Speed Dynamic Along Corridor

(b) Average Speed Dynamic Along Corridor Conflict Directions

Figure 5.8: Average Speed Dynamic Comparison (Austin Network)

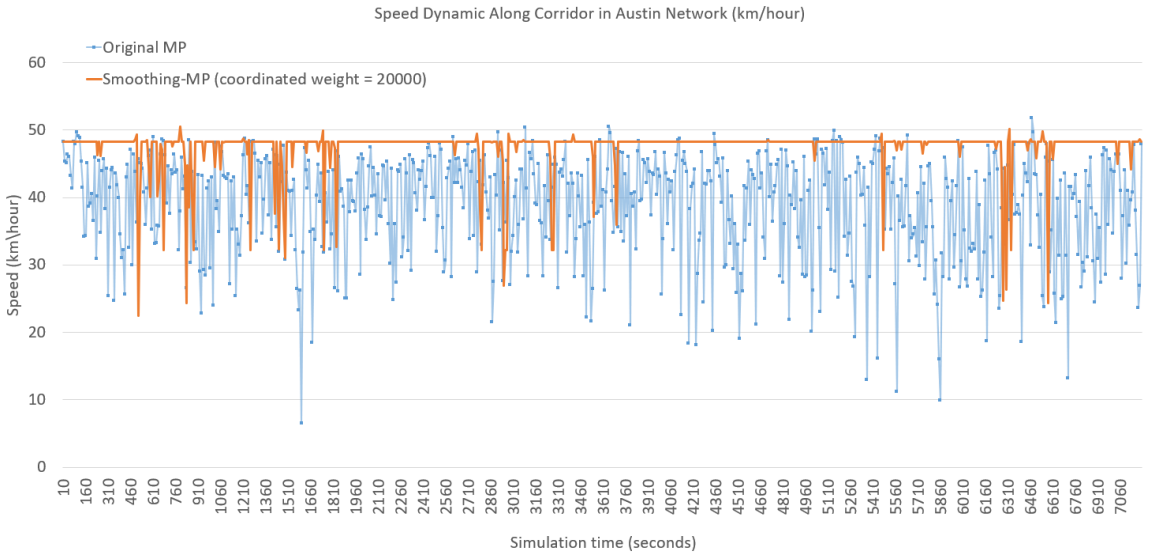

Figure 5.9: Speed Dynamics

delay under the Original MP control significantly exceeds that under the Smoothing-MP with varying weight values, as shown in Figure 5.10a. However, for the corridor's conflict direction in the Grid Network, the average delay under the Original MP control is lower than under the Smoothing-MP with different weight values for vehicle demands of 800, 1600, 2400, 3200, and 3760 vehicles per hour. When vehicle demand equals 3680 and 3840 vehicles per hour, the average delay for both Original MP and Smoothing-MP is comparably high, possibly due to vehicle demand exceeding the stable demand region within the Grid Network. In such circumstances, the Grid Network becomes highly congested, leading to minimal differences between the two controllers along the conflict direction, as depicted in Figure 5.10a.

For the Austin Network, a similar pattern emerges, with the average delay under the Original MP control being considerably higher than that under the Smoothing-MP along the signal coordinated corridor direction, as depicted in Figure 5.11a. Conversely, in the corridor conflict direction, the average delay under the Original MP control remains higher than under the Smoothing-MP control, as shown in Figure 5.11a. Overall, both the Grid Network and the Austin Network exhibit analogous patterns concerning the metric of average delay.

5.5.4 Average Travel Time

The question arises as to whether the implementation of Smoothing-MP will affect the network-level average travel time. Figure 5.12 shows that the network-level average travel time under the Original MP control and Smoothing-MP with varying signal coordination weights and vehicle levels is nearly identical. This observation suggests that, while Smoothing-MP prioritizes signal coordination along the corridor direction, it does not negatively impact the network-level travel time performance.

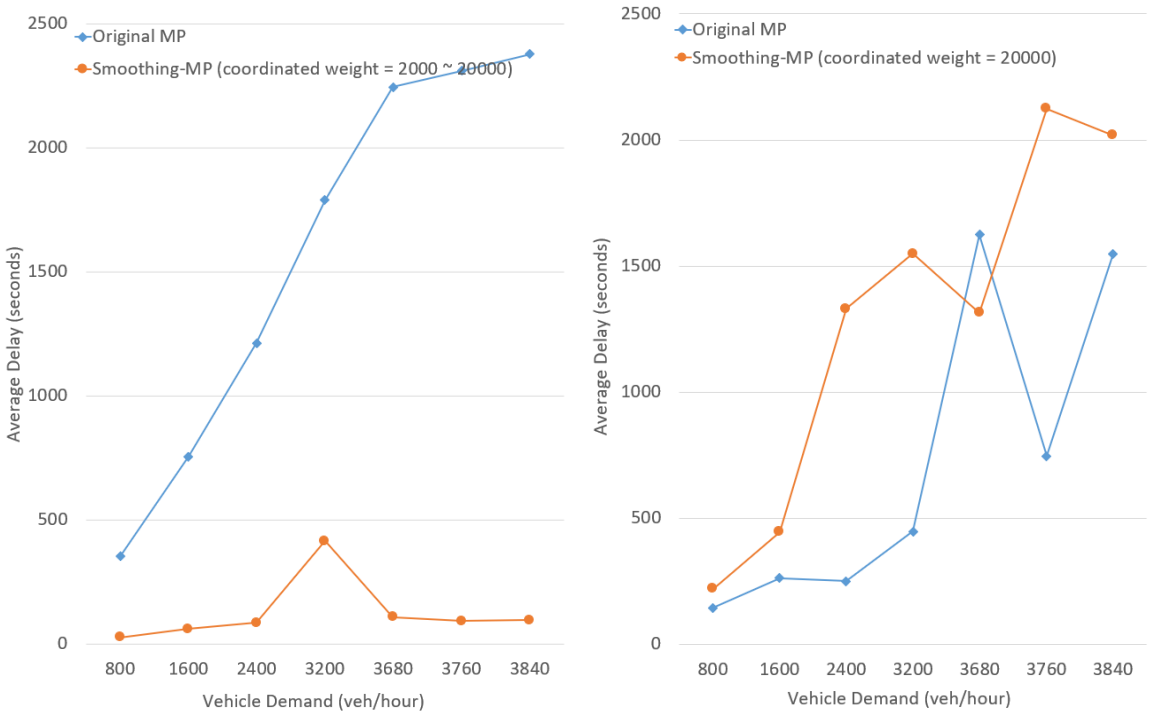

(a) Average Delay Along Corridor

(b) Average Delay Along Corridor Conflicts

Figure 5.10: Average Delay Comparison (Grid Network)

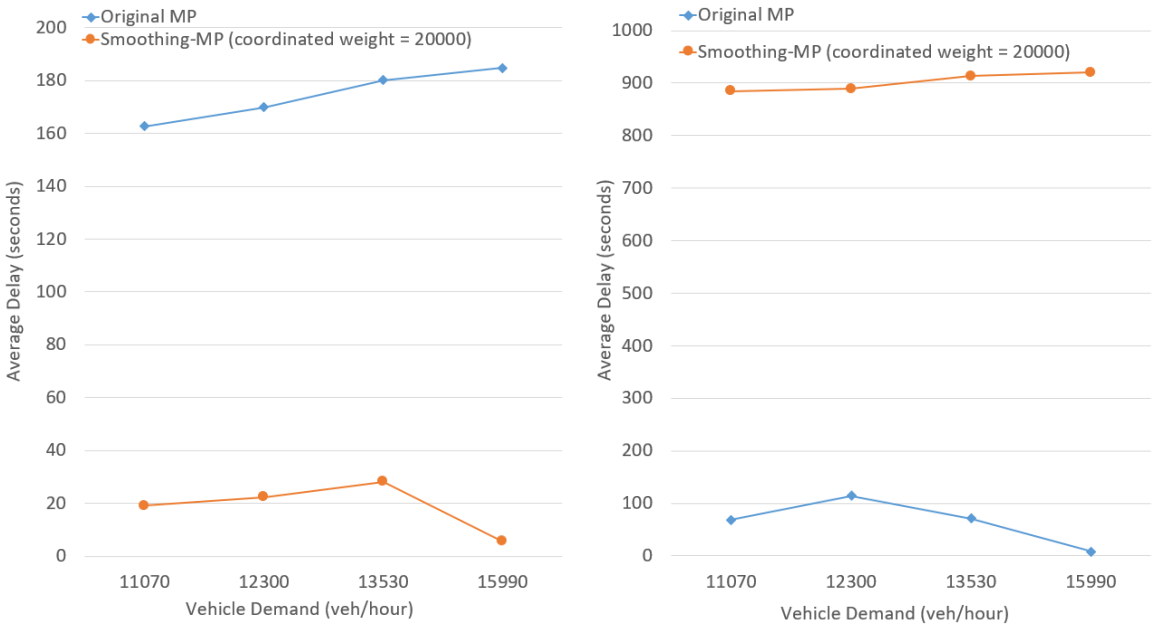

(a) Average Delay Along Corridor

(b) Average Delay Along Corridor Conflict

Figure 5.11: Average Delay Comparison (Grid Network)

5.5.5 Average Fuel Consumption

Fuel consumption stands as a critical parameter for the evaluation of signal control systems. In the current study, we simulate fuel consumption along specific corridors and their associated conflict directions, considering both the Grid Network and the Austin Network under varying vehicle demand levels. In particular, we employ the HBEFA (Handbook Emission Factors for Road Transport) for modeling both fuel consumption and emissions. The HBEFA incorporates vehicle speed, acceleration, and engine technology in determining fuel consumption, a functionality which is comprehensively integrated within the SUMO framework (Krajzewicz et al., 2012; Salles et al., 2020). An examination of both Figure 5.13 and Figure 5.16 elucidates a decline in vehicle fuel consumption corresponding to an increase in the signal coordination weight along the coordinated corridor directions. In stark contrast, an increasing trend is noticeable as the signal coordination weight intensifies

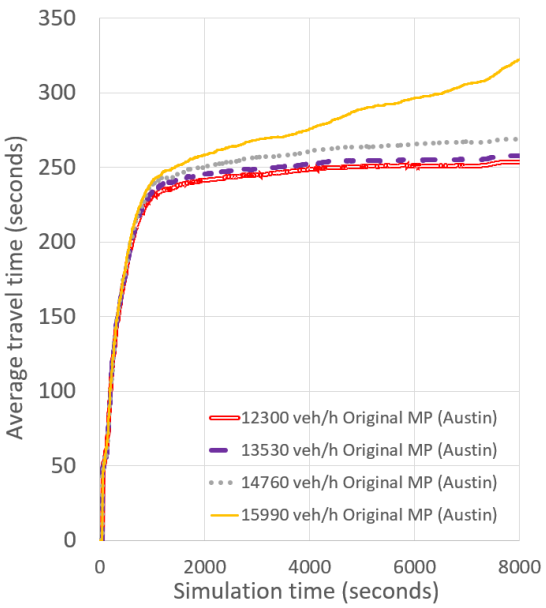

(a) Original MP control

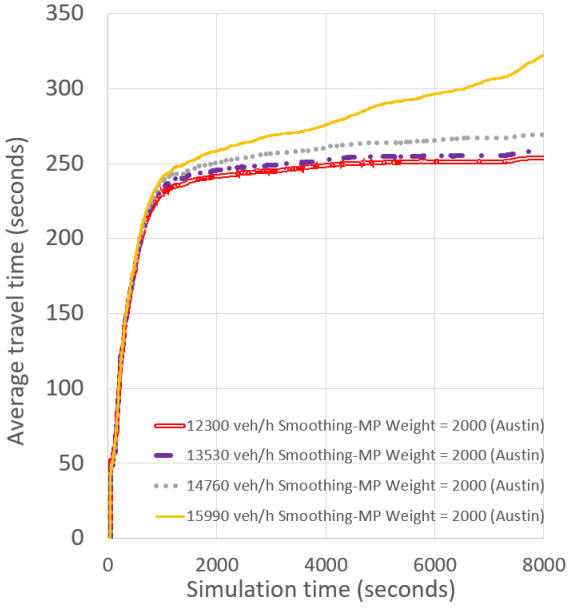

(b) Smoothing-MP, weight = 2000

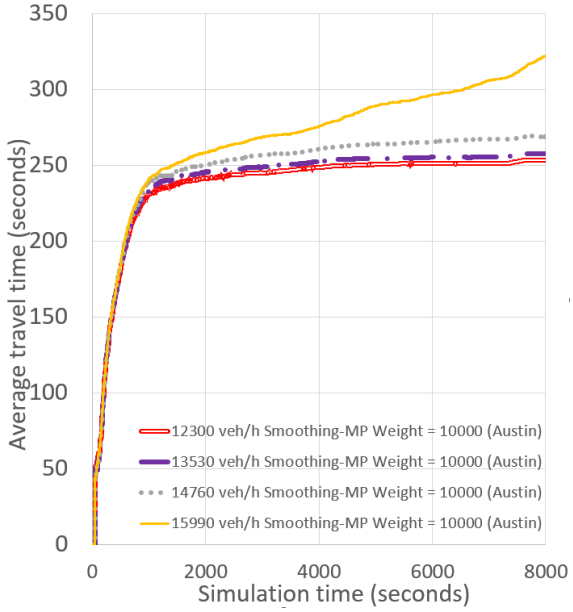

(c) Smoothing-MP, weight = 10000

Figure 5.12: Average Travel Time

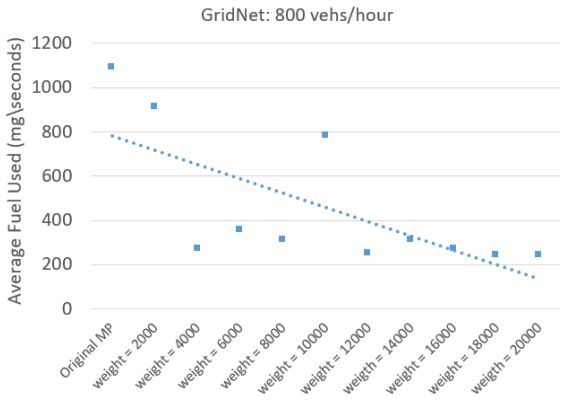

(a) Average Fuel Consumption: 800 vehs/h

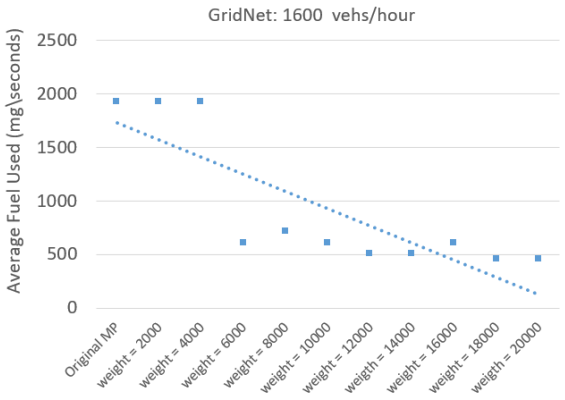

(b) Average Fuel Consumption: 1600 vehs/h

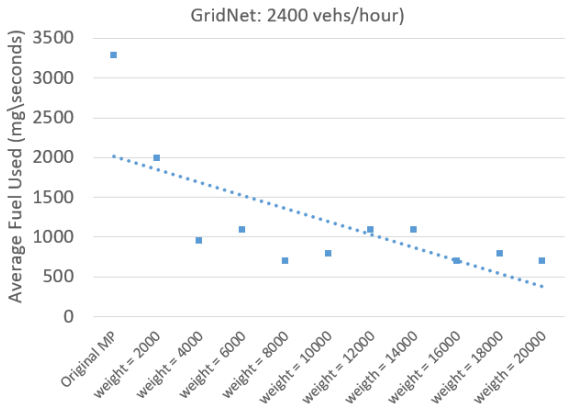

(c) Average Fuel Consumption: 2400 vehs/h

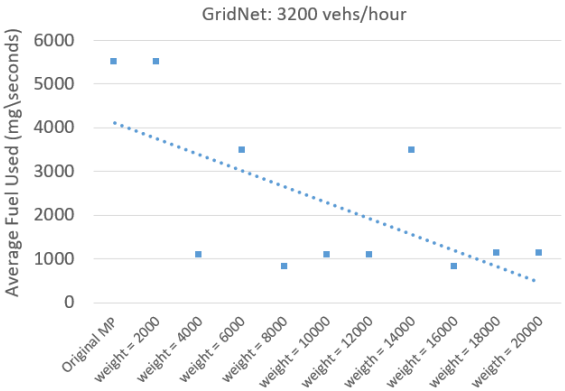

(d) Average Fuel Consumption: 3200 vehs/h

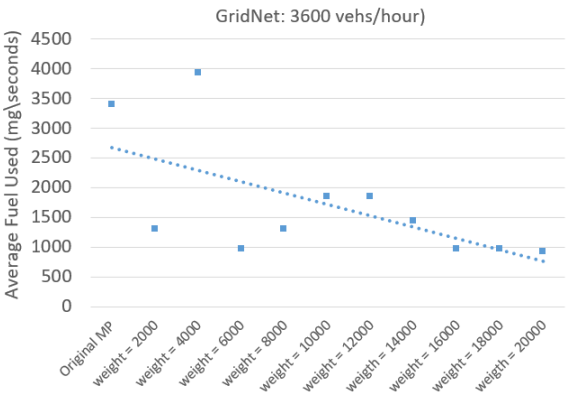

(e) Average Fuel Consumption: 3600 vehs/h

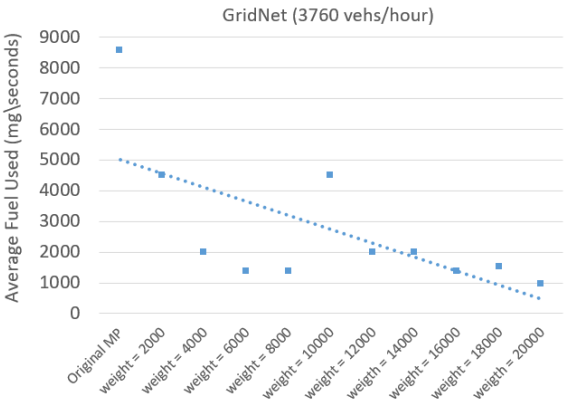

(f) Average Fuel Consumption: 3760 vehs/h

Figure 5.13: Average Fuel Consumption Analysis Along Corridor Direction (Grid Network)

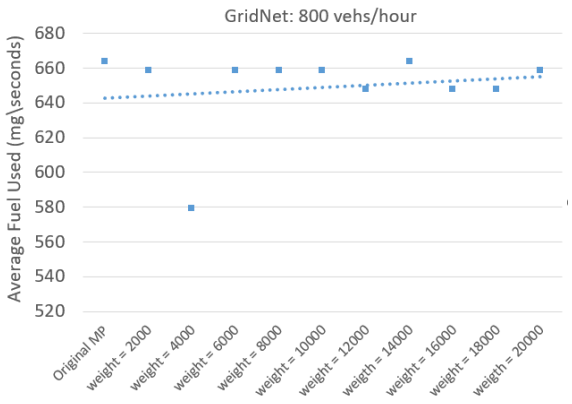

(a) Average Fuel Consumption: 800 vehs/h

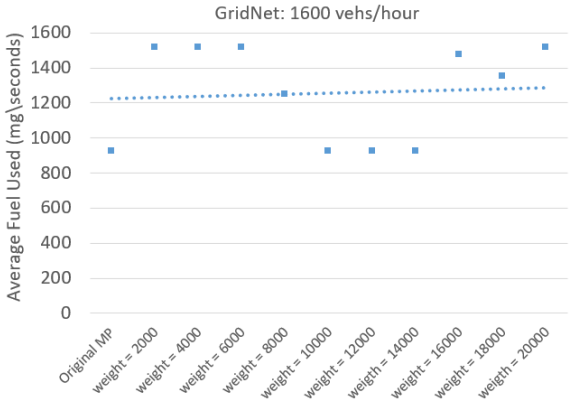

(b) Average Fuel Consumption: 1600 vehs/h

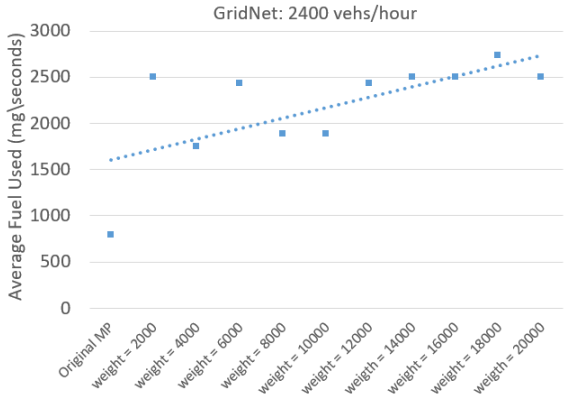

(c) Average Fuel Consumption: 2400 vehs/h

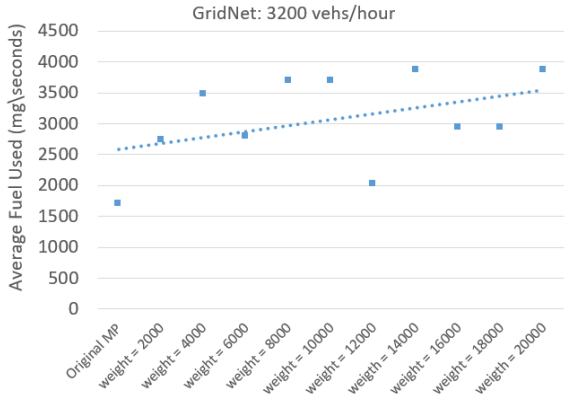

(d) Average Fuel Consumption: 3200 vehs/h

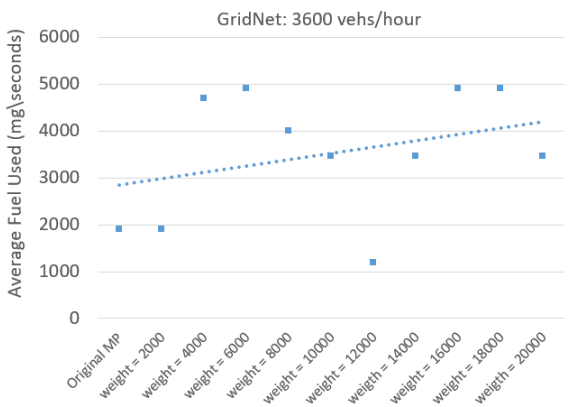

(e) Average Fuel Consumption: 3600 vehs/h

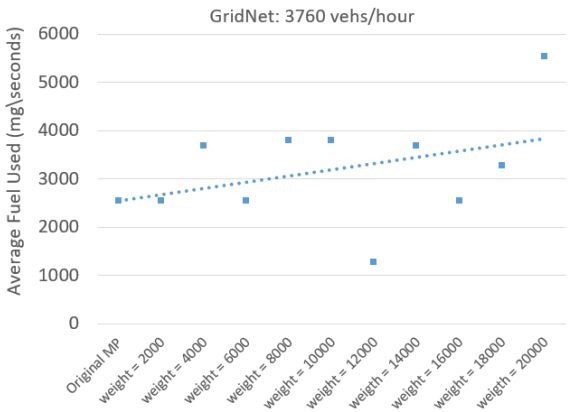

(f) Average Fuel Consumption: 3760 vehs/h

Figure 5.14: Average Fuel Consumption Analysis Along Corridor Direction (Grid Network)

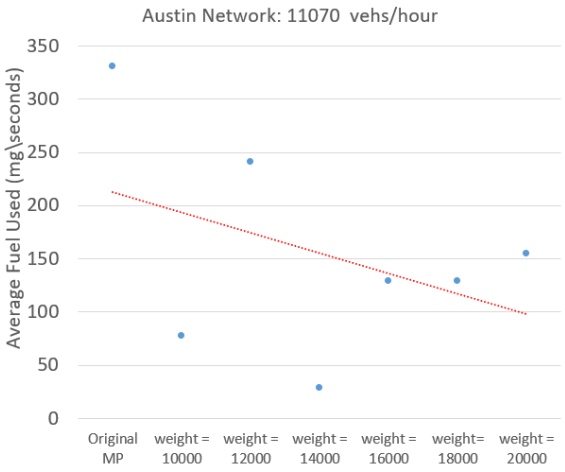

(a) Average Fuel Consumption: 11070 vehs/h

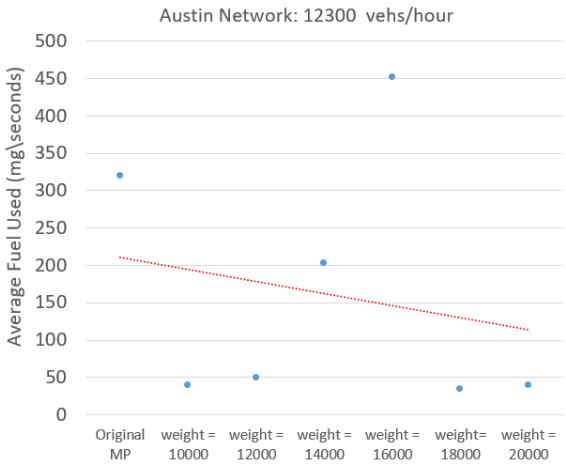

(b) Average Fuel Consumption: 12300 vehs/h

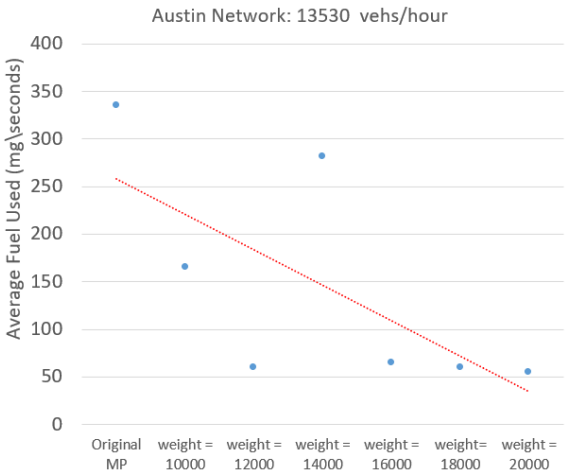

(c) Average Fuel Consumption: 13530 vehs/h

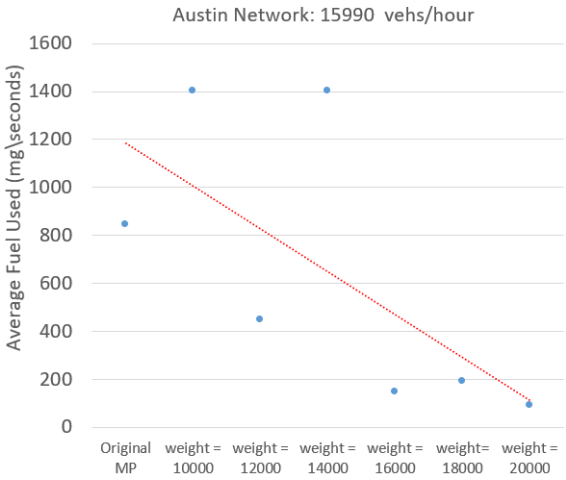

(d) Average Fuel Consumption: 15990 vehs/h

Figure 5.15: Average Fuel Consumption Analysis Along Corridor Direction (Austin Network)

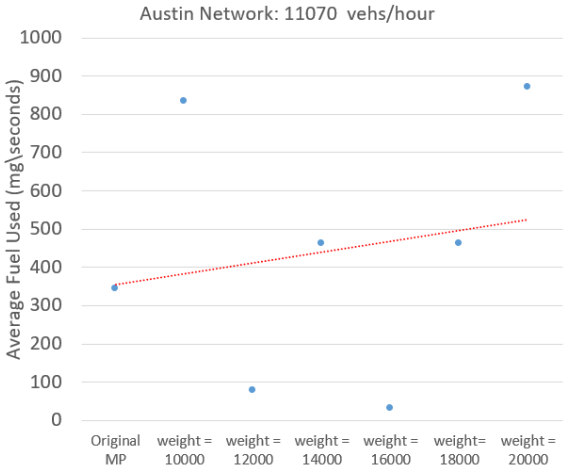

(a) Average Fuel Consumption: 11070 vehs/h

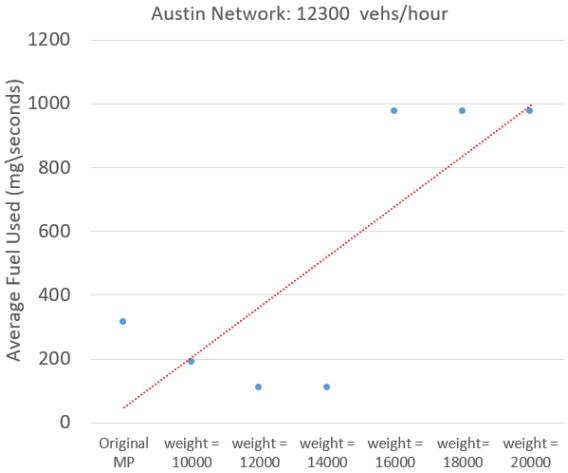

(b) Average Fuel Consumption: 12300 vehs/h

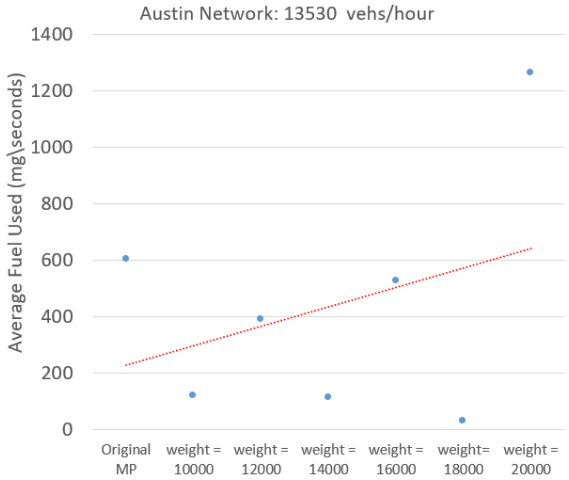

(c) Average Fuel Consumption: 13530 vehs/h

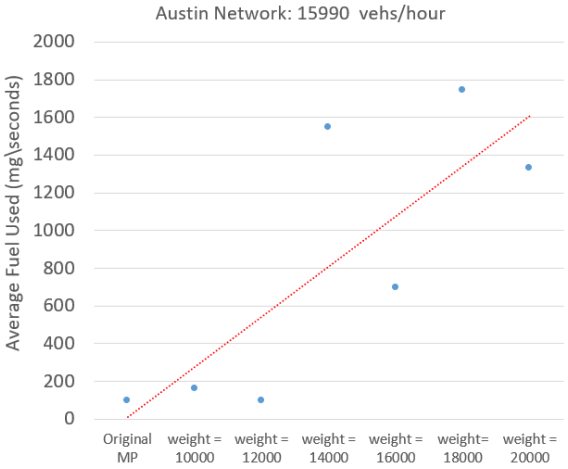

(d) Average Fuel Consumption: 15990 vehs/h

Figure 5.16: Average Fuel Consumption Analysis Along Corridor Conflict Direction (Austin Network)

along the conflict directions of the signal coordination corridor, observed across different vehicular demand levels.

5.6 Conclusions

To our understanding, there exists a gap in current research in the integration of max-pressure (MP) signal timing with signal coordination. Addressing this, our study proposes a pioneering application of MP signal control, which incorporates signal coordination along the corridor for the first time, aimed at smoothing traffic. Moreover, we present a meticulous proof showcasing that our innovative Smoothing-MP approach can maintain maximum stability properties, even while introducing signal coordination. This fresh perspective has the potential to broaden the practical utility of MP control, particularly considering that real-world traffic seldom exhibits uniform distribution across the network.

Numerical results from both the Grid Network and the Downtown Austin Network suggest that the stable region remains unaffected after implementing Smoothing-MP compared to the Original MP control. Regarding corridor directions exhibit higher speeds under Smoothing-MP compared to the Original MP control, while the contrary is true for corridor conflict directions. Based on speed dynamics illustrated in Figure 5.7a to Figure 5.9, we deduce that higher signal coordination weights yield higher average speeds along corridors, while speed dynamics display a reversed pattern at corridor conflict directions. Regarding average delay, corridor directions experience lower average delays under Smoothing-MP compared to the Original MP control, whereas corridor conflict directions register higher average speeds under Smoothing-MP compared to the Original MP control.

Both sets of results indicate that Smoothing-MP prioritizes signal coordination direction over conflict directions. The higher the weight, the greater the level of priority. However, the network-level average number of waiting vehicles and average travel time remain consistent, regardless of the consideration of signal coordination.

Future work includes numerous potential extensions. For instance, integrating Connected and Autonomous Vehicles (CAVs) into the Smoothing-MP control could provide more accurate speed and travel time information, thereby improving signal timing. Another intriguing challenge and topic for future study would be the integration of multimodal traffic and signal coordination within the MP control framework.

Chapter 6

Conclusions

6.1 Summary

This dissertation presents novel contributions to the field of MP control policy, an adaptive traffic signal control strategy with several notable modifications designed to address different traffic conditions and needs.

The first innovation was the implementation of the MP control policy, specifically adjusted to accommodate transit signal priority (MP-TSP). This incorporation required a significant modification to the original MP algorithm to ensure the smooth operation of public transit in urban networks. The numerical analysis performed in the downtown Austin network revealed that despite the MP-TSP having a lower stability region than the original MP control policy, it significantly reduced bus travel times. In addition, it outperformed other fixed time signal controls incorporating TSP and adaptive signal controls, demonstrating lower average travel time for both private vehicles and buses.

The second focus was the development of a pedestrian-friendly max-pressure signal controller (Ped-MP), marking the first time this type of MP control has been proposed. An analytical proof was provided to ensure the maximum stability of the Ped-MP, which aims to increase pedestrian access without significantly impacting vehicle throughput. Simulations in the Sioux Falls network indicated an inverse relationship between pedestrian delay

and tolerance time. Consequently, the Ped-MP could offer more pedestrian-friendly spaces within cities, even in cases with high pedestrian demand.

The third area of focus was the position-weighted back-pressure (PWBP) controller. Originally, the PWBP controller assumed that the density information along the road links could be obtained – a feat easily achieved in simulation but not realistic in a real-world setting, as the density distribution can't be accurately determined without the placement of loop detectors everywhere. To mitigate this challenge, we introduced the approximate position-weighted back-pressure (APWBP) control. This innovative approach requires only two loop detectors per road link, significantly reducing the sensor requirements for practical implementation of the PWBP controller. The APWBP was proven to achieve maximum throughput at the network level using just two loop detectors placed at the upstream and downstream ends of each link. When compared to the original PWBP controller, the APWBP exhibited an almost identical performance, establishing it as a more feasible alternative for implementation.

Finally, previous iterations of the MP controller lacked coordinated phase selection. To address this, we proposed an innovative Smoothing-MP approach which incorporates signal coordination to boost traffic flow efficiency. Mathematical proofs confirmed that this novel control strategy retains maximum stability properties. Numerical results from both the Grid Network and the Downtown Austin Network testified to the effectiveness of the Smoothing-MP approach in maintaining stability within the region and improving average speeds along corridors.

Further adaptations of the MP control policy could include more complex, uncertainty, and real-world considerations (Shi et al., 2022). Examples of these are the integration of Connected and Autonomous Vehicles (CAVs), multi-modal traffic, advanced infrastructure sensors, and perimeter control technologies.

6.2 Future work

I plan to extend some of the work presented in this dissertation and to study interesting research questions that can arise in future transportation systems.

(1) Integration of connected and autonomous vehicles (CAVs) with MP control policy: The growing prevalence of CAVs offers an exciting avenue for future research. CAVs can provide accurate real-time data about their speed, position, and destination, which can be harnessed to refine MP control policies. For example, signal timing could be adjusted based on actual vehicle trajectories rather than traditional aggregated traffic flow models, improving traffic flow and reducing congestion. Additionally, cooperation among CAVs could enable platooning, i.e., groups of vehicles moving together at high speed, which could further enhance road capacity utilization and reduce travel times.

(2) Utilization of advanced infrastructure sensors for more accurate MP signal timing: The accuracy of traffic signal timings under the MP control policy depends on the quality of input data, which could be significantly enhanced by using advanced infrastructure sensors. For example, radar detectors or video cameras could provide detailed information about vehicle counts, speeds, and occupancy levels, allowing for more responsive and efficient signal timings. Moreover, integrating traffic data from multiple sensors could improve the accuracy of traffic state estimation, leading to better traffic control performance.

(3) Integration of perimeter control technologies with MP control: Traffic congestion in city centers is a prevalent issue in many urban areas. Perimeter control, which limits vehicle entry into congested areas, could be combined with the MP control policy to manage traffic demand more effectively. For instance, dynamic tolling could be used to discourage vehicles from entering congested areas during peak periods, while signal timings at the boundary of the controlled area could be adjusted to regulate the flow of vehicles entering and leaving the area. Moreover, the integration of MP control with perimeter control could enhance the stability and throughput of urban networks.

These potential research directions highlight the versatility and potential of the MP control policy. With continued exploration and innovation, this traffic management strategy could play a key role in achieving more efficient, safe, and sustainable urban mobility in the future.

References

Balancing street space for pedestrians and vehicles. https://www.pps.org/article/balancing-street-space-for-pedestrians-and-vehicles. Accessed: 2008-12-31.

N. H. T. S. Administration. US Department of Transportation; Washington, DC, USA, October 2019.

G. Akyol, I. G. Erdagi, M. A. Silgu, and H. B. Celikoglu. Adaptive signal control to enhance effective green times for pedestrians: A case study. *Transportation Research Procedia*, 47:704–711, 2020.

P. Anderson and C. F. Daganzo. Effect of transit signal priority on bus service reliability. *Transportation Research Part B: Methodological*, 132:2–14, 2020.

T. Arsava, Y. Xie, and N. Gartner. Od-netband: an approach for origin–destination based network progression band optimization. *Transportation Research Record*, 2672(18):58–70, 2018.

M. Bayrak and S. I. Guler. Determining optimum transit signal priority implementation locations on a network. *Transportation Research Record*, 2674(10):387–400, 2020.

B. Bing and A. Carter. Scoot: The world's foremost adaptive traffic control system. *TRAFFIC TECHNOLOGY INTERNATIONAL'95*, 1995.

A. Boukerche, D. Zhong, and P. Sun. A novel reinforcement learning-based cooperative traffic signal system through max-pressure control. *IEEE Transactions on Vehicular Technology*, 71(2):1187–1198, 2021.

S. D. Boyles, N. E. Lownes, and A. Unnikrishnan. *Transportation Network Analysis*, volume 1. 0.89 edition, 2021.

S. Cafiso, A. G. Garcia, R. Cavarra, and M. Rojas. Crosswalk safety evaluation using a pedestrian risk index as traffic conflict measure. In *Proceedings of the 3rd International Conference on Road safety and Simulation*, pages 1–15, 2011.

J. Chang, J. Collura, F. Dion, and H. Rakha. Evaluation of service reliability impacts of traffic signal priority strategies for bus transit. *Transportation Research Record*, 1841 (1):23–31, 2003.

R. Chen, J. Hu, M. W. Levin, and D. Rey. Stability-based analysis of autonomous intersection management with pedestrians. *Transportation Research Part C: Emerging Technologies*, 114:463–483, 2020.

N. Chiabaut and A. Barcet. Demonstration and evaluation of an intermittent bus lane strategy. *Public Transport*, 11(3):443–456, 2019.

N. Chiabaut, X. Xie, and L. Leclercq. Road capacity and travel times with bus lanes and intermittent priority activation: analytical investigations. *Transportation Research Record*, 2315(1):182–190, 2012.

E. Christofa and A. Skabardonis. Traffic signal optimization with application of transit signal priority to an isolated intersection. *Transportation Research Record*, 2259(1): 192–201, 2011.

E. Christofa, I. Papamichail, and A. Skabardonis. Person-based traffic responsive signal

control optimization. *IEEE Transactions on Intelligent Transportation Systems*, 14(3): 1278–1289, 2013.

C. G. Claudel and A. M. Bayen. Lax–hopf based incorporation of internal boundary conditions into hamilton–jacobi equation. part i: Theory. *IEEE Transactions on Automatic Control*, 55(5):1142–1157, 2010a.

C. G. Claudel and A. M. Bayen. Lax–hopf based incorporation of internal boundary conditions into hamilton–jacobi equation. part i: Theory. *IEEE Transactions on Automatic Control*, 55(5):1142–1157, 2010b.

C. G. Claudel and A. M. Bayen. Lax–hopf based incorporation of internal boundary conditions into hamilton-jacobi equation. part ii: Computational methods. *IEEE Transactions on Automatic Control*, 55(5):1158–1174, 2010c.

S. L. Cohen and C. Liu. The bandwidth-constrained transyt signal optimization program. *Transportation Research Record*, 1057:1–7, 1986.

G. Currie and H. Lai. Intermittent and dynamic transit lanes: Melbourne, australia, experience. *Transportation Research Record*, 2072(1):49–56, 2008.

G. Currie and A. Shalaby. Active transit signal priority for streetcars: experience in melbourne, australia, and toronto, canada. *Transportation Research Record*, 2042(1):41–49, 2008.

C. F. Daganzo. The cell transmission model, part ii: network traffic. *Transportation Research Part B: Methodological*, 29(2):79–93, 1995.

C. F. Daganzo. A variational formulation of kinematic waves: basic theory and complex boundary conditions. *Transportation Research Part B: Methodological*, 39(2):187–196, 2005a.

C. F. Daganzo. A variational formulation of kinematic waves: Solution methods. *Transportation Research Part B: Methodological*, 39(10):934–950, 2005b.

D. Das, N. V. Altekar, and K. L. Head. Priority-based traffic signal coordination system with multi-modal priority and vehicle actuation in a connected vehicle environment. *Transportation Research Record*, page 03611981221134627, 2022.

M. G. S. de Oliveira and P. C. M. Ribeiro. Production and analysis of coordination plans using a geographic information system. *Transportation Research Part C: Emerging Technologies*, 9(1):53–68, 2001.

T. Deng and J. D. Nelson. Recent developments in bus rapid transit: a review of the literature. *Transport Reviews*, 31(1):69–96, 2011.

J. Ding, M. Yang, W. Wang, C. Xu, and Y. Bao. Strategy for multiobjective transit signal priority with prediction of bus dwell time at stops. *Transportation Research Record*, 2488(1):10–19, 2015.

F. Dion, H. Rakha, and Y. Zhang. Evaluation of potential transit signal priority benefits along a fixed-time signalized arterial. *Journal of Transportation Engineering*, 130(3): 294–303, 2004.

V. Dixit, D. J. Nair, S. Chand, and M. W. Levin. A simple crowdsourced delay-based traffic signal control. *PLoS one*, 15(4):e0230598, 2020.

M. Eichler and C. F. Daganzo. Bus lanes with intermittent priority: Strategy formulae and an evaluation. *Transportation Research Part B: Methodological*, 40(9):731–744, 2006.

D. J. Fagnant and K. Kockelman. Preparing a nation for autonomous vehicles: opportunities, barriers and policy recommendations. *Transportation Research Part A: Policy and Practice*, 77:167–181, 2015.

Y. Feng. *Intelligent traffic control in a connected vehicle environment*. PhD thesis, The University of Arizona, 2015.

N. H. Gartner. *OPAC: A demand-responsive strategy for traffic signal control*. Number 906. 1983.

N. H. Gartner, S. F. Assman, F. Lasaga, and D. L. Hou. A multi-band approach to arterial traffic signal optimization. *Transportation Research Part B: Methodological*, 25(1):55–74, 1991.

J.-T. Girault, V. V. Gayah, I. Guler, and M. Menendez. Exploratory analysis of signal coordination impacts on macroscopic fundamental diagram. *Transportation Research Record*, 2560(1):36–46, 2016.

J. Gregoire, E. Frazzoli, A. de La Fortelle, and T. Wongpiromsarn. Back-pressure traffic signal control with unknown routing rates. *IFAC Proceedings Volumes*, 47(3):11332–11337, 2014a.

J. Gregoire, X. Qian, E. Frazzoli, A. De La Fortelle, and T. Wongpiromsarn. Capacity-aware backpressure traffic signal control. *IEEE Transactions on Control of Network Systems*, 2(2):164–173, 2014b.

Q. Guo, L. Li, and X. J. Ban. Urban traffic signal control with connected and automated vehicles: A survey. *Transportation Research Part C: Emerging Technologies*, 101:313–334, 2019.

K. Han, B. Piccoli, and W. Szeto. Continuous-time link-based kinematic wave model: formulation, solution existence, and well-posedness. *Transportmetrica B: Transport Dynamics*, 4(3):187–222, 2016.

Q. He, K. L. Head, and J. Ding. Pamscod: Platoon-based arterial multi-modal signal

control with online data. *Transportation Research Part C: Emerging Technologies*, 20 (1):164–184, 2012.

Q. He, K. L. Head, and J. Ding. Multi-modal traffic signal control with priority, signal actuation and coordination. *Transportation Research Part C: Emerging Technologies*, 46:65–82, 2014.

D. Heinrichs and J. Jarass. Designing healthy mobility in cities: How urban planning can promote walking and cycling. *Bundesgesundheitsblatt, Gesundheitsforschung, Gesundheitsschutz*, 2020.

P. Hooper, B. Boruff, B. Beesley, H. Badland, and B. Giles-Corti. Testing spatial measures of public open space planning standards with walking and physical activity health outcomes: Findings from the australian national liveability study. *Landscape and Urban Planning*, 171:57–67, 2018.

H. Hu and H. X. Liu. Arterial offset optimization using archived high-resolution traffic signal data. *Transportation Research Part C: Emerging Technologies*, 37:131–144, 2013.

K. M. Hunter-Zaworski, W. C. Kloos, and A. R. Danaher. Bus priority at traffic signals in portland: the powell boulevard pilot project. *Transportation Research Record*, (1503), 1995.

C.-J. Jin, X. Shi, T. Hui, D. Li, and K. Ma. The automatic detection of pedestrians under the high-density conditions by deep learning techniques. *Journal of advanced transportation*, 2021:1–11, 2021.

Z. Ke, Z. Li, Z. Cao, and P. Liu. Enhancing transferability of deep reinforcement learning-based variable speed limit control using transfer learning. *IEEE Transactions on Intelligent Transportation Systems*, 22(7):4684–4695, 2020.

S. Khosravi, B. Beak, K. L. Head, and F. Saleem. Assistive system to improve pedestrians' safety and mobility in a connected vehicle technology environment. *Transportation Research Record*, 2672(19):145–156, 2018.

D. Krajzewicz, J. Erdmann, M. Behrisch, and L. Bieker. Recent development and applications of sumo-simulation of urban mobility. *International Journal on Advances in Systems and Measurements*, 5(3&4), 2012.

T. Le, P. Kovács, N. Walton, H. L. Vu, L. L. Andrew, and S. S. Hoogendoorn. Decentralized signal control for urban road networks. *Transportation Research Part C: Emerging Technologies*, 58:431–450, 2015.

L. Leden, P. Gårder, and C. Johansson. Safe pedestrian crossings for children and elderly. *Accident Analysis & Prevention*, 38(2):289–294, 2006.

M. W. Levin, D. Rey, and A. Schwartz. Max-pressure control of dynamic lane reversal and autonomous intersection management. *Transportmetrica B: Transport Dynamics*, 7(1): 1693–1718, 2019.

M. W. Levin, J. Hu, and M. Odell. Max-pressure signal control with cyclical phase structure. *Transportation Research Part C: Emerging Technologies*, 120:102828, 2020.

H. S. Levinson, S. Zimmerman, J. Clinger, and G. S. Rutherford. Bus rapid transit: An overview. *Journal of Public Transportation*, 5(2):1, 2002.

L. Li and S. E. Jabari. Position weighted backpressure intersection control for urban networks. *Transportation Research Part B: Methodological*, 128:435–461, 2019.

L. Li, V. Okoth, and S. E. Jabari. Backpressure control with estimated queue lengths for urban network traffic. *IET Intelligent Transport Systems*, 15(2):320–330, 2021.

M. Li, Y. Yin, W.-B. Zhang, K. Zhou, and H. Nakamura. Modeling and implementation of adaptive transit signal priority on actuated control systems. *Computer-Aided Civil and Infrastructure Engineering*, 26(4):270–284, 2011.

T. Li, B. Rosenblad, S. Wang, M. Shang, and R. Stern. Exploring energy impacts of cyber-attacks on adaptive cruise control vehicles. In *2023 IEEE Intelligent Vehicles Symposium (IV)*, pages 1–6. IEEE, 2023.

M. Liang, Y. Chao, Y. Tu, and T. Xu. Vehicle pollutant dispersion in the urban atmospheric environment: A review of mechanism, modeling, and application. *Atmosphere*, 14(2): 279, 2023.

M. J. Lighthill and G. B. Whitham. On kinematic waves ii. a theory of traffic flow on long crowded roads. *Proceedings of the Royal Society of London. Series A. Mathematical and Physical Sciences*, 229(1178):317–345, 1955.

Y. Lin, X. Yang, N. Zou, and M. Franz. Transit signal priority control at signalized intersections: a comprehensive review. *Transportation Letters*, 7(3):168–180, 2015.

Y. Lin, X. Yang, and N. Zou. Passive transit signal priority for high transit demand: model formulation and strategy selection. *Transportation Letters*, 11(3):119–129, 2019.

J. D. Little, M. D. Kelson, and N. H. Gartner. Maxband: A versatile program for setting signals on arteries and triangular networks. 1981.

H. Liu and V. V. Gayah. A novel max pressure algorithm based on traffic delay. *arXiv preprint arXiv:2202.03290*, 2022.

J. Liu, H. Zhang, Z. Fu, and Y. Wang. Learning scalable multi-agent coordination by spatial differentiation for traffic signal control. *Engineering Applications of Artificial Intelligence*, 100:104165, 2021.

P. A. Lopez, M. Behrisch, L. Bieker-Walz, J. Erdmann, Y.-P. Flötteröd, R. Hilbrich, L. Lücken, J. Rummel, P. Wagner, and E. Wießner. Microscopic traffic simulation using sumo. In *The 21st IEEE International Conference on Intelligent Transportation Systems*. IEEE, 2018. URL https://elib.dlr.de/124092/.

J. Lv and Y. Zhang. Effect of signal coordination on traffic emission. *Transportation Research Part D: Transport and Environment*, 17(2):149–153, 2012.

K. Ma and X. Li. A deep learning lane-changing decision framework with wide spatiotemporal conditions for connected and automated vehicles. In *2022 IEEE 25th International Conference on Intelligent Transportation Systems (ITSC)*, pages 4036–4041. IEEE, 2022.

K. Ma and H. Wang. Influence of exclusive lanes for connected and autonomous vehicles on freeway traffic flow. *IEEE Access*, 7:50168–50178, 2019.

K. Ma and H. Wang. How connected and automated vehicle–exclusive lanes affect on-ramp junctions. *Journal of Transportation Engineering, Part A: Systems*, 147(2):04020157, 2021.

K. Ma, H. Wang, and T. Ruan. Analysis of road capacity and pollutant emissions: Impacts of connected and automated vehicle platoons on traffic flow. *Physica A: Statistical Mechanics and its Applications*, 583:126301, 2021.

W. Ma, K. L. Head, and Y. Feng. Integrated optimization of transit priority operation at isolated intersections: A person-capacity-based approach. *Transportation Research Part C: Emerging Technologies*, 40:49–62, 2014.

W. Ma, D. Liao, Y. Liu, and H. K. Lo. Optimization of pedestrian phase patterns and signal timings for isolated intersection. *Transportation Research Part C: Emerging Technologies*, 58:502–514, 2015.

W. Ma, K. An, and H. K. Lo. Multi-stage stochastic program to optimize signal timings under coordinated adaptive control. *Transportation Research Part C: Emerging Technologies*, 72:342–359, 2016.

W. Ma, R. Cheng, H. Ke, and J. Zhang. Store-brand production arrangement based on the game theory. *Mathematical Problems in Engineering*, 2018, 2018a.

W. Ma, L. Zou, K. An, N. H. Gartner, and M. Wang. A partition-enabled multi-mode band approach to arterial traffic signal optimization. *IEEE Transactions on Intelligent Transportation Systems*, 20(1):313–322, 2018b.

A. Maipradit, J. Gao, T. Kawakami, and M. Ito. Adaptive traffic control algorithm based on back-pressure and q-learning. In *2019 IEEE Intelligent Transportation Systems Conference (ITSC)*, pages 1995–1999. IEEE, 2019.

D. Manolis, T. Pappa, C. Diakaki, I. Papamichail, and M. Papageorgiou. Centralised versus decentralised signal control of large-scale urban road networks in real time: a simulation study. *IET Intelligent Transport Systems*, 12(8):891–900, 2018.

P. Mercader, W. Uwayid, and J. Haddad. Max-pressure traffic controller based on travel times: An experimental analysis. *Transportation Research Part C: Emerging Technologies*, 110:275–290, 2020.

P. Mirchandani and L. Head. A real-time traffic signal control system: architecture, algorithms, and analysis. *Transportation Research Part C: Emerging Technologies*, 9(6): 415–432, 2001.

E. National Academies of Sciences, Medicine, et al. Signal timing manual. 2015.

G. F. Newell. A simplified theory of kinematic waves in highway traffic, part i: General theory. *Transportation Research Part B: Methodological*, 27(4):281–287, 1993a.

G. F. Newell. A simplified theory of kinematic waves in highway traffic, part ii: Queueing at freeway bottlenecks. *Transportation Research Part B: Methodological*, 27(4):289–303, 1993b.

G. F. Newell. A simplified theory of kinematic waves in highway traffic, part iii: Multi-destination flows. *Transportation Research Part B: Methodological*, 27(4):305–313, 1993c.

G. F. Newell. A simplified car-following theory: a lower order model. *Transportation Research Part B: Methodological*, 36(3):195–205, 2002.

Y. Park and M. Garcia. Pedestrian safety perception and urban street settings. *International Journal of Sustainable Transportation*, 14(11):860–871, 2020.

W. Pian, Y. Wu, X. Qu, J. Cai, and Z. Kou. Spatial-temporal dynamic graph attention networks for ride-hailing demand prediction. *arXiv preprint arXiv:2006.05905*, 2020.

H. Qi, R. Dai, Q. Tang, and X. Hu. Coordinated intersection signal design for mixed traffic flow of human-driven and connected and autonomous vehicles. *IEEE Access*, 8:26067–26084, 2020.

D. Rey and M. W. Levin. Blue phase: Optimal network traffic control for legacy and autonomous vehicles. *Transportation Research Part B: Methodological*, 130:105–129, 2019.

J. Robbennolt and M. W. Levin. Maximum throughput dispatch for shared autonomous vehicles including vehicle rebalancing. *IEEE Transactions on Intelligent Transportation Systems*, 2023.

D. I. Robertson. Transyt: a traffic network study tool. 1969.

E. D. Saldivar-Carranza, M. Hunter, H. Li, J. Mathew, and D. M. Bullock. Longitudinal performance assessment of traffic signal system impacted by long-term interstate construction diversion using connected vehicle data. *Journal of Transportation Technologies*, 11(4):644–659, 2021.

D. Salles, S. Kaufmann, and H.-C. Reuss. Extending the intelligent driver model in sumo and verifying the drive off trajectories with aerial measurements. In *SUMO Conference Proceedings*, volume 1, pages 1–25, 2020.

T. Seo, A. M. Bayen, T. Kusakabe, and Y. Asakura. Traffic state estimation on highway: A comprehensive survey. *Annual Reviews in Control*, 43:128–151, 2017.

L. Shi, Z. Xu, and M. Lejeune. An integer l-shaped method for dynamic order dispatching in autonomous last-mile delivery with demand uncertainty. *arXiv preprint arXiv:2208.09067*, 2022.

A. G. Sims and K. W. Dobinson. The sydney coordinated adaptive traffic (scat) system philosophy and benefits. *IEEE Transactions on Vehicular Technology*, 29(2):130–137, 1980.

J. Stevanovic, A. Stevanovic, P. T. Martin, and T. Bauer. Stochastic optimization of traffic control and transit priority settings in vissim. *Transportation Research Part C: Emerging Technologies*, 16(3):332–349, 2008.

X. Sun and Y. Yin. A simulation study on max pressure control of signalized intersections. *Transportation research record*, 2672(18):117–127, 2018.

B.-S. Tang, K. K. Wong, K. S. Tang, and S. Wai Wong. Walking accessibility to neighbourhood open space in a multi-level urban environment of hong kong. *Environment and Planning B: Urban Analytics and City Science*, 48(5):1340–1356, 2021.

L. Tassiulas and A. Ephremides. Stability properties of constrained queueing systems and scheduling policies for maximum throughput in multihop radio networks. In *29th IEEE Conference on Decision and Control*, pages 2130–2132. IEEE, 1990.

L. T. Truong, M. Sarvi, and G. Currie. An investigation of multiplier effects generated by implementing queue jump lanes at multiple intersections. *Journal of Advanced Transportation*, 50(8):1699–1715, 2016.

P. Varaiya. Max pressure control of a network of signalized intersections. *Transportation Research Part C: Emerging Technologies*, 36:177–195, 2013.

W. S. Vickrey. Congestion theory and transport investment. *The American Economic Review*, 59(2):251–260, 1969.

R. Vincent, A. Mitchell, and D. Robertson. User guide of transyt version 8-trrl report lr888. *Transport and Road Research Laboratory, Crowthorne, Inglaterra*, 1980.

Y. Wadjas and P. G. Furth. Transit signal priority along arterials using advanced detection. *Transportation Research Record*, 1856(1):220–230, 2003.

X. Wang, Y. Yin, Y. Feng, and H. X. Liu. Learning the max pressure control for urban traffic networks considering the phase switching loss. *Transportation Research Part C: Emerging Technologies*, 140:103670, 2022.

F. V. Webster. Traffic signal settings. Technical report, 1958.

H. Wei, C. Chen, G. Zheng, K. Wu, V. Gayah, K. Xu, and Z. Li. Presslight: Learning max pressure control to coordinate traffic signals in arterial network. In *Proceedings of the 25th ACM SIGKDD International Conference on Knowledge Discovery & Data Mining*, pages 1290–1298, 2019.

H. Wei, G. Zheng, V. Gayah, and Z. Li. Recent advances in reinforcement learning for traffic signal control: A survey of models and evaluation. *ACM SIGKDD Explorations Newsletter*, 22(2):12–18, 2021.

S. Wong. Group-based optimisation of signal timings using the transyt traffic model. *Transportation Research Part B: Methodological*, 30(3):217–244, 1996.

S. Wong, W. Wong, C. Leung, and C. Tong. Group-based optimization of a time-dependent transyt traffic model for area traffic control. *Transportation Research Part B: Methodological*, 36(4):291–312, 2002.

T. Wongpiromsarn, T. Uthaicharoenpong, Y. Wang, E. Frazzoli, and D. Wang. Distributed traffic signal control for maximum network throughput. In *2012 15th International IEEE Conference on Intelligent Transportation Systems*, pages 588–595. IEEE, 2012.

K. Wu, M. Lu, and S. I. Guler. Modeling and optimizing bus transit priority along an arterial: A moving bottleneck approach. *Transportation Research Part C: Emerging Technologies*, 121:102873, 2020.

C. Wuthishuwong and A. Traechtler. Vehicle to infrastructure based safe trajectory planning for autonomous intersection management. In *2013 13th International Conference on ITS Telecommunications (ITST)*, pages 175–180. IEEE, 2013.

N. Xiao, E. Frazzoli, Y. Li, Y. Wang, and D. Wang. Pressure releasing policy in traffic signal control with finite queue capacities. In *Decision and Control (CDC), 2014 IEEE 53rd Annual Conference on*, pages 6492–6497. IEEE, 2014.

K. Xu, J. Huang, L. Kong, J. Yu, and G. Chen. Pv-tsc: Learning to control traffic signals for pedestrian and vehicle traffic in 6g era. *IEEE Transactions on Intelligent Transportation Systems*, 2022a.

T. Xu, Y. Bika, and M. Levin. Ped-mp: A pedestrian-friendly max-pressure signal control policy for city networks. *Available at SSRN 4186588*.

T. Xu, M. W. Levin, and M. Cieniawski. A zone-based dynamic queueing model and maximum-stability dispatch policy for shared autonomous vehicles. In *2021 IEEE International Intelligent Transportation Systems Conference (ITSC)*, pages 3827–3832. IEEE, 2021.

T. Xu, S. Barman, M. W. Levin, R. Chen, and T. Li. Integrating public transit signal priority into max-pressure signal control: Methodology and simulation study on a downtown network. *Transportation Research Part C: Emerging Technologies*, 138:103614, 2022b.

T. XU, Y. Bika, and M. Levin. An approximate position-weighted back-pressure traffic signal control policy for traffic networks. *Available at SSRN 4186584*, 2022.

T. Xu, M. Cieniawski, and M. W. Levin. Fms-dispatch: a fast maximum stability dispatch policy for shared autonomous vehicles including exiting passengers under stochastic travel demand. *Transportmetrica A: Transport Science*, pages 1–39, 2023.

H. Yan, F. He, X. Lin, J. Yu, M. Li, and Y. Wang. Network-level multiband signal coordination scheme based on vehicle trajectory data. *Transportation Research Part C: Emerging Technologies*, 107:266–286, 2019.

K. Yang, M. Menendez, and S. I. Guler. Implementing transit signal priority in a connected vehicle environment with and without bus stops. *Transportmetrica B: Transport Dynamics*, 7(1):423–445, 2019a.

M. Yang, Z. Li, Z. Ke, and M. Li. A deep reinforcement learning-based ramp metering control framework for improving traffic operation at freeway weaving sections. In *Proceedings of the Transportation Research Board 98th Annual Meeting, Washington, DC, USA*, pages 13–17, 2019b.

J. Yao, C. Tan, and K. Tang. An optimization model for arterial coordination control based on sampled vehicle trajectories: The stream model. *Transportation Research Part C: Emerging Technologies*, 109:211–232, 2019.

R. Yue. *Determination of Progression Speeds for Traffic Signal Coordination*. PhD thesis, University of Nevada, Reno, 2020.

C. Zhang, Y. Xie, N. H. Gartner, C. Stamatiadis, and T. Arsava. Am-band: an asymmetrical multi-band model for arterial traffic signal coordination. *Transportation Research Part C: Emerging Technologies*, 58:515–531, 2015.

H. Zhang, Y. Nie, and Z. Qian. Modelling network flow with and without link interactions: the cases of point queue, spatial queue and cell transmission model. *Transportmetrica B: Transport Dynamics*, 1(1):33–51, 2013.

L. Zhang, Z. Song, X. Tang, and D. Wang. Signal coordination models for long arterials and grid networks. *Transportation Research Part C: Emerging Technologies*, 71:215–230, 2016.

Y. Zhang and Y. Zhou. Distributed coordination control of traffic network flow using adaptive genetic algorithm based on cloud computing. *Journal of Network and Computer Applications*, 119:110–120, 2018.

Y. Zhang, K. Gao, Y. Zhang, and R. Su. Traffic light scheduling for pedestrian-vehicle mixed-flow networks. *IEEE Transactions on Intelligent Transportation Systems*, 20(4): 1468–1483, 2018.

Y. Zhang, Y. Zhang, and R. Su. Pedestrian-safety-aware traffic light control strategy for urban traffic congestion alleviation. *IEEE Transactions on Intelligent Transportation Systems*, 22(1):178–193, 2019.

L. Zhao, Z. Li, Z. Ke, and M. Li. Fuzzy self-adaptive proportional–integral–derivative control strategy for ramp metering at distance downstream bottlenecks. *IET Intelligent Transport Systems*, 14(4):250–256, 2020.

S. Zheng, M. Li, Z. Ke, Z. Li, et al. Coordinated variable speed limit control for consecutive bottlenecks on freeways using multiagent reinforcement learning. *Journal of advanced transportation*, 2023, 2023.

G. Zhou and A. Gan. Performance of transit signal priority with queue jumper lanes. *Transportation Research Record*, 1925(1):265–271, 2005.

S. Zhou, H. Li, Q. Zhang, M. Gao, and B. Ran. Traffic signal coordination control optimization considering vehicle emissions on urban arterial road. *Journal of Computational Methods in Sciences and Engineering*, 21(1):233–239, 2021.